UNIVERSITY OF PAVIA
FACULTY OF ENGINEERING

DOCTORAL SCHOOL IN ELECTRONICS, COMPUTER SCIENCE AND ELECTRICAL ENGINEERING

CYCLE XXXI

DOCTORAL THESIS

Modeling of Inhomogeneous and Lossy Waveguide Components by the Segmentation Technique Combined with the BI-RME method

Candidate: Battistutta Simone

Supervisor: Prof. Perregrini Luca
Co-supervisor: Prof. Bressan Marco

A.A. 2017/18

To my father

For implicitly pushing me
to become an engineer…

Summary

List of Figures

Abstract

The Boundary Integral-Resonant Mode Expansion (BI-RME) method is an efficient technique for the numerical solution of eigenvalue problems of the type encountered in electromagnetic theory. As highlighted by the huge quantity of scientific publications on it, this specialized numerical method has been developed during the years to analyze several classes of components. But, this evolution has put in evident its most important drawback: even if subsequent versions have some common elements, in order to analyze different classes of components or problems, an *ad hoc* theory development and code implementation was always required. In practice, since the mathematical and physical foundations of this method are not "negligible" and its understanding is not trivial, this drawback has drastically influenced its diffusion: the result was a limitation of the use of the BI-RME method to the laboratory level or implemented into software for the analysis and development of very specialized industrial components.
Since 2013, the Microwave team of the University of Pavia has decided to change the nature of the BI-RME method to overcome its fundamental drawback and to make it more user friendly. The result is a numerical technique that generalize the BI-RME method: it allows analyzing completely arbitrarily shaped waveguide circuits, filled by piecewise homogenous dielectric materials also with losses, with the use of simple and well-known RWG basis functions. The obtained algorithm is called "Generalized BI-RME" method: this Ph.D. thesis represent the work done by the author since 2015 on what concerning the theory development, code implementation and debug of the entire algorithm except the BI-RME solver (whose theory and code implementation is made by Professor Marco Bressan) for which the author has contributed to the debug phase.
The Generalized BI-RME method combines the segmentation technique with an implementation of the BI-RME method: in this way, it is possible to use the same theory and code to analyze passive components that spans from the dielectric-loaded filters to the power dividers or to the orthomode transducers. This combination is necessary since the original BI-RME method doesn't allow directly analyzing inhomogeneous components: to overcome this limitation, the implemented strategy applies the segmentation technic prior the analysis with the BI-RME method, to subdivide the circuit into piecewise homogeneous building blocks.

The Generalized BI-RME method can be conceptually subdivided into three parts. Once defined the geometry, the desired circuit is subdivided into homogeneously filled building blocks: this is the only mandatory requirement during the segmentation phase. In the past combinations of the BI-RME method with the segmentation technique, there were also some constrains on the geometry of the building blocks: with the proposed algorithm, it is only suggested to have, as much as possible, building blocks

with a rectangular parallelepiped shape, the so called “boxed” shape. In this case, it is possible to use a lighter version of the BI-RME method that it is not an *ad hoc* implementation, but only a simplification dictated by the developed theory. The result is a considerably reduction on the computational effort for the boxed building blocks. For the building blocks with an arbitrary shape, the electromagnetic analysis is performed with the BI-RME solver in its general form, so by solving a pure Electric Field Integral Equation (EFIE). Moreover, by carefully choosing the segmentation, it is possible to have identical building blocks in shape and volume: this characteristic could be exploited to implement a sort of block reusability in order to avoid some not necessary electromagnetic analysis (so, to save time). Since the BI-RME method is based on the Boundary Integral Method, it requires the discretization only of the building blocks surfaces instead of the volumes as for the Finite Element Method. A surface mesh made by triangular patches is defined only on some block surfaces like the interconnecting surfaces between building blocks, the surfaces where the external ports lie, and all the surfaces that do not coincide with the cavity walls used for the BI-RME analysis. Respect to what done in the past, in the adopted implementation of the BI-RME method is used a rectangular parallelepiped (“boxed”) shape for the fictitious external cavity resonator instead a sphere one. The boxed shape allows reducing the number of necessary resonant modes, since the volume difference is less than for the sphere case, and of the basis functions, since probably a great part of the sidewalls will coincide with the cavity boundaries. Moreover, for the boxed cavity shape, the Green’s functions are known as series whose convergence speed is enhanced by the Ewald’s technique. In case of boxed building blocks, it is necessary to discretize only the surface magnetic current while, for the arbitrarily shaped ones, it is necessary to discretize both the surface electric and magnetic currents. Another important aspect of the Generalized BI-RME method is the use of simple and well-known Rao-Wilton-Glisson (RWG) basis functions instead using more complex type of basis functions sometimes *ad hoc* developed for the problem under test.

In the second part of the algorithm, each block is analyzed by the BI-RME method. In particular, the electromagnetic behavior of each building block is represented through a Generalized Admittance Matrix (GAM) in form of pole expansion, a wideband and material independent mathematical model. This result is obtained by exploiting the particular calculation of the quasi-static part of the Green’s functions, the Ewald’s technique with its splitting parameter, and the solution of the EFIE problem for the arbitrarily shaped blocks.

In the post-processing phase, the GAMs of all the building blocks are combined together through a circuital cascade procedure in the frequency domain to obtain the GAM of the entire circuit, then converted into S-parameters. In this phase, it is crucial the choosing of the right strategy to achieve the desired accuracy and efficiency during the combination, since the cascade implies the execution of some matrix operations like inversions and multiplications. Before dealing with the circuital cascade, it is necessary to define the sequence by which the building blocks GAMs are combined. The implemented strategy aims to cascade first the building blocks filled by lossless media, and then the ones with dielectric losses or with a surface condition of finite electric conductivity. For a lossless media, the GAM appears purely imaginary since the real part becomes zero. Thanks to this *a priori* knowledge, by combining first the blocks without losses it is possible to work on them with a real algebra: this leads to save a huge amount of computational resources and time since, typically, most of the volume of the analyzable structures is filled by lossless dielectric media (air or vacuum). Moreover, it is reduced also the error produced by the numerical matrix inversion: even if it is known that the inverse of a zero matrix is still a zero matrix, the numerical inversion of the real part of the GAM in the lossless case could not be exactly zero due to the machine precision and this error will propagate. For these purposes, and automated procedure has been implemented to search a path that combine first the lossless building blocks: by adding each time, as much as possible, a block that is connected, at least, with one block

already inserted into the path, this strategy allows controlling the increasing of the matrix dimensions and to reduce the computational time.

Starting from an historical evolution of the BI-RME method to understand the motivations behind this activity, the proposed “Generalized BI-RME” method is explained in Chapter 2 by subdividing it into three parts: pre-processing, so the segmentation phase; EM analysis by the BI-RME method, so the theory adopted; post-processing, for the frequency combination of the GAM related to each circuital block. Some numerical considerations are proposed in Chapter 3 where the effects of the analysis parameters on a simple structure are investigated. In Chapter 4, a series of complex examples are analyzed to illustrate the precision and efficiency of the implemented algorithm, compared with the ones obtainable with a commercial software (ANSYS HFSS). Finally, in Chapter 5 are reported the conclusions and are highlighted some possible future upgrades.

Introduction

Even if the electromagnetic field theory originally introduced by Maxwell remains at the base of an enormity of theoretical studies for the development of analytic techniques, these techniques allow solving an electromagnetic problem with an exact solution only in limited and particular simple cases or under too much simplified assumptions. Some examples of them are the separation of variables, series expansions, integral solutions, perturbation methods and series expansion [1]. On the other hand, the experimental approaches, like the so-called "cut-and-try" approach, could be expensive, time consuming, and not flexible in terms of variation of the project parameters.

The necessity of an alternative approach was already clear in the 1940s due to the increasing of the complexity of the geometries defining the problems. In 1960s, Paris and Hurd wrote in [2]: "*Most problems that can be solved formally (analytically) have been solved*". In fact, the diffusion of the numerical methods started in the mid of the 1960s with the availability of modern high-speed digital computers. Numerical methods allow solving complex problems with an approximated solution. Even if the obtainable solution is approximated, its accuracy can be tuned by properly choosing the parameters used by the specific method. Moreover, their use lead to a remarkable reduction of the project times and costs, as well as a great flexibility and the possibility to investigate non-conventional solutions.

The solution of an electromagnetic (EM) problem through a numerical method can be summarize into three steps [3]:

1- analytical pre-processing of the EM problem to transform it into an algebraic one;
2- solution of the algebraic equations;
3- interpretation of the obtained results.

It is clear that the solution of the same problem can be reached by using different numerical methods, but each one requires a different theoretical elaboration and gives rise to codes with different efficiencies. In general, more is the theoretical elaboration and less will be the computational effort: but, this could limit the application of the same method to different problems (and *vice versa*).

In literature, numerical methods are subdivided in several ways. One of them use to distinguish the numerical methods in general and specialized methods. The general methods allow solving a huge amount of problems thanks to their flexibility but they can suffer of a low accuracy especially in case of reduced computational capabilities. Examples of general methods are the Finite Difference Method, the Finite Element Method, the Method of Moments and the Boundary Element/Integral Method.

The *Finite Difference* method (FD) ([1],[4]) is the oldest and easiest method for the solution of a differential equation: by substituting the derivatives with finite differences (incremental rapport), it is possible to transform the problem into an algebraic equations system. The method is applicable also to structures with complex shape and non-homogeneous medium; moreover, it allows a full-wave analysis with impulse excitation or single frequency analysis by a sinusoidal excitation. On the other side, the application to open regions is complicated and needs to use absorbing boundary conditions (ABC, PML, etc.). It requires the subdivision of the entire domain with a lattice of points and a temporal iteration in order to determine the field in every point at any instant of time: this requires a spatial and temporal step sufficient fine with the consequent increases of the computational effort, time and memory.
The *Finite Element Method* (FEM) [5] may be the most diffuse numerical method in technical environment thanks to its applicability on different fields; even if conceptually complex to understand, the method is based on the discretization of the space with finite elements of canonical shapes like triangle or tetrahedron. On each element, the unknown function (a potential or an EM field component) is approximated with a polynomial whose coefficients are expressed in function of the value assumed by the function on the element vertices. So, the problem is translated to a functional minimization that, thanks to the polynomial approximation, leads to a linear equations system in the values that the unknown function assumes on the vertices of the elements. The FEM method is applicable also to structures with complex shape and non-homogeneous material, and a single frequency analysis is possible with a sinusoidal excitation. It requires the subdivision of the entire domain producing big matrices but sparse; moreover, the application to open regions is complicated and needs to some absorbing boundary conditions.
The *Method of Moment* (MoM) [6] is a powerful mathematical tool that, today, is used for the solution of a great variety of problems, electromagnetics and not. With this tool, it is possible to transform a functional integral-differential equation into an algebraic matrix problem; it provides, then, a general mathematical scheme to which is possible to bring back, practically, all the approaches to the numerical solution of the Maxwell's equation.
The *Boundary Element/Integral Method* (BEM/BIM) [1] is a conceptual easy method based on the representation of the field in all of space as function of the value assumed by the unknown sources placed on the discontinuous surfaces; this is done by formulating the EM problem in terms of an integral equation solved by the Method of Moment. The method is easily applicable to opened or closed structures but with homogeneous mediums and simple geometries. It requires the subdivision only of the surfaces (3D structure) or lines (2D structure) on which are placed the sources: this produces little matrices but fully; moreover, it requires the determination of the analytical or numerical Green's function of the region under test.

The specialized numerical methods are developed to solve a particular problem or to be applied to the analysis of a specific component: so, they are not flexible but, thanks to the theoretical elaboration, it is possible to reach a very high accuracy with, typically, a reduced computational effort. An example of specialized method is the Mode Matching method but, in literature, there are many *ad hoc* techniques for the analysis of dielectric-loaded waveguide filters or more exotic structures.
The *Mode Matching* method (MM) [7] is one of the oldest rigorous techniques for the solution of waveguide resonant cavities and discontinuities; as a consequence, it is less applicable than the general methods. As confirm of the previous rule, even if the effort necessary for the analytical development is remarkable, the computational effort is limited and the calculation speed is higher.

Inside the specialized methods category, there is a sub-class of still specialized methods but developed to solve a particular class of problems or to be applied to the solution of a particular class of components. As for the pure specialized methods, with this class it is possible to reach a very high accuracy even if their application is more flexible. An example is the *Boundary Integral-Resonant Mode Expansion*

method (BI-RME), invented and developed inside the microwave team of the University of Pavia [8]. The BI-RME method is a very efficient and accurate method that allows a full-wave analysis and permits to characterize the component through a mathematical model (i.e., the pole-expansion of the admittance parameters in the frequency domain). Moreover, it leads to the solution of a single linear eigenvalue problem and the modal fields are automatically normalized. However, its nature has represented its most important drawback: in order to be applied to a different class of problems, it required an *ad hoc* theory development and code implementation.

With the activity descripted into this thesis, this drawback has been overcome by creating a new numerical technique that generalize the BI-RME method through the combination of a particular implementation of it with the segmentation technique [9]. The result is the possibility to analyze completely arbitrary 3D components, filled by piecewise homogeneous and lossy dielectric materials, without developing an *ad hoc* theory each time and without losing in accuracy.

Bibliography

[1] M.N.O. Sadiku, *Numerical Techniques in Electromagnetics*, 3rd ed., CRC Press, 2009.

[2] D.T. Paris and F.K. Hurd, *Basic Electromagnetic Theory*, MCGraw-Hill, New York, 1969, p. 166.

[3] R. Sorrentino and G. Bianchi, *Ingegneria delle microonde e radiofrequenze*, McGraw-Hill, Milano 2005.

[4] A. Taflove and S.C. Hagness, *Computational Electrodynamics: The Finite-Difference Time-Domain Method*, 3rd ed., Artech House, 2005.

[5] J.-M. Jin, *The Finite Element Method in Electromagnetics*, 3rd ed., Wiley-IEEE Press, 2014.

[6] R. F. Harrington, *Field Computation by Moment Methods*, IEEE Press, 1993.

[7] R. Mittra and S.W. Lee, *Analytical Techniques in the Theory of Guided Waves*, The Macmillan Company, 1971.

[8] G. Conciauro, M. Guglielmi, and R. Sorrentino, *Advanced Modal Analysis. CAD Techniques for Waveguide Components and Filters*, J. Wiley, 2000.

[9] M. Bressan, S. Battistutta, M. Bozzi and L. Perregrini, "Modeling of Inhomogeneous and Lossy Waveguide Components by the Segmentation Technique Combined with the Calculation of the Green's Function by the Ewald's Method," *IEEE Transactions on Microwave Theory and Techniques*, vol. 66, no. 2, Feb. 2018.

Chapter 1
Historical evolution of the BI-RME method

As originally stated in [1], "*The Boundary Integral-Resonant Mode Expansion (BI-RME) method is an efficient technique for the numerical solution of eigenvalue problems of the type encountered in electromagnetic theory*". It was invented in 1970s by the *emeritus* Professor G. Conciauro, but its improvement and extension were made by the entire Microwave team of the University of Pavia along a temporal period of more than 40 years. In particular, on the development of the BI-RME method, it is right to mention the fundamental work done by Professor M. Bressan, co-supervisor of this activity, who has dedicated its academic life to the study and development of analytical and numerical methods, but also the important contributes given by Professor P. Arcioni, Professor L. Perregrini and Professor M. Bozzi along the years.

Until 1996, the name of this method was not the actual one but the meaning was the same. At the beginning, the BI-RME method was introduced for the calculation of the modes of arbitrarily shaped waveguides [1]-[3] (Fig. 1.1). As indicated by the acronym, this method is based on the Boundary Element/Integral Method (BEM/BIM), but its implementation differs from the original one [4]. The original BIM/BEM is based on the solution of a homogeneous integral equation obtained by enforcing the electric wall boundary condition to the two-dimensional electric field generated in the cross-section by the unknown surface currents on the walls of the circuit under test. Since these currents produce a field radiated into the free space, the Green's functions involved for the field representation is the free space one, so a complex transcendent function of the frequency. By using the Method of Moments (MoM) [5]-[6], the integral equation is transformed into a matrix eigenvalue problem whose eigenvalues represent the resonance frequencies and the eigenvectors the modal currents of the waveguide cross-section. Due to the complex dependency of the free space Green's functions from the frequency, the eigenvalue problem results non-linear and its solution requires the use of iterative methods with very long computational times. The key aspect of the Boundary Integral part of the BI-RME method reported in [1]-[3] was the closing of the structure under test inside a rectangular or circular two-dimensional resonator: the use of this resonator does not perturb the calculation of the cross-section resonant modes since these modes have a null external field. The electric field was represented in a hybrid form consisting of a Boundary Integrals (BI) and a rapidly converging Resonant Mode Expansion (RME), permitting to transform the non-linear eigenvalue problem, arising from the standard boundary integral approach, into a linear one [1]. This transformation was made by introducing a limited number of auxiliary variables (the mode amplitudes), in addition to the variables involved in the representation of the currents on the walls. The disadvantage of increasing the number of unknowns

was largely offset by the advantage of avoiding the lengthy and sometimes unreliable numerical solution of the non-linear eigenvalue problem arising from the conventional boundary method.

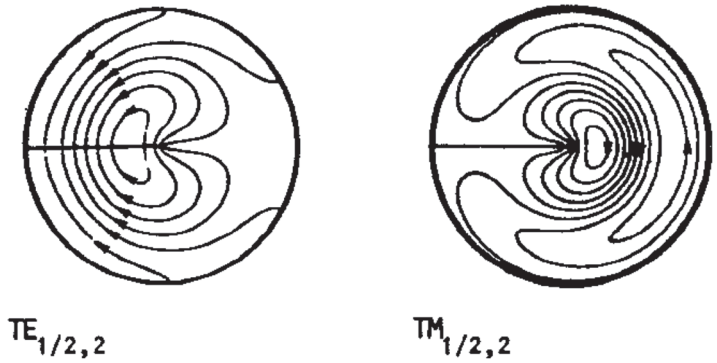

Fig. 1.1. Example of calculated TE and TM mode patterns for a circular waveguide perturbed by a radial fin ([1]-[2]).

Between 1985 and 1995, the same concepts were applied to the study of the resonant modes of arbitrarily shaped cavity resonators thus extending the application of the BI-RME method to the analysis of 3D objects ([7]-[9]). The philosophy was to consider the currents on the walls of the cavity resonator under test acting inside an external fictitious cavity resonator with a spherical shape: this allows a considerable reduction of the computational effort and an increasing of the accuracy thanks to the knowledge of the Green's functions in closed form. In particular, in [7] has been addressed the problem of the calculation of the Green's functions in points near to the source one by extracting the singularity from the modal expression of the dyadic Green's functions. To better model the object surface, in [9] was used a surface mesh, made by triangular patches, since this shape allows to easily representing complex geometries (Fig. 1.2); this fact has been discussed in details by Rao *et al*. in [10] where it was introduced what today are the most widely used type of basis functions in the EM problems, the Rao-Wilton-Glisson (RWG) basis functions.

The first appearance of the BI-RME acronym is dated 1996 when this method was applied to the analysis of arbitrarily shaped H-plane (Fig. 1.3) and E-plane (Fig. 1.5) waveguide components ([11]-[12]). For this works, the BI-RME method was considered like a Method of Moments solution of a pair of linear eigenvalue integral-differential equations, derived directly from the original differential problem. This approach is more suited to describing the mathematical nature of the method and provides a better understanding of the numerical approximations. As result, the EM behavior of the component under test was expressed in terms of its admittance matrix Y in form of pole expansion based on the Kurokawa representation [13]. Moreover, in addition to the extraction of the low-frequency behavior to improve the convergence of the series, the implementation of the BI-RME method also permitted the fast evaluation of the effect of a geometrical deformation on the frequency response, a feature very useful either for optimization or for setting the mechanical tolerances.

Even if the theory of the BI-RME method is more complex than the theory of the conventional BEM/BIM, its numerical implementation is only slightly more complicated. In any case, the efficiency, flexibility and reliability of the codes based on the BI-RME method offset this small disadvantage, as is also the case in comparison with codes based on other popular methods, such as the Finite Element Method [14]. The good features of the BI-RME method are easy to appreciate, especially when many modes have to be determined. For this reason, the BI-RME method is well suited to provide the many modes required by other techniques in cases of geometries where the modes are not available in analytic form. This approach was used in 1996 for the works reported in [15] and [16]: in particular, in [16] was

evaluated the modal coupling coefficients of waveguide step discontinuities like the "triseptum" circular waveguide and the "cross-shaped" waveguide (Fig. 1.4).

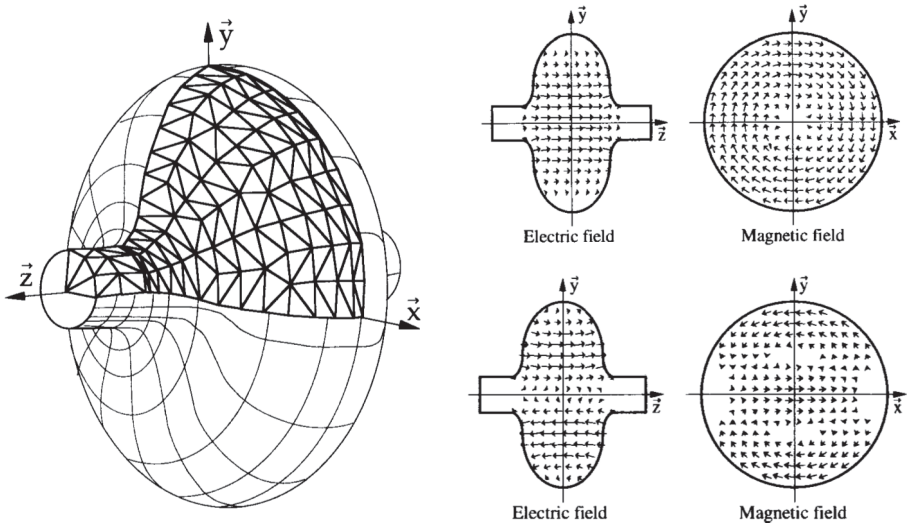

Fig. 1.2. Application of the BI-RME method to the analysis of arbitrarily shaped cavity resonators: the 500 MHz ELETTRA accelerating cavity [9].

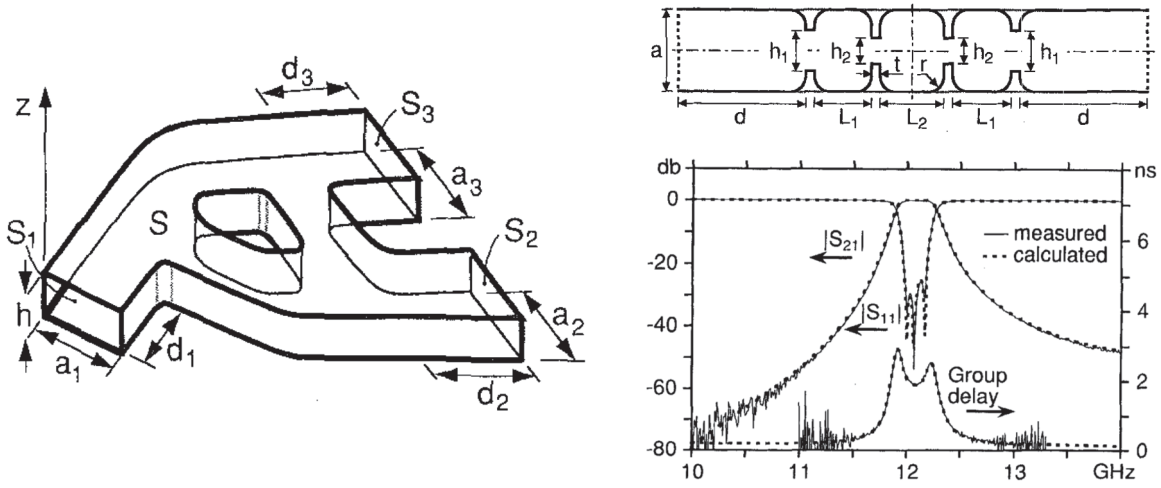

Fig. 1.3. Application of the BI-RME method to the analysis of arbitrarily shaped H-plane waveguide components [11].

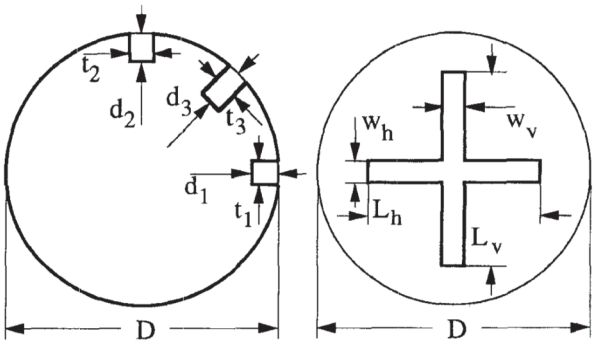

Fig. 1.4. Example of "triseptum" circular waveguide and "cross-shaped" waveguide step discontinuities [16].

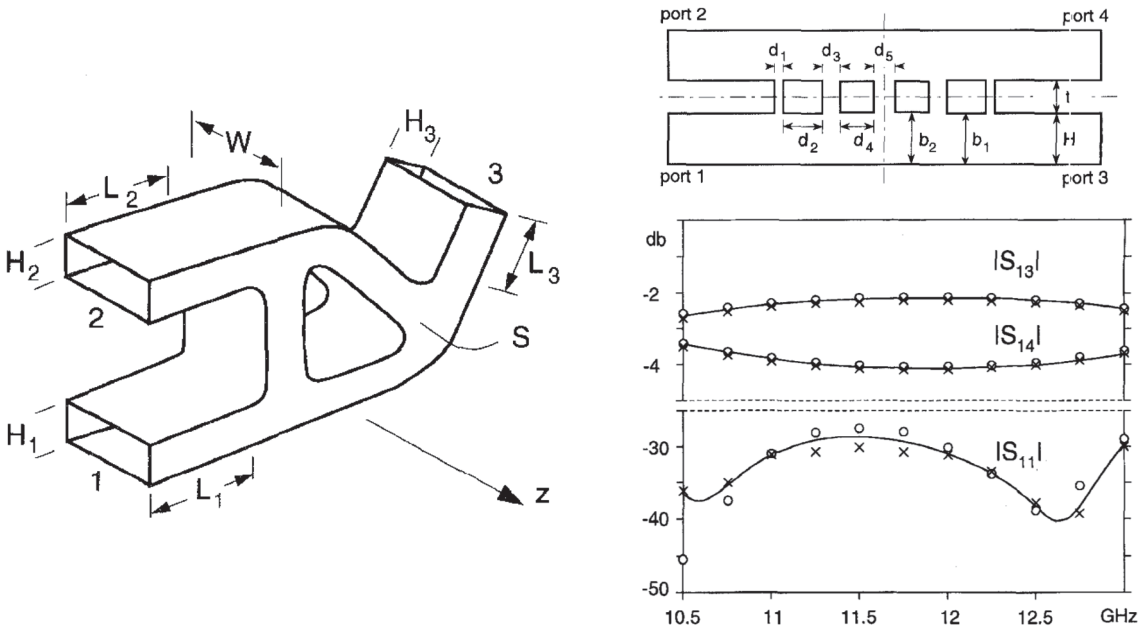

Fig. 1.5. Application of the BI-RME method to the analysis of arbitrarily shaped E-plane waveguide components [12].

Nevertheless the BI-RME method has proved to be a very efficient and reliable method in comparison with codes based on other popular methods, its theoretical and numerical improvements were always a key activity for the Microwave team of the University of Pavia. For example, to enhance its performances, in [17] it was discussed how to minimize the computing time for the evaluation of the double surface integrals arising in the application of the boundary integral method (BIM) to 3D problems. The integrals considered refer to the Green's functions for the scalar and vector potentials and to uniform or linear basis and test functions defined over triangular sub-domains. In particular, in [17] were reported the original analytical formulas for the double surface integrals over coincident triangles involving the singular terms of the Green's functions and it was presented a criterion for obtaining a good compromise between accuracy and computing time in numerical integration.

The admittance matrix representation reported in [11] and [12] is used to characterize the circuit behavior with a wideband mathematical model since the elements obtained by the BI-RME analysis are practically frequency independent. This aspect of the BI-RME method became further important in 1999, when Professors Arcioni and Conciauro present a work entitled "Combination of Generalized Admittance Matrices in the Form of Pole Expansions" [18]. In this work, it was described a novel algorithm for the determination of the wide-band mathematical model of a waveguide component segmented into elementary blocks of known characteristics. Starting from the Y-matrices of the blocks, given in the form of pole expansions in the frequency domain, the algorithm yielded the overall Y-matrix in the same form (Fig. 1.6). Therefore, it could be applied iteratively to find the pole expansion of the Y-matrix of larger and larger waveguide structures. The algorithm was particularly useful if the Y-matrix of the blocks was obtained by the BI–RME method, which yielded the Y-parameters just in the desired form.

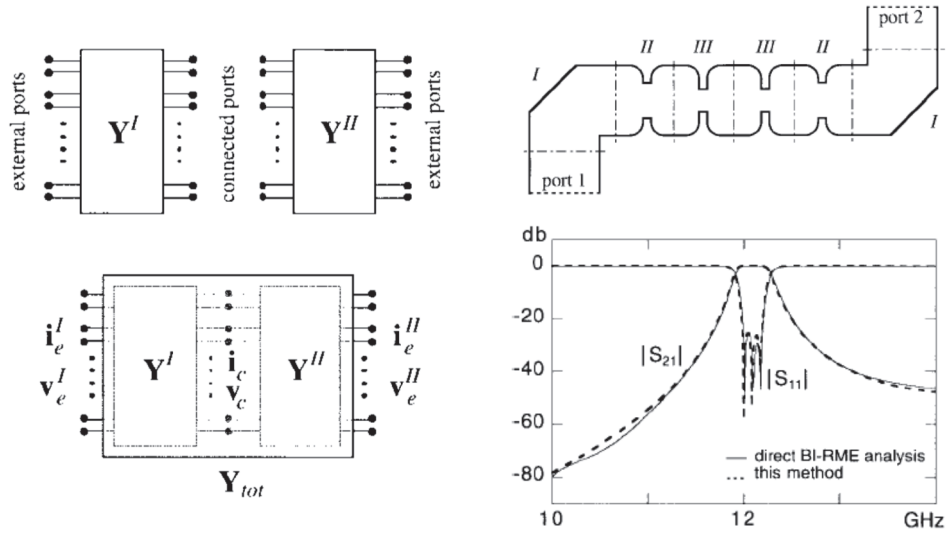

Fig. 1.6. Combination of Generalized Admittance Matrices in the Form of Pole Expansions [18].

In 2000, Professor Conciauro, Eng. Guglielmi and Professor Sorrentino, helped by their teams, published a book entitle "Advanced Modal Analysis: CAD Techniques for Waveguide Components and Filters" [1]. Even if inside it was described some of the most significant developments in the area of modal analysis of passive waveguide components, this was also the occasion to give the first comprehensive description of the BI-RME method. After this event and until 2005, the studies on the BI-RME method were primarily focused on two topics: the analysis of 3D passive components, and the analysis of inductive and capacitive frequency selective surfaces (FSS), whose remarks were used also for the study of shielded planar circuits. In the framework of the analysis of 3D components, in [19] was reported an example of efficient fusion between the analytical calculation of the low frequency terms of the admittance matrix (in the case of long terminal waveguides) and the numerical calculation with the BI-RME method of the resonant wavenumbers and the normalized fields involved by the Resonant Mode Expansion. In [20], it was reported a rigorous and comprehensible explanation of the state of art of the BI-RME method, while, in [21], it was presented an algorithm for the wide-band optimization of H and E-plane waveguide components with irregular shapes. The algorithm used the BI-RME method in conjunction with a variational technique to determine the objective function and its gradient by solving a single electromagnetic problem. The same technique was used to perform a sensitivity analysis to check the effect of the mechanical tolerances on the performance of the component and to estimate the yield for a given manufacturing technology on a large-scale production (Fig. 1.7).

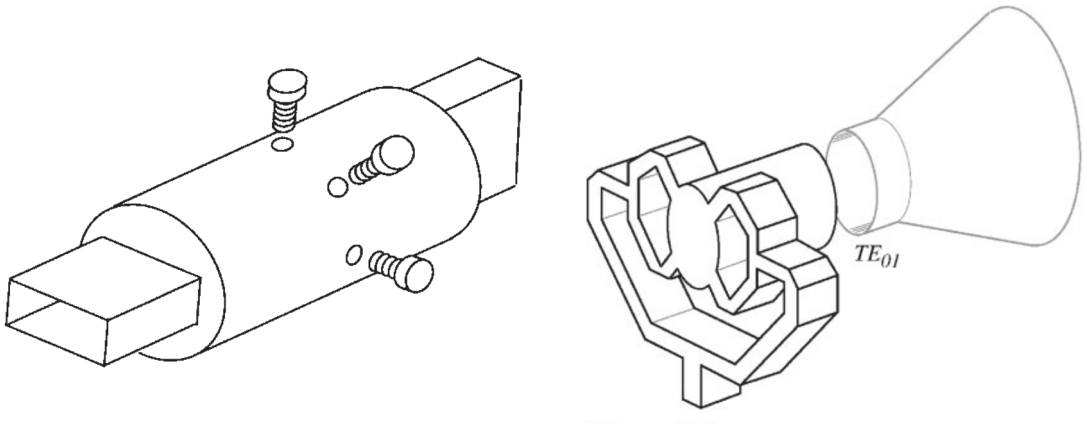

(*a*) (*b*)

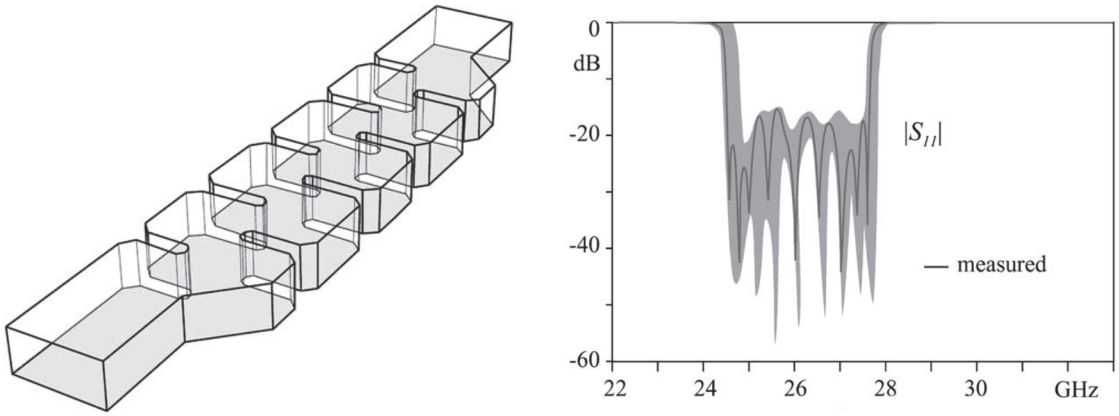

(*c*)

Fig. 1.7. Examples of the 3D components analyzable by the BI-RME method. (*a*) [19], (*b*) [20], (*c*) [21].

Frequency selective surfaces (FSSs) typically consists of a metal plane performed periodically with apertures and possibly backed by a dielectric layer. This type of structures find several applications as filter in microwave as well as in the millimeter wave range ([22]-[23]); the use of arbitrarily shaped apertures adds degrees of freedom in tailoring the frequency behavior of the filter. The analysis by the BI-RME method of frequency selective surfaces started approximately in 1999, where an efficient algorithm was presented for the first time [22]. Then, this algorithm was improved and applied also to the analysis of quasi-optical filters consisting of thick metal screens perforated periodically with arbitrarily shaped apertures [24]. The algorithm was based on the expression of the electromagnetic field in free space as a combination of Floquet modes, and the field on each aperture was obtained as Method of Moment solution of the integral equation resulting from matching the fields across the aperture. The flexibility, accuracy, and rapidity of the proposed algorithm depend on the use of the Boundary Integral-Resonant Mode Expansion method in the numerical determination of the entire domain basis functions since the application of the Method of Moment is more efficient using this type of basis functions as reported in [25] (Fig. 1.10). Always in [24] was proposed the analysis of two different quasi-optical filters operating at 8 GHz and 280 GHz, compared with experimental data as well as with other simulations (Fig. 1.8). In both cases, the whole analysis required few seconds on a standard workstation and the theoretical results showed a very good agreement with the measured data in a wide frequency band. Moreover, this hybrid MoM/BI-RME approach was capable to handle completely arbitrary shapes. Then, in 2003, the capabilities of the BI-RME method to analyze FSSs was extended from the inductive to the capacitive FSSs. In particular, the algorithm was used for the analysis of printed periodic structures, consisting of a multi-layered array of metal patches in a stratified dielectric medium, illuminated by a uniform plane-wave [26]. The patches may have an arbitrary shape, and both metal conductivity and dielectric losses were considered (Fig. 1.9).

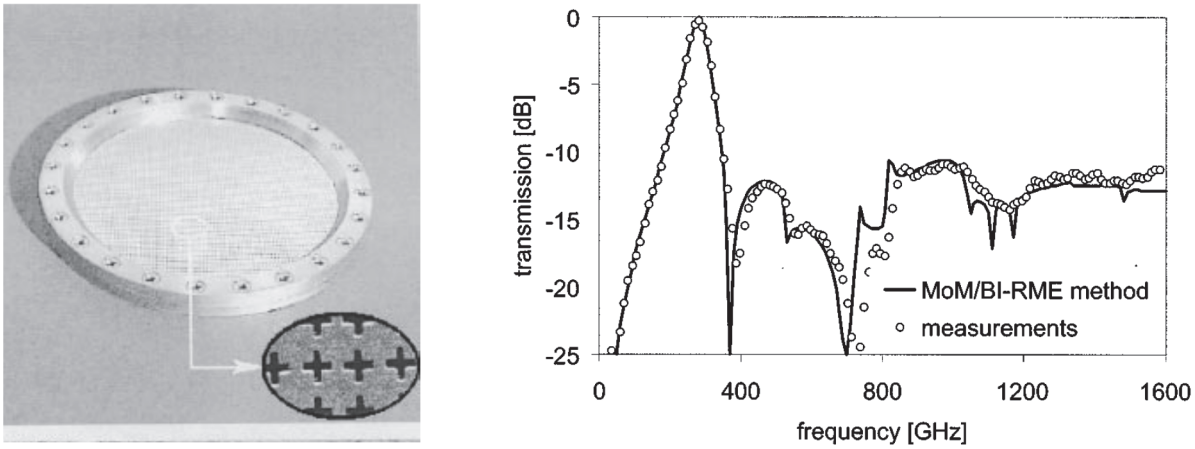

Fig. 1.8. Application of the hybrid MoM/BI-RME method to the analysis of quasi-optical filters [24].

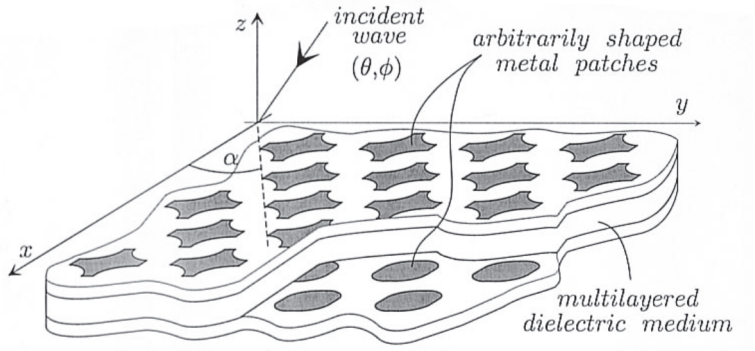

(*a*)

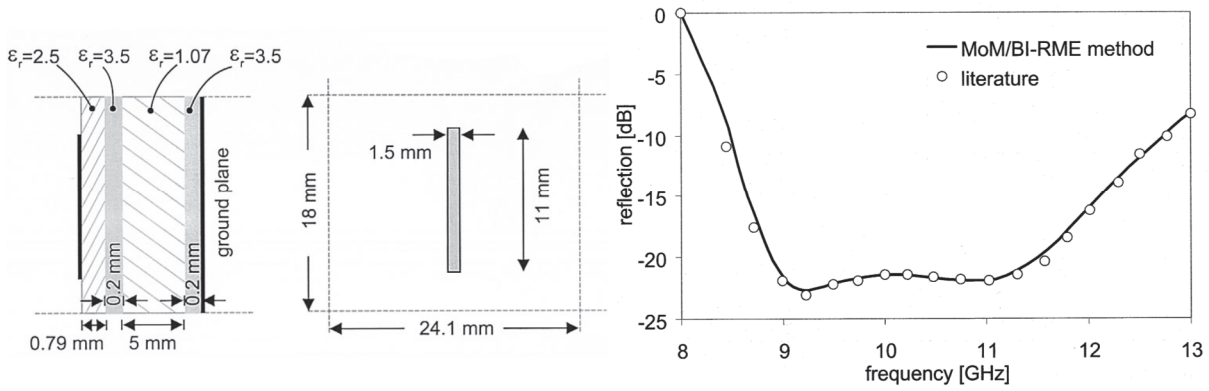

(*b*) (*c*)

Fig. 1.9. Analysis of multi-layered printed FSS with the hybrid MoM/BI-RME approach. (*a*) Schematic representation. Periodic array of rectangular patches on a grounded multi-layered dielectric medium: (*b*) side and front view of the unit cell and (*c*) reflection coefficient of the fundamental mode versus frequency [26].

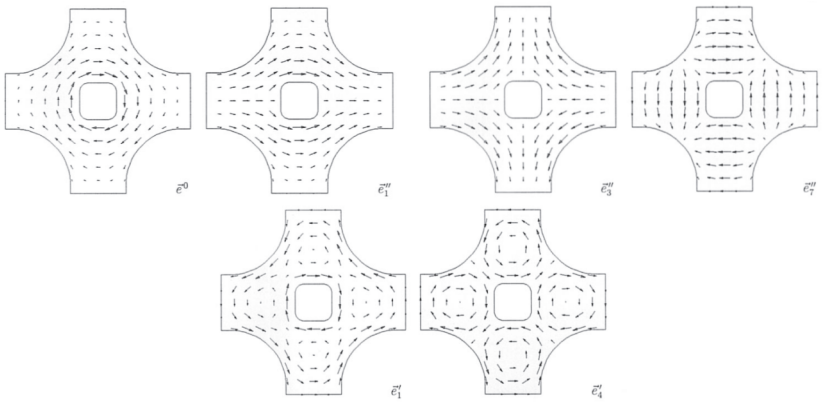

Fig. 1.10. Some of the first entire-domain vector basis functions used for representing the electric current density on a multiply-connected patch with a rounded cross shape [26].

In the framework of the analysis of planar components, the approach used was derived by the one proposed for the FSS. In particular, in [27] it was presented an approach for the analysis of shielded microstrip circuits, composed of a number of thin metallic areas with arbitrary shapes and finite conductivity, embedded in a multi-layered lossy medium (Fig. 1.11). The analysis was based on the solution of an integral equation (IE) obtained by enforcing the proper boundary condition to the electric field on the metallic areas. The IE was solved by using the Method of Moments with entire domain basis functions, which was numerically determined by the BI–RME method. The use of the BI–RME method allowed for the efficient calculation of the basis functions independently on the shape of the domain, thus permitting the analysis of a wide class of circuits. Another important remark is dated 2003: differently from the standard integral approaches, the proposed method led to a state-space model of the circuit [28]. This model directly permitted to find the admittance matrix in the form of a reduced-order pole expansion in the S-domain through standard Krylov sub-space techniques (Fig. 1.12). Then, in 2005, the hybrid MoM/BI-RME method found application also to the analysis of the dispersion diagram of planar Electromagnetic Band-Gap structures (EBG) [29] (Fig. 1.13).

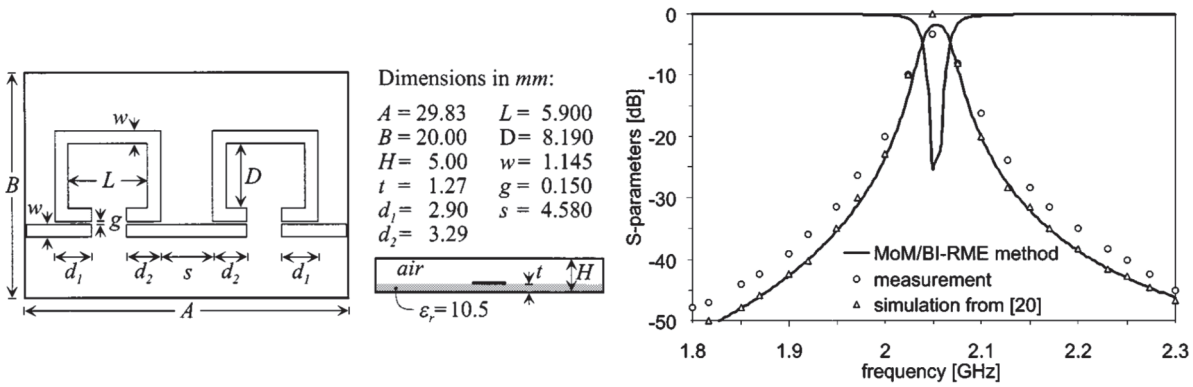

Fig. 1.11. Application of the hybrid MoM/BI–RME technique to the analysis of boxed MMICs [27].

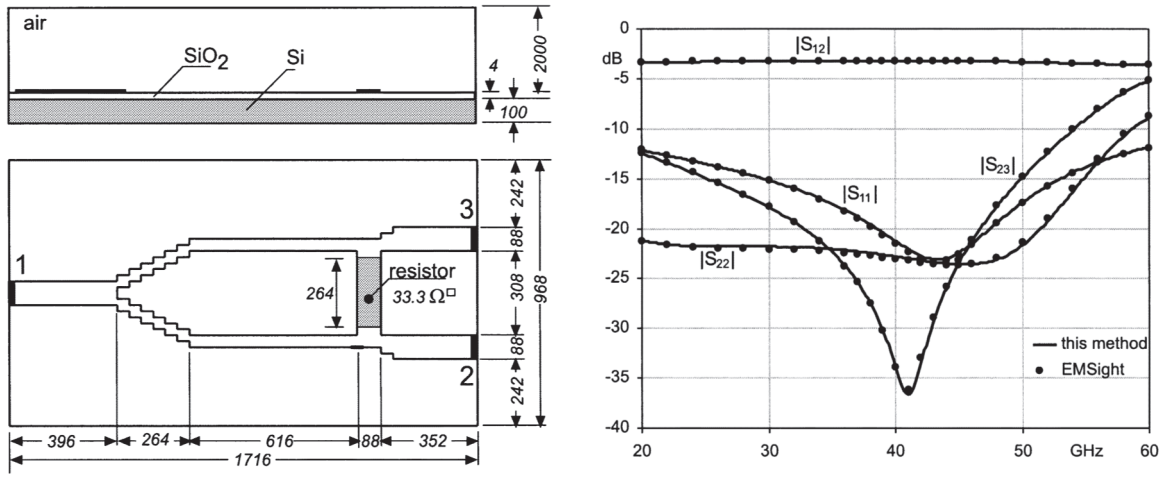

Fig. 1.12. Application of the hybrid MoM/BI–RME technique to the S-domain modelling of planar circuits on semiconducting substrates [28].

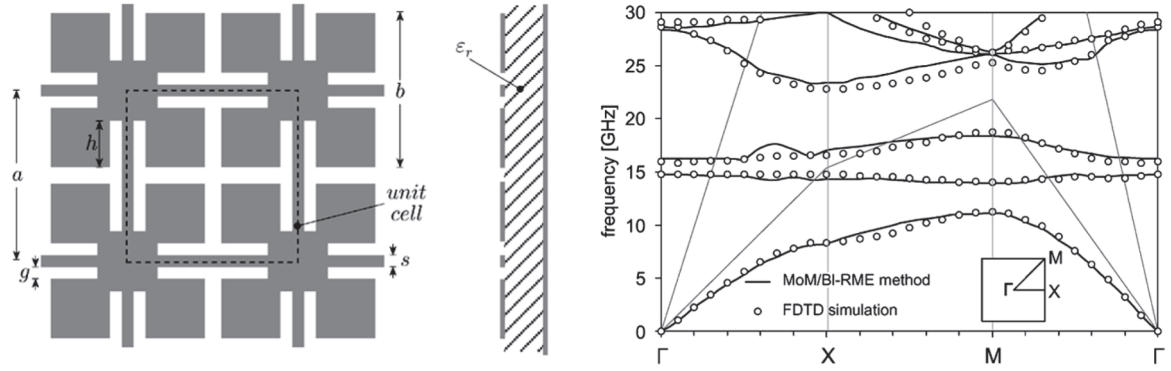

Fig. 1.13. Dispersion diagram of planar Electromagnetic Band-Gap structures (EBG) calculated by the MoM/BI-RME method [29].

Between 2005 and 2013, the activities of the Microwave team concerning the development of the BI-RME method were focused on the analysis of circuits in Surface Integrated Waveguide (SIW) technology and waveguide circuits, primarily filters, with metal insets or dielectric resonators. The conductive thread between these two research fields was the segmentation of the structure under test into unit cell; then, each unit cell was subdivided into homogeneously filled sub-circuits whose analysis with the BI-RME method was easier or more efficient. In this way, each sub-element was characterized with a mathematical model. The overall behavior was obtained by combining all the sub-elements models for each unit cell, and then combining the unit cells them self. Modern microwave and millimeter-wave systems require low-cost, broadband, and low-profile components, able to perform different functions. The integration of all these building blocks on a single substrate is a very attractive solution, especially in the millimeter-wave range, but the main drawback of this approach is represented by the radiation losses, which become critical in the millimeter-wave range [30]. The Substrate Integrated Waveguide technology represents a very promising candidate for circuits and components operating in the microwave, millimeter-wave and terahertz region. Substrate integrated waveguides belong to the family of substrate integrated circuits and are fabricated by using two rows of conducting cylinders and/or slots embedded in a dielectric substrate that connect two parallel metal plates [31]-[33]. The basic step for the design of transmission lines based on the SIW concept is the development of a fast and reliable code for the determination of the dispersion properties of the SIW modes [30]. For this purpose, the BI-RME method was used to create a novel analysis method in conjunction with the

Floquet theorem and the segmentation technique. First, the structure was subdivided into unit cells, so very simple and redundant parts of the circuit. If necessary, each unit cell was segmented again in a number of sub circuits, consisting of either the dielectric-filled portion or air holes. Each sub circuit was characterized separately by its generalized admittance matrix (GAM) calculated by using the BI-RME method (Fig. 1.14). All GAMs were then combined in order to determine the GAM of the unit cell of the SIW and the dispersion diagram of the first modes could be calculated ([30], [32] and [33]). Moreover, in [33] the BI-RME method was used to model the conductive, dielectric and radiating losses in SIW circuits with a perturbation technique; these elements were then added to the generalized admittance representation as independent terms (Fig. 1.15). To simplify the circuital analysis of pseudo-periodic structures like a SIW circuit, in [34] was presented a novel technique for the automatic, self-consistent and direct determination of wide-band lumped-element equivalent circuit models of SIW discontinuities. Also in this case, the technique was based on the full-wave analysis of SIW components by using the BI-RME method to characterize them with a generalized admittance matrix in the form of a pole expansion in the frequency domain. This expression permitted to directly identify the topology of a multimodal equivalent circuit and the values of its lumped elements, thus avoiding any initial guess or fitting procedure. The proposed method found application on the creation of libraries of parametric models of SIW discontinuities to easily represent the behavior of each unit cell and to use them inside simpler circuital solvers respect the more complicated full-wave software (Fig. 1.16).

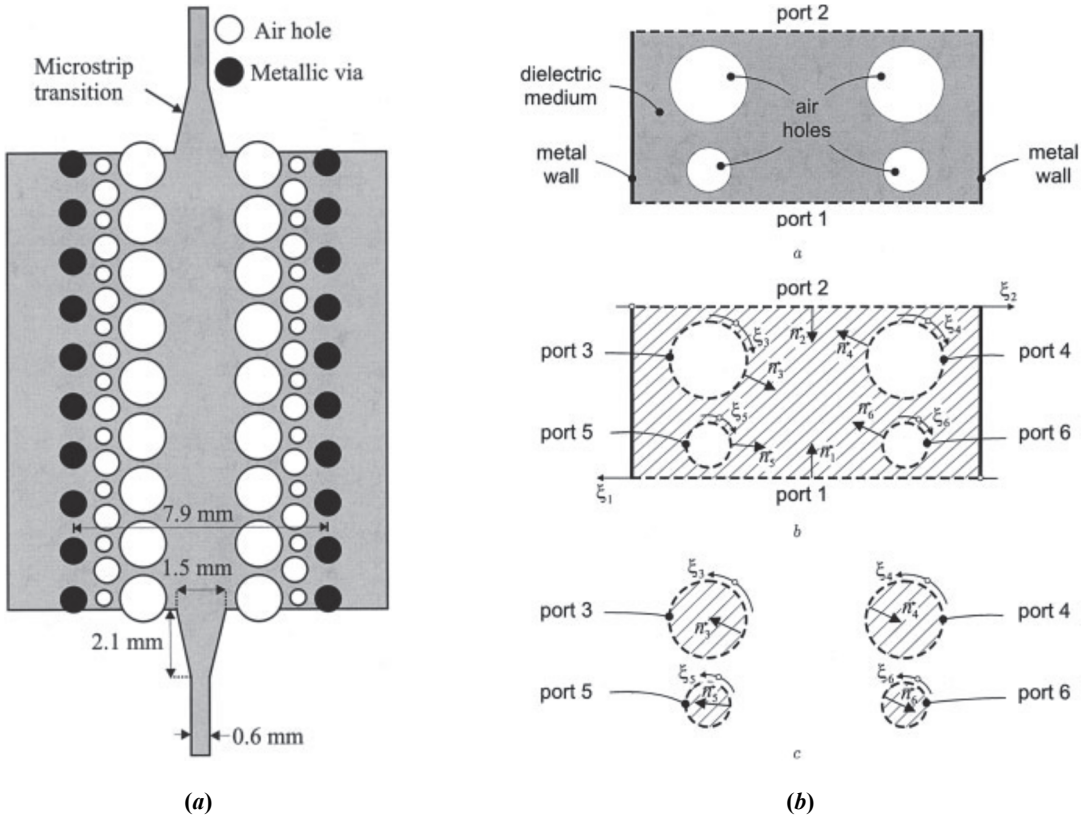

(*a*) (*b*)

Fig. 1.14. (*a*) Example of SIW circuit, (*b*) schematization of the proposed approach based on the Floquet theorem, the segmentation technique, and the BI-RME method [30].

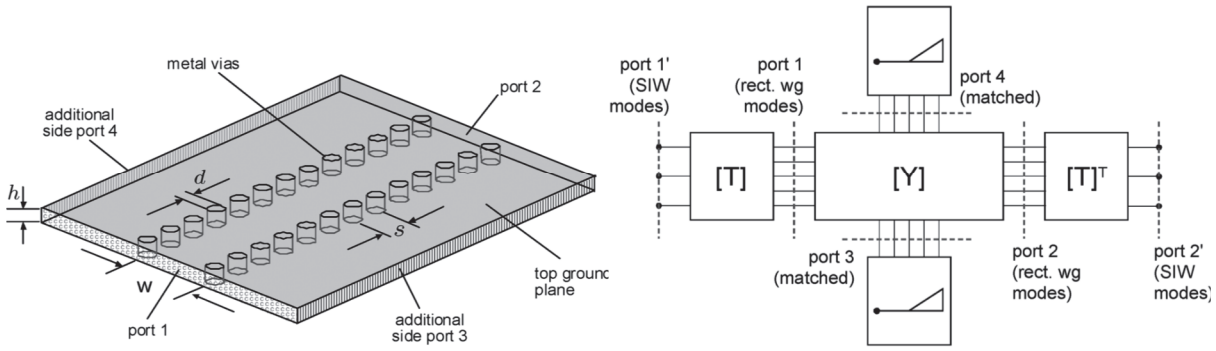

(*a*) (*b*)

$$Y_{ij}(k_0) = \frac{A_{ij}}{j\eta_0 k_0} + \sigma_d B_{ij} + \frac{jk_0\varepsilon_r}{\eta_0} B_{ij} + \frac{k_0^2 \varepsilon_r^{3/2}}{\eta_0} \sum_{p=1}^{P} \frac{C_{ip} C_{ip}}{k'_p Q_p \left(k'^2_p + jk_0 k'_p \varepsilon_r^{1/2} / Q_p - k_0^2 \varepsilon_r \right)} + \frac{jk_0^3 \varepsilon_r^2}{\eta_0} \sum_{p=1}^{P} \frac{C_{ip} C_{ip}}{k'^2_p \left(k'^2_p + jk_0 k'_p \varepsilon_r^{1/2} / Q_p - k_0^2 \varepsilon_r \right)}.$$

(*c*)

Fig. 1.15. Geometry of a lossy SIW circuit. (*a*) Physical model considered in the BI-RME analysis, with additional side radiation ports. (*b*) Circuit schematic with the ports definition. (*c*) GAM formulation to consider the losses [33].

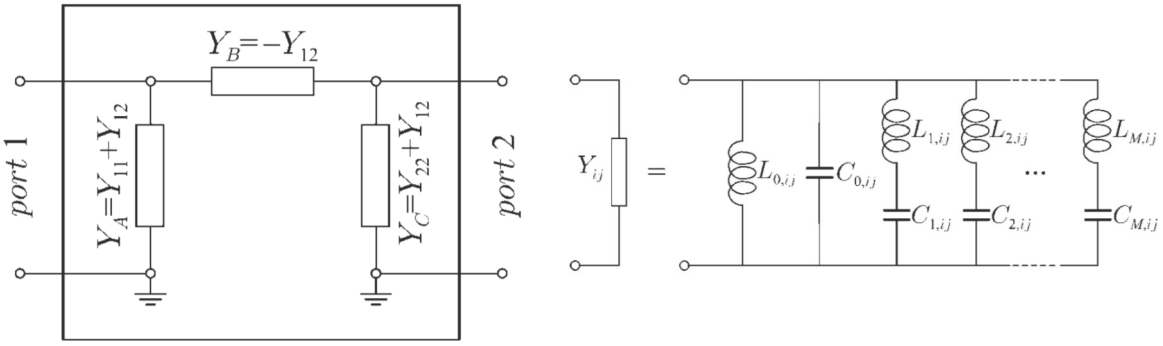

(*a*) (*b*)

Fig. 1.16. Topology of the generic p-type equivalent circuit model, in the case of a two-port component (*a*). Equivalent circuit model of Y_{ij}, directly derived from the BI-RME analysis (*b*) [34].

Even if the SIW technology represents a very promising candidate for the future evolution of the circuits, for the applications where the losses (dielectric or conductive) are a critical aspect (i.e., when it is necessary to handle high power), is still practically mandatory to use traditional waveguide circuits. In this framework, the BI-RME method, combined with the segmentation technique, was used to analyzed piecewise homogeneous circuits like dielectric loaded filters, or to analyze filters with particular topologies. By starting from this last class, the BI–RME method was applied to the modelling of rectangular waveguides with complicated radially symmetric metal insets [35] (Fig. 1.17 and Fig. 1.18). In this work, a self-consistent new theory was presented to fully exploit the peculiarities of the considered class of structures, thus straightforwardly leading to the system equations. The efficiency of the BI-RME method was further enhanced application because the currents on the waveguide walls was not involved in the calculation. For this reason, the Method of Moments discretization of the field equations led to a mathematical model whose order was much smaller than in the general BI-RME approach as well as in other boundary integral methods. Due to the state-space formulation of this model, a wide-band representation of the generalized admittance matrix of the structure was easily found in the form of a pole expansion in the S-domain by the calculation of a reasonably small number of eigensolutions of a matrix eigenvalue problem. Instead, in [36], a state-space integral-equation (SS-IE) formulation based on the standard BI-RME technique was employed for the accurate analysis of rectangular three-dimensional cavities loaded with cylindrical dielectric resonators placed at any arbitrary position inside the cavity (Fig. 1.19). The electric equivalent polarization charge and current densities were employed for the rigorous characterization of a dielectric obstacle immersed into free space. The presented technique permitted to calculate in a very efficient way a large number of solenoidal modes. The resonant frequencies of dielectric-loaded cavities were calculated and compared with data from literature and a commercial finite element method software. An example of application is reported in [37] where the novel technique was first validated through the accurate analysis of a dielectric loaded rectangular cavity, and a simple stop-band structure based on such basic building block (Fig. 1.20). Then, making use of a computer-aided design tool, a four-pole band-pass filter based on dielectric loaded resonators was efficiently designed. Also in this case, the accuracy of the proposed method was validated through successful comparisons with data from technical literature and available commercial software.

During the years, the implementations of the BI-RME method has been translated into some *ad hoc* software. For example, '*Pagoda'*, for the calculation of the electromagnetic field distribution of unusual coaxial cross-sections (for the Ericsson Radio System); '*ANAPLAN-W*', for the wideband modelling of arbitrarily shaped H and E-plane components ([38], [39]); '*ACID*', for the analysis and optimization of capacitive and inductive FSS with arbitrary shapes and/or number of layers (used for the analysis and development of dichroic mirrors for the European Space Agency - ESA); '*MIF*', to calculate the scattering parameters and the group delay of Metal Insert Filters (MIF); '*INDFILT*', which computes the scattering parameters of inductive filters based on the insertion of thick irises in a rectangular waveguide.

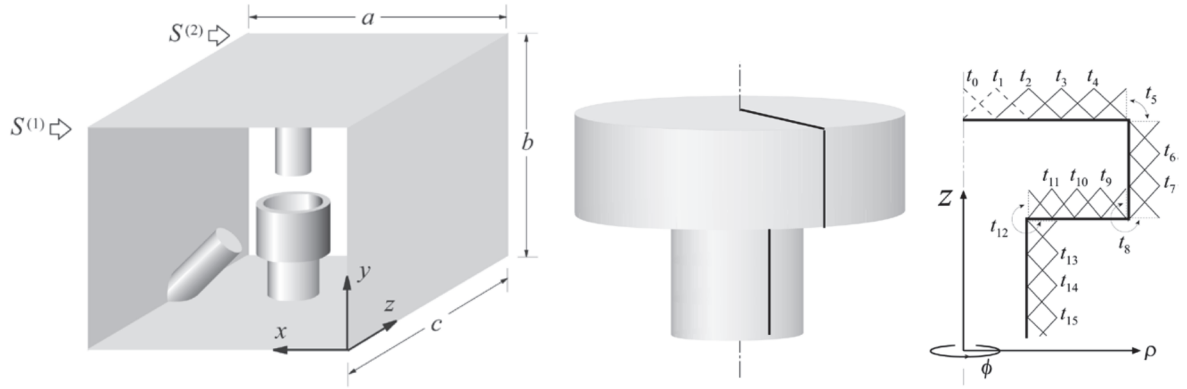

(*a*) (*b*)

Fig. 1.17. Rectangular waveguide with metal insets (*a*) and an overview of the definition of the triangular basis functions defined on the metal inset surface (*b*) [35].

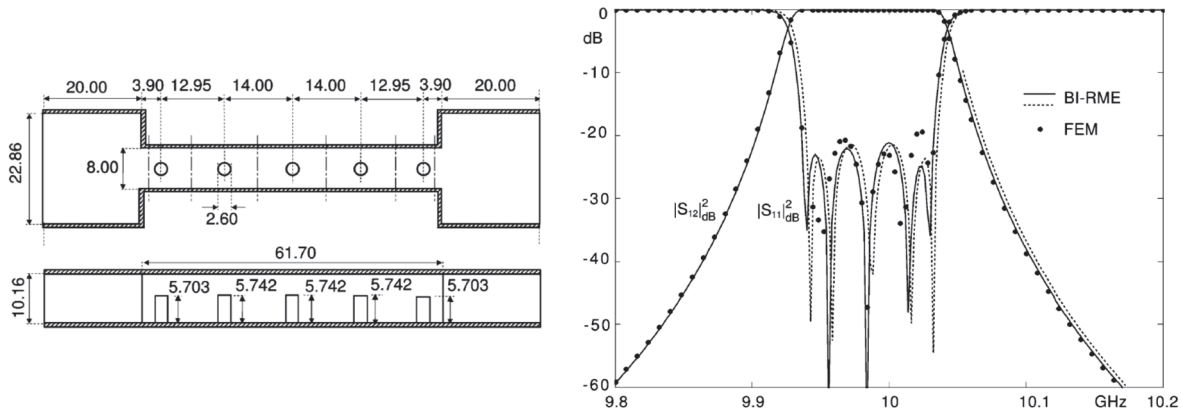

Fig. 1.18. Reflection and transmission losses of an evanescent-mode filter calculated by the BI–RME method and a frequency-by-frequency cascading procedure in different times. Solid curves: long calculation, dotted curves: short calculation [35].

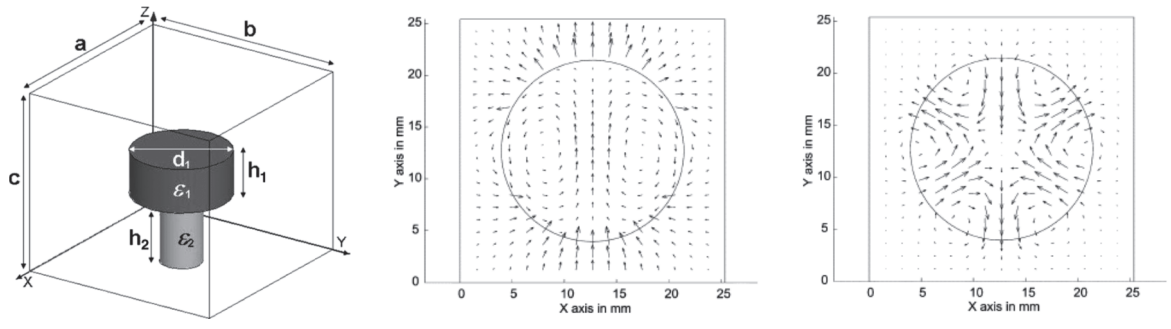

(*a*) (*b*) (*c*)

Fig. 1.19. Rectangular cavity loaded with a cylindrical dielectric resonator (*a*). Example of electric (*b*) and magnetic (*c*) fields distributions [36].

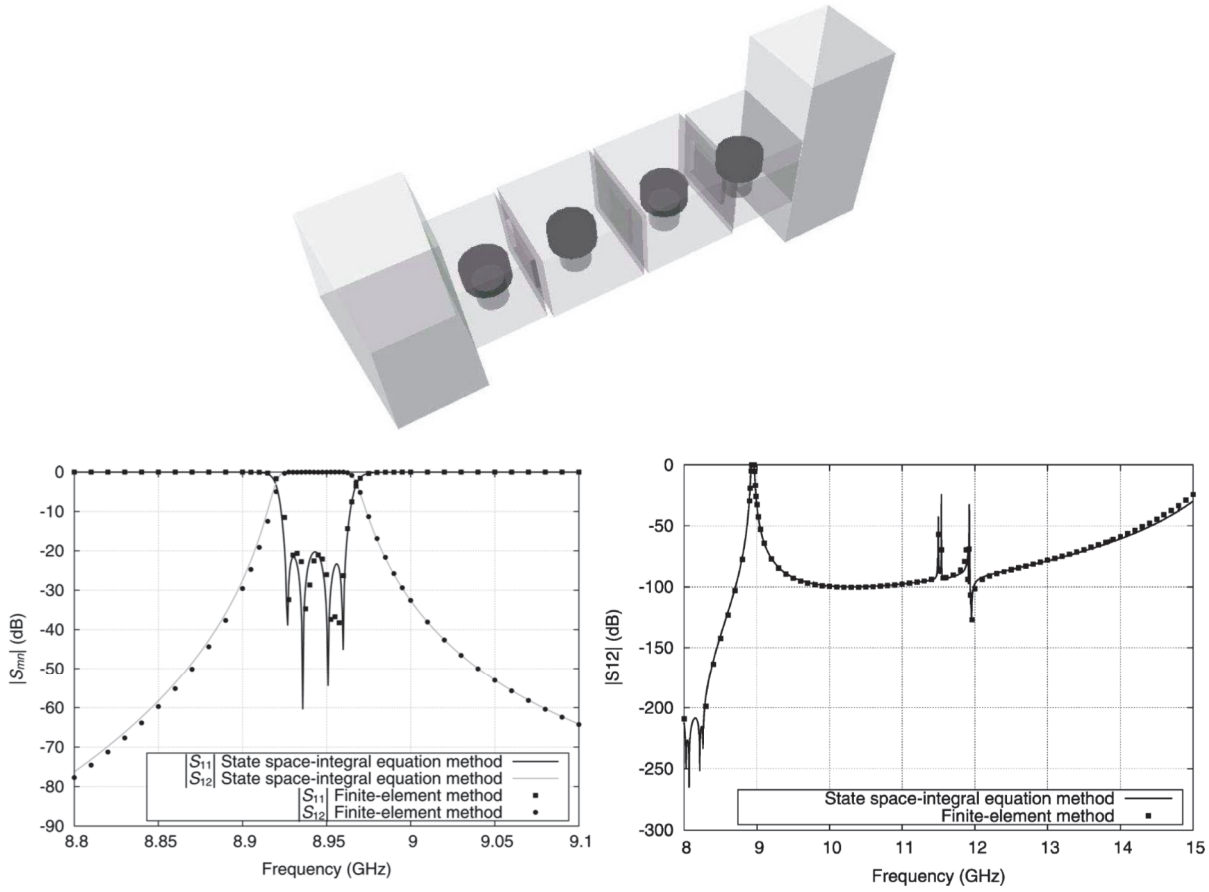

Fig. 1.20. Four-pole bandpass filter based on dielectric resonators in rectangular waveguide technology: comparison of the bandpass and out of band responses between the state space-integral equation method and a commercial software based on the FEM method (ANSYS HFSS) [37].

As highlighted by this historical overview, during the years, the BI-RME method has been modified and adapted in order to analyze several classes of components. But, this type of evolution has put in evident the most important drawback of this method: even if subsequent versions have some common elements, in order to analyze different classes of components or problems, an *ad hoc* theory development and code implementation was always required. In practice, since the mathematical and physical foundations of this method are not "negligible" and its understanding is not trivial, this drawback has drastically influenced its diffusion: the result was a limitation of the use of the BI-RME method to the laboratory level or to the development of software for the analysis and development of very specialized industrial components.

Since the 2013, the Microwave team of the University of Pavia has decided to change the nature of the BI-RME method to overcome its fundamental drawback and to make it more user friendly. The result is a numerical technique that generalize the BI-RME method and permits to analyze completely arbitrarily shaped waveguide circuits, filled by piecewise homogenous dielectric materials also with losses, with the use of simple and well-known RWG basis functions ([40]-[49]). This is possible by combining the segmentation technique with an implementation of the BI-RME method: in this way, it is possible to use the same theory and code to analyze passive components that spans from the dielectric-loaded filters to the power dividers or to the orthomode transducers.

Bibliography

[1] G. Conciauro, M. Guglielmi, and R. Sorrentino, *Advanced Modal Analysis. CAD Techniques for Waveguide Components and Filters*, J. Wiley, 2000.

[2] M. Bressan and G. Conciauro, "Un metodo numerico per lo studio dei modi TM in guide d'onda fortemente perturbate da conduttori cilindrici disposti assialmente," *II Riunione Nazionale di Elettromagnetismo Applicato*, Pavia (Italy), 1978.

[3] G. Conciauro, M. Bressan and C. Zuffada, "Waveguide Modes Via an Integral Equation Leading to a Linear Matrix Eigenvalue Problem," *IEEE Trans. on Microwave Theory and Techniques*, vol. MTT-32, no. 11, Nov. 1984.

[4] M. Bozzi, "Analisi di Giunzioni 3D in Guida D'Onda: Valutazione dei Termini Quasi-Statici della Matrice di Ammettenza Generalizzata," M.S. thesis, University of Pavia, Pavia (Italy), 1996.

[5] R. F. Harrington, *Field Computation by Moment Methods*, New York, Macmillian, 1968.

[6] M. M. Ney, "Method of Moments as Applied to Electromagnetic Problems", *IEEE Trans. on Microwave Theory and Techniques*, vol. MTT-33, no. 10, Oct. 1985.

[7] M. Bressan and G. Conciauro, "Singularity Extraction from the Electric Green's Function for a Spherical Resonator," *IEEE Trans. on Microwave Theory and Techniques*, vol. MTT-33, no. 5, May 1985.

[8] P. Arcioni, M. Bressan and G. Conciauro, "A new algorithm for the wide-band analysis of arbitrarily shaped planar circuits," *IEEE Trans. on Microwave Theory and Techniques*, vol. 36, no. 10, Oct. 1988.

[9] P. Arcioni, M. Bressan and L. Perregrini, "A new boundary integral approach to the determination of the resonant modes of arbitrarily shaped cavities," *IEEE Trans. on Microwave Theory and Techniques*, vol. 43, no. 8, Aug. 1995.

[10] S. Rao, D. Wilton and A. Glisson, "Electromagnetic scattering by surfaces of arbitrary shape," *IEEE Trans. on Antennas and Propagation*, vol. AP-30, no. 3, May 1982.

[11] G. Conciauro, P. Arcioni, M. Bressan and L. Perregrini, "Wideband modeling of arbitrarily shaped H-plane waveguide components by the boundary integral-resonant mode expansion method," *IEEE Trans. on Microwave Theory and Techniques*, vol. 44, no. 7, Jul. 1996.

[12] P. Arcioni, M. Bressan, G. Conciauro and L. Perregrini, "Wideband modeling of arbitrarily shaped E-plane waveguide components by the boundary integral-resonant mode expansion method," *IEEE Trans. on Microwave Theory and Techniques*, vol. 44, no. 11, Nov. 1996.

[13] K. Kurokawa, *An Introduction to the Theory of Microwave Circuits*, New York, Academic Press, 1969, sec. 4.2.

[14] J.M. Jin, *The Finite Element Method in Electromagnetics*, 3rd ed., Wiley-IEEE Press, 2014

[15] G. Conciauro, M. Bressan and P. Gamba, "Analysis of guided modes in multilayer/multiconductor structures by the boundary integral-resonant mode expansion method," *IEEE Trans. on Microwave Theory and Techniques*, vol. 44, no. 5, May 1996.

[16] P. Arcioni, "Fast evaluation of modal coupling coefficients of waveguide step discontinuities," *IEEE Microwave and Guided Wave Letters*, vol. 6, no. 6, June 1996.

[17] P. Arcioni, M. Bressan and L. Perregrini, "On the Evaluation of the Double Surface Integrals Arising in the Application of the Boundary Integral Method to 3-D Problems," *IEEE Trans. on Microwave Theory and Techniques*, vol. 45, no. 3, Mar 1997.

[18] P. Arcioni and G. Conciauro, "Combination of generalized admittance matrices in the form of pole expansions," *IEEE Trans. on Microwave Theory and Techniques*, vol. 47, no. 10, Oct. 1999.

[19] P. Arcioni, M. Bozzi, M. Bressan and L. Perregrini, "A Novel CAD Tool for the Wideband Modeling of 3D Waveguide Components," *International Journal of RF and Microwave Computer–Aided Engineering*, vol. 10, no. 3, May 2000.

[20] P. Arcioni, M. Bozzi, M. Bressan, G. Conciauro and L. Perregrini, "Frequency/Time-Domain Modeling of 3D Waveguide Structures by a BI-RME Approach," *International journal of numerical modelling: electronic networks, devices and fields*, vol. 15, pp. 3-21, 2002.

[21] P. Arcioni, M. Bozzi, M. Bressan, G. Conciauro and L. Perregrini, "Fast optimization, tolerance analysis, and yield estimation of H-/E-plane waveguide components with irregular shapes," *IEEE Trans. on Microwave Theory and Techniques*, vol. 52, no. 1, Jan. 2004.

[22] M. Bozzi and L. Perregrini, "Efficient analysis of thin conductive screens perforated periodically with arbitrarily shaped apertures," *Electronics Letters*, vol. 35, no. 13, June 1999.

[23] R. Mittra, C. H. Chan and T. Cwik, "Techniques for analyzing frequency selective surfaces-a review," *Proceedings of the IEEE*, vol. 76, no. 12, Dec. 1988.

[24] M. Bozzi and L. Perregrini, J. Weinzierl and C. Winnewisser, "Efficient Analysis of Quasi-Optical Filters by a Hybrid MoM/BI-RME Method," *IEEE Trans. on Antennas and Propagation*, vol. 49, no. 7, Jul. 2001.

[25] C.-C. Chen, "Transmission through a Conducting Screen Perforated Periodically with Apertures," *IEEE Trans. on Microwave Theory and Techniques*, vol. 18, no. 9, Sep. 1970.

[26] M. Bozzi and L. Perregrini, "Analysis of Multilayered Printed Frequency Selective Surfaces by the MoM/BI-RME Method," *IEEE Trans. on Antennas and Propagation*, vol. 51, no. 10, Oct. 2003.

[27] M. Bozzi, L. Perregrini, A. Alvarez Melcon, M. Guglielmi and G. Conciauro, "MoM/BI-RME Analysis of Boxed MMICs with Arbitrarily Shaped Metallizations," *IEEE Trans. on Microwave Theory and Techniques*, vol. 49, no. 12, Dec. 2001.

[28] G. Conciauro, P. Arcioni and M. Bressan, "State-space Integral-equation method for the S-domain modeling of planar circuits on semiconducting substrates," *IEEE Trans. on Microwave Theory and Techniques*, vol. 51, no. 12, Dec. 2003.

[29] M. Bozzi, S. Germani, L. Minelli, L. Perregrini and P. de Maagt, "Efficient Calculation of the Dispersion Diagram of Planar Electromagnetic Band-Gap Structures by the MoM/BI-RME Method," *IEEE Trans. on Antennas and Propagation*, vol. 53, no. 1, Jan. 2005.

[30] M. Bozzi, D. Deslandes, P. Arcioni, L. Perregrini, K. Wu and G. Conciauro, "Efficient Analysis and Experimental Verification of Substrate Integrated Slab Waveguides for Wideband Microwave Applications" *International Journal of RF and Microwave Computer–Aided Engineering*, vol. 15, no. 3, May 2005.

[31] F. Xu and K. Wu, "Guided-wave and leakage characteristics of substrate integrated waveguide," *IEEE Trans. on Microwave Theory and Techniques*, vol. 53, no. 1, Jan. 2005.

[32] D. Deslandes and K. Wu, "Accurate modeling, wave mechanisms, and design considerations of a substrate integrated waveguide," *IEEE Trans. on Microwave Theory and Techniques*, vol. 54, no. 6, Jun. 2006.

[33] M. Bozzi, L. Perregrini and K. Wu, "Modeling of Conductor, Dielectric and Radiation Losses in Substrate Integrated Waveguide by the Boundary Integral-Resonant Mode Expansion Method," *IEEE Trans. on Microwave Theory and Techniques*, vol. 56, no. 12, Dec. 2008.

[34] M. Bozzi, L. Perregrini and K. Wu, "A Novel Technique for the Direct Determination of Multi-mode Equivalent Circuit Models for Substrate Integrated Waveguide Discontinuities," *International Journal of RF and Microwave Computer–Aided Engineering*, vol. 9, no. 4, Jul. 2009.

[35] F. Mira, M. Bressan, G. Conciauro, B. G. Martinez and V. E. B. Esbert, "Fast S-domain modeling of rectangular waveguides with radially symmetric metal insets," *IEEE Trans. on Microwave Theory and Techniques*, vol. 53, no. 4, Apr. 2005.

[36] J. Gil, A. M. Perez, B. Gimeno, M. Bressan, V. E. Boria and G. Conciauro, "Analysis of Cylindrical Dielectric Resonators in Rectangular Cavities Using a State-Space Integral-Equation Method," *IEEE Microwave and Wireless Components Letters*, vol. 16, no. 12, Dec. 2006.

[37] J. Gil, A. A. San Blas, C. Vicente, B. Gimeno, M. Bressan, V. E. Boria, G. Conciauro, M. Maestre, "Full-Wave Analysis and Design of Dielectric-Loaded Waveguide Filters Using a State-Space Integral-Equation Method," *IEEE Trans. on Microwave Theory and Techniques*, vol. 57, no. 1, Jan. 2009.

[38] P. Arcioni, M. Bressan, G. Conciauro, L. Perregrini and G. Gatti, "ANAPLAN-W: a CAD Tool for E/H-Plane Waveguide Circuits," *ESA - Preparing for the Future*, vol. 6, n. 1, Mar. 1996.

[39] P. Arcioni, M. Bressan, G. Conciauro and L. Perregrini, "ANAPLAN-W on a Sun platform," *Final Report*, ESA Contract 10966/94/NL/NB, Mar. 1995.

[40] M. Bressan, S. Battistutta, M. Bozzi and L. Perregrini, "Modeling of Inhomogeneous and Lossy Waveguide Components by the Segmentation Technique Combined with the Calculation of the Green's Function by the Ewald's Method," *IEEE Trans. on Microwave Theory and Techniques*, vol. 66, no. 2, Feb. 2018.

[41] S. Battistutta, M. Bozzi, M. Bressan and L. Perregrini, "Analysis of Dielectric-Loaded Waveguide Filters by the Generalized BI-RME Method," *2018 48th European Microwave Conference (EuMC)*, Madrid, Spain, Sept. 23–28, 2018.

[42] S. Battistutta, M. Bozzi, M. Bressan and L. Perregrini, "Generalized BI-RME Method applied to the Analysis of Dielectric-Loaded Waveguide Components," *2018 IEEE MTT-S International Conference on Numerical Electromagnetic and Multiphysics Modeling and Optimization for RF, Microwave, and Terahertz Applications (NEMO)*, Reykjavik, Iceland, Aug. 08-10, 2018.

[43] S. Battistutta, M. Bozzi, M. Bressan and L. Perregrini, "Analysis of a Matched Turnstile Junction by the BI-RME Method and the Segmentation Technique," *2018 Baltic URSI Symposium (URSI)*, Poznań, Poland, May 15–17, 2018.

[44] S. Battistutta, M. Bozzi, M. Bressan and L. Perregrini, "Extension of the BI-RME Method to the Analysis of Piecewise-Homogeneous Waveguide Components Including Arbitrarily Shaped Building Blocks," *2017 47th European Microwave Conference (EuMC)*, Nurnberg, DE, Oct. 9–12, 2017.

[45] S. Battistutta, M. Bressan, M. Bozzi and L. Perregrini, "Material Characterization Through a Full-Wave Approach Based on the BI-RME Method," *2017 IEEE MTT-S International Microwave Workshop Series on Advanced Materials and Processes for RF and THz Applications (IMWS-AMP)*, Pavia, Italy, Sep. 20-22, 2017.

[46] S. Battistutta, M. Bressan, M. Bozzi and L. Perregrini, "A Fast Numerical Technique for the Determination of Electrical Properties of Materials," *2017 IEEE MTT-S International Conference on Numerical Electromagnetic and Multiphysics Modeling and Optimization for RF, Microwave, and Terahertz Applications (NEMO)*, Sevilla, Spain, May 17-19, 2017.

[47] S. Battistutta, M. Bozzi, M. Bressan, M. Pasian and L. Perregrini, "Modeling of Inhomogeneous and Lossy Components by the BI-RME Method and the Segmentation Technique," *2016 46th European Microwave Conference (EuMC)*, London, UK, Oct. 3–7, 2016.

[48] S. Battistutta, M. Bozzi, M. Bressan, M. Pasian and L. Perregrini, "Application of the BI-RME Method to the Analysis of Piecewise-Homogeneous Waveguide Components," *2016 IEEE MTT-S International Conference on Numerical Electromagnetic and Multiphysics Modeling and Optimization for RF, Microwave, and Terahertz Applications (NEMO),* Beijing, China, July 27-29, 2016.

[49] S. Battistutta, M. Bozzi, M. Bressan, M. Pasian and L. Perregrini, "Modeling of Waveguide Components by the BI-RME Method with the Ewald Green's Function and the Segmentation Technique," *2016 IEEE MTT-S International Microwave Symposium (IMS)*, San Francisco, CA, USA, May 22 – 27, 2016.

Chapter 2
The Generalized BI-RME method

As already mentioned in the previous Chapter, the "Generalized BI-RME" method is a numerical technique that generalize the traditional BI-RME method to analyze different classes of components by removing the necessity of an *ad hoc* theory development and code implementation. Thanks to this change of direction, the fundamental drawback of the BI-RME method has been overcame. The adopted solution consist on the combination of a particular implementation of the BI-RME method with the segmentation technique and it permits to analyze completely arbitrarily shaped waveguide circuits, filled by piecewise homogenous and lossy dielectric materials, with the use of simple and well-known RWG basis functions ([1]-[12]).
This Ph.D. thesis represent the work done by the author since 2015 on what concerning the theory development, code implementation and debug of the entire algorithm except the BI-RME solver (whose theory and code implementation is made by Professor Marco Bressan) for which the author has contributed to the debug phase.

Based on the historical overview done in the previous Chapter, with the BI-RME method it is not possible to directly analyze piecewise homogeneous components: to overcome this limitation, the strategy implemented in the Generalized BI-RME method consist into applying the segmentation technic prior the analysis with the BI-RME method. To summarize the proposed numerical technique prior its full explanation, the Generalized BI-RME method can be conceptually subdivided into three parts, as indicated by the flowchart in Fig. 2.1. Once defined the geometry of the desired circuit, in the first part it is subdivided into homogeneously filled building blocks (BBs): this is the only mandatory requirement during the segmentation phase. Then, it is necessary to define also the surface mesh on the building blocks boundaries based on some rules dictated by the successive electromagnetic analysis phase. In the second part, each block is analyzed by the BI-RME method subdividing them into two categories based on the block shape. In particular, for the building blocks with a rectangular parallelepiped shape, the analysis is performed with an easier and faster version of the implemented BI-RME method called "boxed" approach; while, for the blocks with a different shape, it is used the general version called "arbitrarily shaped" approach. The results of the electromagnetic analysis of each building block are combined in the third part of the algorithm to form a generalized admittance matrix (GAM) in form of pole expansion, so a wideband and material independent mathematical model of the block behavior. Once obtained the GAMs elements of all the building blocks, they are combined together through a circuital cascade procedure in the frequency domain to obtain the GAM of the entire circuit; then, the admittance matrix behavior is transformed into S-parameters.

The Pre-Processing phase as well as the EM Analysis and the Post-Processing ones will be explained in details in the next sub-sections, by considering both theoretical and practical aspects.

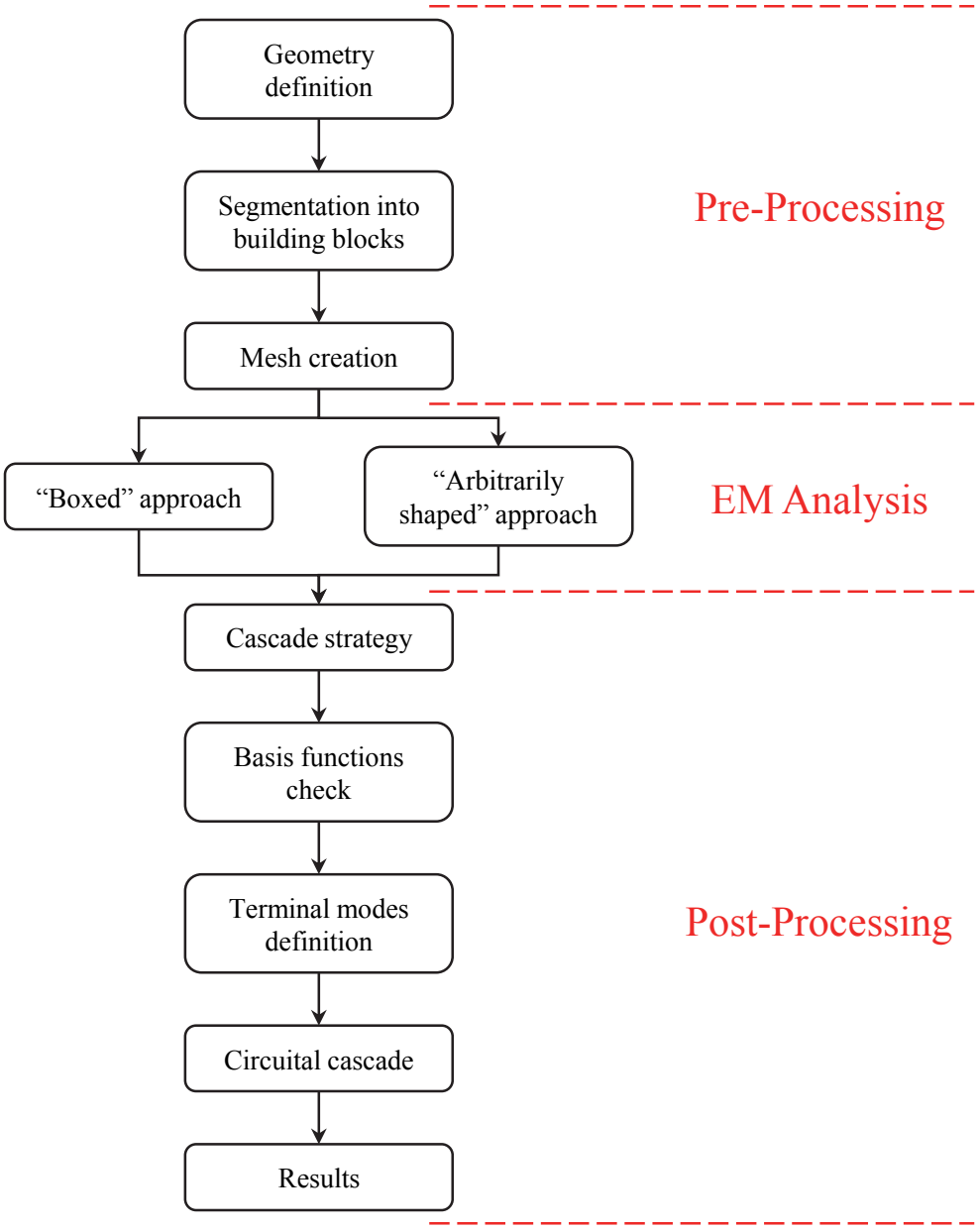

Fig. 2.1. Conceptual flowchart of the Generalized BI-RME method.

2.1 The Pre-Processing phase

In order to understand the Generalized BI-RME method, it is better to refer to a simple example like the structure reported in Fig. 2.2. This arbitrarily shaped 3D waveguide component is filled by three different dielectric material, each one characterized by its relative dielectric constant and the dielectric conductivity (but, it is possible also to characterized them in terms of dielectric loss tangents or real and imaginary part of the relative dielectric constants). Since the BI-RME method can be used only to directly analyze homogenous components, the first step of this algorithm consists into the segmentation of the proposed circuit into homogeneously filled building blocks (BBs). As already outlined, this is the only mandatory requirement: in Fig. 2.3 it is proposed a possible segmentation that satisfy this constrain. In the past combinations of the BI-RME method with the segmentation technique, there were also some constrains on the geometry of the building blocks: primarily, they were related to the adopted type of basis functions and/or to the specific target in terms of class of components (i.e., waveguide filters made by cylindrical dielectric resonator: obviously, the constrain was to have a cylindrical shaped blocks for the resonator). Even if in the proposed algorithm there are no constrains about the geometry of the building blocks, it is better to have, as much as possible, building blocks with a rectangular parallelepiped shape, the so called "boxed" shape. This suggestion comes from the electromagnetic analysis phase because, in this case, it is possible to use a lighter version of the BI-RME method. This is not an *ad hoc* implementation of the solver respect to the general one: it is only a simplification dictated by the theory developed and/or the implemented code that allows a considerable reduction of the computational effort and to save time. In general, it is difficult to subdivide a circuit into only boxed building blocks without losing in representation accuracy (i.e., by representing rounded angles with sharped ones): in fact, it is practically mandatory to have building blocks with a not defined *a priori* shape, the so called "arbitrarily" shaped blocks. For them, the electromagnetic analysis is performed with the BI-RME solver without simplification, so by solving a pure Electric Field Integral Equation (EFIE). By observing the Fig. 2.3, the proposed segmentation allows having four boxed building blocks (practically, waveguide sections, highlighted in light red in Fig. 2.4) and five arbitrarily shaped blocks (highlighted in light green in Fig. 2.5). Moreover, some blocks are practically identical in shape and volume: this is related to the specific segmentation and, especially in symmetric structures, could be exploited to avoid some not necessary EM analysis. In practice, by implementing some *ad hoc* techniques to have the same mash over identical blocks, or by using geometrically non-conformal domain decomposition methods to map the analysis results, it is possible to analyze only one block for each identical block set by saving a lot of computational effort.

Since the BI-RME method is based on the Boundary Integral Method, it requires the discretization only of the building blocks surfaces instead of the volumes as for the Finite Element Method. As suggested by Rao *et al*. [1], a surface mesh made by triangular patches represents the best trade-off between the accuracy of the surface details representation, and the simplicity of the type of basis functions definable on it. Thanks to the particular implementation of the BI-RME method, it is not necessary to mesh always the entire block surface. In particular, it is necessary to mesh the interconnecting surfaces between building blocks, the surfaces where the external ports lie, and all the surfaces that do not coincide with the cavity walls used for the BI-RME analysis. The last statement is not always true because it depends on the building block shape. To understand the mesh process, it is necessary to anticipate some details about the BI-RME analysis. A key aspect of the application of the BI-RME method to the analysis of 3D components is the closing of the element under test inside a fictitious external cavity resonator with a known shape. In the past implementations, the most used shape was the sphere, for which the Green's functions are known in closed form. However, this shape had some drawbacks. One of them was the

too high difference between the sphere volume and the circuit one: this implied the necessity to find a huge amount of resonant modes, so a bigger eigenvalue problem.

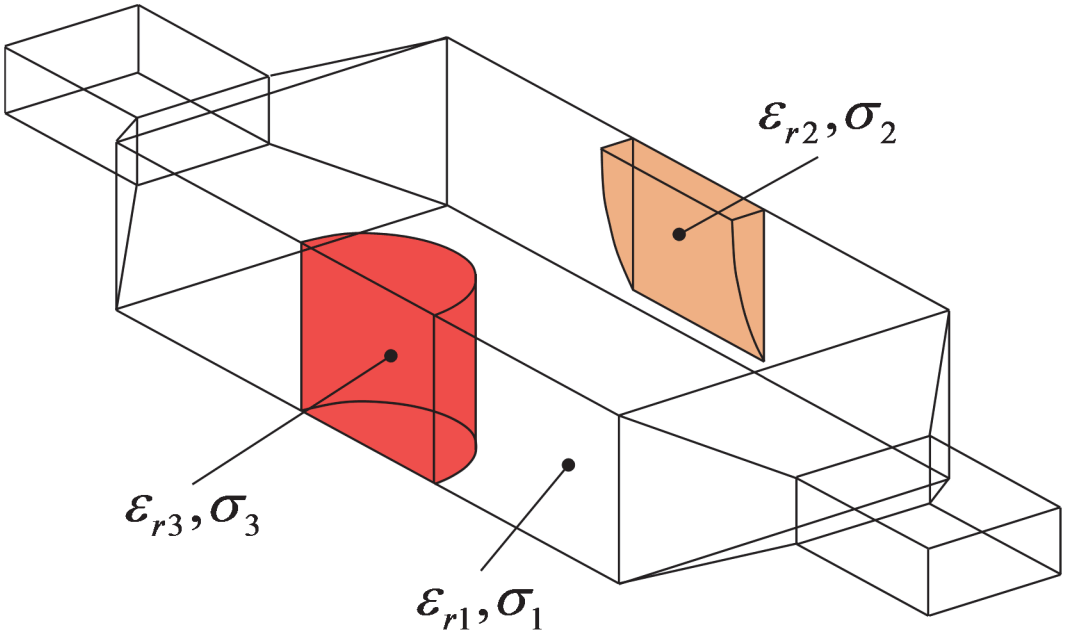

Fig. 2.2. Example of piecewise homogeneous arbitrarily shaped 3D waveguide component.

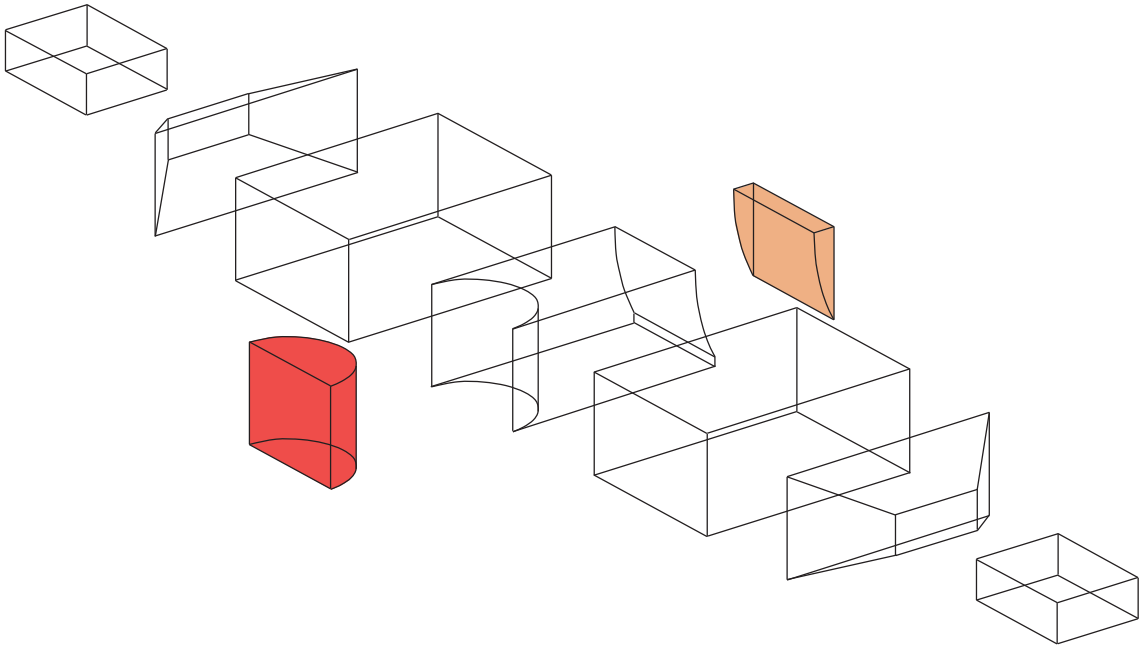

Fig. 2.3. A possible segmentation into homogeneous building blocks.

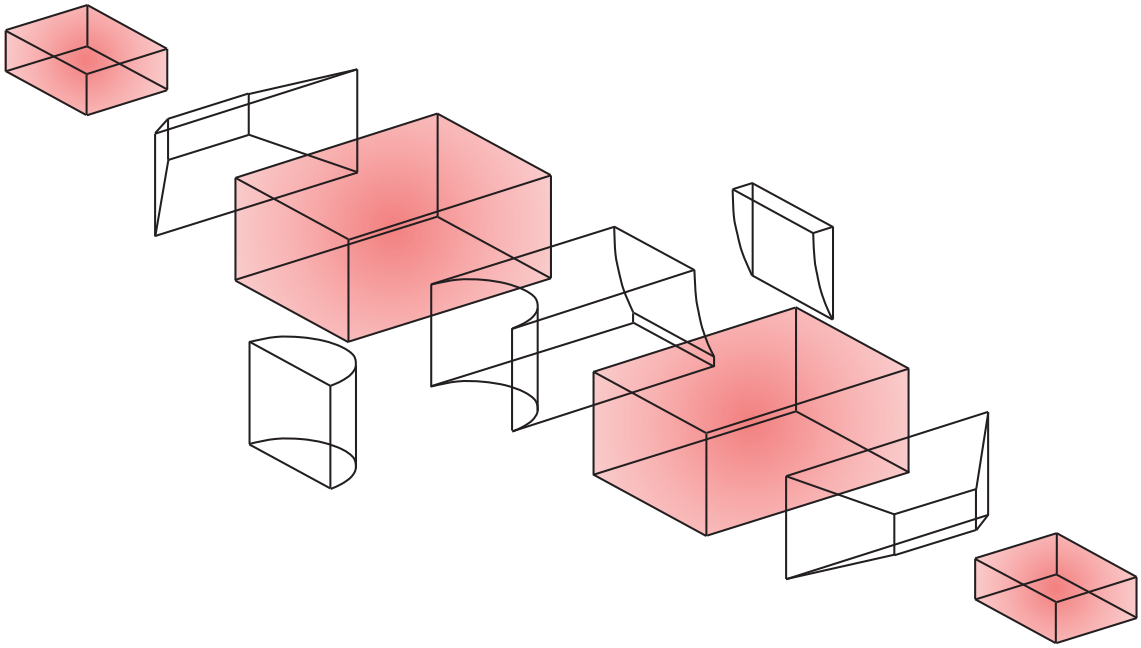

Fig. 2.4. Building blocks with a boxed shape highlighted in light red.

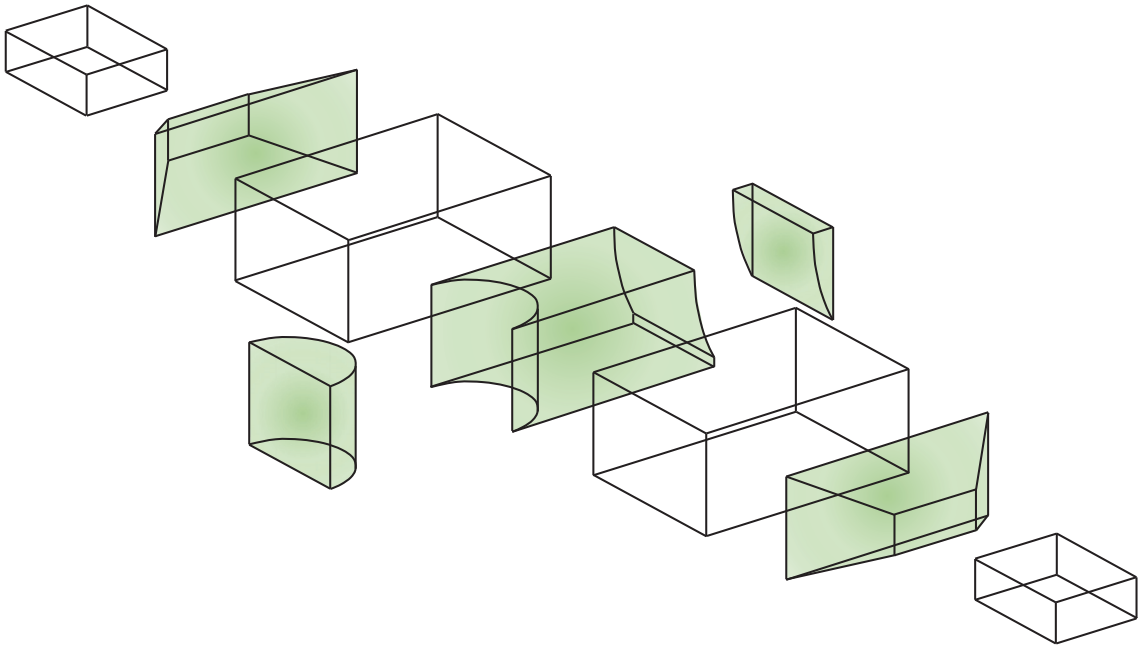

Fig. 2.5. Building blocks with an arbitrary shape highlighted in light green.

Moreover, with the sphere it was difficult to have a considerable portion of the object boundary coincident with the resonator one: so, it was practically always necessary to define the basis functions over the great part of the object boundary with a considerable amount of memory requirement and computational effort. In practice, as already shown in Fig. 2.3, it is possible to have building blocks with a shape near to the boxed one, so with some sidewalls with a planar shape. The actual implementation of the BI-RME method uses a rectangular parallelepiped ("boxed") shape for the fictitious external cavity resonator. For this shape, the Green's functions are known as series whose convergence speed can be tuned (more details in the next sub-section). The boxed shape permits to reduce the number of necessary resonant modes, since the volume difference is less than the sphere case, and of the basis functions, since probably a great part of the sidewalls will coincide with the cavity boundary. The subdivision of the building blocks between boxed and arbitrarily shaped starts to be important in this phase because it define which surfaces need to be meshed.

Boxed building blocks

For the boxed building blocks, if no metallic losses conditions are defined, it is necessary to mesh only the interconnecting surfaces between building blocks as well as the surfaces where an external port is defined. For example, by considering the structure element reported in Fig. 2.6, it is necessary to mesh only the three surfaces highlighted in yellow because they are interconnecting surfaces coinciding or partially coinciding with the cavity walls. As mentioned previously, with the boxed approach it is not necessary to solve an EFIE problem. In fact, the imposed mesh will be used to discretize only the surface magnetic current $\vec{M}$ because, in this case, the surface electric current $\vec{J}$ is not defined on the part of the building block boundary that coincide with the cavity walls since, on that, the electric wall condition is automatically satisfy. On the other hand, the magnetic current $\vec{M}$, which represent the excitation of the building block at the interconnecting surfaces, is not defined on the part of building block surfaces that are bounded by a metallic surface ([9], [11]-[12]). For example, if the building block under test is a waveguide with a rectangular cross-section, its shape will fit perfectly the cavity volume; so, it is necessary to mesh and then to discretize the surface magnetic current only on the two surfaces that coincide with the waveguide ports. In case of building blocks on whose surfaces it is defined a metallic loss condition (so, metal with a finite conductivity), it is necessary to mesh them in order to discretize the magnetic current: as explained in the Post-Processing sub-section, this condition is treated as the cascade with a fictitious block whose admittance matrix depends by the finite conductivity.

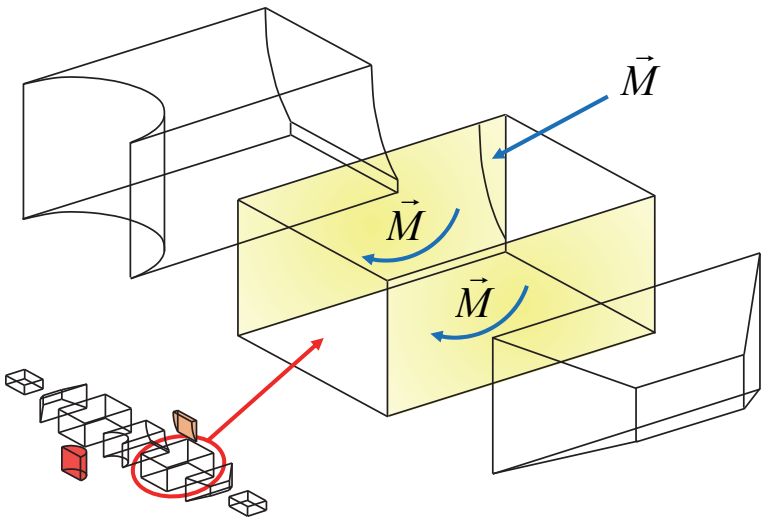

Fig. 2.6. Graphical example of which surfaces need to be meshed in case of boxed building block.

Arbitrarily shaped building blocks

Since the volume of an arbitrarily shaped building block doesn't fit the volume of the boxed external resonator, it is necessary to solve a pure EFIE problem. In general, it is necessary to discretize both the surface electric and magnetic currents: in this case, there are two possible distinct situations or combinations of both.

By considering the structure element reported in Fig. 2.7, this building block represent the metallic transition between two different waveguide cross-sections. For the surfaces highlighted in light yellow, since they totally/partially coincide with the external cavity walls, they need to be meshed in order to discretize only the surface magnetic current. For the surfaces highlighted in light blue, since they don't coincide with the external cavity walls and they are made by PEC (Perfectly Electric Conductor), they need to be meshed in order to discretize only the surface electric current for the same reasons explained in the boxed case ([4] and [6]).

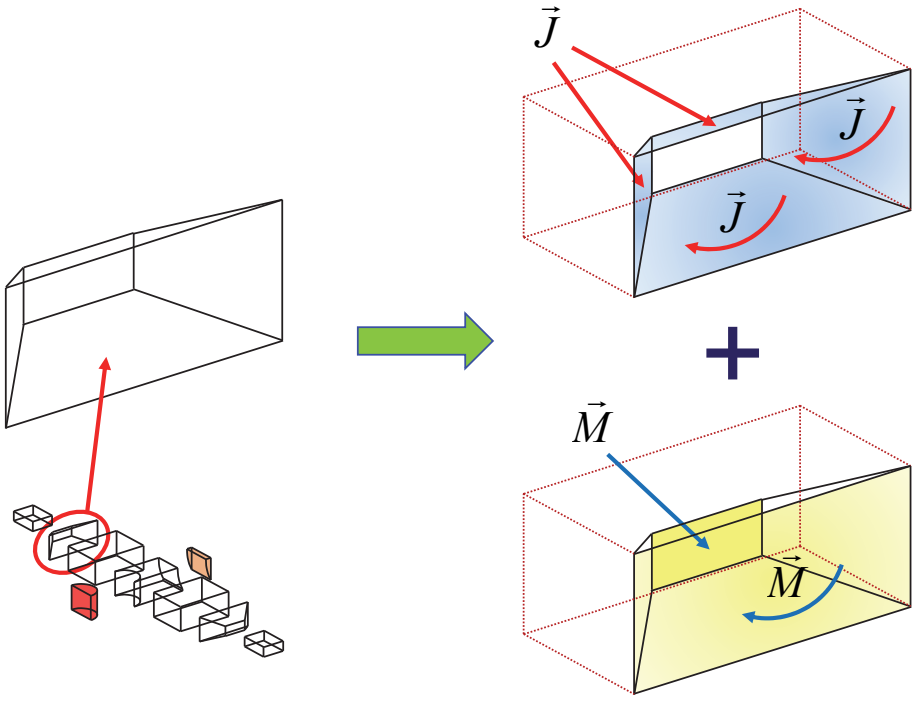

Fig. 2.7. Graphical example of the single definition of the electric and magnetic currents in case of arbitrarily shaped building blocks.

By considering the circuit part reported in Fig. 2.8, this building block represent the interconnection between two empty waveguides and two dielectric blocks. As for the previous case, since the surfaces highlighted in light yellow totally/partially coincide with the external cavity walls, they need to be meshed in order to discretize only the surface magnetic current $\vec{M}$. For the surfaces highlighted in light green, since they are the interconnections with the dielectric blocks and don't coincide with the external cavity walls, they need to be meshed in order to discretize both the surface electric $\vec{J}$ and magnetic $\vec{M}$ currents ([1] and [3]). In practice, the only case where it is necessary to discretize both the currents, it is when an interconnecting surface doesn't lie on the external cavity walls. Also in this case, if on the building block surface it is defined a metallic loss condition, it is necessary to mesh them in order to discretize the magnetic current.

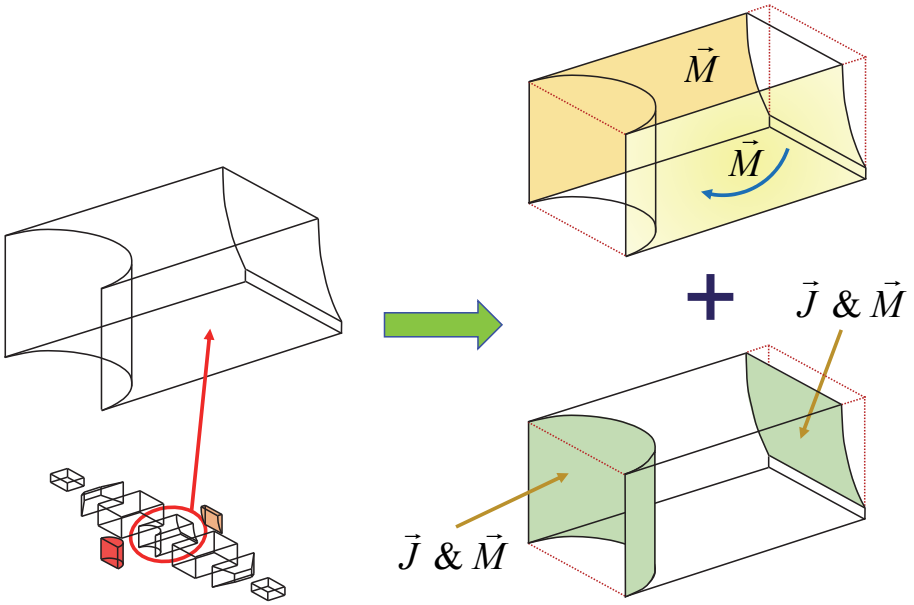

Fig. 2.8. Graphical example of the definition of both the electric and magnetic currents in case of arbitrarily shaped building blocks.

2.1.1. Implementation details

In practice, the Pre-Processing phase is done by combining a third-part software and a homemade MATLAB tool: the result is a textual file used as input file for the next phase. In this way, it is possible to separate the EM analysis and recombination parts to the specific software or tools used for the geometry definition and meshing. For the meshing procedure, it is used a third-part software, called GiD, developed by the International Center for Numerical Methods in Engineering (CIMNE), a research center with headquarters in Barcelona (Spain). As reported on the website related to it (*www.gidhome.com*): *"GiD has been designed to cover all the common needs in numerical simulation field from pre to post processing phases: geometrical modelling, effective definition of analysis data, meshing, data transfer to analysis software, as well as the visualization of numerical results. So, it is a universal, adaptive and user-friendly pre and post processor; it allows generating all the information required for the analysis of any problem in science and engineering using numerical methods. Moreover, it is easy to adapt it to any numerical simulation code because the GiD's input and output formats can be customized and made compatible with any existing software"*. The geometry of the waveguide circuit under test can be designed on other software and imported (either in the entire or segmented version), or directly drawn in GiD. Thanks to its customization capability, it is possible to define a "Problem Type": this is a collection of instructions in order to add some conditions like terminal ports, metallic losses, electric walls, etc., to add materials and information related to the problem like frequency parameters and measurement units. Depending by the user ability, it is possible to directly drown the structure under test or to import it from another software though a geometrical file (i.e. ".stp" or ".step"). The second solution is the most useful one because, by supposing to use another software to draw the structure, the only key point is to draw the structure already segmented into building blocks (Fig. 2.9).

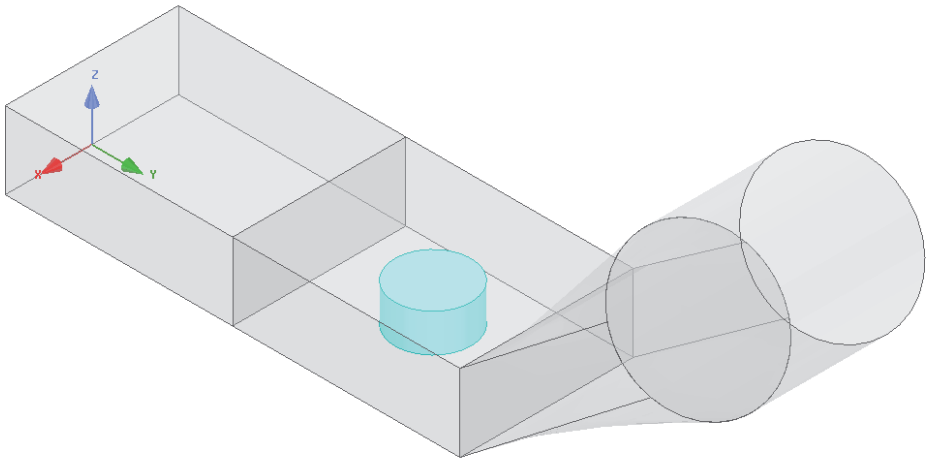

Fig. 2.9. Example of a piecewise homogeneous waveguide circuit already segmented into homogeneous building blocks.

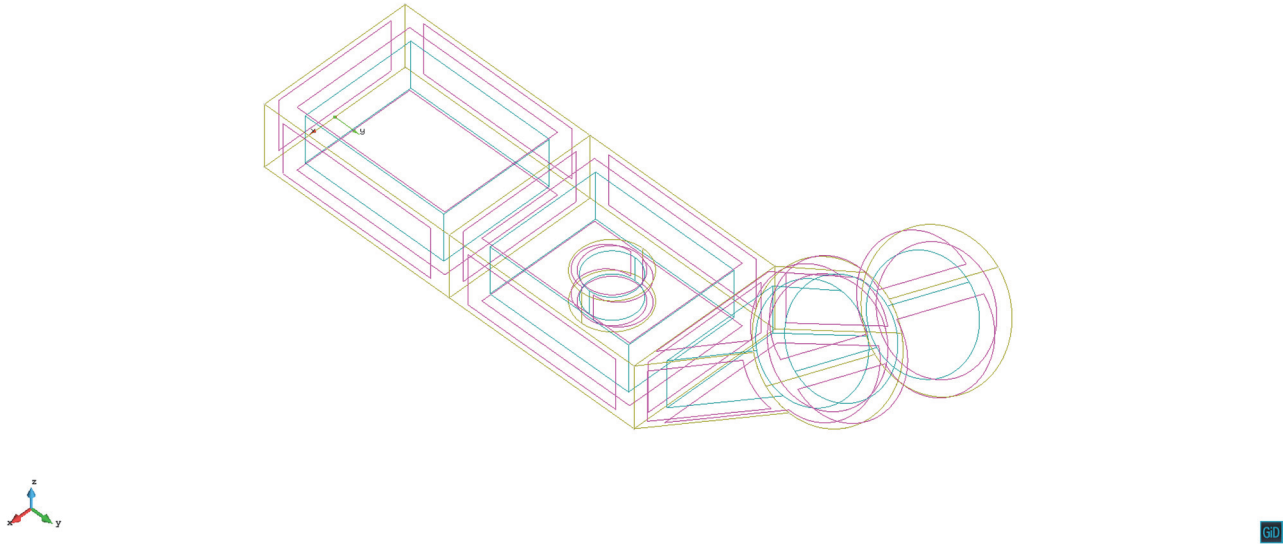

Fig. 2.10. View of the imported structure into GiD

The example structure reported in Fig. 2.9 is made by five building blocks, one of which (the light blue one) is filled by a dielectric material with characteristics different from the vacuum one that fills the great part of the component. In Fig. 2.10 is shown the geometrical structure of the component under test as appear into GiD.

According to which indicated for the original BI-RME method, the basic dimension for the triangle edges must be equal or lower than a quarter of wavelength at the highest interested frequency. Typically, a good rule of thumb is to have a triangle edge length equal to

$$\frac{\lambda_0}{10\sqrt{\varepsilon'}} = \frac{c_0 / f_{\max}}{10\sqrt{\varepsilon'}} \tag{2.1}$$

Obviously, this length needs to be tuned based on the particular situation or building block shape since it has not been implemented jet an automated mesh refinement tool like the one proposed by the commercial software ANSYS HFSS. For example, if the block positioning is critical in terms of field variations, it is necessary to define on it a finer mesh; moreover, it is necessary to reduce the mesh step if the block has a dimension smaller respect to the upper defined mesh step or it has a particular shape.

On the other hand, if a block is placed in a circuit point where the fields are negligible, it is possible to relax the mesh step by choosing an edge length greater than what suggested by (2.1). In general, it is better to use an "Unstructured mesh" because the irregular distribution of the mesh triangles allows better following the field variations and to reduce the discretization error. In Fig. 2.11 is reported an example of possible mash and visualizations.

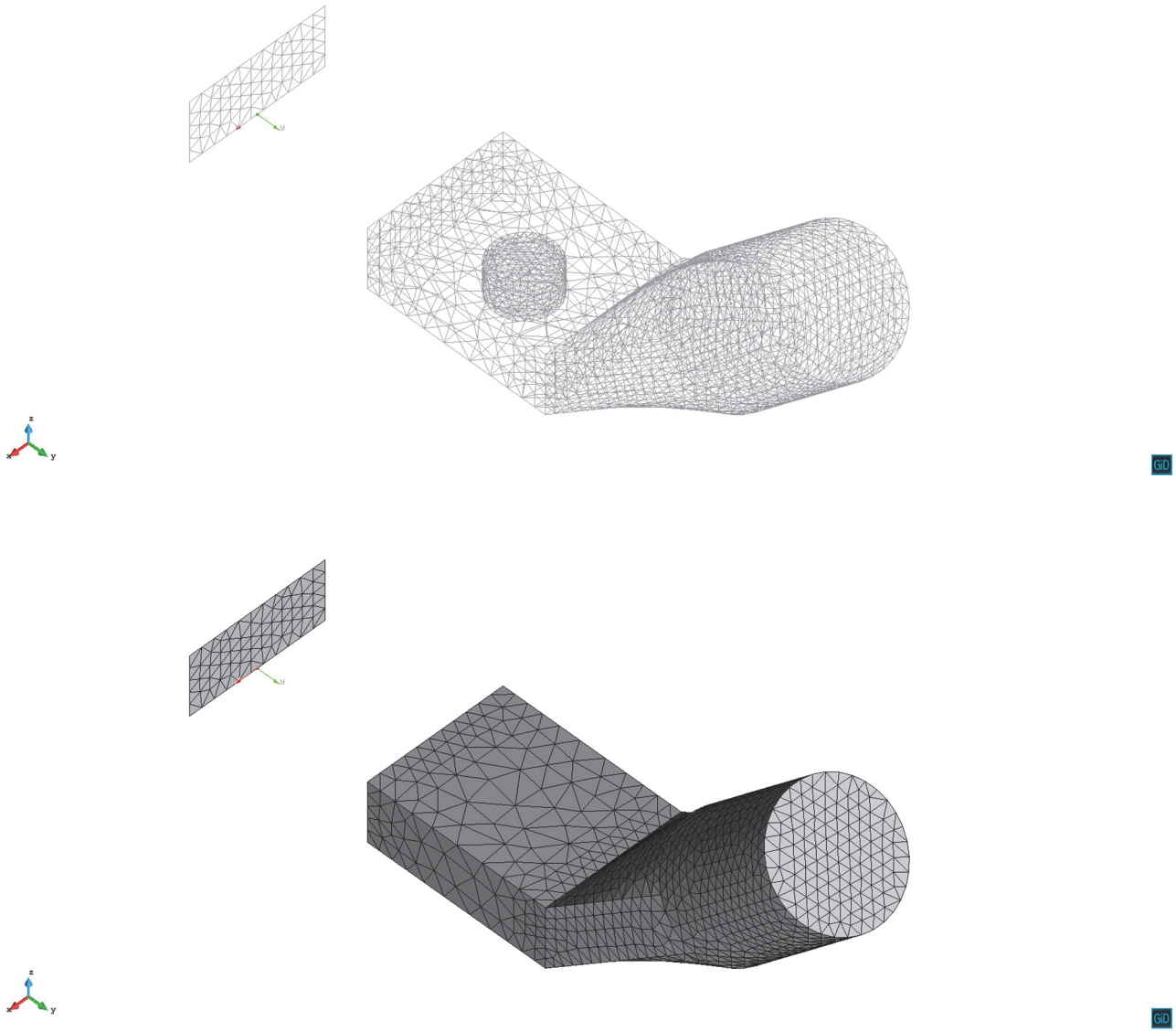

Fig. 2.11. Example of possible mash and visualizations.

Once created the desired mesh and added the necessary conditions, materials and problem data, two textual files are exported from GiD with geometrical, mesh and user added information. These information are manipulated by an automated homemade MATLAB tool to put them in the form required by the input file; moreover, this tool performs a set of operation on the acquired data since not all the information are directly obtainable by GiD. Even if this operation may seam easy, the obtained tool is made by a main file plus thirty-three user defined functions with more than 2000 effective code lines (about 5000 by considering the comments lines). Thanks to the code modularity, it is easier to modify the procedure in order to add future upgrades. The obtained file will content information regarding the frequency parameters; the mesh nodes with IDs and coordinates; the mesh triangles with several information; the boxed blocks as well as the arbitrarily shaped ones with information about the

dimensions, coordinates, material, number of triangles defined on the boundary surfaces and their IDs; the external ports with their shape and vectors; eventually, the finite conductivity in case of metallic losses, and the electric wall conditions.

Since the entire structure (so, also all the building blocks) is placed over a fixed grid, at first glance only the building blocks with all the boundary surfaces parallel to the coordinated plans could be threat as boxed blocks. Unfortunately, this easy approach did not identify as boxed blocks the building blocks with a rectangular parallelepiped shape rotated respect the coordinated axes: so, these blocks were identified as arbitrarily shaped blocks with a consequent increasing of the computational time. To overcome this drawback, an automated procedure has been implemented to determine the rotation matrix to be applied to the building blocks in order to see them as boxed blocks. In particular, the rotation matrix can be obtained independently by the number of rotations and angles. First, it is necessary to define two coordinate systems: the first one is the canonical one (called $\{S_0\}=\{x, y, z\}$), the second one is a system in solidarity with the rotated block whose axes directions are defined by the block sides (called $\{S_1\}=\{i, j, k\}$). Then, it is necessary to transpose the block into the origin of the canonical coordinate system: in this way, the origins of $\{S_1\}$ and $\{S_0\}$ will coincides (Fig. 2.12).

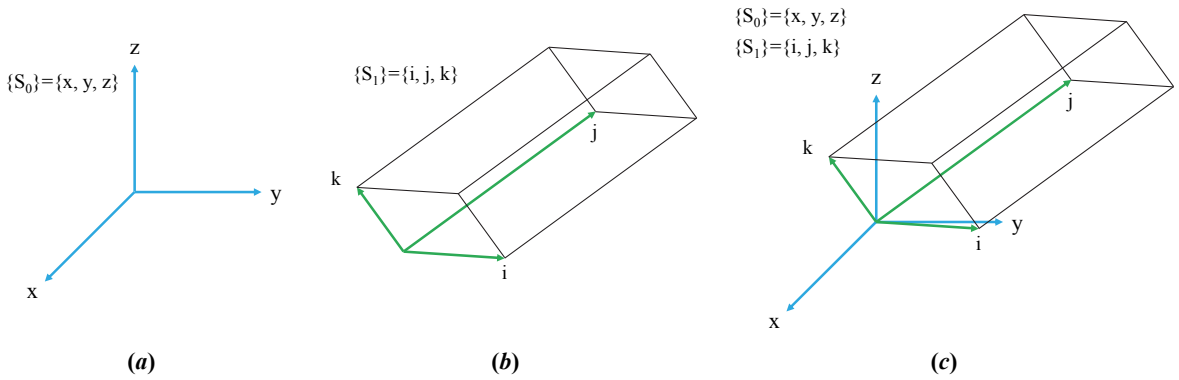

Fig. 2.12. (*a*) Canonical coordinate system $\{S_0\}$, (*b*) Coordinate system in solidarity with the rotated block $\{S_1\}$, (*c*) $\{S_1\}$ transposed into the origin of $\{S_0\}$.

Each axis of $\{S_1\}$ can be represented as rotation of the axes of $\{S_0\}$, where the elements of this rotation are the cosines of the angles formed by the axis under test and the axes of $\{S_0\}$. In this way, each axis of $\{S_1\}$ can be represented with elements into $\{S_0\}$ (Fig. 2.13).

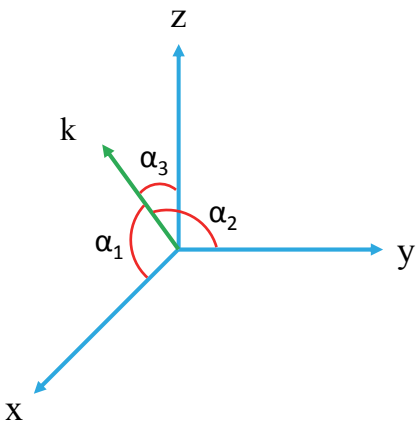

$$ {}^{\{S_0\}}k^{\{S_1\}} = \begin{bmatrix} \cos\alpha_1 \\ \cos\alpha_2 \\ \cos\alpha_3 \end{bmatrix} $$

Fig. 2.13. Example of a $\{S_1\}$ axis represented as rotation of the axes of $\{S_0\}$ by using the cosines of the angles formed by the axis under test and the axes of $\{S_0\}$.

Once computed the representations for each axis of $\{S_1\}$, they are combined to form the rotation matrix R from $\{S_0\}$ to $\{S_1\}$. To obtain the rotation matrix from $\{S_1\}$ to $\{S_0\}$, it is sufficient to transpose the previous one since it is orthogonal ($R^{-1}=R^T$).

Another relevant aspect of this Pre-Processing phase is related to the information associated to each triangle. Even if a triangle can be defined under different situations, each triangle will lie, at least, on one building block; so, for each triangle are provided the identifiers of the building blocks on the positive and/or negative direction of the triangle normal vector. For example, by considering the Fig. 2.14, the building block "A" is on the positive direction of the triangle normal vector, while the building block "B" on the negative one.

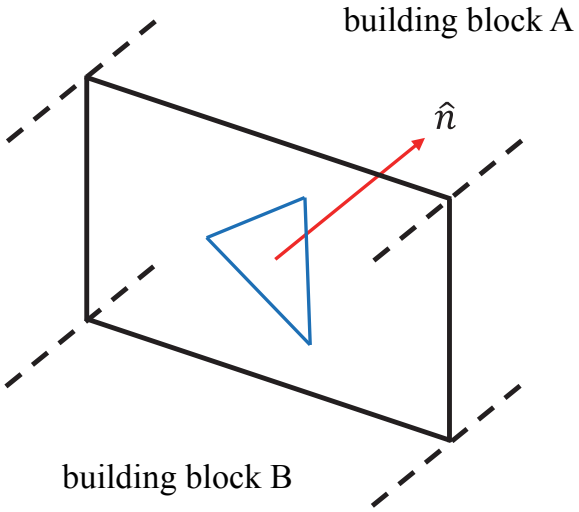

Fig. 2.14

In case of boxed blocks, it is trivial to obtain this information from the triangle normal vector coordinates and the blocks ones because the *a priori* knowledge of the block shape adds some degrees of freedom useful to simplify the procedure. The situation becomes complicated when the triangle is defined over the boundary of one or two arbitrarily shaped blocks. In this case, to understand the normal vector direction of each triangle, first it is necessary to define a segment by using, as starting point, a test point P_T on the normal direction of the current triangle, and as ending one, an external point P_0 defined univocally for the entire structure. If this segment doesn't intersect any triangle or the number of intersection is even, the triangle normal direction is outgoing respect the volume surface on which it is defined; otherwise, if the number of intersection is odd, the triangle normal direction is incoming (Fig. 2.15). In practice, to perform this test it is necessary to mesh the entire block surface: obviously, the triangles not necessary for the BI-RME analysis will be deleted prior the file creation. Practically, two loops are evaluated: the external one is executed on the useful triangles for the BI-RME analysis (one for each surface since all the triangles pertain to the same surface will have the same incoming or outgoing normal direction), while the internal one is executed on all the triangles associated to the volume under test (so, also the not useful ones).

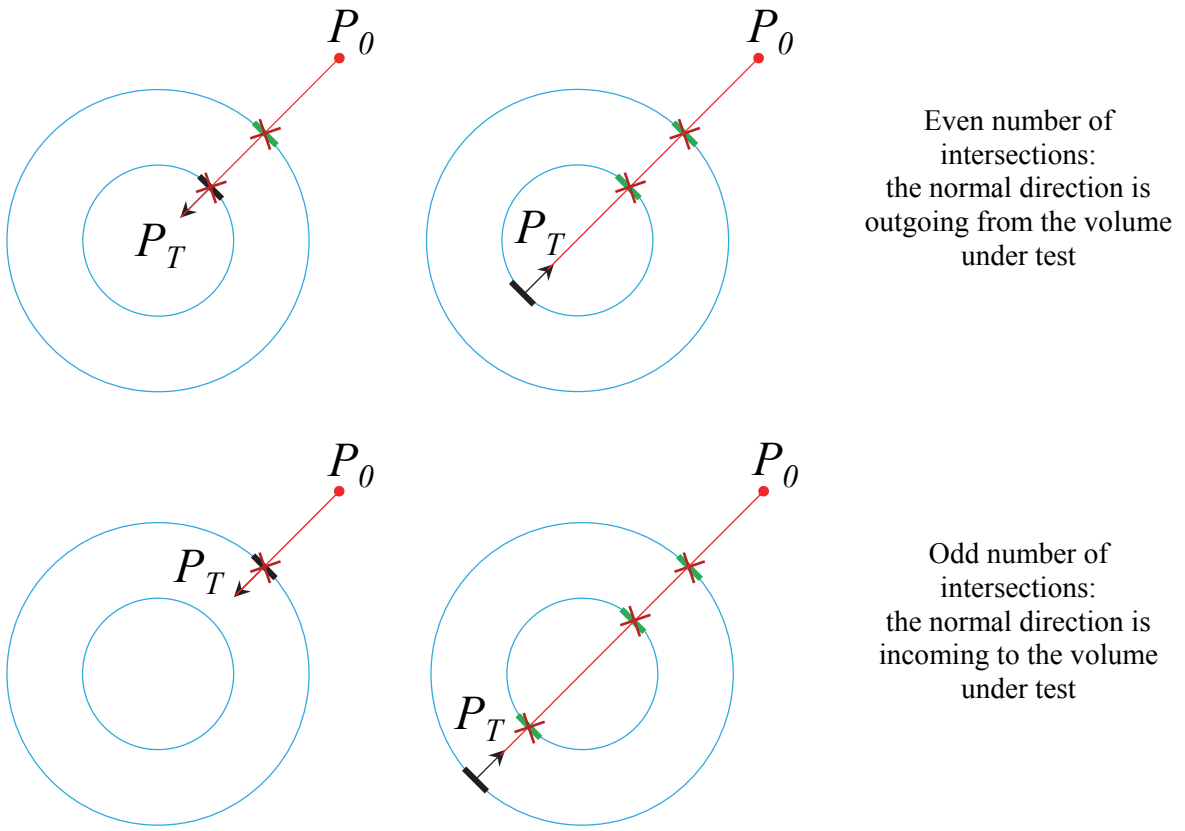

Fig. 2.15. Graphical explanation of the intersection rule: test triangle (inner loop) in black line; other triangle (outer loop) in green line.

Once chosen the point on the test triangle normal direction (P_T) and the external point (P_0), a set of operations are performed on each triangle of the inner loop. After the calculation of the normal vector (2.2), a local non-orthogonal reference system for the current inner loop triangle is calculated; then, P_T and P_0 are evaluated into the new reference system by solving the following equation system (2.3) where P_x could be the test point or the external one.

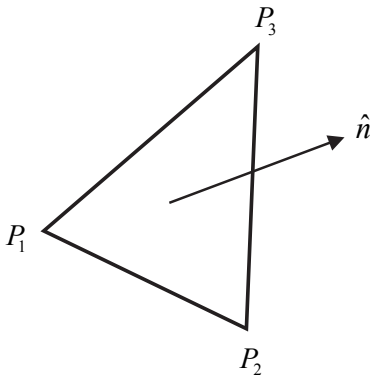

$$\hat{n} = \frac{\vec{v}}{2A}$$
$$A = \frac{1}{2}\left(\vec{v}^T\vec{v}\right)$$
$$\vec{v} = \left(P_2 - P_1\right)\times\left(P_3 - P_1\right) \qquad (2.2)$$

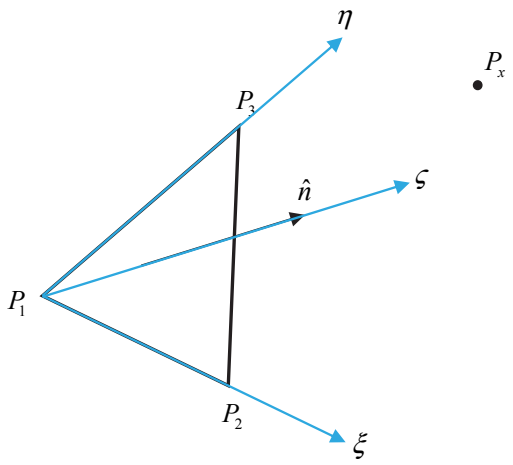

$$\overrightarrow{P_1P_2} = P_2 - P_1$$
$$\overrightarrow{P_1P_3} = P_3 - P_1$$
$$\overrightarrow{P_1P_x} = P_x - P_1$$
$$\begin{cases} \overrightarrow{P_1P_2} \cdot \left(\overrightarrow{P_1P_2}\xi_x + \overrightarrow{P_1P_3}\eta_x \right) = \overrightarrow{P_1P_2} \cdot \overrightarrow{P_1P_x} \\ \overrightarrow{P_1P_3} \cdot \left(\overrightarrow{P_1P_2}\xi_x + \overrightarrow{P_1P_3}\eta_x \right) = \overrightarrow{P_1P_3} \cdot \overrightarrow{P_1P_x} \\ \varsigma_x = \overrightarrow{P_1P_x} \cdot \hat{n} \end{cases} \tag{2.3}$$

The result is the P_x point translated into the local reference system ($\tilde{P}_x = \{\xi_x, \eta_x, \varsigma_x\}$). Then, the solution of the straight line-plane intersection equation is calculated and the coordinates of the eventually intersection point $\tilde{P}_I = \{\xi_I, \eta_I, \varsigma_I\}$ in the local reference system are obtained (2.4).

$$s = \frac{-b}{a} \qquad \rightarrow \quad \tilde{P}_I = \tilde{P}_0 + \left(\tilde{P}_T - \tilde{P}_0 \right) s \tag{2.4}$$
$$a = \varsigma_{\tilde{P}_T} - \varsigma_{\tilde{P}_0} \quad b = \varsigma_{\tilde{P}_0}$$

Where $\varsigma_{\tilde{P}_x}$ indicates the third coordinate of the point. To understand if the intersection falls inside the triangle, the following conditions need to be satisfied:

$$a \neq 0$$
$$b \neq 0$$
$$\xi_I > 0 \quad \xi_I < 1$$
$$\eta_I > 0 \quad \eta_I < 1$$
$$0 < \xi_I + \eta_I < 1$$

If the above conditions are not satisfied, there are different possible scenarios:

- if $a = 0$ and $b \neq 0$, the straight line doesn't intersect the area of the triangle under test;
- if $a = 0$ and $b = 0$, it is necessary to change P_0 because there are infinite solutions;
- if $\xi_I = 0$ and $0 < \eta_I < 1$, it is necessary to change P_0 because the intersection is on the triangle side along ξ;
- if $\eta_I = 0$ and $0 < \xi_I < 1$, it is necessary to change P_0 because the intersection is on the triangle side along η;
- if $\xi_I > 0$, $\eta_I > 0$ and $\xi_I + \eta_I + \varsigma_I = 1$, it is necessary to change P_0 because the intersection is on the third triangle side;
- if $\xi_I = 0$, and $\eta_I = 0$, it is necessary to change P_0 because the intersection is on the reference system origin (centered on P_1);
- if $\xi_I = 0$, and $\eta_I = 1$, it is necessary to change P_0 because the intersection is on the P_3 point;
- if $\xi_I = 1$, and $\eta_I = 0$, it is necessary to change P_0 because the intersection is on the P_2 point.

If the above conditions are satisfied, the last task is to check if the intersection is between P_T and P_0.

2.2 The Electromagnetic Analysis

As outlined in Chapter 1, the BI-RME method permits to represent the building block behavior with a particular expression of the generalized admittance matrix (GAM), and the calculation of the GAM terms through the solution of a single frequency-independent eigenvalue problem obtained by imposing an Electric Field Integral Equation (EFIE). In the 3D implementation adopted for this work, the BI-RME method is based on the Green's function of a rectangular (box) cavity resonator [15]: in particular, only the quasi-static Green's function in the Coulomb gauge need to be calculated ([13], Ch. 5). The efficiency of this approach strongly depends on the efficiency of the computation of the pertinent Green's function. In fact, the filling of the matrices requires the computation of the Green's function in a very large number of different points, and often represents the largest part of the computation time. When dealing with periodic structures or rectangular enclosures, the Green's functions are naturally expressed by infinite series, either in the spatial or in the spectral domain. Both representations, however, have very poor convergence properties. In its early paper, Ewald [16] proposed to transform the slowly converging series representing the electric potential in a lattice, into the sum of two rapidly converging series: the first one expressed in the spectral domain, while the second one in the spatial one. The transformation is based on splitting an integral from zero to infinity, representing the free-space Green's function, into two parts by introducing a splitting parameter. The two parts of the integral are rearranged in different ways, in order to make the first to converge rapidly near to zero and the second near to infinity. The splitting parameter plays an important role on the numerical convergence of both terms. A number of authors used the Ewald's summation technique to build up efficient codes for the analysis of periodic structures or to enhance the convergence of the Green's functions ([17]-[22]). In particular, some authors discussed the application of the Ewald's method to the calculation of the dynamic potential Green's function in the case of rectangular enclosures in 2D or 3D ([23]-[26]). However, on the quasi-static expression of the 3D rectangular Green's function accelerated by the Ewald technique was presented a very preliminary work in [14], where only the final formulas were reported, but without a discussion on the derivation technique. The availability of rapidly converging expressions of the quasi-static Green's functions for a rectangular cavity greatly enlarges the set of structures that can be efficiently analyzed by the BI-RME method (see, for instance, [15], [27]). In this sub-section, the representation of the quasi-static Green's function of a box by the Ewald technique is fully discussed, and details for its efficient numerical calculation are reported. Particular attention is paid to the mathematical representation of the Green's functions and of their derivative, as well as to the discussion of some relevant implementation issues. In particular, the extraction of the singularity is discussed, and a technique for the choice of the Ewald splitting parameter is derived, aiming not only to control the error in the calculation of the Green's functions, but also to minimize the computing time for a specific implementation on a given computing platform. Then, two paragraphs are dedicated to the analysis of boxed and arbitrarily shaped building blocks based on the Green's functions.

From a practical point of view, a homemade MATLAB program does the management of the electromagnetic analysis as well as the post-processing phase. Its tasks comprise the acquirement of the input file from the pre-processing phase, the preparation of the necessary data structures for the electromagnetic analysis and, then, the results combination in order to obtain the S-parameters representation of the overall circuit behavior. Since the BI-RME analysis of each building block is executed by using a solver written in FORTRAN language and compiled, the MATLAB program needs to write the necessary information inside a textual file. The results are written inside a series of textual files whose information are acquired, checked and prepared by the MATLAB program for the frequency circuital cascade procedure in the post-processing phase.

2.2.1. The Green's functions of a boxed homogeneous cavity

Let us consider the rectangular box Ω with volume V shown in Fig. 2.16, bounded by electric walls at $x = 0, x = a, y = 0, y = b, z = 0$, and $z = c$, and filled by a homogeneous and isotropic medium. Assuming $\vec{J}$ and $\vec{M}$ are the electric and magnetic current sources in the region, the electric and magnetic fields in Ω can be expressed as ([13] Ch. 2)

$$\vec{E} = -\nabla\phi^e - \varepsilon^{-1}\nabla\times\vec{F} - j\omega\vec{A} \tag{2.5}$$

$$\vec{H} = -\nabla\phi^m + \mu^{-1}\nabla\times\vec{A} - j\omega\vec{F} \tag{2.6}$$

$$\phi^e(\vec{r}) = -\frac{1}{j\omega\varepsilon}\int g^e(\vec{r},\vec{r}')\nabla_s'\cdot\vec{J}(\vec{r}')d\vec{r}' \tag{2.7}$$

$$\phi^m(\vec{r}) = -\frac{1}{j\omega\mu}\int g^m(\vec{r},\vec{r}')\nabla_s'\cdot\vec{M}(\vec{r}')d\vec{r}' \tag{2.8}$$

$$\vec{A}(\vec{r}) = \mu\int \overleftrightarrow{G}_0^A(\vec{r},\vec{r}')\cdot\vec{J}(\vec{r}')d\vec{r}' + \mu\sum_{m=1}^{\infty}\frac{\omega^2\varepsilon\mu}{k_m^2\left(k_m^2-\omega^2\varepsilon\mu\right)}\vec{\mathrm{E}}_m(\vec{r})\int\vec{\mathrm{E}}_m\cdot\vec{J}\,d\vec{r} \tag{2.9}$$

$$\vec{F}(\vec{r}) = \varepsilon\int \overleftrightarrow{G}_0^F(\vec{r},\vec{r}')\cdot\vec{M}(\vec{r}')d\vec{r}' + \varepsilon\sum_{m=1}^{\infty}\frac{\omega^2\varepsilon\mu}{k_m^2\left(k_m^2-\omega^2\varepsilon\mu\right)}\vec{\mathrm{H}}_m(\vec{r})\int\vec{\mathrm{H}}_m\cdot\vec{M}\,d\vec{r} \tag{2.10}$$

where

$$\vec{r} = x\vec{u}_x + y\vec{u}_y + z\vec{u}_z \tag{2.11}$$

$$\vec{r}' = x'\vec{u}_x + y'\vec{u}_y + z'\vec{u}_z \tag{2.12}$$

represent the field and source points in Ω and ∇_s is the surface differential operator. In the theory of cavity resonator, the field is split into its irrotational and solenoidal parts. In terms of potentials, this splitting corresponds to the use of the so-called 'Coulomb gauge condition', where the scalar potentials correspond to the static potentials generated by the electric and magnetic charges and the vector potentials are solenoidal [28]. By using these potentials, g^e and g^m represent the quasi-static Green's functions of the box for the electric and magnetic scalar potentials. The dyadic Green's functions for the electric and magnetic vector potentials are represented, respectively, as the sum of the quasi-static dyadic Green's functions of the box for the electric $\overleftrightarrow{G}_0^A$ and magnetic $\overleftrightarrow{G}_0^F$ vector potentials, and the resonant mode expansions involving the electric $\vec{\mathrm{E}}_m$ and magnetic $\vec{\mathrm{H}}_m$ modal fields, and the resonant wavenumber k_m of the mth resonant mode of the box, as reported in (2.9) and (2.10).

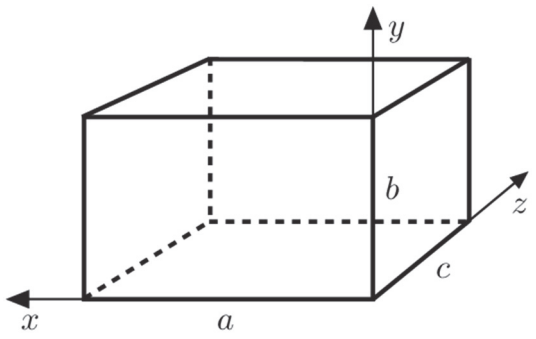

Fig. 2.16. The rectangular cavity geometry

The modal fields are normalized so that

$$\int \vec{\mathrm{E}}_m \cdot \vec{\mathrm{E}}_n \, dV = \delta_{mn} \qquad \int \vec{\mathrm{H}}_m \cdot \vec{\mathrm{H}}_n \, dV = \delta_{mn} \tag{2.13}$$

where δ_{mn} is the Kronecker delta. The static Green's functions for the scalar and vector potential of electric and magnetic type satisfy the following differential equations [29]

$$\begin{cases} \nabla^2 g^e(\vec{r},\vec{r}') = -\delta(\vec{r}-\vec{r}') \\ g^e(\vec{r},\vec{r}') = 0 \qquad \text{on the boundary} \end{cases} \tag{2.14}$$

$$\begin{cases} \nabla\times\nabla\times\overleftrightarrow{G}_0^A(\vec{r},\vec{r}') = \overleftrightarrow{\mathrm{I}}\,\delta(\vec{r}-\vec{r}') - \nabla\nabla' g^e(\vec{r},\vec{r}') \\ \nabla\cdot\overleftrightarrow{G}_0^A(\vec{r},\vec{r}') = 0 \\ \vec{n}\times\overleftrightarrow{G}_0^A(\vec{r},\vec{r}') = 0 \qquad \text{on the boundary} \end{cases} \tag{2.15}$$

$$\begin{cases} \nabla^2 g^m(\vec{r},\vec{r}') = -\delta(\vec{r}-\vec{r}') + \dfrac{1}{V} \\ \vec{n}\cdot\nabla g^m(\vec{r},\vec{r}') = 0 \qquad \text{on the boundary} \end{cases} \tag{2.16}$$

$$\begin{cases} \nabla\times\nabla\times\overleftrightarrow{G}_0^F(\vec{r},\vec{r}') = \overleftrightarrow{\mathrm{I}}\,\delta(\vec{r}-\vec{r}') - \nabla\nabla' g^m(\vec{r},\vec{r}') \\ \nabla\cdot\overleftrightarrow{G}_0^F(\vec{r},\vec{r}') = 0 \\ \vec{n}\times\nabla\times\overleftrightarrow{G}_0^F(\vec{r},\vec{r}') = 0 \qquad \text{on the boundary} \end{cases} \tag{2.17}$$

where $\vec{n}$is the unit vector normal to the boundary, $\overleftrightarrow{\mathrm{I}}$ is the unit dyadic, and V is the volume of the cavity Ω. The term $1/V$ appearing in the equation of g^m derives from the fact that the scalar magnetic Green's function is defined in the extended sense [29] on the space of zero–mean functions. The Green's function can be represented through two periodic scalar functions g and f, with period $2a$, $2b$, and $2c$ along x, y, and z, respectively, in the following form [30]

$$g^e(\vec{r},\vec{r}') = \sum_i i_x i_y i_z \, g(u_i, v_i, w_i) \tag{2.18}$$

$$g^m(\vec{r},\vec{r}') = \sum_i g(u_i, v_i, w_i) \tag{2.19}$$

$$\overleftrightarrow{G}_0^A(\vec{r},\vec{r}') = \sum_i i_x i_y i_z \left[\vec{\mathrm{I}}_i \, g(u_i,v_i,w_i) - \nabla\nabla' f(u_i,v_i,w_i)\right] \tag{2.20}$$

$$\overleftrightarrow{G}_0^F(\vec{r},\vec{r}') = \sum_i \left[\vec{\mathrm{I}}_i \, g(u_i,v_i,w_i) - \nabla\nabla' f(u_i,v_i,w_i)\right] \tag{2.21}$$

where the indices i_x, i_y and i_z may assume the value ±1, and $\sum_i$ indicates the summation over the eight possible combinations of the values of i_x, i_y and i_z. Moreover,

$$u_i = x - i_x x' \tag{2.22}$$

$$v_i = y - i_y y' \tag{2.23}$$

$$w_i = z - i_z z' \tag{2.24}$$

$$\vec{\mathrm{I}}_i = \vec{u}_x\vec{u}_x i_x + \vec{u}_y\vec{u}_y i_y + \vec{u}_z\vec{u}_z i_z \tag{2.25}$$

For a rectangular cavity, the functions *g* and *f* can be easily expressed either as eigenfunction expansions or as infinite image series. However, the convergence of both types of series is extremely slow. In fact, on the one hand the spectral series requires a very large number of eigenfunctions to approximate the delta source, and, on the other hand, the contribution of the images in the spatial series remains significant up to a distance much larger than the cavity dimensions. To overcome this problem and accelerate the convergence, the Ewald's summation technique can be adopted [16]. Both functions *g* and *f* can be expressed as the sum of two terms: the firsts, denoted by $g^{(1)}$ and $f^{(1)}$, are eigenfunction expansions in the spectral domain, and the seconds, denoted by $g^{(2)}$ and $f^{(2)}$, are functions of distances between the field and the image points in the spatial domain:

$$g(u,v,w)=\underbrace{\frac{1}{abc}\sum_m \frac{e^{-k_m^2\eta^2/4}}{k_m^2}C_m}_{g^{(1)}}\underbrace{-\frac{\eta^2}{32abc}+\frac{1}{4\pi}\sum_n \frac{\operatorname{erfc}(R_n/\eta)}{R_n}}_{g^{(2)}} \tag{2.26}$$

$$f(u,v,w)=\underbrace{\frac{1}{abc}\sum_m \frac{e^{-k_m^2\eta^2/4}}{k_m^4}\left(1+k_m^2\,\eta^2/4\right)C_m}_{f^{(1)}}+\underbrace{\frac{1}{8\pi}\sum_n\left(\frac{\eta\, e^{-R_n^2/\eta^2}}{\sqrt{\pi}}-R_n\operatorname{erfc}(R_n/\eta)\right)}_{f^{(2)}} \tag{2.27}$$

where

$$k_m=\sqrt{\left(k_m^x\right)^2+\left(k_m^y\right)^2+\left(k_m^z\right)^2} \tag{2.28}$$

$$k_m^x=\pi\frac{m_x}{a},\qquad k_m^y=\pi\frac{m_y}{b},\qquad k_m^z=\pi\frac{m_z}{c}, \tag{2.29}$$

$$C_m=\frac{\cos\left(k_m^x u\right)\cos\left(k_m^y v\right)\cos\left(k_m^z w\right)}{2^{\delta_{om_x}+\delta_{om_y}+\delta_{om_z}}} \tag{2.30}$$

$$\vec{R}_n=\left(u+2n_x a\right)\vec{u}_x+\left(v+2n_y b\right)\vec{u}_y+\left(w+2n_z c\right)\vec{u}_z \tag{2.31}$$

$$R_n=\left|\vec{R}_n\right| \tag{2.32}$$

In the previous expressions, η is the Ewald splitting parameter, $\sum_m$ indicates the sum over all the possible combinations of non-negative integer values of m_x, m_y, and m_z (excluding $m_x = m_y = m_z = 0$), $\sum_n$ indicates the sum over all the possible combinations of integer values of n_x, n_y, and n_z (positive, negative, and zero). It is noted that $g^{(1)}$ in (2.26) is a zero mean function, whereas the extra term $-\eta^2/(32abc)$ in (2.26), independent of $\vec{r}$ and $\vec{r}\,'$, counterbalances the non-zero mean value of the remaining part of $g^{(2)}$, thus leading to an overall zero-mean *g* function.

For the calculation of the electromagnetic fields, the expressions of ∇g^e, ∇g^m, $\nabla\times\vec{\vec{G}}_0^A$, and $\nabla\times\vec{\vec{G}}_0^F$ need also to be evaluated. Starting from (2.18)-(2.21), it can be easily demonstrated that

$$\nabla g^e\left(\vec{r},\vec{r}\,'\right)=\sum_i i_x i_y i_z \nabla g\left(u_i,v_i,w_i\right) \tag{2.33}$$

$$\nabla g^m\left(\vec{r},\vec{r}\,'\right)=\sum_i \nabla g\left(u_i,v_i,w_i\right) \tag{2.34}$$

$$\begin{aligned}\nabla\times\vec{\vec{G}}_0^A\left(\vec{r},\vec{r}\,'\right)&=\sum_i i_x i_y i_z \nabla g\left(u_i,v_i,w_i\right)\times\vec{\mathrm{I}}_i\\&=-\sum_i \vec{\mathrm{I}}_i\times\nabla' g\left(u_i,v_i,w_i\right)\end{aligned} \tag{2.35}$$

$$\nabla\times\vec{\vec{G}}_0^F\left(\vec{r},\vec{r}'\right)=\sum_i\nabla g\left(u_i,v_i,w_i\right)\times\vec{\mathrm{I}}_i \tag{2.36}$$

and, therefore, they depends on ∇g , whose expression is

$$\nabla g\left(u,v,w\right)=\underbrace{-\frac{1}{abc}\sum_m\frac{e^{-k_m^2\eta^2/4}}{k_m}\vec{S}_m}_{\nabla g^{(1)}}\underbrace{-\frac{1}{4\pi}\sum_n\left(\frac{2e^{-R_n^2/\eta^2}}{\eta\sqrt{\pi}}+\frac{\mathrm{erfc}\left(R_n/\eta\right)}{R_n}\right)\frac{\vec{R}_n}{R_n^2}}_{\nabla g^{(2)}} \tag{2.37}$$

where

$$\begin{aligned}\vec{S}_m=&\vec{u}_x\frac{k_m^x}{k_m}\frac{\sin\left(k_m^x u\right)\cos\left(k_m^y v\right)\cos\left(k_m^z w\right)}{2^{\delta_{om_y}+\delta_{om_z}}}\\&+\vec{u}_y\frac{k_m^y}{k_m}\frac{\cos\left(k_m^x u\right)\sin\left(k_m^y v\right)\cos\left(k_m^z w\right)}{2^{\delta_{om_x}+\delta_{om_z}}}\\&+\vec{u}_z\frac{k_m^z}{k_m}\frac{\cos\left(k_m^x u\right)\cos\left(k_m^y v\right)\sin\left(k_m^z w\right)}{2^{\delta_{om_x}+\delta_{om_y}}}\end{aligned} \tag{2.38}$$

For the sake of completeness, since it is required in (2.20) and (2.21), also the expression of ∇f is provided:

$$\nabla f\left(u,v,w\right)=\underbrace{-\frac{1}{abc}\sum_m\frac{e^{-k_m^2\eta^2/4}}{k_m^3}\left(1+k_m^2\eta^2/4\right)\vec{S}_m}_{\nabla f^{(1)}}\underbrace{-\frac{1}{8\pi}\sum_n\mathrm{erfc}\left(R_n/\eta\right)\frac{\vec{R}_n}{R_n}}_{\nabla f^{(2)}} \tag{2.39}$$

Since *g* and *f* are even periodic functions of *u*, *v*, and *w*, the components of ∇g and ∇f have the same periodicity, and their components are either even or odd functions.

2.2.2. Numerical considerations about the Green's functions

For an efficient calculation of the Green's functions, it is necessary to highlight some numerical hints like the extraction of the singularity as well as the truncation of the series and their convergence properties. Then, some expressions are derived for the selection of the splitting parameter that minimize the computing time for a prescribed accuracy.

Extraction of the singularity

When the Green's functions are used for setting-up an electric field integral equation (EFIE), only the values of *g*, *f*, and ∇g are needed. The functions *g* and ∇g are singular in *u = v = w = 0* and in all the periodic corresponding points. On the contrary, *f* is limited in the whole domain, but exhibits an irregular behaviour (a cuspid) in the origin. For this reason, the numerical calculation of the integrals involving *f* may become unacceptably inaccurate. Extracting the singular or irregular terms in {0, 0, 0} it results

$$g\left(u,v,w\right)=\frac{1}{4\pi R_0}+\underline{g}\left(u,v,w\right) \tag{2.40}$$

$$f(u,v,w) = -\frac{R_0}{8\pi} + \underline{f}(u,v,w) \tag{2.41}$$

$$\nabla g(u,v,w) = -\frac{\vec{R}_0}{4\pi R_0^3} + \nabla \underline{g}(u,v,w) \tag{2.42}$$

where

$$\vec{R}_0 = \vec{R}_{\{0,0,0\}} = u\,\vec{u}_x + v\,\vec{u}_y + w\,\vec{u}_z \qquad R_0 = \left|\vec{R}_0\right|$$

and

$$\underline{g}(u,v,w) = g^{(1)} - \frac{\eta^2}{32\,abc} + \frac{1}{4\pi}\left(-\frac{\operatorname{erf}(R_0/\eta)}{R_0} + \sum_n{}^{*}\frac{\operatorname{erfc}(R_n/\eta)}{R_n}\right) \tag{2.43}$$

$$\underline{f}(u,v,w) = f^{(1)} + \frac{1}{8\pi}\left[\frac{\eta e^{-R_0^2/\eta^2}}{\sqrt{\pi}} + R_0 \operatorname{erf}(R_0/\eta) + \sum_n{}^{*}\left(\frac{\eta e^{-R_n^2/\eta^2}}{\sqrt{\pi}} - R_n \operatorname{erfc}(R_n/\eta)\right)\right] \tag{2.44}$$

$$\begin{aligned}\nabla \underline{g}(u,v,w) = \nabla g^{(1)} &- \left(\frac{2e^{-R_0^2/\eta^2}}{\eta\sqrt{\pi}} - \frac{\operatorname{erfc}(R_0/\eta)}{R_0}\right)\frac{\vec{R}_0}{4\pi R_0^2} \\ &- \sum_n{}^{*}\left(\frac{2e^{-R_n^2/\eta^2}}{\eta\sqrt{\pi}} - \frac{\operatorname{erfc}(R_n/\eta)}{R_n}\right)\frac{\vec{R}_n}{4\pi R_n^2}\end{aligned} \tag{2.45}$$

where $\sum_n{}^{*}$ differs from $\sum_n$ only because the term corresponding to $n_x = n_y = n_z = 0$ is excluded. After the singularity extraction, the functions g, f e ∇g are finite and regular in $u = v = w = 0$.

Truncation of the series and choice of the splitting parameter to optimize the computing time

The accuracy and computing time in the calculation of the Green's functions strongly depends on the truncation of the spectral and spatial series, as well as in the proper choice of the splitting parameter η. This subject has been already addressed in the literature (see, for instance, [17]–[26], [31]), where the choice of the splitting parameter is discussed in the case of the 3D dynamic Green's functions and of the 2D static and dynamic case. In this section, it is outlined the derivation of the criterion for the series truncation and of the choice of the splitting parameter to guarantee a prescribed accuracy in the calculation of the scalar functions f and g and of their gradients. Let us assume to include in the spectral series all the terms satisfying the conditions

$$k_m \le k_M \tag{2.46}$$

Under this condition the number of terms N_k to be included in the modal series in (2.26), (2.27), (2.37) , and (2.39) can be approximated by the asymptotic expression

$$N_k \approx \frac{(k_M l)^3}{6\pi^2} + \frac{(k_M l)^2\,\underline{l}}{8\pi} + \frac{(k_M l)\,\overline{l}}{4\pi} \tag{2.47}$$

where

$$l = \sqrt[3]{abc} \qquad \underline{l} = \frac{l}{a} + \frac{l}{b} + \frac{l}{c} \qquad \overline{l} = \frac{a+b+c}{l} \tag{2.48}$$

Analogously, assuming to include in the spatial series all the terms satisfying the conditions

$$\min(R_n) \leq R_N \tag{2.49}$$

Where min (R_n) is the minimum value of R_n for u, v and w comprised in the intervals $[-a, a]$, $[-b, b]$, and $[-c, c]$, respectively, the number of terms N_R included in the spatial series can be approximated as

$$N_R \approx \frac{\pi(R_N/l)^3}{6} + \frac{\pi(R_N/l)^2}{4}\bar{l} + (R_N/l)\underline{l} \tag{2.50}$$

Once N_k and N_R are calculated through (2.47) and (2.50), it is possible to estimate the error in the truncation of the series by considering their reminders. The errors depends on k_M, R_N, η, and on the shape of the cavity through $\bar{l}$ and $\underline{l}$. Considering the a-dimensional functions lg, f/l, $l^2\nabla g$, and ∇f, for which it is meaningful to define the absolute error, by running a large number of numerical calculations varying all the above parameters, it was verified that the maximum absolute error is below 10^{-N_c} (i.e., N_c digits of accuracy) when

$$\underline{k}_M = \frac{k_M \eta}{2} = \sqrt{\ln(10) N_c} \tag{2.51}$$

$$\underline{R}_N = \frac{R_N}{\eta} = \sqrt{\ln(10) N_c} \tag{2.52}$$

Moreover, it also resulted that the error is almost independent from the value of η in the range $0.3l < \eta < 2l$. Therefore, a variation of η in this interval will change k_M and R_N (keeping constant $\underline{k}_M$ and $\underline{R}_N$), without almost any effect on the overall precision. However, changing the values of k_M and R_N will impact the computing time. The overall computing time of the Green's functions can be estimated as

$$T = T_{0k} + T_{0R} + N_k T_{1k} + N_R T_{1R} \tag{2.53}$$

where T_{0k} and T_{0R} are bias times independent of the number of terms of the series, whereas T_{1k} and T_{1R} are the computing times for a single term of the spectral and spatial series, respectively. These partial times can be easily obtained by running a test calculation of the Green's function on the computer used, and, therefore, they are assumed as known. By substituting (2.47) and (2.50) in (2.53) and deriving with respect to η, with some approximations it can be demonstrated that a good estimate of the value of η providing the minimum computing time is

$$\eta = l \sqrt[4]{\frac{2\underline{l} T_{1k}}{\pi^2 \bar{l} T_{1R}}} \tag{2.54}$$

To confirm the correctness of the above estimate, several numerical tests have been conducted. As an example, Fig. 2.17 reports the case of a box with dimensions a = 5.4 mm, b = 8.7 mm, and c = 7.1 mm, when the precision is set to N_c = 6 digits. The curves are obtained by changing the value of η and calculating the truncating values k_M, R_N by using (2.51) and (2.52). In particular, the dashed curve is the computing time estimated by the asymptotic expression of the number of terms in the series, while the solid uneven red curve is the real computing time. It is observed that close to the minimum the quantization of the number of modes and images in the calculation of the series is more sensitive, but

the asymptotic expression well represents the real behaviour, and (2.54) gives a very good *a priori* estimate of the value of the splitting parameter η minimizing the computing time.

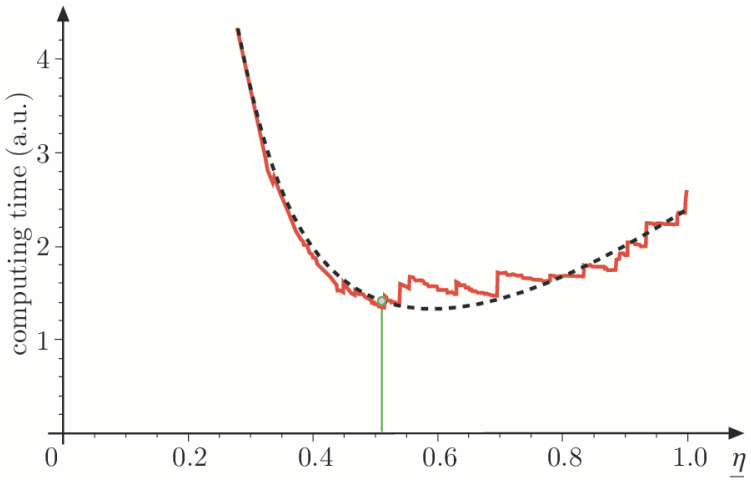

Fig. 2.17. Computing time (arbitrary units) vs the value of the normalized splitting parameter $\eta = \eta/\ell$, in the case a = 5.4 mm, b = 8.7 mm, c = 7.1 mm, and N_c = 6. The vertical line indicates the optimal value of η, calculated by using (2.54).

2.2.3. Electromagnetic analysis of Arbitrarily shaped objects

The analysis of an arbitrarily shaped block represents the general situation, so a case where the block boundary walls don't coincide with the cavity ones. Since the aim of the electromagnetic analysis is to represent the building block behavior as a generalize admittance matrix (GAM), the electric wall boundary condition needs to be enforced on the building block surface S_V to determine the unknown surface electric current $\vec{J}$ for a given surface magnetic current excitation $\vec{M}$. However, since the block is enclosed within a metallic box, this condition is automatically fulfilled on the part of the block surface coincident with the box faces and on which it is not defined an interconnecting surface with other blocks. Elsewhere, the condition

$$\vec{E}_{\tan} = \hat{n} \times \vec{M} \tag{2.55}$$

is imposed, which leads to the following Electric Field Integral Equation (EFIE)

$$\frac{1}{j\omega\varepsilon}\int \nabla_s \nabla_s' g^e(\vec{r},\vec{r}') \cdot \vec{J}(\vec{r}')\, d\vec{r}' + j\omega\mu \left[\int \vec{\vec{G}}_0^A(\vec{r},\vec{r}') \cdot \vec{J}(\vec{r}')\, d\vec{r}' + \sum_{m=1}^{\infty} a_m \vec{\mathrm{E}}_m(\vec{r}) \right]_{\tan}$$

$$= -\left[\frac{1}{2}\hat{n} \times \vec{M} + \mathrm{PV}\left(\int \nabla \times \vec{\vec{G}}_0^F(\vec{r},\vec{r}') \cdot \vec{M}(\vec{r}')\, d\vec{r}' \right) \right]_{\tan} \tag{2.56}$$

where PV means the principal value, and the mode amplitudes auxiliary variables have been introduced and are defined as

$$a_m = \frac{\omega^2 \varepsilon \mu}{k_m^2 \left(k_m^2 - \omega^2 \varepsilon \mu \right)} \left(\int \vec{\mathrm{E}}_m \cdot \vec{J}\, d\vec{r} + \frac{\varepsilon}{\mu} \int \vec{\mathrm{H}}_m \cdot \vec{M}\, d\vec{r} \right) \tag{2.57}$$

The tangential electric field on the surface of the block can be represented as

$$\vec{E}_{\tan} = \hat{n} \times \vec{M} = \sum_{i=1}^{n} v_i \, \hat{n} \times \vec{f}_i \tag{2.58}$$

where v_i have the meaning of generalized voltages, and $\vec{f}$ is the ith RWG basis function [13]. This type of basis function (Fig. 2.18) is well known, commonly and widely used for its simplicity and properties: no normal component of the current to the boundary domain (so, no line of charges exists along it) while the normal one to the common edge is constant and continuous across the edge (its normal flux density to common edge is unitary). The relationship between the generalized voltages v_i and currents i_i is given by

$$i_i = -\int_{S_V} \vec{f}_i \cdot \vec{H}_{\tan} \, dS \tag{2.59}$$

where S_V is the support of the ith RWG basis function. The EFIE (2.56) is solved with the Method of Moment together with (2.57). As a first step, the surface currents $\vec{J}$ and $\vec{M}$ are represented as a combination of RWG basis functions

$$\vec{J} = \sum_{j=1}^{N} w_j \vec{f}_j \qquad \vec{M} = \sum_{j=1}^{N} v_j \vec{f}_j \tag{2.60}$$

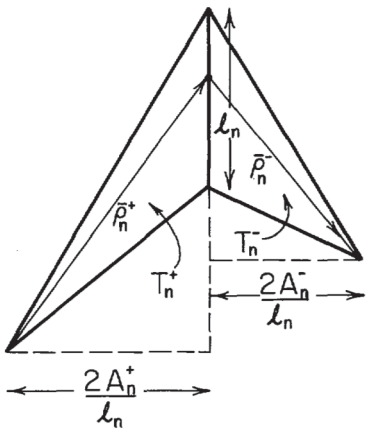

$$\vec{f}(\vec{r}) = \begin{cases} \dfrac{l_n}{2A_n^+} \vec{\rho}_n^+, & \vec{r} \text{ in } \mathrm{T}_n^+ \\ \dfrac{l_n}{2A_n^-} \vec{\rho}_n^-, & \vec{r} \text{ in } \mathrm{T}_n^- \\ 0, & \text{otherwise} \end{cases}$$

Fig. 2.18. Graphical and theoretical representation of the RWG basis functions [13].

By substituting (2.6) in (2.59), representing the surface currents with the (2.60) and exploiting the particular BI-RME representation of the Green's functions, the integral equation is converted into a linear eigenvalue problem. After some manipulation along the line reported in [28], it is possible to represent the behavior of the block under test in terms of its Generalized Admittance Matrix (GAM) in form of pole expansion relating the ith and the jth basis functions

$$Y_{ij}(k_0) = \frac{A_{ij}}{j\eta_0 k_0} + j\frac{k_0}{\eta_0}(\varepsilon' - j\varepsilon'')B_{ij} + j\frac{k_0}{\eta_0}(\varepsilon' - j\varepsilon'')\sum_{p=1}^{P}\frac{C_{ip}C_{jp}}{k_p^2 - k_0^2(\varepsilon' - j\varepsilon'')} \tag{2.61}$$

where $k_0 = \omega\sqrt{\varepsilon_0\mu_0}$; $\eta_0 = \sqrt{\mu_0/\varepsilon_0}$; ε' and ε'' are the real and imaginary part of the relative dielectric constant of the material filling the building block; A_{ij} and B_{ij} represents the inductive and capacitive quasi-static interaction; C_{ip} is related to the projection of the magnetic field of the pth resonant modes on the ith basis function; k_p is the pth resonant wavenumbers of the building block bounded by perfect

metallic walls [32]. In the summation are retained all resonant modes with $k_p \leq \xi\omega_{\max}\sqrt{\varepsilon_0\mu_0}\sqrt{\varepsilon'}$, where $\omega_{\max}$ is the maximum angular frequency of interest for the analysis of the circuit, and ξ typically range from 2 to 4 ([13], Ch. 6). An important aspect is that the quantities A_{ij}, B_{ij} and C_{ip} are wideband (so, frequency-independent) and material independent. Moreover, since the material properties appear explicitly in (2.61), the GAM of each building block can be computed for different materials without the execution of the full-wave analysis each time (this is possible if the initial analysis is done with the higher expected value of ε').

2.2.4. Electromagnetic analysis of Boxed shaped objects

As already reported, a boxed shaped block is a building block with a rectangular parallelepiped shape: so, the cavity volume is completely filled by the block itself and their boundary surfaces will coincide. In this case, the analysis is simplified respect the general one since only the interconnecting surfaces between two blocks need to be meshed using triangular patches. On these surfaces, it is necessary to define the RWG basis functions to represent the surface magnetic current $\vec{M}$ since the perfect electric wall condition on metallic walls is naturally taken into account by the Green's function of the box. In fact, the surface electric current $\vec{J}$ is not defined on the part of the building block boundary that coincide with the cavity walls since, on that, the electric wall condition is automatically satisfy. As mentioned, with the boxed approach it is not necessary to solve an EFIE problem and the quantity of interest for the GAM formulation are obtained as projection on the basis functions. In particular, since the aim is always the representation of the building block behavior as a generalize admittance matrix (GAM), first it is necessary to insert (2.8)-(2.10) into (2.6). Then, introducing into it the electric and magnetic surface currents representation (2.60), and substituting the obtained equation for the H field into (2.59) , after some manipulation it is possible to obtain the same GAM representation of (2.61). However, in this case, the frequency-independent terms A_{ij} and B_{ij} are obtained by projecting the Green's functions on the RWG basis functions

$$A_{ij} = \int_S \int_{S'} \left(\nabla \cdot \vec{f}_i(\vec{r})\right) g^m(\vec{r},\vec{r}\,') \nabla' \cdot \vec{f}_j(\vec{r}\,') dS\, dS' \tag{2.62}$$

$$B_{ij} = \int_S \int_{S'} \vec{f}_i(\vec{r}) \cdot \vec{\vec{G}}_0^F(\vec{r},\vec{r}\,') \cdot \vec{f}_j(\vec{r}\,') dS\, dS' \tag{2.63}$$

where $\vec{f}_i$ is the ith RWG sub-domain vector basis function, define in [13], and S is its domain of definition. Moreover, the terms C_{ip} are given by

$$C_{ip} = \int_S \vec{f}_i(\vec{r}) \cdot \vec{\mathrm{H}}_m(\vec{r})\, dS \tag{2.64}$$

where $\vec{\mathrm{H}}_m$ is the normalized magnetic modal field of the mth resonant mode of the box. The integrals are calculated numerically, typically by adopting Gaussian quadrature rules. However, when the domains of the basis functions are partly overlapped or contiguous, the integrals (2.62) and (2.63), involving the singular part of the Green's functions, are calculated using the analytical expressions given in [33], [34].

2.3 The Post-Processing phase

Once terminated the electromagnetic analysis of all building blocks by the BI-RME solver, the output files are acquired and their content checked and prepared for the post-processing phase. All tasks after the EM analysis are performed by the previously mentioned MATLAB program. Even if the content of the next paragraphs may seem easy to understand, from a practical point of view there are a series of problems and situations to carefully manage in order to ensure the correctness and accuracy of the results as well as the code efficiency. To give an idea, the MATLAB tool is made by a main file and forty-seven user defined functions with more than 5300 effective code lines (about 19000 by considering the comments lines). Also in this case, thanks to the code modularity, it is easy to modify the MATLAB tool in order to add future upgrades.

The most important part of the post-processing phase is the frequency-by-frequency circuital cascade of the building blocks GAMs. Before starting this operation, it is necessary to prepare the data and to choose a strategy to achieve the desired accuracy and efficiency during the combination. For a circuital cascade, each building block is treated as a circuital block whose ports are the basis functions defined on it. As reported in [13], the domain of definition of a RWG basis function is composed by two adjacent triangles. Since each couple of adjacent triangles has one shared edge, it is possible to think the basis function as locked to it. Therefore, first it is necessary to map the basis functions of each block to the edges of the entire structure under test. After do that, it is necessary to check if all the basis functions are correct: since the BI-RME solver works only on the mesh defined on each block, it does not have any information about the building blocks interconnections. For example, by considering the proposed segmentation for a tee-junction reported in Fig. 2.19*a*, the building block 1 (BB 1) has three meshed sidewalls since they are the interconnections with the other blocks (Fig. 2.19*b*). From a mesh viewpoint, the three sidewalls are treated by the BI-RME solver as a unique surface by defining also the basis functions on the couples of triangles defined across the surfaces (so, on the corner edge highlighted in green in Fig. 2.19*b*). But, these basis functions are not correct because, on the connected blocks, they are not defined since the corner edge of the building block 1 lie to the metallic boundary of the interconnecting surfaces where, by definition, it is not possible to discretize the surface magnetic current.

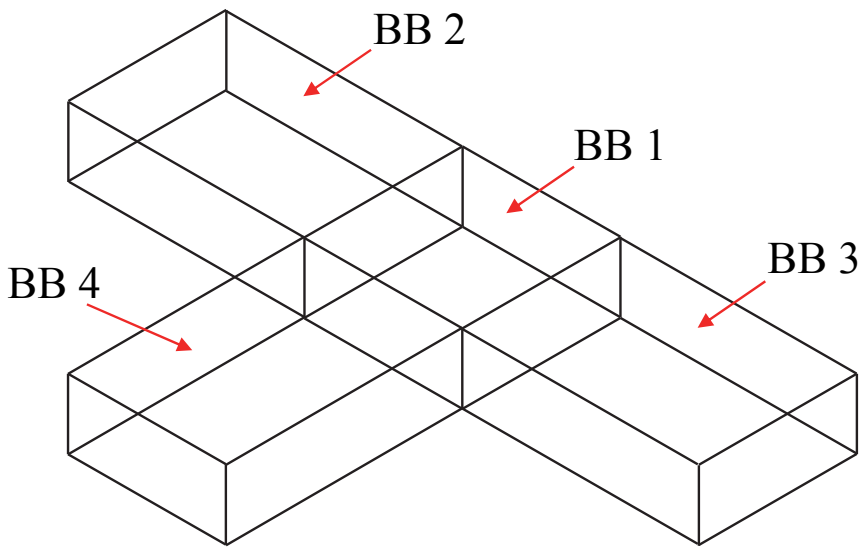

(*a*)

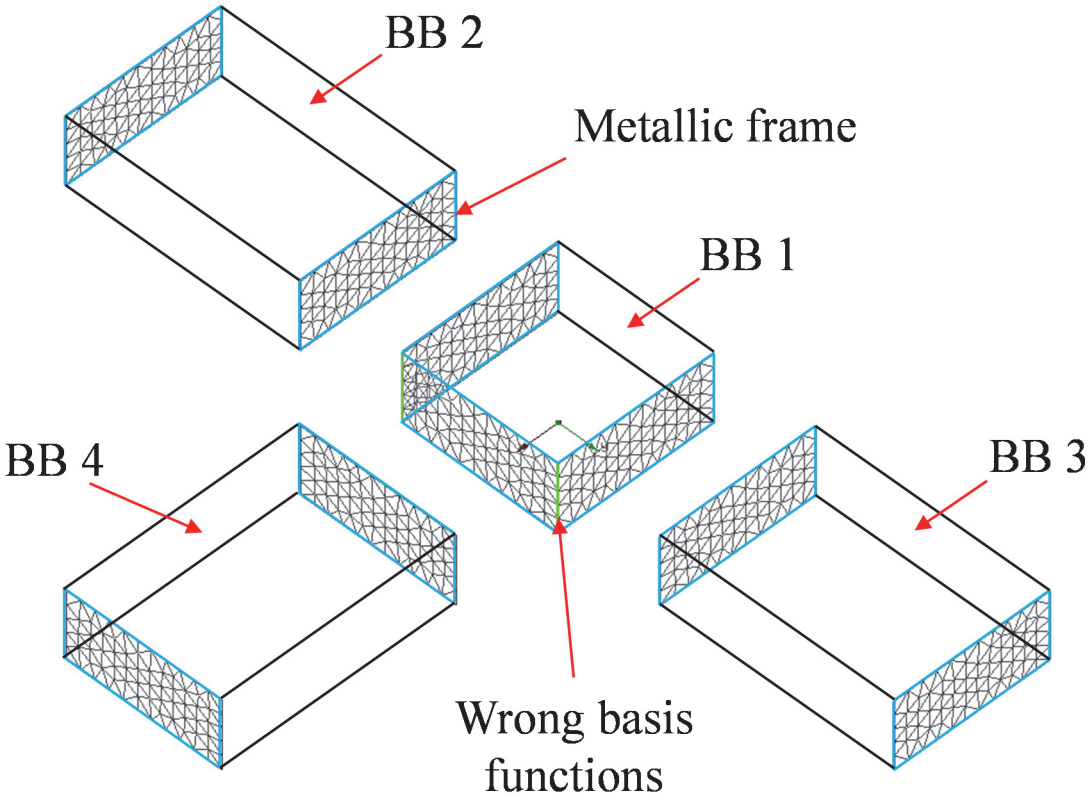

(*b*)

Fig. 2.19. Graphical explanation of the wrong basis functions problem.

2.3.1. Choice of the cascade strategy

Before dealing with the circuital cascade, it is necessary to define its strategy: also called cascade path, it is the sequence of building blocks that define how their GAMs needs to be combined. This sequence is obtained starting from the information about the blocks interconnections and the material filling them. Since the cascade implies the execution of some matrix operations like inversions and multiplications, the optimal choice of the cascade path is crucial because it will determine the computational performances. The implemented strategy aims to cascade first the building blocks filled by lossless media, and then the ones with dielectric losses or with a surface condition of finite electric conductivity. As will be explained in the next paragraphs, the finite electric conductivity is treated as the cascade of the building block under test with a fictitious block whose admittance matrix depends on the electric conductivity. The reasons behind this strategy are the results of some considerations. The first one comes from the observation of the (2.61): for a lossless media, ε'' is equal to 0; so, the GAM appears purely imaginary since the real part becomes zero. Thanks to this *a priori* knowledge, by combining first the blocks without losses it is possible to work on them with a real algebra; then, for the combination with the first lossy block, the GAM of the cascade front will be shift to the complex algebra by adding a zero-real part. This leads to save a huge amount of computational resources and time since, typically, most of the volume of the analyzable structures is filled by lossless dielectric media (air or vacuum). The second consideration is a consequence of the first one: thanks to the real algebra, the accuracy of the results will be better. This statement is related to the matrix operations involved in the GAMs cascade (like numerical inversion): even if it is known that the inverse of a zero matrix is still a

zero matrix, the numerical inversion of the zero-real part of the GAM could not be exactly zero due to the machine precision and this error will propagate. Another peculiar aspect of the proposed strategy is that the path is computed by adding each time, as much as possible, a block that is connected, at least, with one block already inserted into the path: this allows controlling the increasing of the matrix dimensions. To define the cascade strategy, first of all the building blocks are subdivided into two groups based on the ε'' value: equal to zero, called '*BBwoLosses*', or different from zero, called '*BBwLosses*'. The starting block of the cascade path is chosen with the following considerations:

- if exists at least one block without losses on which it is defined an external port, it is set as the starting block;
- if all ports lie on blocks with losses, if there's at least one block without losses, it will be the starting block;
- otherwise, since all blocks have losses, the block where the first port lies is chosen as starting block.

The choice of the cascade path (called '*CascadePath*' in the next procedure) is done in two consecutive iterative steps where all the building blocks are analysed: first, it is necessary to define the path for the lossless building blocks; then, the one for the lossy blocks. Each time, the building blocks connected to block under test are checked and the lossless ones are inserted inside a group called '*nextBBs*', from which the block for the next iteration is chosen. Obviously, since it is necessary to compute first the path for the lossless blocks, the building blocks filled with a lossy media connected to the one under test will be inserted into a dedicated group (called '*nextBBwLosses*') to be analysed in the second phase.

Procedure for lossless building blocks

To procedure used to define the lossless cascade path is illustrated in the flowchart of Fig. 2.20. To easily follow it, each instruction here reported is numbered in the same way as the associated block in the flowchart; moreover, for sake of simplicity, some coding acronyms are used.

1. The starting block is chosen and the next blocks group (*nextBBs*) is filled with its connected building blocks.
2. The candidate block to be added to the cascade path (called block under test - *BB_ut*) is the first one of the *nextBBs* group.
3. A check is done in order to verify if the block under test has been already inserted into the cascade path (*CascadePath*): in positive case, it is deleted from the next blocks group (*nextBBs*) and its connected blocks are not added to *nextBBs* because already inserted (go to point 7). Otherwise, the *BB_ut* has not yet inserted into the cascade path and needs to be analysed (go to point 4).
4. A check is done on the dielectric characteristics of the media filling the *BB_ut*: in fact, it is sufficient to check if the *BB_ut* is part or not of the *BBwLosses* group: in positive case, it is necessary to go to point 5; otherwise, go to point 6.
5. Since the block under test is a lossy block, it is not directly added to the cascade path and it is investigated if it has been already inserted into the *nextBBwLosses* group.
   5a. If the *BB_ut* has been already inserted into *nextBBwLosses*, it is deleted from *nextBBs* and its connected blocks are not added to the next blocks group (*nextBBs*) because already inserted (go to point 7).
   5b. Otherwise, the *BB_ut* has not been yet investigated: it is added to the *nextBBwLosses* group and its connected blocks are added to the next blocks group (*nextBBs* - go to point 7).

6. Since the block under test is a lossless block, it is inserted inside the cascade path; then, its connected blocks are added into the *nextBBs* and the *BB_ut* it is deleted from this group.
7. Obviously, from the *nextBBs* group are removed the building blocks already inserted into the cascade path.
8. From the *BBwoLosses* group are removed the building blocks already inserted into the cascade path.
9. If the *nextBBs* group is not empty, the procedure continues from point 2. Otherwise, also the *BBwoLosses* is checked:
   9a. if it is empty, this means that there are not hidden lossless blocks (so, blocks surrounded by different layers of only lossy blocks) and the procedure ends by updating the *nextBBwLosses* group with the lossy blocks not yet investigated (from *BBwLosses*).
   9b. Otherwise, there are some lossless building blocks not already analysed (hidden blocks): the first element of the *BBwoLosses* list will inserted into the *nextBBs* one. The procedure continues from point 2.

Once do that, the starting building block from which it is necessary to switch to the complex algebra is set to the position inside the cascade path after the last lossless block. If the number of building blocks inside the temporary cascade path is equal to the total number of blocks inside the project, this means that there are no dielectric lossy blocks. If there are metallic losses, the associated fictitious blocks will be the only elements with losses: so, they are added at the end of the cascade path because it is necessary for them to switch to the complex algebra. Otherwise, this means that it is necessary to compute the optimal lossy path because there are some lossy blocks inside the project.

Procedure for lossy building blocks

If there are metallic losses, the associated fictitious blocks are added at the end of the previously obtained cascade path. If there are no hidden blocks, the lossy blocks of the *nextBBwLosses* group are directly inserted at the end of the cascade path because already recorded inside the group based on the connectivity; otherwise, it is executed a loop over the lossy blocks (*nextBBwLosses*) with the creation of an internal jump list. In every iteration, the lossy block under test is added to the end of the cascade path; moreover, the connected blocks to it not yet inserted into the cascade path are added to a dedicated list. Finally, the jump list is updated with the block under test and the not yet inserted one. The procedure is iterated until all the lossy building blocks have been investigated.

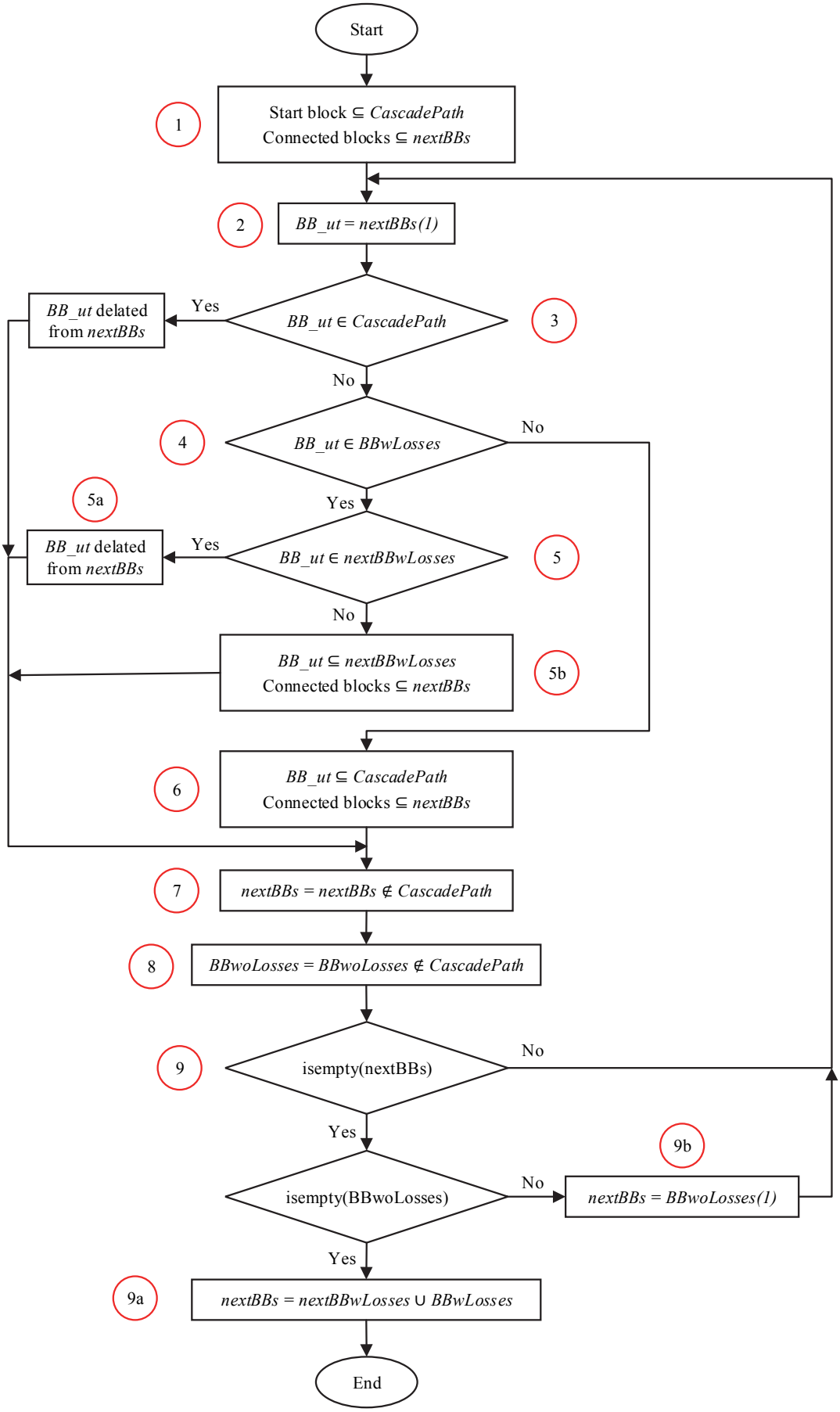

Fig. 2.20. Flowchart for the lossless cascade procedure.

2.3.2. The "partially connected" basis functions

For the next frequency-by-frequency cascade operation, each building block is treated as a circuital block whose ports are the basis functions: in fact, each term of the admittance matrix relates a current and a voltage ([5] and [9]). Due to the generalization of the proposed EM numerical technique, each building block is not a waveguide circuital block on which it is possible to clearly identify the interconnecting ports (like what required by the Mode Matching technique). Therefore, when cascading the matrices of two building blocks A and B (Fig. 2.21), there are three possible situations (one more respect the past implementations of the BI-RME method combined with the segmentation technique):

i. the corresponding basis functions of the two blocks are defined on triangles lying on the interface surface (*connected basis functions*), and the corresponding current and voltage disappear when the two blocks are cascaded;

ii. the basis functions of the two blocks have only one shared triangle lying on the interface surface (*partially connected basis functions*), and the corresponding current and voltage are combined but partly survive when the two blocks are cascaded;

iii. the basis functions of either blocks have no shared triangles (*not connected basis functions*), and the corresponding current and voltage are not affected by the cascade process.

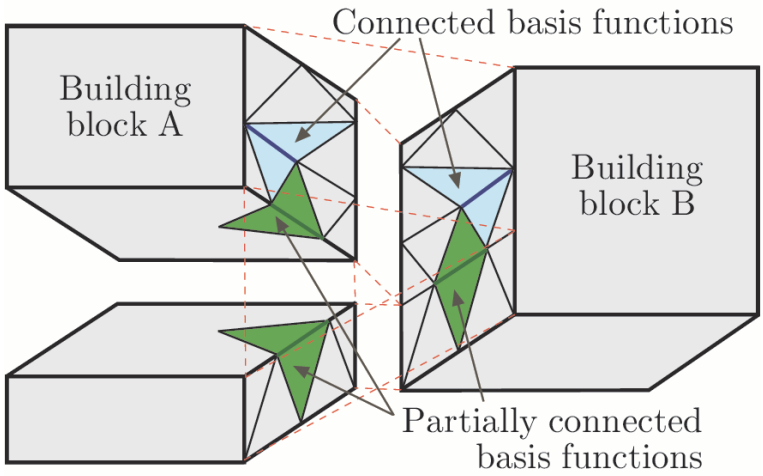

Fig. 2.21. Identification of connected and partially connected basis functions

In the cascade of two building blocks, the generalized voltages must be set equal if the basic functions have opposite directions. Only in this way the magnetic currents placed on the boundary of the blocks to take account of the discontinuity of the tangential component of the electric field when the volumes are separated, they cancel each other and the continuity of the tangential component of the electric field on the interface is re-established. In practice, if the orientation of the basic functions is the same, it is necessary to change the sign to one of two by acting on the sign of the voltage and current into the admittance matrix (row and column). This task is automatically performed during the BI-RME analysis by defining the normal vector of the basis function to have an incoming direction respect the building block. In case of partially connected basis functions, the sign adjustment is not possible during BI-RME analysis but it requires a post-processing. For each partially connected basis function, all blocks on which it appears are selected and ordered based on the position inside the cascade path. In order to correctly define the sign of the them, it is necessary to observe the correspondence between the triangles defining their domain. In particular, the first and second triangles that define the basis function on one block are compared with the ones on the next block through an iterative procedure. Starting from the

first building block of the cascade path on which the basis function appears, the first and second triangles are assumed as master information: it is possible to refer to them as *master_tri_a* and *master_tri_b*. Then, considering the second building block of the cascade path on which the basis function appears, the first and second triangles are assumed as slave information: it is possible to refer to them as *slave_tri_a* and *slave_tri_b*. This information will be updated during the procedure. If two partially connected basis functions have the same direction, the starting/ending triangles will be the same. If two basis functions have an opposite direction, the starting/ending triangles of the first one will coincide with the ending/starting one of the second basis function. Once understood if it is necessary to change a sign, the procedure requires the prediction of the starting and ending triangles of the basis function obtained combined the two previous ones. To summarize:

- *master_tri_a* = *slave_tri_a*: it is necessary to change the sign. The resulting basis function will have *master_tri_a* = *slave_tri_b* while the *master_tri_b* is kept the same.
- *master_tri_b* = *slave_tri_b*: it is necessary to change the sign. The resulting basis function will have *master_tri_b* = *slave_tri_a* while the *master_tri_a* is kept the same.
- *master_tri_a* = *slave_tri_b*: it is not necessary to change the sign. The resulting basis function will have *master_tri_a* = *slave_tri_a* while the *master_tri_b* is kept the same.
- *master_tri_b* = *slave_tri_a*: it is not necessary to change the sign. The resulting basis function will have *master_tri_b* = *slave_tri_b* while the *master_tri_a* is kept the same.

To better understand the situation, please consider Fig. 2.22-Fig. 2.23.

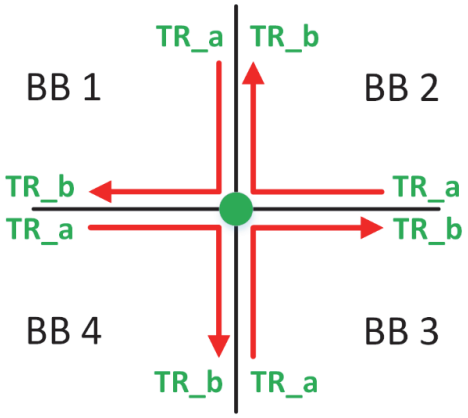

Fig. 2.22

All the basis functions have the right orientation: it is not necessary to change the signs.

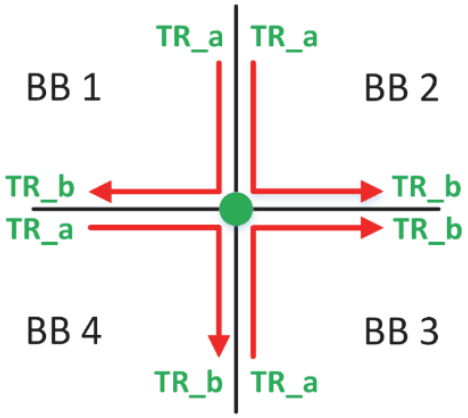

Fig. 2.23

The basis function on BB 2 has the same orientation of the one inside the BB 1 (same TR_a): it is necessary to change the sign into the admittance matrix of BB 2. The resulting basis function (obtained as combination of the ones of BB 1 and 2) will have the following orientation:

master_tri_a = *slave_tri_b* of BB 2 (TR_b)

master_tri_b = *slave_tri_b* of BB 1 (TR_b)

Then, since the orientation will be correct respect the basis function of BB 3, and this last has a correct orientation respect the one of BB 4, no more signs need to be changed.

2.3.3. Terminal port modes

With the BI-RME analysis, each block is characterized through a generalized admittance matrix: so, the combination of them is still a GAM. In order to represent the overall circuit behavior in terms of S-parameters, it is necessary to transform the obtained GAM into a Y-matrix. For this purpose, if on a building block is defined a rectangular terminal port, its modal fields are defined during the BI-RME analysis since this shape is linked with the one of the cavity resonator. In fact, it is possible to impose the desired terminal mode or set of terminal modes; otherwise, it is possible to impose all the propagating modes inside a given frequency range. In practice, even if the rectangular cross-section is the most widely used shape for the waveguide terminal ports, it is necessary to provide also the possibility to use other shapes like the circular and the coaxial ones (Fig. 2.24); moreover, sometimes it is necessary to use not conventional shapes for the terminal ports. To accomplish these requirements, there are two possibilities. The first one involves the implementation inside the BI-RME solver of the necessary formulas. However, this approach is not in line with the philosophy behind the Generalized BI-RME method and the code modularity because it requires the development of *ad hoc* features inside the BI-RME solver. Moreover, even if for the circular and coaxial shapes this task may be easy since the formulas are well known, it is not the same for terminal ports with a completely arbitrary shape. The second approach, the adopted one, is based on the definition of the RWG basis functions also on the terminal ports, and the projection of them on the port modes [4] (Fig. 2.25). This is based on the solution of (2.65) to build a projection matrix used to pre/post multiply the GAM of the building block on which it is defined the terminal port.

$$\int_{S_i} \vec{f}_i(\vec{r}) \cdot \hat{n} \times \vec{e}_{mn}(\vec{r}) dS = \sum_{j=1}^{N} a_j \int_{S_i \cap S_j} \vec{f}_i(\vec{r}) \cdot \vec{f}_j(\vec{r}) dS \quad \forall i \tag{2.65}$$

In (2.65), $\vec{f}_i(\vec{r})$ is the *i*th RWG basis function used as test for the Galerkin method, and S_i is its support; $\vec{f}_j(\vec{r})$ is the *j*th RWG basis function defined on the terminal port, and $S_i \cap S_j$ is the common triangle of the *i*th and *j*th RWG supports. In this equation, the unknown quantity is the coefficient a_j associated to the *j*th basis function: once solved the equation for each terminal port basis functions, the projection matrix is obtained. Even if from (2.65) it is evident that this procedure needs to be executed for each mode defined over the terminal port, the proposed approach is completely independent from the shape of the terminal port. In fact, it requires only to know the electric modal vector of the port mode and not how this data have been obtained. In practice, even if inside the MATLAB program have been implemented the formulas for the circular and coaxial canonical shapes, it is compatible with the calculation of the modal vector quantities also by third part tools. For example, a possibility could be the use of the 1970s BI-RME method since it was developed to find the modal vectors of arbitrary waveguide cross-sections.

In the following paragraphs are reported the formulas and the conventions used for the rectangular port modes inside the BI-RME solver, and the ones used for the circular and coaxial shapes to define the modal vectors for the projection phase.

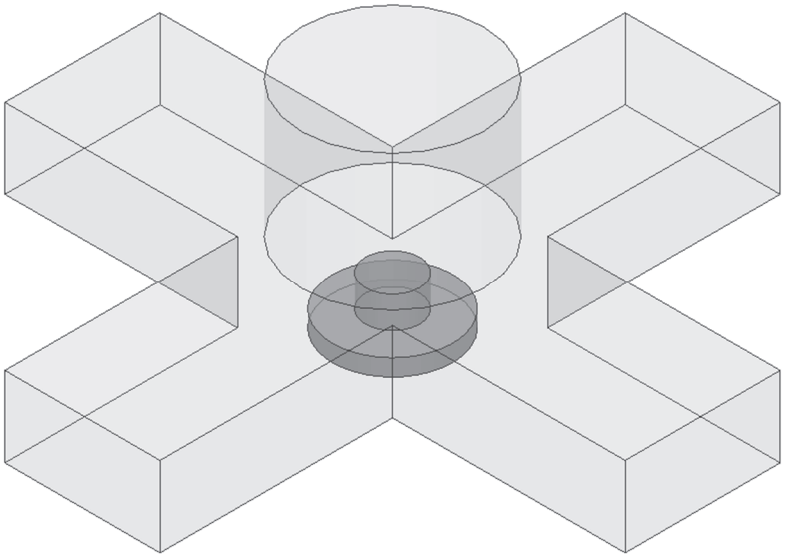

Fig. 2.24. Example of waveguide circuit with rectangular and circular terminal ports: a turnstile junction [4].

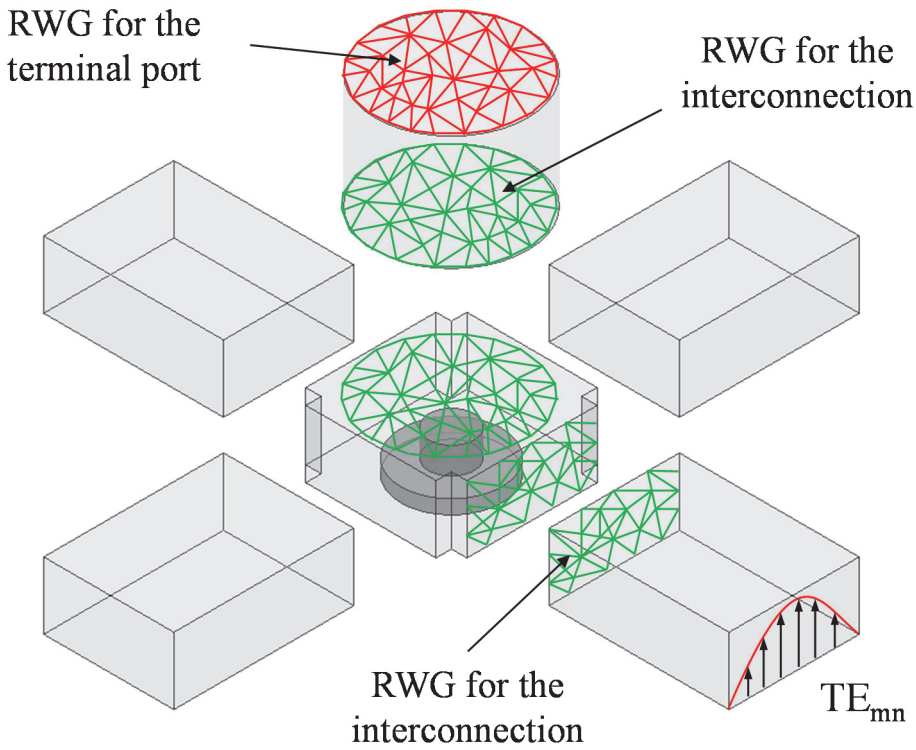

Fig. 2.25. Definition of the RWG basis functions on the not rectangular terminal port for the projection phase.

Rectangular ports

For the rectangular modes definition inside the BI-RME solver, it is used a formulation related to the local reference coordinate of Fig. 2.26.

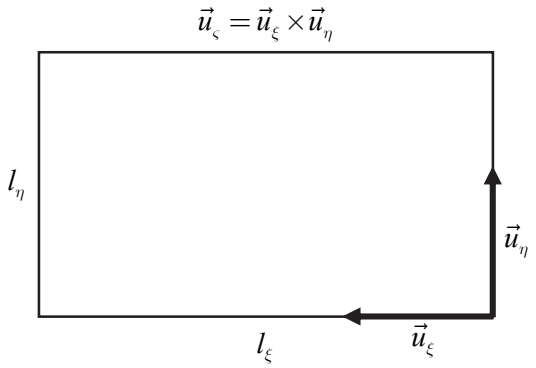

Fig. 2.26. Representation of the local coordinate system for a rectangular port.

Here, l_η, l_ξ and $\vec{u}_\eta$, $\vec{u}_\xi$ represent, respectively, the lengths of the edges and the unit vectors on η and ξ directions, while $\vec{u}_\varsigma$ is the unit vector pointing inside the port. In this way, it is possible to write the electric and magnetic normalized fields components as:

$$\vec{e}_{mn}^{TE} = N_{mn}\left[\vec{u}_\xi \frac{k_\eta}{k_t} C_\xi S_\eta - \vec{u}_\eta \frac{k_\xi}{k_t} S_\xi C_\eta\right] \qquad \vec{e}_{mn}^{TM} = N_{mn}\left[-\vec{u}_\xi \frac{k_\xi}{k_t} C_\xi S_\eta - \vec{u}_\eta \frac{k_\eta}{k_t} S_\xi C_\eta\right] \tag{2.66}$$

$$\vec{h}_{mn}^{TE} = N_{mn}\left[\vec{u}_\xi \frac{k_\xi}{k_t} S_\xi C_\eta + \vec{u}_\eta \frac{k_\eta}{k_t} C_\xi S_\eta\right] \qquad \vec{h}_{mn}^{TM} = N_{mn}\left[\vec{u}_\xi \frac{k_\eta}{k_t} S_\xi C_\eta - \vec{u}_\eta \frac{k_\xi}{k_t} C_\xi S_\eta\right] \tag{2.67}$$

where

$$k_\xi = \frac{m\pi}{l_\xi} \qquad k_\eta = \frac{n\pi}{l_\eta} \qquad k_t = \sqrt{k_\xi^2 + k_\eta^2} \tag{2.68}$$

$$C_\xi = \cos k_\xi \xi \qquad C_\eta = \cos k_\eta \eta \tag{2.69}$$

$$S_\xi = \sin k_\xi \xi \qquad S_\eta = \sin k_\eta \eta \tag{2.70}$$

$$N_{mn} = \sqrt{\frac{2-\delta_{0m}}{l_\xi}\frac{2-\delta_{0n}}{l_\eta}} \qquad \delta_{0m} = \begin{cases} 1, & m = 0 \\ 0 & m \neq 0 \end{cases} \qquad \delta_{0n} = \begin{cases} 1, & n = 0 \\ 0 & n \neq 0 \end{cases} \tag{2.71}$$

Circular ports

In case of circular ports, the formulas for the modal vectors are taken from [35] and here reported.

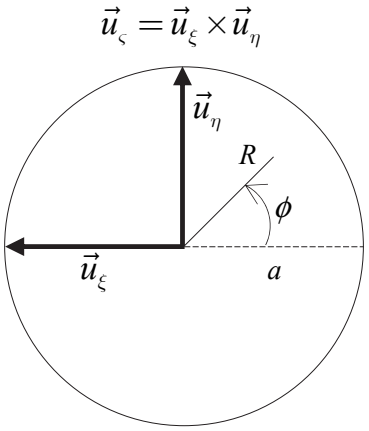

Fig. 2.27. Representation of the local coordinate system for a circular port.

In Fig. 2.27, $\vec{u}_\eta$, $\vec{u}_\xi$ represent the unit vectors on η and ξ directions, while $\vec{u}_\varsigma$ is the unit vector pointing inside the port. It is possible to write the electric and magnetic normalized fields components as:

$$\vec{e}_{np}^{TM} = \frac{\sqrt{\delta_n/\pi}}{J_{n+1}(\chi_{np})}\left(-\vec{u}_R \frac{J'_n(\chi_{np}R/a)}{a}\begin{Bmatrix}\cos n\phi \\ \sin n\phi\end{Bmatrix} + \vec{u}_\phi \frac{nJ_n(\chi_{np}R/a)}{\chi_{np}R}\begin{Bmatrix}\sin n\phi \\ -\cos n\phi\end{Bmatrix}\right) \tag{2.72}$$

$$\vec{h}_{np}^{TM} = \frac{\sqrt{\delta_n/\pi}}{J_{n+1}(\chi_{np})}\left(+\vec{u}_R \frac{nJ_n(\chi_{np}R/a)}{\chi_{np}R}\begin{Bmatrix}-\sin n\phi \\ \cos n\phi\end{Bmatrix} - \vec{u}_\phi \frac{J'_n(\chi_{np}R/a)}{a}\begin{Bmatrix}\cos n\phi \\ \sin n\phi\end{Bmatrix}\right) \tag{2.73}$$

$$\vec{e}_{np}^{TE} = \frac{1}{J_n(\chi'_{np})}\sqrt{\frac{\delta_n}{\pi(\chi'^{\,2}_{np} - n^2)}}\left(+\vec{u}_R \frac{nJ_n(\chi'_{np}R/a)}{R}\begin{Bmatrix}\sin n\phi \\ -\cos n\phi\end{Bmatrix} + \vec{u}_\phi \frac{\chi'_{np}J'_n(\chi'_{np}R/a)}{a}\begin{Bmatrix}\cos n\phi \\ \sin n\phi\end{Bmatrix}\right) \tag{2.74}$$

$$\vec{h}_{np}^{TE} = \frac{1}{J_n(\chi'_{np})}\sqrt{\frac{\delta_n}{\pi(\chi'^{\,2}_{np} - n^2)}}\left(-\vec{u}_R \frac{\chi'_{np}J'_n(\chi'_{np}R/a)}{a}\begin{Bmatrix}\cos n\phi \\ \sin n\phi\end{Bmatrix} + \vec{u}_\phi \frac{nJ_n(\chi'_{np}R/a)}{R}\begin{Bmatrix}\sin n\phi \\ -\cos n\phi\end{Bmatrix}\right) \tag{2.75}$$

where R and ϕ are respectively the radial and angular distances of the point under test from the origin; χ_{np} is the pth root of the Bessel's equation $J_n(\chi) = 0$ (zero excluded); χ'_{np} is the pth root of the Bessel's equation $J'_n(\chi) = 0$ (zero excluded); n is the order of the Bessel's equation ($n = 0, 1, 2, \ldots$); p is the zero number of the Bessel's equation ($p = 1, 2, \ldots$). Moreover,

$$J'_n(\chi) = \frac{dJ_n(\chi)}{d\chi} \qquad \delta_n = \begin{Bmatrix}1 & n=0 \\ 2 & n\neq 0\end{Bmatrix} \tag{2.76}$$

Coaxial ports

In case of coaxial ports, only the TEM mode is considered: the formulas for the modal vectors are taken from [35] and here reported.

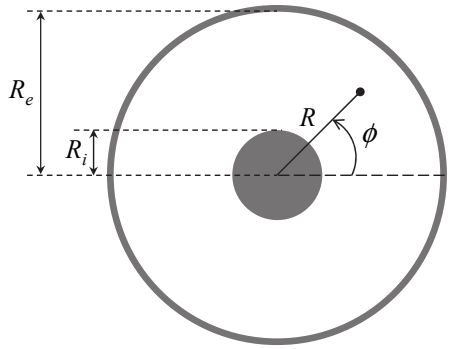

Fig. 2.28. Coaxial port.

$$\vec{e}^{TEM} = \frac{1}{R\ln\left(R_e/R_i\right)}\vec{u}_R \tag{2.77}$$

$$\vec{h}^{TEM} = \frac{1}{2\pi R}\vec{u}_\phi \tag{2.78}$$

where R and ϕ are, respectively, the radial and angular distances of the point under test from the origin; R_e and R_i are, respectively, the outer and inner radius of the coaxial port.

2.3.4. GAMs frequency combination

Before starting with the cascade, it is possible to do some considerations in order to speed-up the process. By observing the GAM formula (2.61), also reported here, it is possible to identify some terms that are frequency independent: in particular, beyond the terms A, B, C and k_p that are, by definition, frequency independent, also η_0, ε' and ε'' are frequency independent.

$$Y_{ij}(k_0) = \frac{A_{ij}}{j\eta_0 k_0} + j\frac{k_0}{\eta_0}(\varepsilon' - j\varepsilon'')B_{ij} + j\frac{k_0}{\eta_0}(\varepsilon' - j\varepsilon'')\sum_{p=1}^{P}\frac{C_{ip}C_{jp}}{k_p^2 - k_0^2(\varepsilon' - j\varepsilon'')}$$

In practice, some parts of the admittance matrix of each block can be calculated outside the frequency loop by saving a lot of time and computational effort. Starting from equation (2.61), it is possible to write the GAM formula as

$$Y_{ij}(k_0) = \frac{1}{k_0}Y_{ij}^{A} + k_0 Y_{ij}^{B} + k_0\,\mathrm{ext}\sum_{p=1}^{P}\frac{C_{ip}C_{jp}}{k_p^2 - k_0^2\tilde{\varepsilon}} \tag{2.79}$$

where

$$Y_{ij}^{A} = \frac{A_{ij}}{j\eta_0} \qquad Y_{ij}^{B} = j\frac{(\varepsilon' - j\varepsilon'')}{\eta_0}B_{ij} \qquad \mathrm{ext} = j\frac{(\varepsilon' - j\varepsilon'')}{\eta_0} \qquad \tilde{\varepsilon} = (\varepsilon' - j\varepsilon'') \tag{2.80}$$

Inside the MATLAB program, a dedicated function performs the following tasks for each building block:

- loading of the EM results from the BI-RME output files;
- creation of the frequency independent parts of (2.79) and preparing them for the right algebra;
- eventually, it deletes the not correct basis functions;
- eventually, it changes the sings of the partially connected basis functions;
- eventually, it prepares the metallic losses fictitious GAM for the closing conditions (for the theory, please refer to the next paragraph).

Another important operation executed prior the frequency-by-frequency cascade is the modes projection. Even if this operation can be conceptually executed after the cascade to transform the GAM of the circuit into an S-matrix, the coefficients that form the projection matrix are frequency independent. Moreover, the projection consists into the pre/post product of the GAM of the terminal building blocks by the associated projection matrix **T**: thanks to the GAM formulation, when this operation is executed over the terms in (2.79) of the terminal building blocks, it leads to the following matrix formulation

$$\mathbf{Y}(k_0) = \frac{1}{k_0}\mathbf{Y}^{\mathrm{A}} + k_0\mathbf{Y}^{\mathrm{B}} + k_0\,\mathrm{ext}\,\mathbf{Y}^{\mathrm{C}}\mathrm{diag}\left(\frac{1}{\mathbf{K}^2 - k_0^2\tilde{\varepsilon}}\right)\left(\mathbf{Y}^{\mathrm{C}}\right)^{T} \tag{2.81}$$

where

$$\mathbf{Y}^{\mathrm{A}} = \frac{1}{j\eta_0}\mathbf{T}\mathbf{A}\mathbf{T}^{T} \qquad \mathbf{Y}^{\mathrm{B}} = \frac{(\varepsilon' - j\varepsilon'')}{j\eta_0}\mathbf{T}\mathbf{B}\mathbf{T}^{T} \qquad \mathrm{ext} = j\frac{(\varepsilon' - j\varepsilon'')}{\eta_0} \qquad \mathbf{Y}^{\mathrm{C}} = \mathbf{T}\mathbf{C} \tag{2.82}$$

and, obviously, **A**, **B**, **C** and **K** are the matrix representations of A_{ij}, B_{ij}, C_{ij} and k_p, respectively.

Once prepared the frequency independent parts of the admittance matrices and done the modes projection, it's time to determine the interconnecting elements necessary for the cascade operation. In

particular, a dedicated function combines the interconnections data of the building blocks based on the cascade path. At each step of the cascade operation, only the GAM of a single building block is combined with the cascade front. For this purpose, from an interconnecting point of view, it is necessary to simulate the cascade operation by understanding the subdivision between connected, not connected and partially connected basis functions between the cascade front and the block to be added. To simplify the operations, it is used the association between each basis function and the edge shared between the triangles defining the domain; moreover, a counter is associated to each edge on which is defined a partially connected basis function. This is necessary because the same edge can be shared by more than three partially connected basis functions. The procedure starts by defining two containers: the first one, called *tmp_Edge_FdB*, to contain the association edges - basis functions that survive after each combination step; the second one, called *tmp_PC_count*, for the counters associated to each shared edge after each combination step (for the partially connected basis functions). At the beginning, *tmp_Edge_FdB* will contain the relative information of the first building block of the cascade path. Thanks to an *a priori* knowledge on the partially connected basis functions, if an edge is shared between three blocks, the corresponding *tmp_PC_count* counter is set equal to 1; if the edge is shared between four blocks, the corresponding *tmp_PC_count* counter is set equal to 2, and so on; otherwise, it is set to 0. For each cascade step, a set of information regarding the connected, not connected and partially connected basis functions are stored to easily identify the associated elements into the GAM during the cascade. The operations sequence is here reported:

1. For the first cascade step, the first block to be added (block under test) is the second one inside the cascade path. Also for it are defined two containers with the same meaning of the previous ones: *Edge_FdB_bbut* and *PC_count_bbut*.
2. Identification of the not connected basis functions (*EdgesNC*), so the elements not in the intersection between *tmp_Edge_FdB* and *Edge_FdB_bbut*.
3. Identification of the connected basis functions (*EdgesCC*), so the elements in the intersection between *tmp_Edge_FdB* and *Edge_FdB_bbut* with at least one *tmp_PC_count* equal to 0.
4. Identification of the partially connected basis functions (*TPedges*). In the combination of two building blocks on which an edge is shared between three blocks, the corresponding counter will figure into *tmp_PC_count* with a value reduced to 0 for the next cascade step. When the associated basis function will be combined with the same on the third block on which it appears, the combination of 0 and 1 counters will produce the disappearing of the edge from the list of shared ones because it will be consider as a connected edge. To summarize, if an edge is shared between three block, its counter will be equal to 1; the combination of two 1s will produce a 0, and the combination 0 and 1 cause the absorption of the edge.
   In the combination of two building blocks on which an edge is shared between four blocks, the corresponding counter will figure into *tmp_PC_count* with a value reduced to 1 for the next cascade step. When this edge will be combined with the third block on which it appears, the combination of 2 and 1 counters will not produce the absorption of the edge because it is necessary to combine it with the fourth block. To summarize, if an edge is shared between four blocks, its counter will be equal to 2; the combination of two 2 will produce a 1, the combination 2 and 1 will produce a 0, and the combination 2 and 0 cause the absorption of the edge. An edge will be considered a shared edge only if the corresponding counter into *tmp_PC_count* and *PC_count_bbut* differ from 0.
5. Creation of the new *tmp_Edge_FdB* as concatenation of *EdgesNC* and *TPedges*.
6. Creation of the new *tmp_PC_count* by following the rules listed above.

Finite metallic conductivity condition

In case of finite metallic conductivity condition (so, not a PEC material), first it is necessary to mesh also the surfaces where the condition is assigned to discretize the surface magnetic current $\vec{M}$ even if those surfaces are part of or coincides with the cavity walls. From the theory point of view, first it is necessary to represent the EM power that flows in the positive direction of a generic surface S_V

$$P = \frac{1}{2}\int_{S_V} \vec{E}\times\vec{H}^{*}\cdot\hat{n}\,dS_V = \frac{1}{2}\int_{S_V} \hat{n}\times\vec{E}\cdot\vec{H}^{*}\,dS_V \tag{2.83}$$

The magnetic current can be expressed in terms of the electric field

$$\vec{M} = -\hat{n}\times\vec{E} = \vec{E}_{\tan} \tag{2.84}$$

Moreover, as reported in (2.58), the surface magnetic current can be written as the combination of basis functions weighted by some useful coefficients

$$\vec{M} = -\hat{n}\times\vec{E} = \vec{E}_{\tan} = \sum_{i=1}^{n} v_i\,\vec{f}_i \tag{2.85}$$

where v_i have the meaning of generalized voltages, and $\vec{f}$ is the ith RWG basis function [13]. By substituting (2.85) in (2.83), the power can be written as

$$P = \frac{1}{2}\int_{S_V} \hat{n}\times\vec{E}\cdot\vec{H}^{*}\,dS_V = -\frac{1}{2}\sum_{i=1}^{n} v_i \int_{S_V} \vec{f}_i\cdot\vec{H}^{*}\,dS_V \tag{2.86}$$

From a circuital point of view, (2.86) can be written as

$$P = \frac{1}{2}\sum_i v_i i_i^{*} \tag{2.87}$$

where

$$i_i = -\int_{S_V} \vec{f}_i\cdot\vec{H}\,dS_V \tag{2.88}$$

In the case of non-perfect electric conductor, the electric and magnetic fields on the volume surface must satisfy the Leontovič condition

$$\hat{n}\times\vec{E} = R_S(1+j)\vec{H}_{\tan} \tag{2.89}$$

from which it is possible to deduce the tangential component of the magnetic field:

$$\vec{H}_{\tan} = \frac{1}{R_S(1+j)}\hat{n}\times\vec{E} \tag{2.90}$$

By substituting (2.85) inside (2.90) and introducing the result in (2.88), the expression of the current become:

$$i_i = -\int_{S_V} \vec{f}_i\cdot\left(-\frac{1}{R_S(1+j)}\sum_j v_j\vec{f}_j\right)dS_V = \frac{1}{R_S(1+j)}\sum_j v_j\int_{S_V}\vec{f}_i\cdot\vec{f}_j\,dS_V \tag{2.91}$$

This expression relates the surface current with the voltages used in order to represent the electric field. Therefore, by inserting all the coefficients in a matrix and by dividing the current for that, an admittance matrix expression is finally obtained, whose elements are:

$$y_{ij} = \frac{i_i}{v_j} = \frac{1}{R_S(1+j)} \int_{S_V} \vec{f}_i \cdot \vec{f}_j \, dS_V = \frac{1}{R_S(1+j)} y_{ij}^0 \tag{2.92}$$

where

$$R_S = \frac{1}{\delta\sigma} = \frac{1}{\sigma}\sqrt{\pi f \mu_0 \sigma} = \sqrt{\frac{\pi f \mu_0}{\sigma}} \tag{2.93}$$

is the surface resistance that depends by the conductivity σ and the frequency *f*; y_{ij}^0 is an integral between basis functions that differs from zero only on the intersection of the domain of definition of the *i*th and *j*th basis functions. In fact, this quantity has the dimension of an admittance matrix and it is used as base for the closing condition fictitious block. In practice, it is not necessary to calculate the y_{ij}^0 terms since they are already calculated during the BI-RME analysis of the building block on which it has been define the finite conductivity condition; so, only necessary to identify the basis functions involved by the imposed condition and to calculate the frequency dependent term during the frequency-by-frequency cascade.

Frequency-by-frequency circuital GAMs cascade

In theory, a frequency-by-frequency cascade technique is not the most efficient way to combine the EM characterization of each building block. In fact, in case of lossless media, a modified version of the efficient frequency-independent cascading technique discussed in [36] can be adopted. However, since its extension to lossy building blocks and to the use of the partially connected basis functions is not trivial and not yet available, a frequency-by-frequency procedure is actually adopted for the Generalized BI-RME method. Due to the presence of the partially connected basis functions, the traditional theory for the cascade of two admittance matrices [14] has been modified in order to combine them in a parallel way [5]. The admittance matrices are partitioned into 3-by-3 sub-matrices. According to the symbols defined in Fig. 2.29, the matrices of blocks A and B are partitioned as follows:

$$\begin{bmatrix} \mathbf{I}_\mathrm{n}^\mathrm{A} \\ \mathbf{I}_\mathrm{p}^\mathrm{A} \\ \mathbf{I}_\mathrm{c}^\mathrm{A} \end{bmatrix} = \begin{bmatrix} \mathbf{Y}_\mathrm{nn}^\mathrm{A} & \mathbf{Y}_\mathrm{np}^\mathrm{A} & \mathbf{Y}_\mathrm{nc}^\mathrm{A} \\ \mathbf{Y}_\mathrm{pn}^\mathrm{A} & \mathbf{Y}_\mathrm{pp}^\mathrm{A} & \mathbf{Y}_\mathrm{pc}^\mathrm{A} \\ \mathbf{Y}_\mathrm{cn}^\mathrm{A} & \mathbf{Y}_\mathrm{cp}^\mathrm{A} & \mathbf{Y}_\mathrm{cc}^\mathrm{A} \end{bmatrix} \begin{bmatrix} \mathbf{V}_\mathrm{n}^\mathrm{A} \\ \mathbf{V}_\mathrm{p}^\mathrm{A} \\ \mathbf{V}_\mathrm{c}^\mathrm{A} \end{bmatrix} \tag{2.94}$$

$$\begin{bmatrix} \mathbf{I}_\mathrm{n}^\mathrm{B} \\ \mathbf{I}_\mathrm{p}^\mathrm{B} \\ \mathbf{I}_\mathrm{c}^\mathrm{B} \end{bmatrix} = \begin{bmatrix} \mathbf{Y}_\mathrm{nn}^\mathrm{B} & \mathbf{Y}_\mathrm{np}^\mathrm{B} & \mathbf{Y}_\mathrm{nc}^\mathrm{B} \\ \mathbf{Y}_\mathrm{pn}^\mathrm{B} & \mathbf{Y}_\mathrm{pp}^\mathrm{B} & \mathbf{Y}_\mathrm{pc}^\mathrm{B} \\ \mathbf{Y}_\mathrm{cn}^\mathrm{B} & \mathbf{Y}_\mathrm{cp}^\mathrm{B} & \mathbf{Y}_\mathrm{cc}^\mathrm{B} \end{bmatrix} \begin{bmatrix} \mathbf{V}_\mathrm{n}^\mathrm{B} \\ \mathbf{V}_\mathrm{p}^\mathrm{B} \\ \mathbf{V}_\mathrm{c}^\mathrm{B} \end{bmatrix} \tag{2.95}$$

where the subscripts “n”, “p”, and “c” refer to not connected, partially connected, and connected basis functions, respectively. Since the building blocks are filled by an isotropic material, the GAMs (2.94) and (2.95) are symmetric. By imposing the Kirchhoff’s laws on currents and voltages for the connected and partially connected ports,

$$\mathbf{V}_\mathrm{c}^\mathrm{A} = \mathbf{V}_\mathrm{c}^\mathrm{B} = \mathbf{V}_\mathrm{c} \qquad \mathbf{V}_\mathrm{p}^\mathrm{A} = \mathbf{V}_\mathrm{p}^\mathrm{B} = \mathbf{V}_\mathrm{p} \tag{2.96}$$

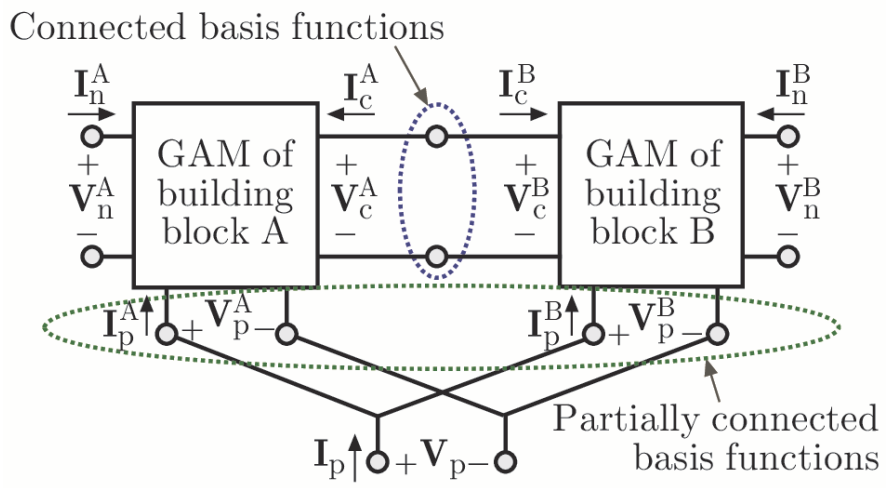

Fig. 2.29. Circuital representation of two building blocks during the cascade procedure.

$$-\mathbf{I}_c^A = \mathbf{I}_c^B = \mathbf{I}_c \qquad \mathbf{I}_p^A + \mathbf{I}_p^B \triangleq \mathbf{I}_p \tag{2.97}$$

the following equations are obtained:

$$\mathbf{I}_n^A = \mathbf{Y}_{nn}^A \mathbf{V}_n^A + \mathbf{Y}_{np}^A \mathbf{V}_p + \mathbf{Y}_{nc}^A \mathbf{V}_c \tag{2.98}$$

$$\mathbf{I}_n^B = \mathbf{Y}_{nn}^B \mathbf{V}_n^B + \mathbf{Y}_{np}^B \mathbf{V}_p + \mathbf{Y}_{nc}^B \mathbf{V}_c \tag{2.99}$$

$$\mathbf{I}_p = \mathbf{Y}_{pn}^A \mathbf{V}_n^A + \mathbf{Y}_{pp}^A \mathbf{V}_p + \mathbf{Y}_{pc}^A \mathbf{V}_c + \mathbf{Y}_{pn}^B \mathbf{V}_n^B + \mathbf{Y}_{pp}^B \mathbf{V}_p + \mathbf{Y}_{pc}^B \mathbf{V}_c \tag{2.100}$$

$$-\mathbf{Y}_{cn}^A \mathbf{V}_n^A - \mathbf{Y}_{cp}^A \mathbf{V}_p + \mathbf{Y}_{cc}^A \mathbf{V}_c = \mathbf{Y}_{cn}^B \mathbf{V}_n^B + \mathbf{Y}_{cp}^B \mathbf{V}_p + \mathbf{Y}_{cc}^B \mathbf{V}_c \tag{2.101}$$

From the equation (2.101) it is possible to derive $\mathbf{V}_c$ obtaining

$$\begin{aligned} \left(\mathbf{Y}_{cc}^A + \mathbf{Y}_{cc}^B\right)\mathbf{V}_c &= -\left(\mathbf{Y}_{cn}^A \mathbf{V}_n^A + \mathbf{Y}_{cn}^B \mathbf{V}_n^B + \left(\mathbf{Y}_{cp}^A + \mathbf{Y}_{cp}^B\right)\mathbf{V}_p\right) \\ \mathbf{V}_c &= -\mathbf{Z}\,\mathbf{Y}_{cn}^A \mathbf{V}_n^A - \mathbf{Z}\,\mathbf{Y}_{cn}^B \mathbf{V}_n^B - \mathbf{Z}\left(\mathbf{Y}_{cp}^A + \mathbf{Y}_{cp}^B\right)\mathbf{V}_p \end{aligned} \tag{2.102}$$

where

$$\mathbf{Z} = \left(\mathbf{Y}_{cc}^A + \mathbf{Y}_{cc}^B\right)^{-1} \tag{2.103}$$

Then, introducing (2.102) with (2.103) into (2.98)-(2.100), the following final equations are obtained:

$$\mathbf{I}_n^A = \left(\mathbf{Y}_{nn}^A - \mathbf{Y}_{nc}^A \mathbf{Z}\,\mathbf{Y}_{cn}^A\right)\mathbf{V}_n^A + \left(-\mathbf{Y}_{nc}^A \mathbf{Z}\,\mathbf{Y}_{cn}^B\right)\mathbf{V}_n^B + \left(\mathbf{Y}_{np}^A - \mathbf{Y}_{nc}^A \mathbf{Z}\left(\mathbf{Y}_{cp}^A + \mathbf{Y}_{cp}^B\right)\right)\mathbf{V}_p \tag{2.104}$$

$$\mathbf{I}_n^B = \left(-\mathbf{Y}_{nc}^B \mathbf{Z}\,\mathbf{Y}_{cn}^A\right)\mathbf{V}_n^A + \left(\mathbf{Y}_{nn}^B - \mathbf{Y}_{nc}^B \mathbf{Z}\,\mathbf{Y}_{cn}^B\right)\mathbf{V}_n^B + \left(\mathbf{Y}_{np}^B - \mathbf{Y}_{nc}^B \mathbf{Z}\left(\mathbf{Y}_{cp}^A + \mathbf{Y}_{cp}^B\right)\right)\mathbf{V}_p \tag{2.105}$$

$$\begin{aligned} \mathbf{I}_p = &\left(\mathbf{Y}_{pn}^A - \left(\mathbf{Y}_{pc}^A + \mathbf{Y}_{pc}^B\right)\mathbf{Z}\,\mathbf{Y}_{cn}^A\right)\mathbf{V}_n^A + \left(\mathbf{Y}_{pn}^B - \left(\mathbf{Y}_{pc}^A + \mathbf{Y}_{pc}^B\right)\mathbf{Z}\,\mathbf{Y}_{cn}^B\right) \\ &+ \left(\left(\mathbf{Y}_{pp}^A + \mathbf{Y}_{pp}^B\right) - \left(\mathbf{Y}_{pc}^A + \mathbf{Y}_{pc}^B\right)\mathbf{Z}\left(\mathbf{Y}_{cp}^A + \mathbf{Y}_{cp}^B\right)\right)\mathbf{V}_p \end{aligned} \tag{2.106}$$

Moreover, by using the symmetry properties of the GAMs blocks, the (2.104)-(2.106) can be easily written in matrix form

$$\begin{bmatrix}\mathbf{I}_{\mathrm{n}}^{\mathrm{A}}\\ \mathbf{I}_{\mathrm{n}}^{\mathrm{B}}\\ \mathbf{I}_{\mathrm{p}}\end{bmatrix}=\left(\begin{bmatrix}\mathbf{Y}_{\mathrm{nn}}^{\mathrm{A}} & 0 & \mathbf{Y}_{\mathrm{np}}^{\mathrm{A}}\\ 0 & \mathbf{Y}_{\mathrm{nn}}^{\mathrm{B}} & 0\\ \left(\mathbf{Y}_{\mathrm{np}}^{\mathrm{A}}\right)^{T} & 0 & \mathbf{Y}_{\mathrm{pp}}^{\mathrm{A}}+\mathbf{Y}_{\mathrm{pp}}^{\mathrm{B}}\end{bmatrix}-\begin{bmatrix}\mathbf{Y}_{\mathrm{nc}}^{\mathrm{A}}\\ \mathbf{Y}_{\mathrm{nc}}^{\mathrm{B}}\\ \mathbf{Y}_{\mathrm{pc}}^{\mathrm{A}}+\mathbf{Y}_{\mathrm{pc}}^{\mathrm{B}}\end{bmatrix}\mathbf{Z}\begin{bmatrix}\mathbf{Y}_{\mathrm{nc}}^{\mathrm{A}}\\ \mathbf{Y}_{\mathrm{nc}}^{\mathrm{B}}\\ \mathbf{Y}_{\mathrm{pc}}^{\mathrm{A}}+\mathbf{Y}_{\mathrm{pc}}^{\mathrm{B}}\end{bmatrix}^{T}\right)\begin{bmatrix}\mathbf{V}_{\mathrm{n}}^{\mathrm{A}}\\ \mathbf{V}_{\mathrm{n}}^{\mathrm{B}}\\ \mathbf{V}_{\mathrm{p}}\end{bmatrix} \tag{2.107}$$

Finally, after cascading all the blocks, the scattering parameters are retrieved from the final Y-matrix by using the standard matrix transformation involving the characteristic impedances of the terminal waveguide modes

$$\mathbf{S}=\left(\mathbf{Y}_0+\mathbf{Y}_{\mathrm{TOT}}\right)^{-1}\left(\mathbf{Y}_0-\mathbf{Y}_{\mathrm{TOT}}\right) \tag{2.108}$$

where

$$Y_{0_{TE_{mn}}}=\frac{1}{Z_{0_{TE_{mn}}}}=\frac{\gamma_{mn}}{j\eta k}\qquad Y_{0_{TE_{mn}}}=\frac{1}{Z_{0_{TE_{mn}}}}=\frac{\gamma_{mn}}{j\eta k}\qquad Y_{0_{TEM}}=\frac{1}{Z_{0_{TEM}}}=\frac{1}{\frac{\eta}{2\pi}\ln\frac{R_e}{R_i}} \tag{2.109}$$

$$\gamma_{mn}=\sqrt{\kappa_{mn}^2-k^2}\qquad \eta=\frac{\eta_0}{\sqrt{\varepsilon'-j\varepsilon''}}\qquad k=k_0\sqrt{\varepsilon'-j\varepsilon''} \tag{2.110}$$

In the previous formulas, κ_{mn} is the cut-off wavenumber of the *mn*th mode of the desired terminal port, while η_0 and k_0 are respectively the characteristic impedance and the wavenumber of the vacuum.

Bibliography

[1] S. Battistutta, M. Bozzi, M. Bressan and L. Perregrini, "Analysis of Dielectric-Loaded Waveguide Filters by the Generalized BI-RME Method," *2018 48th European Microwave Conference (EuMC)*, Madrid, Spain, Sept. 23–28, 2018.

[2] S. Battistutta, M. Bozzi, M. Bressan and L. Perregrini, "Analysis of Inhomogeneous Waveguide Components by the BI-RME Method," *XXII Riunione Nazionale di Elettromagnetismo (XXII RiNEm)*, Cagliari, Italy, Sept. 03-06, 2018.

[3] S. Battistutta, M. Bozzi, M. Bressan and L. Perregrini, "Generalized BI-RME Method applied to the Analysis of Dielectric-Loaded Waveguide Components," *2018 IEEE MTT-S International Conference on Numerical Electromagnetic and Multiphysics Modeling and Optimization for RF, Microwave, and Terahertz Applications (NEMO)*, Reykjavik, Iceland, Aug. 08-10, 2018.

[4] S. Battistutta, M. Bozzi, M. Bressan and L. Perregrini, "Analysis of a Matched Turnstile Junction by the BI-RME Method and the Segmentation Technique," *2018 Baltic URSI Symposium (URSI)*, Poznań, Poland, May 15–17, 2018.

[5] M. Bressan, S. Battistutta, M. Bozzi and L. Perregrini, "Modeling of Inhomogeneous and Lossy Waveguide Components by the Segmentation Technique Combined With the Calculation of Green's Function by Ewald's Method," *IEEE Transactions on Microwave Theory and Techniques*, vol. 66, no. 2, Feb. 2018.

[6] S. Battistutta, M. Bozzi, M. Bressan and L. Perregrini, "Extension of the BI-RME Method to the Analysis of Piecewise-Homogeneous Waveguide Components Including Arbitrarily Shaped Building Blocks," *2017 47th European Microwave Conference (EuMC)*, Nurnberg, DE, Oct. 9–12, 2017.

[7] S. Battistutta, M. Bressan, M. Bozzi and L. Perregrini, "Material Characterization Through a Full-Wave Approach Based on the BI-RME Method," *2017 IEEE MTT-S International Microwave Workshop Series on Advanced Materials and Processes for RF and THz Applications (IMWS-AMP)*, Pavia, Italy, Sep. 20-22, 2017.

[8] S. Battistutta, M. Bressan, M. Bozzi and L. Perregrini, "A Fast Numerical Technique for the Determination of Electrical Properties of Materials," *2017 IEEE MTT-S International Conference on Numerical Electromagnetic and Multiphysics Modeling and Optimization for RF, Microwave, and Terahertz Applications (NEMO)*, Sevilla, Spain, May 17-19, 2017.

[9] S. Battistutta, M. Bozzi, M. Bressan, M. Pasian and L. Perregrini, "Modeling of Inhomogeneous and Lossy Components by the BI-RME Method and the Segmentation Technique," *2016 46th European Microwave Conference (EuMC)*, London, UK, Oct. 3–7, 2016.

[10] S. Battistutta, M. Bozzi, M. Bressan, M. Pasian and L. Perregrini, "The BI-RME Method Combined with the Segmentation Technique Applied to the Modeling of 3D Components," *XXI Riunione Nazionale di Elettromagnetismo (XXI RiNEm)*, Parma, Italy, Sept. 12-14, 2016.

[11] S. Battistutta, M. Bozzi, M. Bressan, M. Pasian and L. Perregrini, "Application of the BI-RME Method to the Analysis of Piecewise-Homogeneous Waveguide Components," *2016 IEEE MTT-S International Conference on Numerical Electromagnetic and Multiphysics Modeling and Optimization for RF, Microwave, and Terahertz Applications (NEMO),* Beijing, China, July 27-29, 2016.

[12] S. Battistutta, M. Bozzi, M. Bressan, M. Pasian and L. Perregrini, "Modeling of Waveguide Components by the BI-RME Method with the Ewald Green's Function and the Segmentation Technique," *2016 IEEE MTT-S International Microwave Symposium (IMS)*, San Francisco, CA, USA, May 22 – 27, 2016.

[13] S. Rao, D. Wilton and A. Glisson, "Electromagnetic scattering by surfaces of arbitrary shape," *IEEE Trans. on Antennas and Propagation*, vol. AP-30, no. 3, May 1982.

[14] G. Conciauro, M. Guglielmi, and R. Sorrentino, *Advanced Modal Analysis. CAD Techniques for Waveguide Components and Filters*, J. Wiley, 2000.

[15] M. Bressan, L. Perregrini and E. Regini, "BI-RME modeling of 3D waveguide components enhanced by the Ewald technique," *IEEE International Microwave Symposium (MTT-S 2000)*, June 11-16, 2000.

[16] P. P. Ewald, "Die Berechnung optisher und electrostatishen Gitterpotentiale", *Ann. Phys.*, vol. 64, 1921.

[17] T.F. Eibert, J.L. Volakis, D.R. Wilton, and D.R. Jackson, "Hybrid FE/BI modeling of 3-D doubly periodic structures utilizing triangular prismatic elements and MPIE formulation accelerated by the Ewald transformation," *IEEE Trans. on Antennas and Propagation*, vol. 47, no. 5, May 1999.

[18] Y. Yu and C. H. Chan, "Efficient hybrib spatial and spectral techniques in analyzing planar periodic structures with nonuniform discretizations," *IEEE Trans. on Microwave Theory and Techniques*, vol. MTT 48, no. 10, Oct. 2000.

[19] K. E. Jordan, G. R. Richter, and P. Sheng "An efficient numerical evaluation of the Green's function for the Helmholtz operator on periodic structures", *Journal of Computational Physics*, vol. 63, no. 1, Mar. 1986.

[20] F. Capolino, D. R. Wilton, and W. A. Johnson, "Efficient computation of the 2D Green's function for 1D periodic layered structures using the Ewald method", *IEEE Antennas and Propagation Society International Symposium*, vol. 1, Jun. 16-21, 2002.

[21] G. Lovat, P. Burghignoli, and R. Araneo, "Efficient evaluation of the 3-D periodic Green's function through the Ewald method," *IEEE Trans. on Microwave Theory and Techniques*, vol. 56, no. 9, Nov. 2009.

[22] M. J. Park and S. Nam, "Rapid summation of the Green's function in the shielded planar structures", *IEEE Microwave and Guided Wave Letters*, vol. 7, no. 10, Oct. 1997.

[23] M. J. Park, J. Park, and S. Nam, "Efficient calculation of the Green's function for the rectangular cavity", *IEEE Microwave and Guided Waves Letters*, vol. 8, no. 3, Mar. 1998.

[24] M. J. Park and S. Nam, "Rapid summation of the Green's function for the rectangular waveguide," *IEEE Trans. on Microwave Theory and Techniques*, vol. 46, no. 12, Dec. 1998.

[25] A. Borji and S. Safavi-Naeini, "Fast convergent Green's function in a rectangular enclosure," *IEEE Antennas and Propagation Society International Symposium*, vol. 4, Jun. 22-27, 2003.

[26] F. J. P. Soler, F. D. Q. Pereira, D. C. Rebenaque, A. A. Melcon, and J. R. Mosig, "A novel efficient technique for the calculation of the Green's functions in rectangular waveguides based on accelerated series decomposition," *IEEE Trans. on Antennas and Propagation*, vol. 56, no. 10, Oct. 2008.

[27] F. Mira Perez, M. Bressan, G. Conciauro, B. Gimeno, and V. Boria "State-space/integral-equation method for fast s-domain modelling of rectangular waveguides with cylindrically-symmetric metal insets", *IEEE Trans. on Microwave Theory and Techniques*, vol. 53, no. 4, Apr. 2005.

[28] P. Arcioni, M. Bozzi, M. Bressan and L. Perregrini, "A Novel CAD Tool for the Wideband Modeling of 3D Waveguide Components," *International Journal of RF and Microwave Computer–Aided Engineering*, vol. 10, no. 3, May 2000.

[29] J. Van Bladel, *Electromagnetic Fields*, Publishing Corporation, 1985.

[30] A. Borji and S. Safavi-Naeini, "Rapid calculation of the Green's function in a rectangular enclosure with application to conductor loaded cavity resonators," *IEEE Trans. on Microwave Theory and Techniques*, vol. 52, no. 7, Jul. 2004.

[31] A. Kustepeli and A.Q. Martin, "On the splitting parameter in the Ewald method", *IEEE Microwave Guided Wave Lett.,* vol. 10, no. 5, May 2000.

[32] M. Bozzi, L. Perregrini and K. Wu, "Modeling of Conductor, Dielectric and Radiation Losses in Substrate Integrated Waveguide by the Boundary Integral-Resonant Mode Expansion Method," *IEEE Trans. on Microwave Theory and Techniques*, vol. 56, no. 12, Dec 2008.

[33] D.R. Wilton, S.M. Rao, A.W. Glisson, D.H. Schaubert, O.M. Al-Bundak, and C.M. Butler, "Potential integrals for uniform and linear source distributions on polygonal and polyhedral domains", *IEEE Trans. Antennas Propagation*, vol. 32, no. 3, Mar. 1984

[34] P. Arcioni, M. Bressan, and L. Perregrini, "On the evaluation of the double surface integrals arising in the application of the boundary integral method to 3-D problems", *IEEE Trans. on Microwave Theory and Techniques*, vol. 45, no. 3, Mar. 1997.

[35] G. Conciauro, *Introduzione alle onde elettromagnetiche*, McGraw-Hill, Milano 1993.

[36] P. Arcioni and G. Conciauro, "Combination of generalized admittance matrices in the form of pole-expansions," *IEEE Trans. on Microwave Theory and Techniques*, vol. 47, no. 10, Oct. 1999.

Chapter 3
Numerical Considerations

In this Chapter, some numerical considerations are provided in order to explain the influence of the segmentation and meshing phase, as well as the parameters of the BI-RME solver, on the accuracy of the results and on the general algorithm performances. In particular, the effects of the BI-RME parameters are tested on a very simple structure for a given segmentation and mesh.

Despite the goodness of the results shown in the next chapter, it is right to make some considerations about the implementation of the Generalized BI-RME algorithm. The proposed numerical method has been implemented in MATLAB language with the BI-RME solver written in FORTRAN language and compile. Moreover, for the pre-processing phase, a third-party software and an *ad hoc* MATLAB tool are used. Starting to talk about the pre-processing, this phase requires, obviously, the interaction with the user to segment and mesh the structure, and to create the input file. Nevertheless the importance of this part is focused on how the circuit is segmented and meshed, a good feature not yet implemented could be an automatic segmentation and mesh refinement base on the field intensity, like what done by the commercial software (like ANSYS HFSS). In this way could be possible to reduce the human error. Another point on which it is possible to gain a lot in terms of memory usage, computational effort, data reusability, and time is the integration inside a unique software with the same language (i.e. C++) of both the MATLAB pre and post-processing parts and the electromagnetic solver. As mentioned, actually the adopted strategy uses three different tools to compose the algorithm with exchange of files between them. In particular, for the BI-RME analysis it is necessary to write an input file for each building blocks; the BI-RME solver needs to read it, do its job, and then to write a series of output files whose content dimensions are related to the number of basis functions and modes. The files with the results of the EM analysis are then red from the post processing MATLAB tool. It is universally known that the reading and writing of textual files is time consuming: obviously, this strategy is good in a development and debug phase where it is necessary to separate the single tasks, but not for and operative or commercial phase. Furthermore, also the pre and post-processing tools are still written with a development and debug purpose: so, there are some operations executed over the building blocks or the mesh elements that are intentionally done not in the most efficient way in order to gain in terms of an easier operation in presence of problems or to add new features. Finally, the frequency-by-frequency circuital cascade is an easy but not efficient approach to combine the results: so, it is suggested especially for a limited number of frequency points. On the other side, the use of a frequency-independent algorithm on the line of what done in the past is justified for a huge number of frequency points. In particular, it involves the solution of an N-1 eigenvalue problems (N is equal to the total

number of building blocks) whose dimension is dictated by the resonant modes and by the basis functions.

3.1 General considerations about segmentation, mesh and BI-RME parameters

Segmentation

For some methods, it is a fundamental step, for other ones not so much important... for the Generalized BI-RME method the segmentation phase represent the first key aspect. As explained in the pre-processing sub-section, in order to reduce the computational effort, it is better to have a segmentation with, as much as possible, "boxed" building blocks (rectangular parallelepiped shape) respect the "arbitrarily" ones. In this way, it is possible to employ the simplify version of the BI-RME solver by avoiding the EFIE solution. Moreover, it is needful to choose the right position and number of building blocks. To explain this aspect, it is better to refer to the tee-junction reported in Fig. 3.1, where are proposed three possible segmentations with them meshes. The segmentation into 4 building blocks proposed in Fig. 3.1*a* allows reducing the volume of each building block thus reducing the computational time for the volumetric modes calculation during the BI-RME analyze. However, the proposed mesh has the greater number of triangles (708) respect the other two (it has been used the same mesh step) and this requires more time for the computation of the Green's functions, the integrals, and, then, for the cascade process because the matrices dimensions are linked with the number of basis functions. So, the benefits of the volume reduction are drastically overcome by the necessity of more triangles. The segmentation into 3 building blocks proposed in Fig. 3.1*b* represents an initial good trade-off between volume and triangles (590): so, at first glance, it may seem the right choice. In practice, if the building block shape is the boxed one, the volumetric modes calculation is trivial since they are obtained with analytical formulas. Therefore, it is better to try to reduce one more time the number of triangles especially to speed-up the circuital cascade because it is executed frequency-by-frequency. In case of a huge number of frequency point, the time spent for the cascade process will overcame the one for the Green's functions and for the integrals. Finally, the segmentation into 2 building blocks proposed in Fig. 3.1*c* represents the best trade-off between volume and triangles (472). Moreover, it is suggested to avoid the segmentation in which parts of the circuits where the field has a huge intensity of it manifests a strong or fast variation. For example, in Fig. 3.2 is proposed a bad segmentation: in fact, the segmentation is not wrong but it requires a very fine (and expensive on the computational and memory point of view) mesh. To conclude the speech about the segmentation, it is not possible to reduce the volume keeping fixed the mesh step and the number of volumetric modes because this produce a loss in the accuracy. On the other hand, it is not convenient to reduce the blocks size to something near a "pixel" because it requires to increase the number of volumetric modes and to reduce the mesh step; moreover, this will raise the computational time for the cascade process. The last consideration about the segmentation is linked to a possible upgrade of the algorithm: having building blocks with the same shape and volume will help to save a lot of time for the EM analysis in case of block reusability (this requires also to have the same mesh or to know how map different meshes).

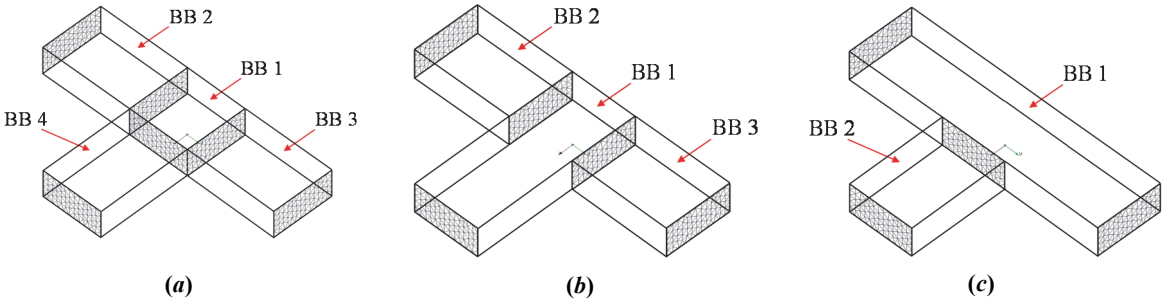

Fig. 3.1. Three possible segmentation, with their meshes, for a tee-junction.

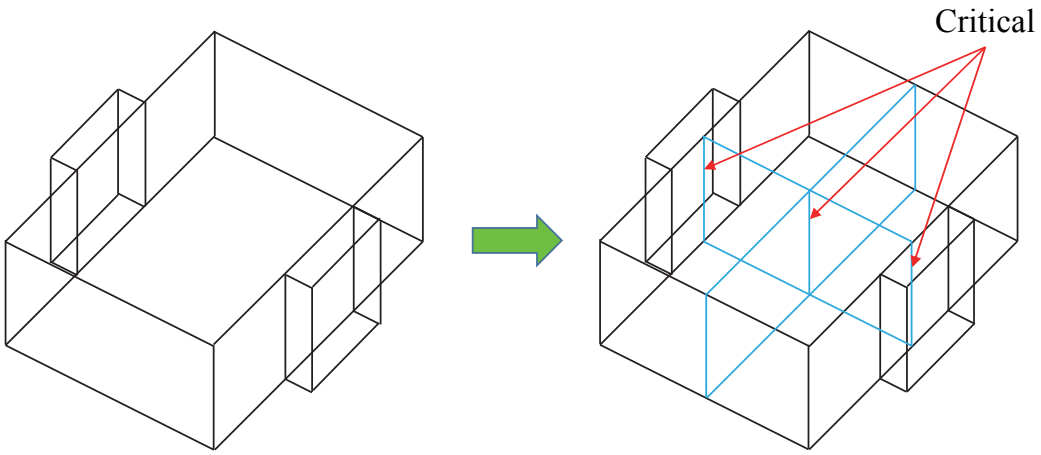

Fig. 3.2. Example of not optimal segmentation.

Mesh

In general, the mesh is the most important factor: if the mesh is underestimate (especially on the external ports) the fields representation will result not appropriate even with all the other parameters set to the best values. As previously mentioned, a good rule of thumb is to have a basic dimension for the triangle edges equal to or lower than a one over ten wavelength at the highest interested frequency. In fact, the proposed formula was

$$\frac{\lambda_0}{10\sqrt{\varepsilon'}} = \frac{c_0 / f_{\max}}{10\sqrt{\varepsilon'}}$$

This length needs to be tuned based on the particular situation or building block shape since it has not been implemented jet an automated mesh refinement tool like the one proposed by the commercial software ANSYS HFSS. For example, by considering the segmentation of Fig. 3.2, since the blocks are jointed in a critical point in terms of field variation and intensity, it is necessary to use a finer mesh. Another common situation is when the building block dimensions are lower than the starting mesh step or with it is not possible to well represent the field's variation on the block surfaces. On the other hand, if a block is placed in a circuit point where the fields are negligible, it is possible to relax the mesh step by choosing an edge length greater than what suggested. By talking about the mesh type, the shape of the elements is blocked in the Generalized BI-RME method by the type of basis functions that will be defined on it; moreover, the triangular shape is optimal for surface mashes to well represent the block shape. GiD lets to create "Structured" and "Unstructured" but, to randomize the error on the discretization of a continue quantity (i.e., a surface current) it is suggested to use an unstructured mesh.

Parameters of the BI-RME solver

Even if the mesh has a crucial impact on the accuracy of the results, it is possible to tune some parameters of the BI-RME solver to balance the accuracy and the computational effort:

- Accuracy factor (*ACC* - ξ): it is the value that, multiply to the maximum frequency of interest (via k_0), extends the modal series in order to obtain a better precision on the desired frequency range. The accuracy of the modal series increased with the value of ACC but this requires more time for the BI-RME analysis as well as for the determination of the GAMs.
- Precision of the Green's functions (*FdG*): it represents the number of significant digits after dot for the truncation of the Green's functions approximation. More digits implies more precision but this requires more time for the BI-RME analysis; as results of some previous experiments, the precision variations become less appreciable after 4 digits.
- Order of the "Gaussian" integration rules (*IRU*): the "Gauss" method is a polynomial interpolation method where the function is interpolated by a polynomial that must be integrated exactly. To each *IRU* value is associated a number of points (that are internal to each triangle) by which is possible to integrate exactly a polynomial whose order is equal to the *IRU* value. The accuracy of the numerical solution of the integrals will increase considerably with the IRU value but the time requires by the BI-RME analysis will increase dramatically with the square of the number of points dictated by the IRU

IRU	1	2	3	4	5	6	7	8	9	10
Points	1	3	4	6	7	12	13	16	19	25

3.2 Effects of the BI-RME parameters

In this sub-section are reported the results obtained testing the effects of the BI-RME solver parameters: in particular, the attention is focused on the frequency error for a very simple structure analyzed taking fixed the segmentation and mesh. The structure considered is a WR-90 waveguide with a dielectric block positioned at the center of the cross section of the structure (Fig. 3.3). The dielectric block has a relative dielectric constant $\varepsilon_r = 10$ and a loss tangent of $tan\delta = 0.001$, while its shape is cubic ("boxed"). The component is subdivided into 7 building blocks (Fig. 3.4*a*) and, in Fig. 3.4*b*, is reported the adopted unstructured mesh with about 2450 triangles.

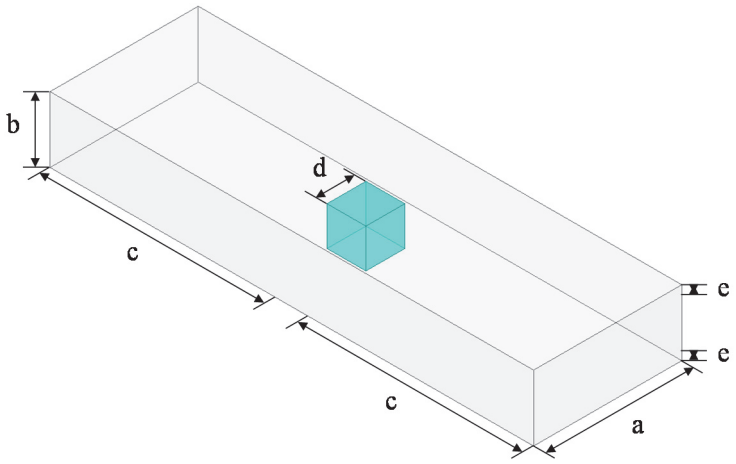

Quantity	Length [mm]
a	22.86
b	10.16
c	34.29
d	6
e	2.08

Fig. 3.3. WR-90 waveguide with dielectric block used to test the BI-RME solver parameters.

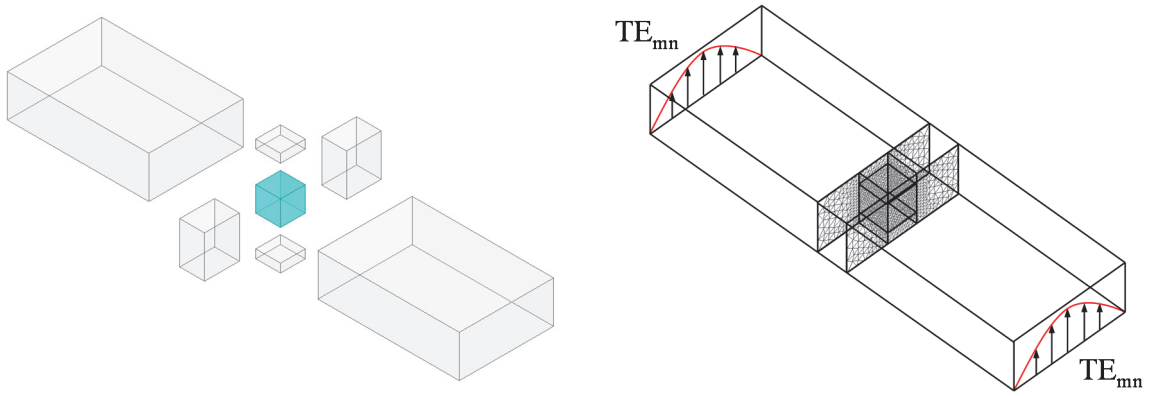

(*a*) (*b*)

Fig. 3.4. WR-90 waveguide with dielectric block used to test the BI-RME solver parameters: (*a*) Segmentation into building blocks; (*b*) The adopted mesh.

This structure has been analyzed with all the BI-RME solver parameters combination inside the following ranges:

- IRU range: from 2 to 7 with a step width of 1;
- ACC range: from 2 to 8 with a step width of 0.5.

For what concerning the number of digits after dot for the Green's functions, based on some tests done in the past on other WR-90 circuits, after 4 digits the results was practically the same: so, this value has been used for the proposed test.

In the following graphs are reported the frequency errors obtained by comparing the resonance frequency of the reference (obtained with ANSYS HFSS) with the ones obtained by analyzing the proposed structure with the Generalized BI-RME method. In particular, it is evaluated the relative frequency error (%) for each Gaussian integration rule (IRU) as function of the accuracy parameter (ACC) for the extension of the modal series calculation (Fig. 3.5). Moreover, it is evaluated also the mean times for the single frequency point (Fig. 3.6), and the mean times for the BI-RME analysis of each building block (Fig. 3.7).

By analyzing the reported data in Fig. 3.5, it is clear that the relative frequency error percentage decrease with a monotone behavior as the accuracy factor for the modal series extension increases. In this sense, after an accuracy factor of 5, there's no more gain in terms of error reduction due to the increasing of modes. The only way to experience an error reduction after this value is to increase the integration rule. The unusual behavior for the ACC = 2.5 can be due to different reasons. First, also the reference is obtained with a numerical method: so, also it could suffer of convergence issues. Another aspect could be the error due to the frequency discretization of both results. To reduce the error after an accuracy factor of 5, it is possible to choose a higher order integration rule. Unfortunately, by increasing the integration rule, the mean time required by the BI-RME analysis increases with an important rate (Fig. 3.7): this behavior is justified by the fact that, by increasing the integration rule, the number of points for each triangle on with the integrals are evaluated increases with a non-linear rule. Even if the BI-RME time increases also by increasing the accuracy factor, its effect is more important on the mean time for the single frequency points (Fig. 3.6) because it increases the dimension of the matrices related to the modal part of the Generalized Admittance Matrix. Therefore, for the proposed structure the best trade-off between the relative frequency error and the computational effort is obtained by choosing an accuracy factor (ACC) of 5 and a Gaussian integration rule (IRU) of 4.

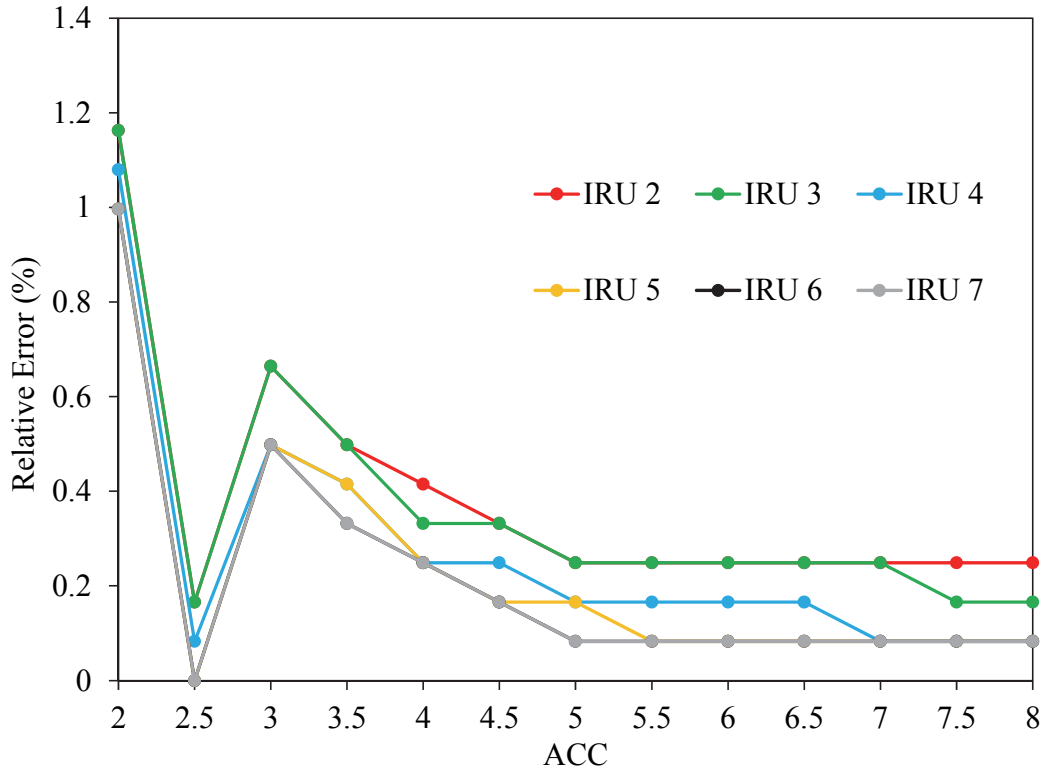

Fig. 3.5. Relative error (%): study of the influence of the Gaussian integration rules (IRU) as function of the accuracy parameter (ACC).

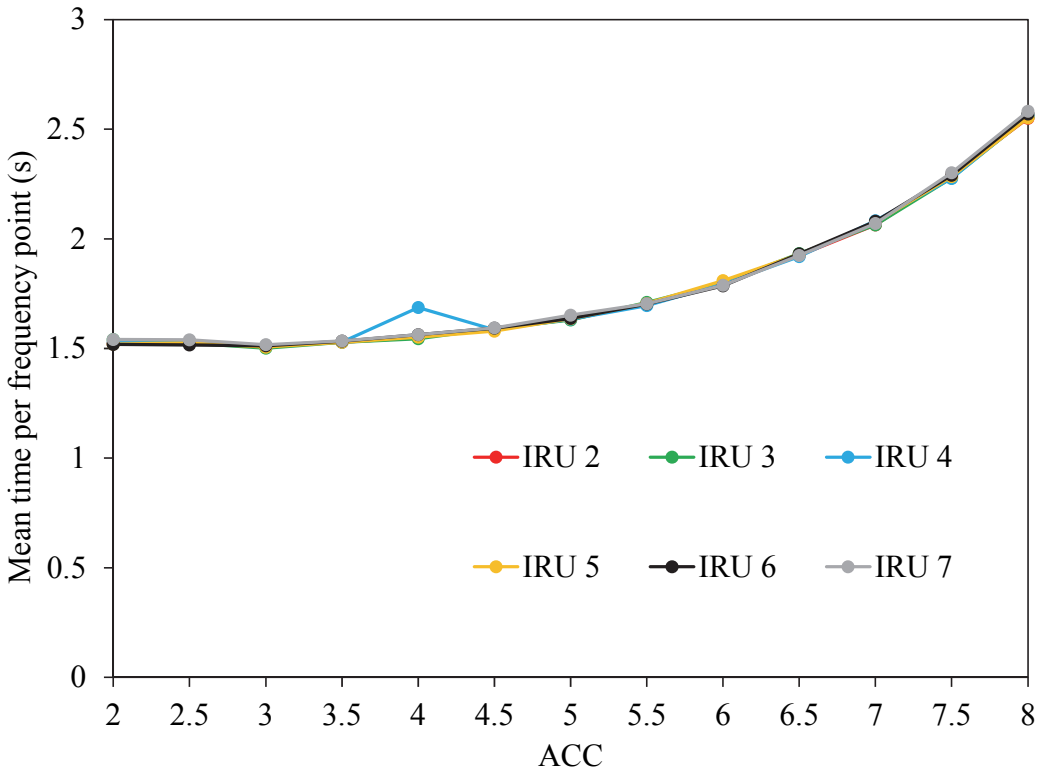

Fig. 3.6. Mean time per frequency point (s): study of the influence of the Gaussian integration rules (IRU) as function of the accuracy parameter (ACC).

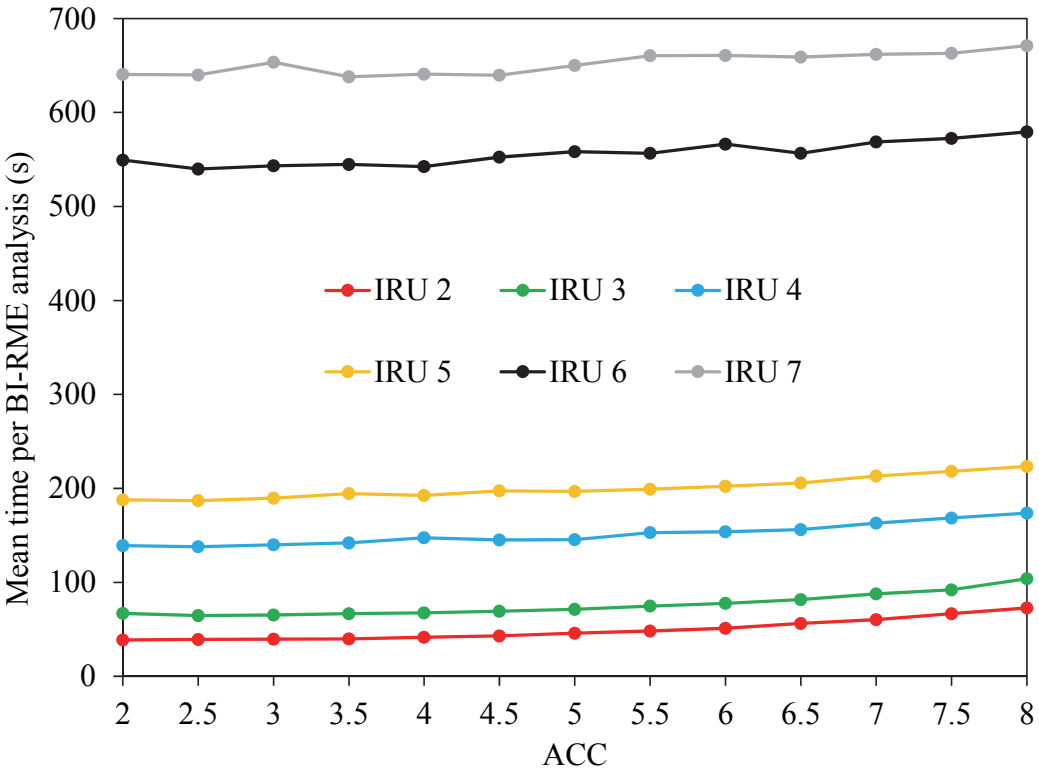

Fig. 3.7. Mean time per BI-RME analysis (s): study of the influence of the Gaussian integration rules (IRU) as function of the accuracy parameter (ACC).

Chapter 4
Examples

In this Chapter, a series of examples are presented to demonstrate the effectiveness of the proposed algorithm. All the examples are analyzed with the Generalized BI-RME method and the results are compared with the ones obtained with ANSYS HFSS. In particular, first are reported some examples of structures segmented into boxed blocks; then, the attention is focus on true arbitrarily shaped circuits. In both cases are proposed examples loaded or not with dielectric elements, with or without dielectric losses.

As already told, the reported examples have been analyzed with the proposed numerical method and, for comparison, with a commercial software implementing a FEM method (ANSYS HFSS). By definition, a numerical method allows working out a complex problem, not solvable with analytical approaches, with an approximated solution, which accuracy can always be tuned. So, even if the results are obtained by choosing the right parameters in order to have a good convergence, a little discrepancy can exist since both are numerical methods. In fact, it is not possible to determine which of the two results is the correct one: this could only be possible by comparing the numerical method solution with an exact one given by an analytical method. Moreover, a little discrepancy can be due to the fact that ANSYS HFSS implements an automatic mesh refinement system, based on the fields intensity, contrary to what is done with the Generalized BI-RME method. In particular, no mesh refinements are implemented: actually, the mesh is created by the user and it is based on their electromagnetic knowledge, on the implemented segmentation and on the nature of the component under test. Another necessary consideration is about timing and memory requirements. The Generalized BI-RME method is a homemade project still in the development phase: so, the code structure is designed to have a full control and debug capability and, typically, this is not compliant with the commercial purpose of the reference software; therefore, it is not compiled. In this sense, having a timing and memory usage equal or greater than the one of the commercial software it is not a sign of bad numerical method or implementation but it needs to be interpreted as a point on which it is possible to do better for the next upgrades. Moreover, the proposed examples are analyzed without exploiting the block reusability and the symmetries since there is no control on the mesh generation for this purpose. All timings are given as CPU time since it is the exact amount of time that the CPU has spent processing data for a specific task such as doing arithmetic and logic operations. The frequency independent times of the Generalized BI-RME method are not reported since they are almost irrelevant. The simulations were performed on a computer equipped with an Intel Core^{TM} i7 @ 3.6 GHz, 32 GB of RAM, Win 8.1.

4.1 Dual-band orthomode transducer (OMT)

The first proposed example is a dual-band orthomode transducer (OMT - Fig. 4.1*a*), taken from [1], whose results obtained with the Generalized BI-RME method have been published in [2]-[4]. The micromachining process adopted for manufacturing the OMT, which is based on Thick SU-8 Photo-Resist technology, leads to a structure with sharp edges that can be segmented into boxed building blocks without any loss of accuracy in the geometry representation. The OMT is designed to transmit the vertical polarized signal from port 1 to port 3 in the frequency band 75-82 GHz, and the horizontally polarized signal from port 2 to port 4 in the frequency band 95-105 GHz (Fig. 4.1*a*), in both cases with a return loss better than 25 dB. The rectangular waveguides are standard WR10 ($a = 2.54$ mm, $b = 1.27$ mm), and all the physical dimensions of the OMT are provided in [1]. The structure has been analyzed by the Generalized BI-RME method adopting the "boxed" thanks to the micromachining process: in particular, its geometry minimizes to 9 the number of rectangular parallelepiped shaped building blocks adopted in the segmentation phase (Fig. 4.1*b*). Two different mesh sizes have been adopted: a coarse mesh, with an average triangle dimension of about $\lambda/8$, and a fine mesh, with an average triangle dimension of about $\lambda/12$. In terms of BI-RME parameters, for the accuracy parameter ACC has been used a value of 3 while, for the quadrature Gaussian rule adopted for the integrations, a 6-point ($IRU = 4$). Fig. 4.2 shows the comparison between the simulation results obtained with the proposed algorithm and ANSYS HFSS: in particular, in Fig. 4.2*a* is detailed the behavior of the component in terms of matching on the rectangular waveguides, while, in Fig. 4.2*b*, the results obtained in terms of transmission. A very good agreement is observed over the whole frequency band, also in the case of the coarse mesh used for a quick initial study. Two components connected back-to-back (Fig. 4.1*c*) were also analyzed: in Fig. 4.3*a* is detailed the behavior of the component in terms of matching on the rectangular waveguides, while, in Fig. 4.3*b*, the results obtained in terms of transmission. Also in this case, the simulation results shown a very good agreement. In Table I and Table II are summarized the timings, while, in Table III and Table IV the maximum amounts of memory required by the ANSYS simulation and by the Generalized BI-RME method for both the structures.

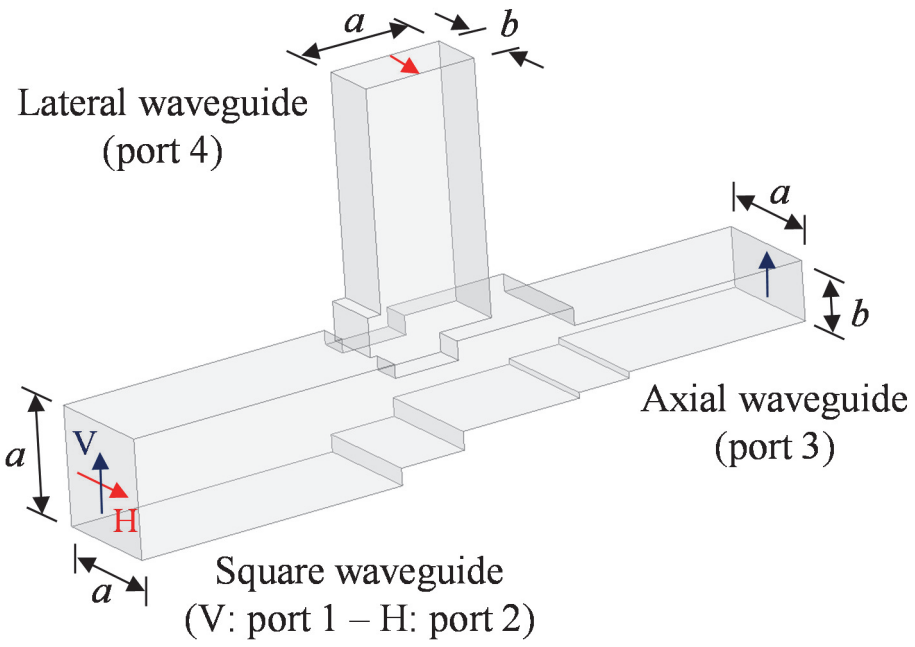

(*a*)

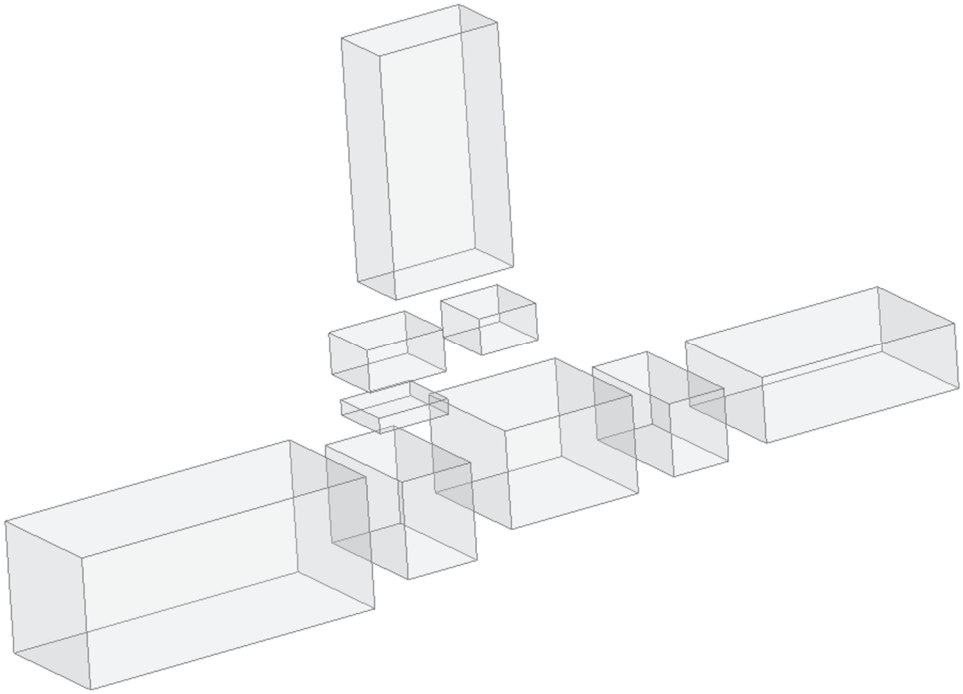

(*b*)

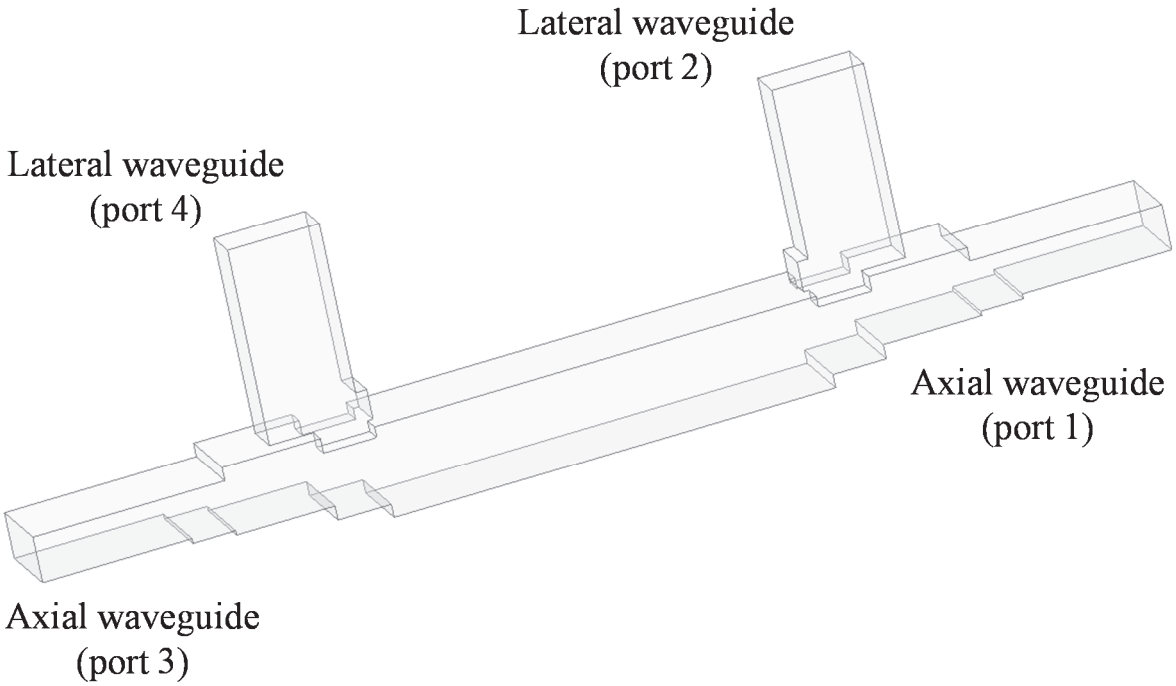

(*c*)

Fig. 4.1. The OMT proposed in [1]: (*a*) geometry of the whole structure with the port polarizations; (*b*) the component segmented into boxed building blocks: (*c*) geometry of the structure connected in back-to-back configuration.

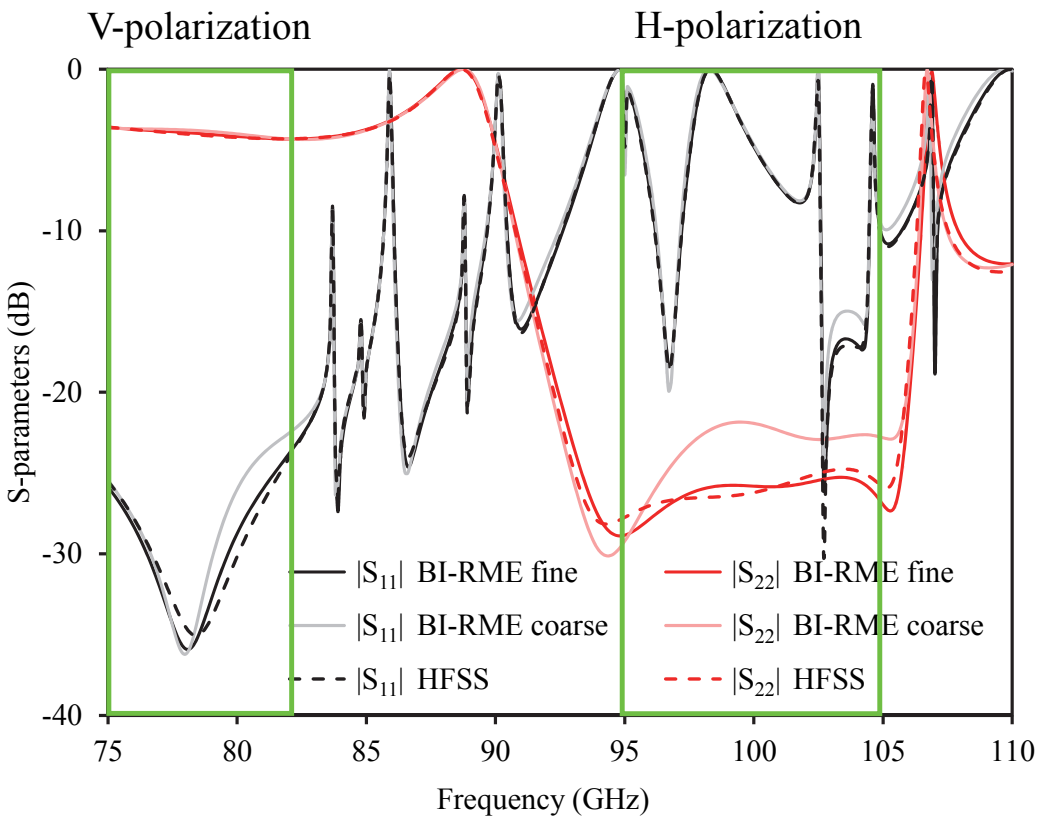

(*a*)

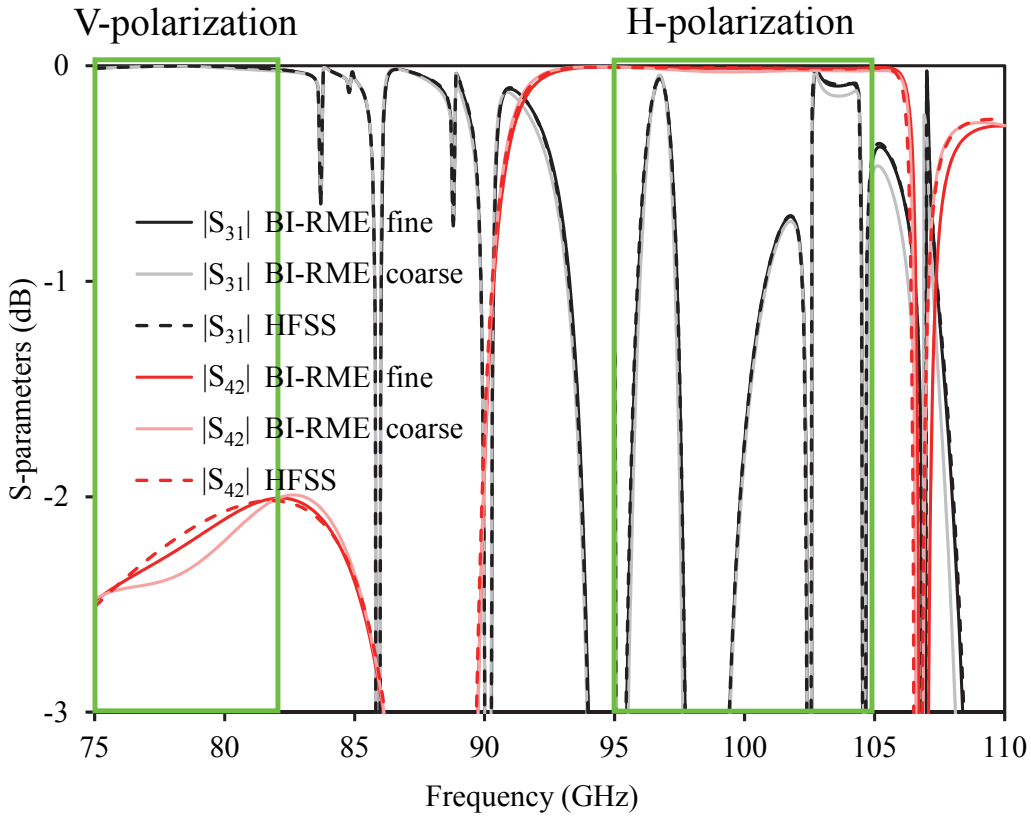

(*b*)

Fig. 4.2. Comparison of the OMT frequency response ([2]-[4]): (*a*) matching results; (*b*) transmission results.

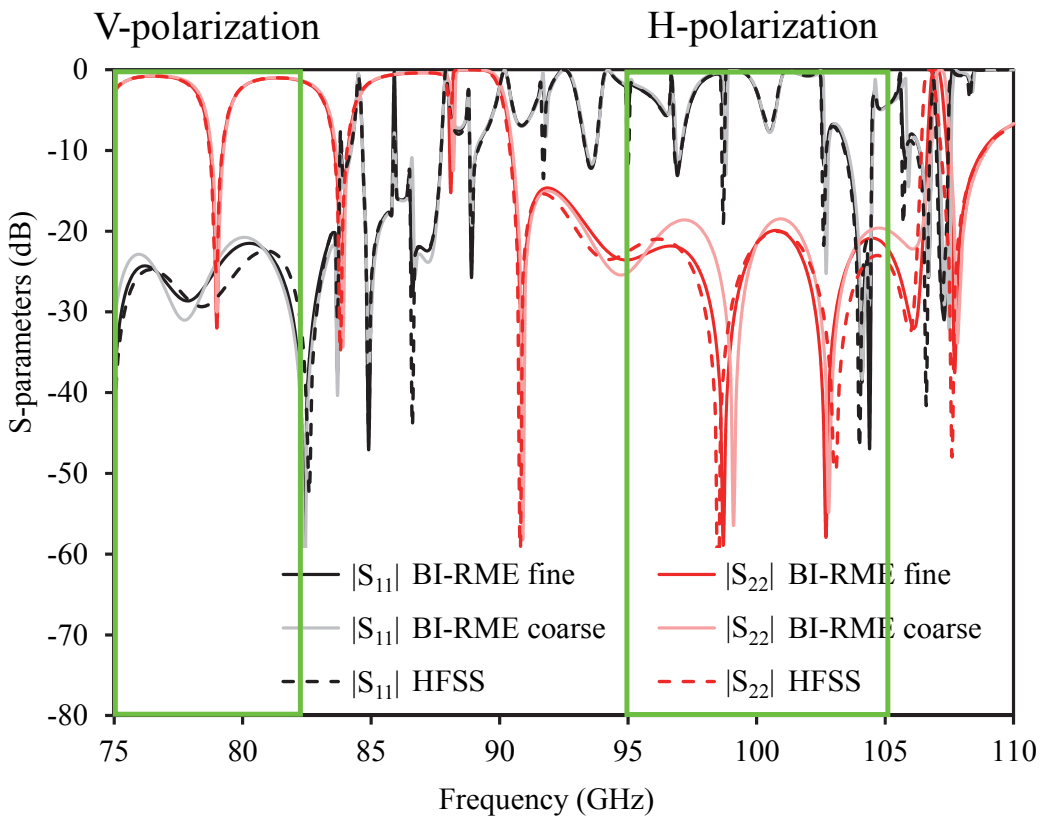

(*a*)

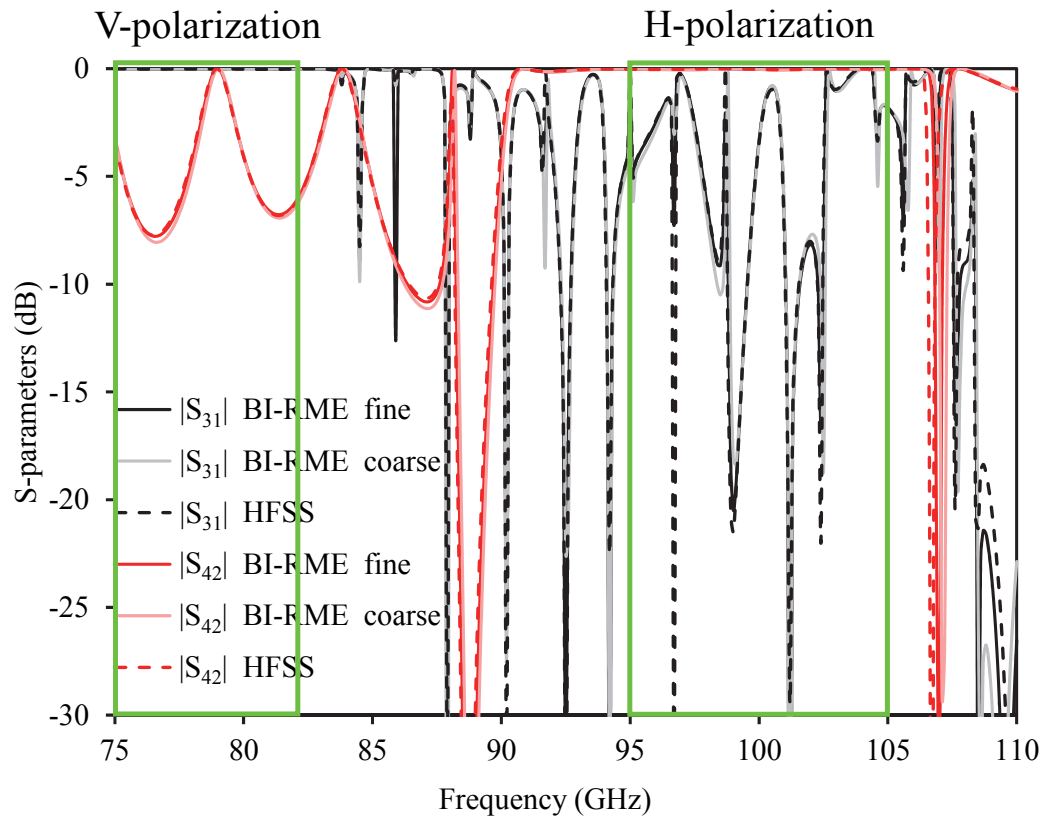

(*b*)

Fig. 4.3. Comparison of the OMT back-to-back frequency response: (*a*) matching results; (*b*) transmission results.

ANSYS HFSS	CPU Time (s)
Convergence: 15 points	500
Interpolating analysis: 70 real frequency points	6090
Total	**6590**

Generalized BI-RME method – coarse mesh	CPU Time (s)
BI-RME analysis	94
MATLAB frequency cascade: 351 frequency points	20
Total	**114**

Generalized BI-RME method – fine mesh	CPU Time (s)
BI-RME analysis	2908
MATLAB frequency cascade: 351 frequency points	389
Total	**3297**

Table I. Timing comparison for the dual-band orthomode transducer.

ANSYS HFSS	CPU Time (s)
Convergence: 15 points	469
Interpolating analysis: 70 real frequency points	9001
Total	**9470**

Generalized BI-RME method – coarse mesh	CPU Time (s)
BI-RME analysis	188
MATLAB frequency cascade: 351 frequency points	42
Total	**230**

Generalized BI-RME method – fine mesh	CPU Time (s)
BI-RME analysis	5816
MATLAB frequency cascade: 351 frequency points	827
Total	**6643**

Table II. Timing comparison for the dual-band orthomode transducer in back-to-back configuration.

ANSYS HFSS	Memory (MB)
Maximum amount	2180

Generalized BI-RME method – coarse mesh	Memory (MB)
Maximum amount	59

Generalized BI-RME method – fine mesh	Memory (MB)
Maximum amount	441

Table III. Maximum memory requirement comparison for the dual-band orthomode transducer.

ANSYS HFSS	Memory (MB)
Maximum amount	3060

Generalized BI-RME method – coarse mesh	Memory (MB)
Maximum amount	317

Generalized BI-RME method – fine mesh	Memory (MB)
Maximum amount	934

Table IV. Maximum memory requirement comparison for the dual-band orthomode transducer in back-to-back configuration.

4.2 Eight-poles eight-zeros TM dual-mode cavities filter

In this sub-section, it is proposed an eight-poles eight-zeros TM dual-mode cavities filter, originally proposed in [5], whose results obtained with the Generalized BI-RME method have been published in [6]. The filter is based on empty TM dual-mode cavities, which employ both resonant and non-resonating modes to provide reflection and transmission zeros. The overall geometry of the filter is sketched in Fig. 4.4*a*. All the dimensions are provided in [[5], Fig. 15 and Tab. II]. The filter is designed to have a passband of about 150 MHz around 10 GHz, and an out-of-band rejection of about 80 dB in the lower stop band and up to 11 GHz. Due to the large out-of-band rejection and the presence of eight transmission zeros, the analysis of this structure is particularly challenging. It is worth noting that in [5] the filter was tuned by screws after fabrication. Since the penetration of the tuning screws is not provided, and since they practically only affect the passband, the structure has been analyzed without tuning. Due to its geometry, the structure has been segmented into 19 boxes (see Fig. 4.4*b*). The interface surfaces were meshed with 1860 triangles, and overall 2790 RWG basis functions were defined. Since each cascade procedure involves only two blocks, the frequency-by-frequency matrix manipulations in (2.107) involves only a small subset of these basis functions, and the dimension of the matrix to be inverted in (2.103) is usually in the order of tens. A Gaussian integration rule with six points per triangle was used for the projection of the Green's function on the basis functions ((2.62)-(2.64)), the coefficient for the truncation of the series in (2.61) was $\xi = 4$, and the number of digits of accuracy for the calculation of the Green's function was $N_c = 4$. Fig. 4.5 shows the very good agreement between the results of the proposed method and the HFSS simulations. In the out-of-band the results agree also very well with the experimental results shown in [[5], Fig. 17], the only discrepancy in the passband being due to the absence of the tuning screws. For properly identifying the positions of the zeros, a frequency step of 4 MHz was adopted, resulting into 750 frequency points. As reported in Table V, the CPU time was about 840 s for the calculation of the quasi-static terms A_{ij}, B_{ij}, C_{ip} and k_p, and 0.116 s per frequency point for the cascading procedure. Overall, the proposed method required less than 16 minutes of CPU time, with a memory allocation of about 76 MB. As a comparison, HFSS took about one hour for the convergence and 17 minutes per frequency point with the interpolating method, which required 45 frequency points due to the uneven behavior of the filter response. The overall CPU time of HFSS was more than 10 hours, with an overall memory allocation of about 16 GB. This great amount of time was due to the imposition of a finer mesh on some critical points since the proposed one by the automatic refinement system produced a frequency shift. In Table V are summarized the timings, while, in Table VI the maximum amounts of memory required by the ANSYS simulation and by the Generalized BI-RME method for both the structures.

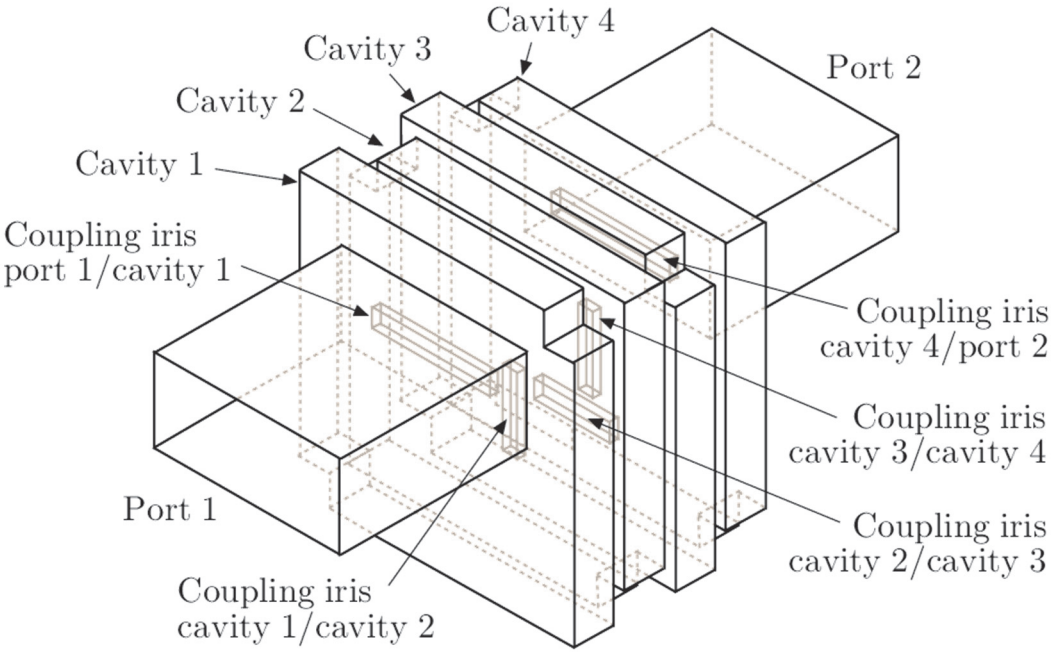

(*a*)

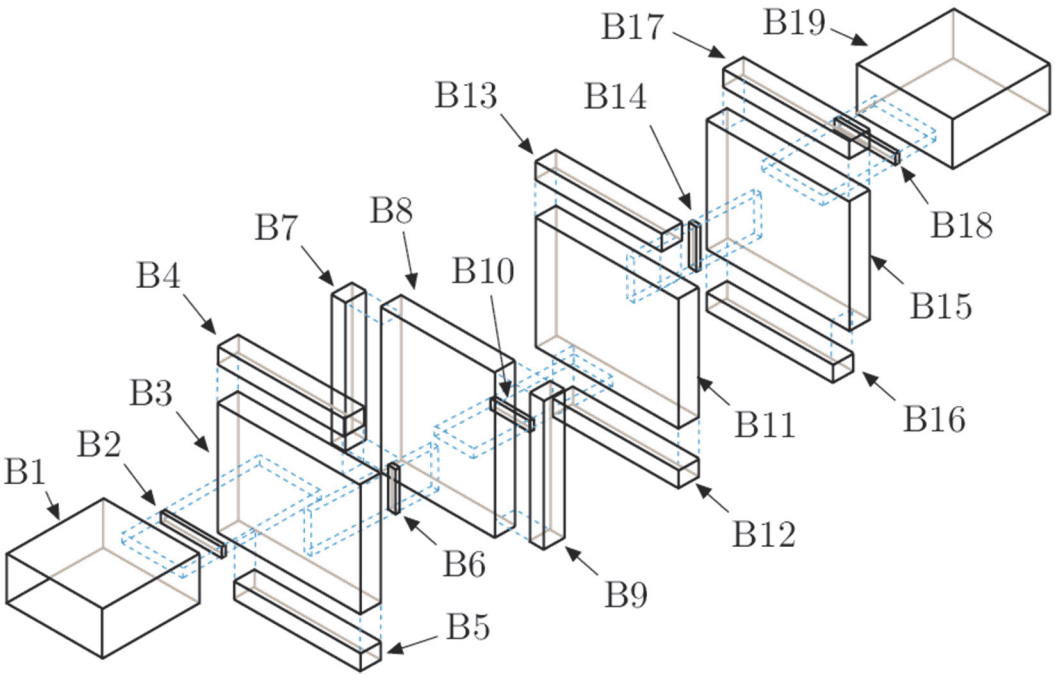

(*b*)

Fig. 4.4. Geometry of the eight-poles eight-zeros TM dual-mode cavities filter considered to validate the proposed numerical technique [5]: (*a*) Sketch of the filter geometry; (*b*) Segmentation into building blocks.

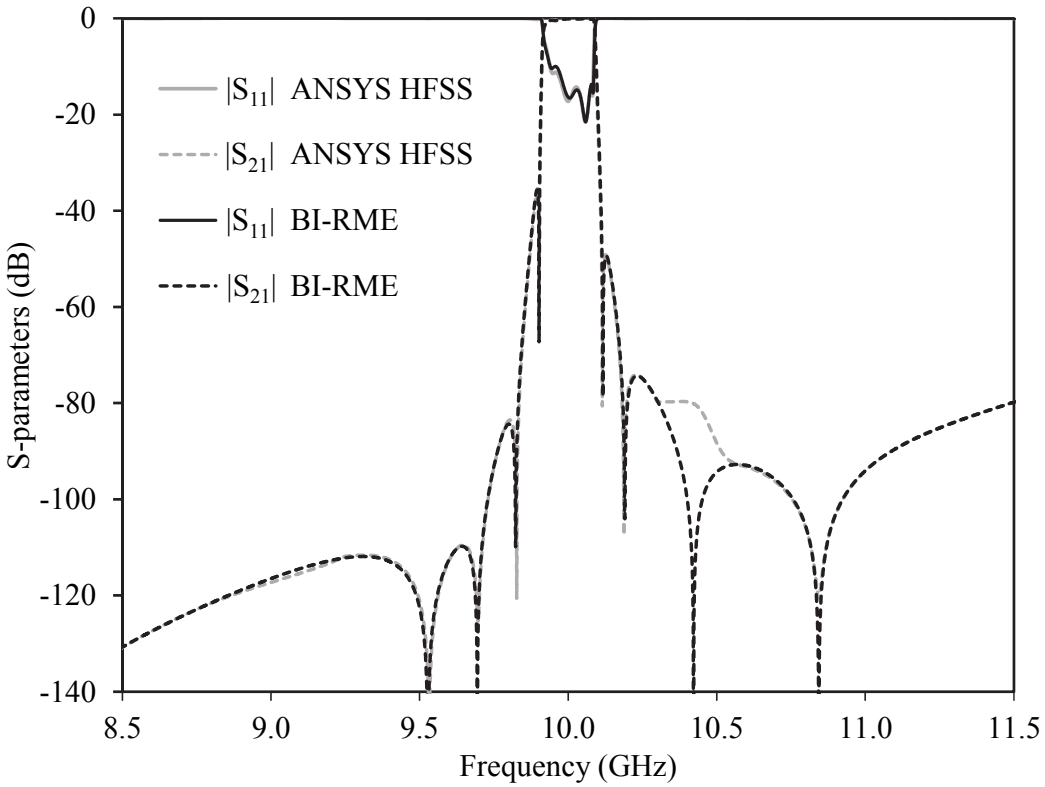

Fig. 4.5. Comparison of the frequency responses of the eight-poles eight-zeros TM dual-mode cavities filter (Fig. 4.4) between the Generalized BI-RME method and ANSYS HFSS [6].

ANSYS HFSS	CPU Time (s)
Convergence: 15 points	3529
Interpolating analysis: 45 real frequency points	38731
Total	**42260**

Generalized BI-RME method	CPU Time (s)
BI-RME analysis	842
MATLAB frequency cascade: 750 frequency points	88
Total	**930**

Table V. Timing comparison for the eight-poles eight-zeros TM dual-mode cavities filter.

ANSYS HFSS	Memory (MB)
Maximum amount	16000

Generalized BI-RME method	Memory (MB)
Maximum amount	76

Table VI. Maximum memory requirement comparison for the eight-poles eight-zeros TM dual-mode cavities filter.

4.3 WR-90 waveguide with a cubic dielectric resonator

The third example is the structure used for the study of the effects of the BI-RME parameters. In particular, it consists of a cubic dielectric resonator ($d \times d \times d$) symmetrically placed in a standard WR-90 waveguide (Fig. 4.6). The resonator has a relative dielectric constant $\varepsilon_r = 10$ and a loss tangent of $tan\delta = 0.001$. Although the geometry of this structure is simple, this component is fully three-dimensional and permits to demonstrates the capability of the code to handle piecewise homogeneous and lossy materials. The component is subdivided into 7 boxed building blocks (Fig. 4.7*a*) and, in Fig. 4.7*b*, is reported the adopted unstructured mesh with about 2450 triangles. This structure has been analyzed with a Gaussian integration rule with six points per triangle, the coefficient for the truncation of the series in (2.61) was $\xi = 5$, and the number of digits of accuracy for the calculation of the Green's function was $N_c = 4$. For properly identifying the resonance, a frequency step of 10 MHz was adopted, resulting into 401 frequency points. The comparison between the simulation results obtained using the proposed method and those obtained by ANSYS HFSS are reported in Fig. 4.8. A good agreement is observed, apart from a small frequency shift of about 0.02 GHz probably due to convergence issues, at the resonance the insertion loss estimated by the proposed technique is about 0.0242 dB, while HFSS calculated 0.0239 dB: so, pretty the same value. As reported in Table VII, the CPU time was about 920 s for the BI-RME analysis, and 1.81 s per frequency point for the cascading procedure. Overall, the proposed method required less than 28 minutes of CPU time, with a memory allocation of about 0.934 GB. As a comparison, HFSS took about half an hour for the convergence and less than 10 minutes per frequency point with the interpolating method, which required 11 frequency points. The overall CPU time of HFSS was less than 2.5 hours, with an overall memory allocation of about 5 GB. In Table VII are summarized the timings, while, in Table VIII the maximum amounts of memory required by the ANSYS simulation and by the Generalized BI-RME method for both the structures.

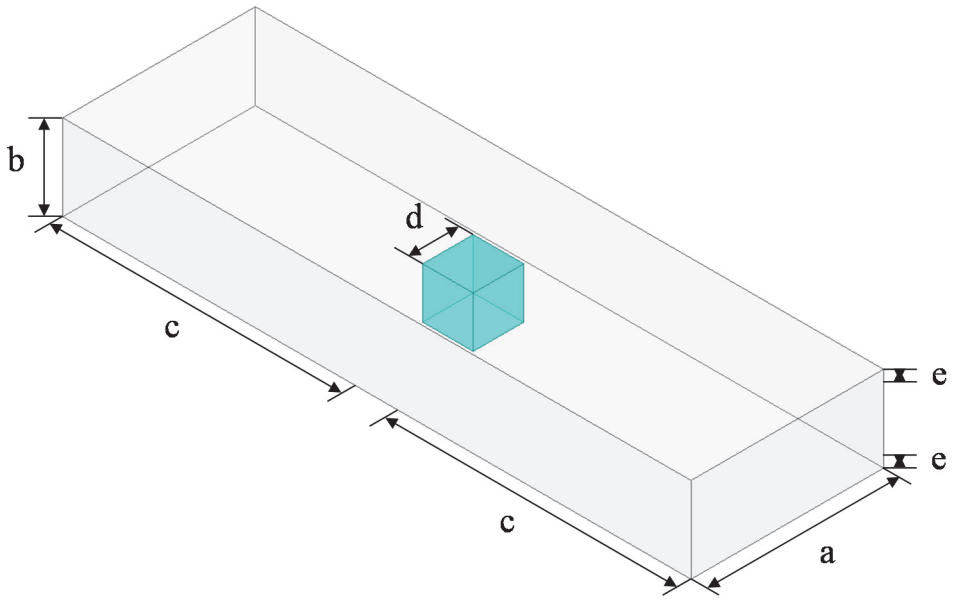

Fig. 4.6. Cubic dielectric resonator symmetrically placed in a standard WR-90 waveguide (dimensions in mm: a = 22.86, b = 10.16, c = 34.29, d = 6, e = 2.08).

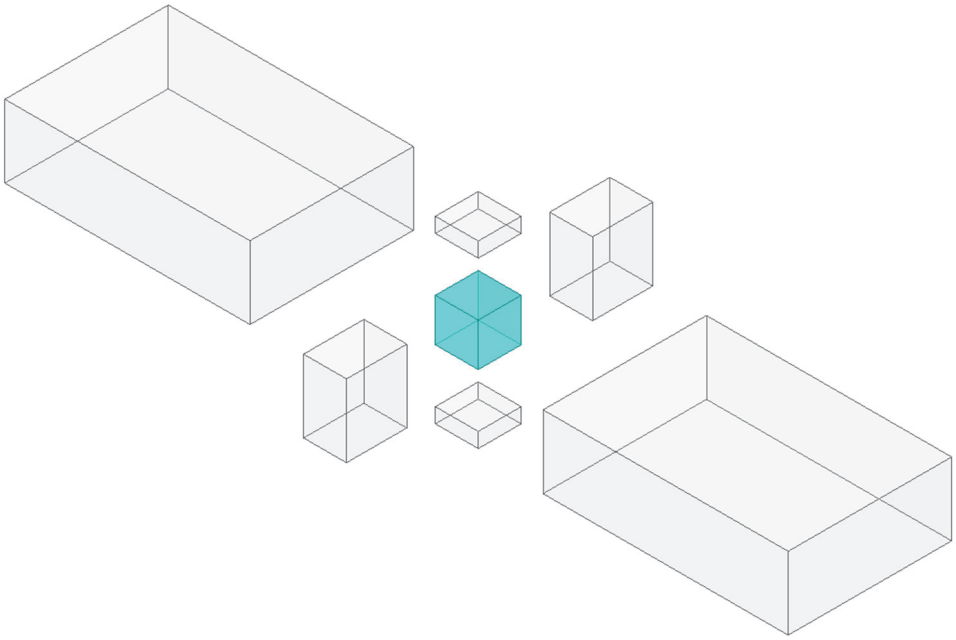

(*a*)

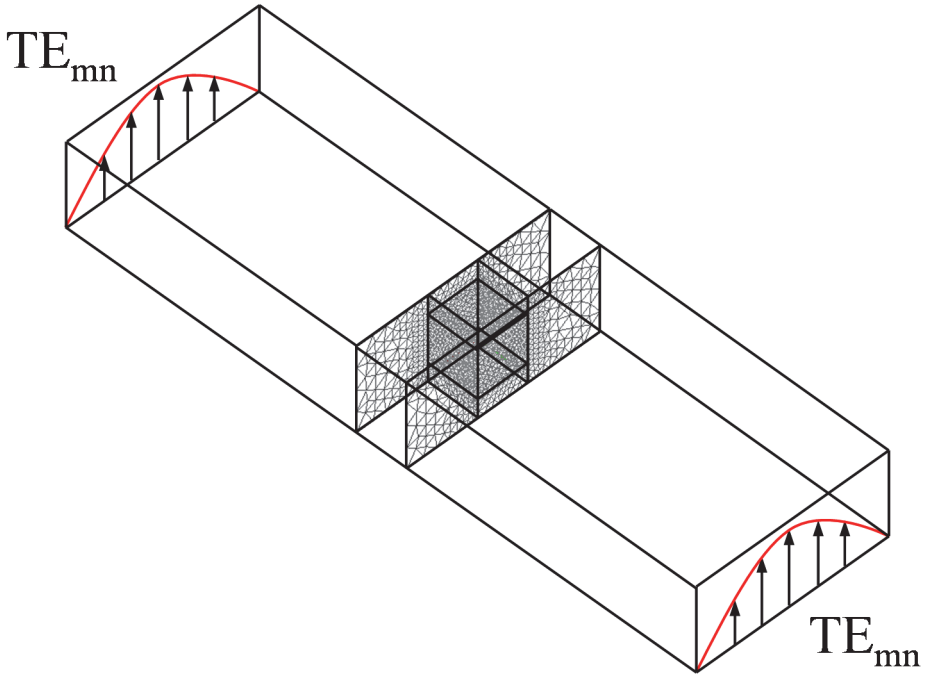

(*b*)

Fig. 4.7. Cubic dielectric resonator symmetrically placed in a standard WR-90 waveguide: (*a*) Segmentation into building blocks; (*b*) The adopted mesh.

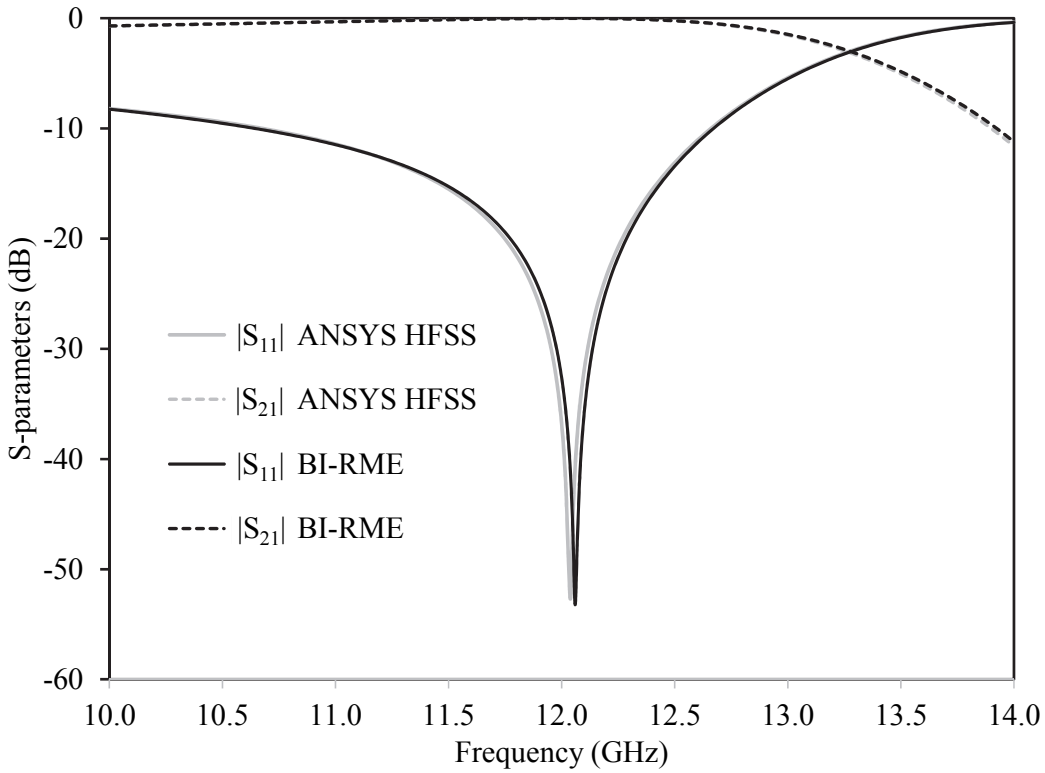

Fig. 4.8. Comparison of the frequency responses of the WR-90 waveguide with cubic dielectric resonator (Fig. 4.7) between the Generalized BI-RME method and ANSYS HFSS.

ANSYS HFSS	CPU Time (s)
Convergence: 15 points	2026
Interpolating analysis: 11 real frequency points	6677
Total	**8703**

Generalized BI-RME method	CPU Time (s)
BI-RME analysis	919
MATLAB frequency cascade: 401 frequency points	725
Total	**1644**

Table VII. Timing comparison for the cubic dielectric resonator symmetrically placed in a standard WR-90 waveguide.

ANSYS HFSS	Memory (MB)
Maximum amount	5070

Generalized BI-RME method	Memory (MB)
Maximum amount	934

Table VIII. Maximum memory requirement comparison for the cubic dielectric resonator symmetrically placed in a standard WR-90 waveguide.

4.4 Dielectric resonator filter on a waveguide section below cut-off

In this sub-section, the analysis of a more complex dielectric resonators waveguide filter is reported. Originally presented in [7], it is based on two dielectric slab-loaded below cut-off waveguide section, as shown in Fig. 4.9*a*-*b*. Moreover, the dielectric slab is metallized on both sides to reduce the length of the coupling section and improve the stopband attenuation [7]. The resonators are realized using a material with relative dielectric constant $\varepsilon_r = 2.2$ and loss tangent $tan\delta = 0.001$ (all the dimensions are reported in the caption of Fig. 4.9). The structure has been analyses with the Generalized BI-RME method adopting a segmentation into 13 boxed building blocks. The mesh shown in Fig. 4.9*c* was adopted to accurately represent the electromagnetic field on the surfaces, leading to the definition of about 3000 RWG basis functions overall. In the BI-RME representation of each block, all the resonant modes up to four times the maximum frequency of interest were include in the summation in (2.61). Moreover, it has been used a Gaussian integration rule with six points per triangle and four digits of accuracy for the calculation of the Green's function. For properly identifying the resonance position, a frequency step of 20 MHz was adopted, resulting into 1101 frequency points. Fig. 4.10*a* shows the comparison between the simulation results obtained with the proposed algorithm and ANSYS HFSS. A very good agreement is observed over a very large frequency band. It is noted that the effect of the losses of the material on the insertion loss of the filter is accurately modelled (see the close-up of the two passbands in Fig. 4.10*b*). Furthermore, it is worth nothing that the agreement is very good also in the first spurious band and until the upper frequency limit of 40 GHz even if the mesh elements dimension was calculated to cover the desired passband. The obtained results were published in [3] and [8] but, due to some convergence issues, they presented a little frequency shift now solved, as demonstrated by Fig. 4.10. As shown in Table IX, the CPU time was about 1751 s for the BI-RME analysis, and 3.58 s per frequency point for the cascading procedure. Overall, the proposed method required less than 110 minutes of CPU time due to the huge number of frequency points: in fact, by observing only the band of interest (18 - 26 GHz) that requires 401 frequency points, the overall CPU time becomes about 53 minutes. In terms of maximum memory allocation, the Generalized BI-RME method has required about 1.349 GB. As a comparison, HFSS took about ten minutes for the convergence and less than 3 minutes per frequency point with the interpolating method, which required 20 frequency points. The overall CPU time of HFSS was about one hour, with an overall memory allocation of about 3.94 GB. In Table IX are summarized the timings, while, in Table X the maximum amounts of memory required by the ANSYS simulation and by the Generalized BI-RME method for both the structures.

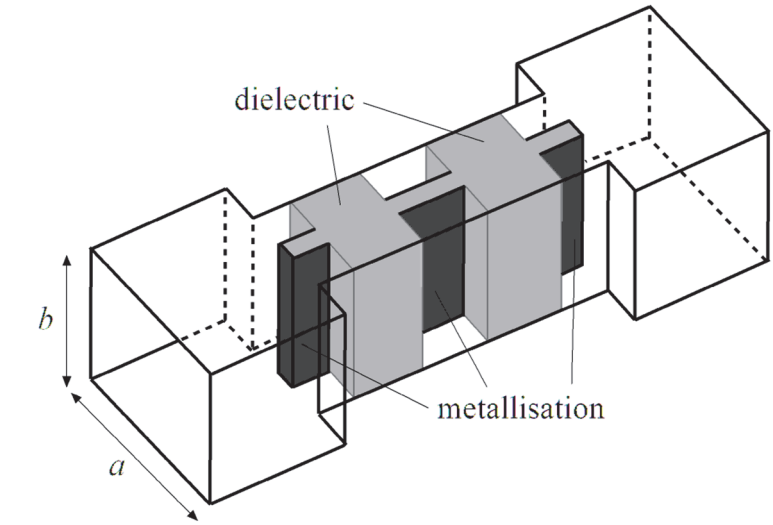

(*a*)

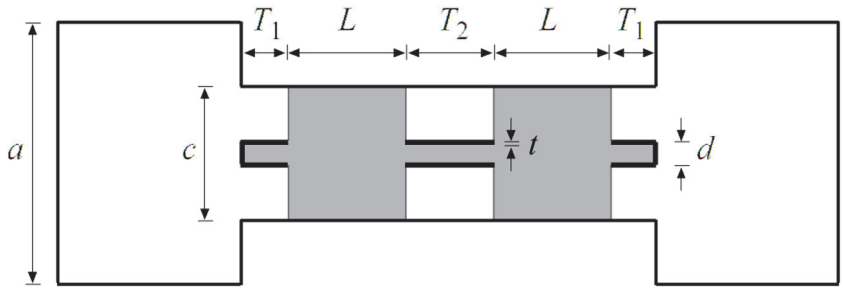

(*b*)

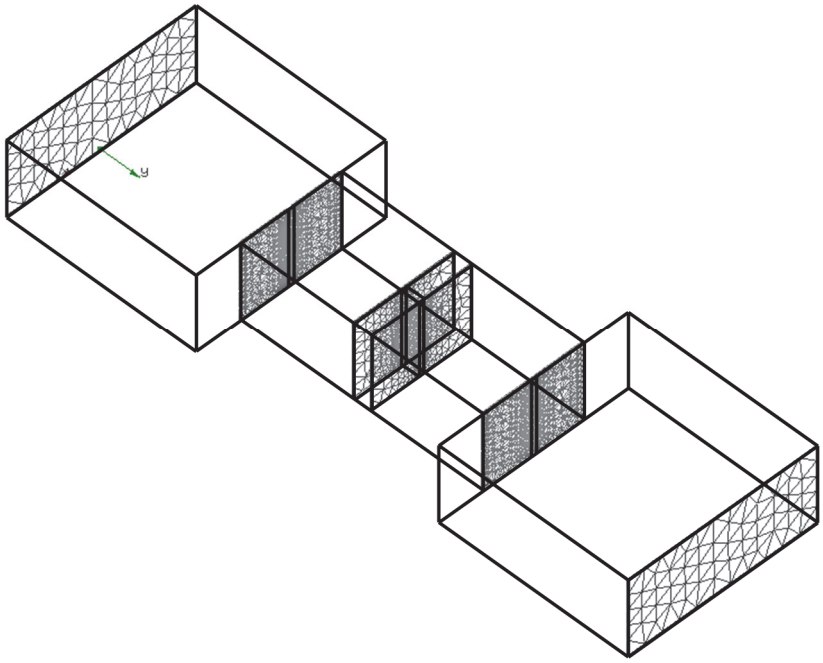

(*c*)

Fig. 4.9. Dielectric resonator filter on a waveguide section below cut-off [7]: (*a*-*b*) Geometry of the filter (dimensions in mm: $a = 10.7$, $b = 4.32$, $c = 5.689$, $d = 0.254$, $T_1 = 0.1$, $T_2 = 1.0$, $L = 6.3$; metal thickness of the internal septa $t = 0.017$); (*c*) Mesh adopted in the interconnecting surfaces for the analysis of the filter.

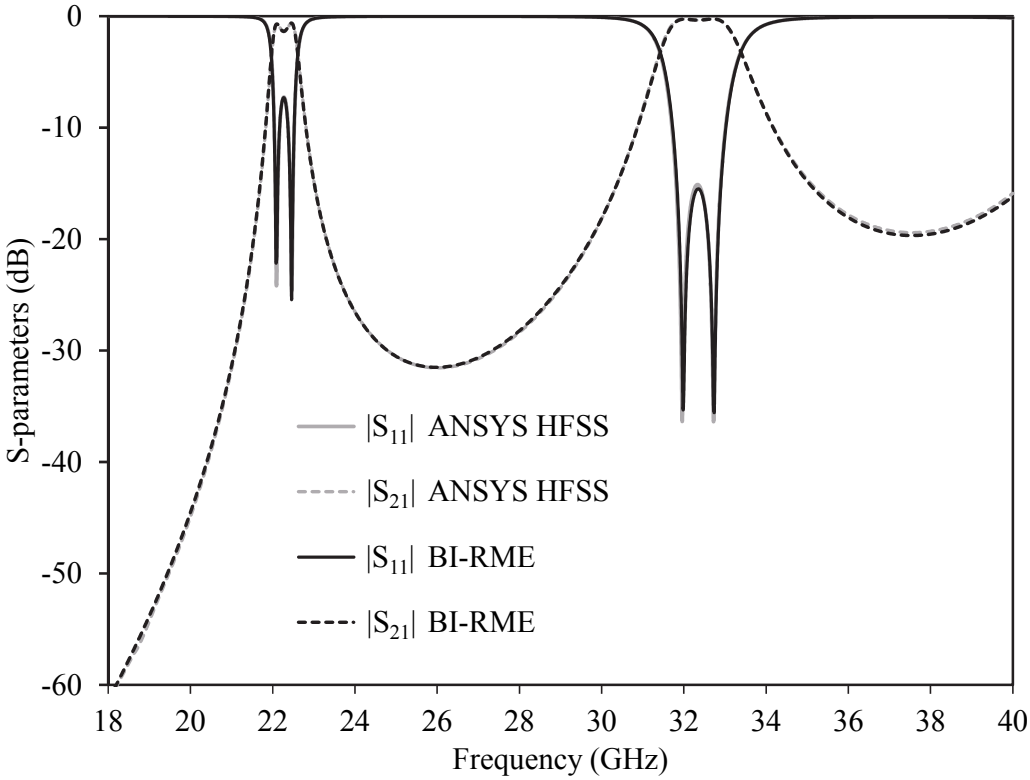

(*a*)

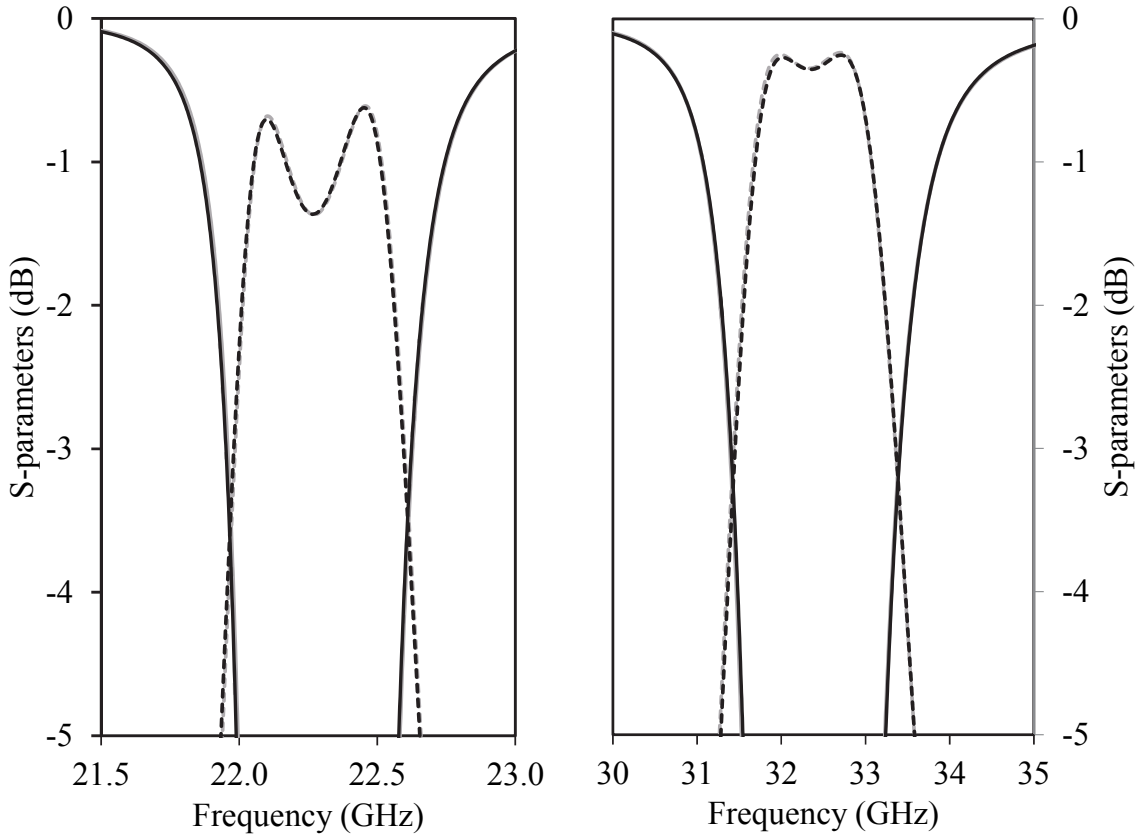

(*b*)

Fig. 4.10. Dielectric resonator filter on a waveguide section below cut-off (Fig. 4.9): (*a*) Comparison between the simulated frequency response calculated by the proposed technique and by ANSYS HFSS; (*b*) Close-up of the scattering parameters in the two passbands ([3] and [8]).

ANSYS HFSS	CPU Time (s)
Convergence: 15 points	642
Interpolating analysis: 20 real frequency points	3079
Total	**3721**

Generalized BI-RME method	CPU Time (s)
BI-RME analysis	1751
MATLAB frequency cascade: 1101 frequency points	3945
Total	**5695**

Table IX. Timing comparison for the dielectric resonator filter on a waveguide section below cut-off.

ANSYS HFSS	Memory (MB)
Maximum amount	3940

Generalized BI-RME method	Memory (MB)
Maximum amount	1349

Table X. Maximum memory requirement comparison for the dielectric resonator filter on a waveguide section below cut-off.

4.5 Diplexer based on rectangular ring resonators filters

The next structure analyzed with the Generalized BI-RME method is the diplexer originally presented in [9], whose results are reported in [6]. The diplexer is based on a central rectangular waveguide, connected with two miniaturized evanescent mode waveguide filters using rectangular ring resonators (RRRs), as shown in Fig. 4.11*a*. The RRRs are printed on a Duroid 5880 dielectric slab with relative dielectric constant $\varepsilon_r = 2.2$ and loss tangent $tan\delta = 9 \cdot 10^{-4}$ (all dimensions are available [[9], Sec. IV]). This diplexer is designed to have the passbands at 32 GHz and 36 GHz, with a 3% passband bandwidth at both frequencies. For the analysis with the proposed method, the structure was segmented into 22 homogeneous building blocks as shown in Fig. 4.11*b*. The presence of evanescent mode waveguides and of printed resonators makes the analysis particularly challenging. In fact, in excess of 10000 triangles were defined overall, with a particular refinement around the RRRs, leading to about 15000 basis functions. Also for this example, a Gaussian integration rule with six points per triangle was used, and $\xi = 4$ and $N_c = 4$ were adopted. For the analysis, a frequency step of 250 MHz was adopted, resulting into 54 frequency points. Fig. 4.12 shows the comparison between the simulation results obtained with the proposed algorithm and ANSYS HFSS: in particular, it shows a good agreement between the results of the proposed method and the HFSS simulations, not only for the passband response, but also for the more critical calculation of the isolation. Due to the large mesh refinement needed in the RRRs for the representation of the resonant fields, both the proposed technique and HFSS required a larger computing time than the previous example. The CPU time for the proposed method was more than 500 minutes for the calculation of the quasi-static BI-RME terms and about 200 s per frequency point for the cascading procedure. Overall, the proposed method required less than 200 minutes. However, it is in line with the CPU time of HFSS, which required about 7 hours with the interpolation method. Also in this case, the memory allocation of the proposed method was less than the one required by HFSS. It is worth noting that the computing time of the proposed method can be significantly reduced by reusing the quasi-static calculation for identical blocks and by exploiting the symmetries of the blocks. In Table XI are summarized the timings, while, in Table XII the maximum amounts of memory required by the ANSYS simulation and by the Generalized BI-RME method for both the structures.

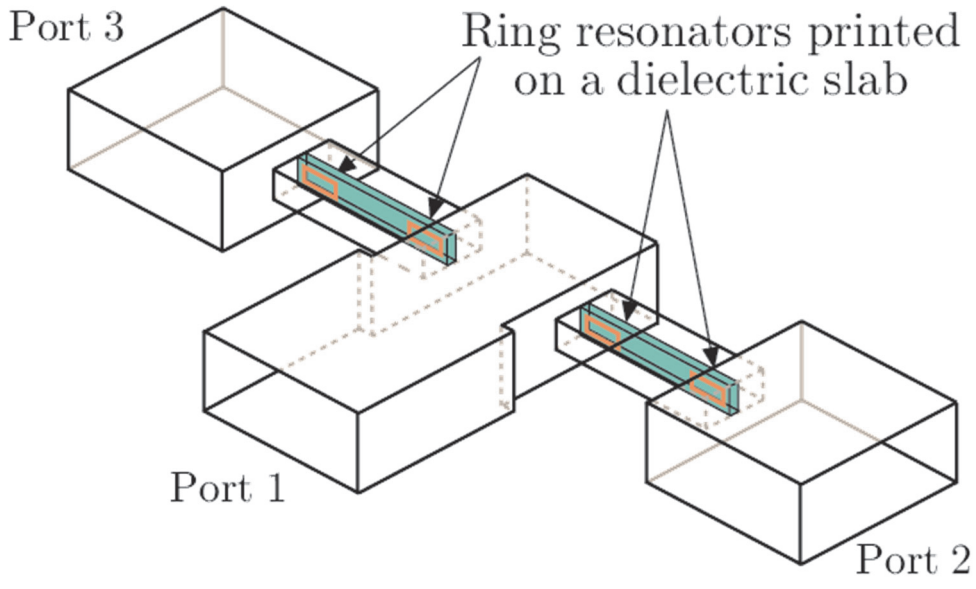

(*a*)

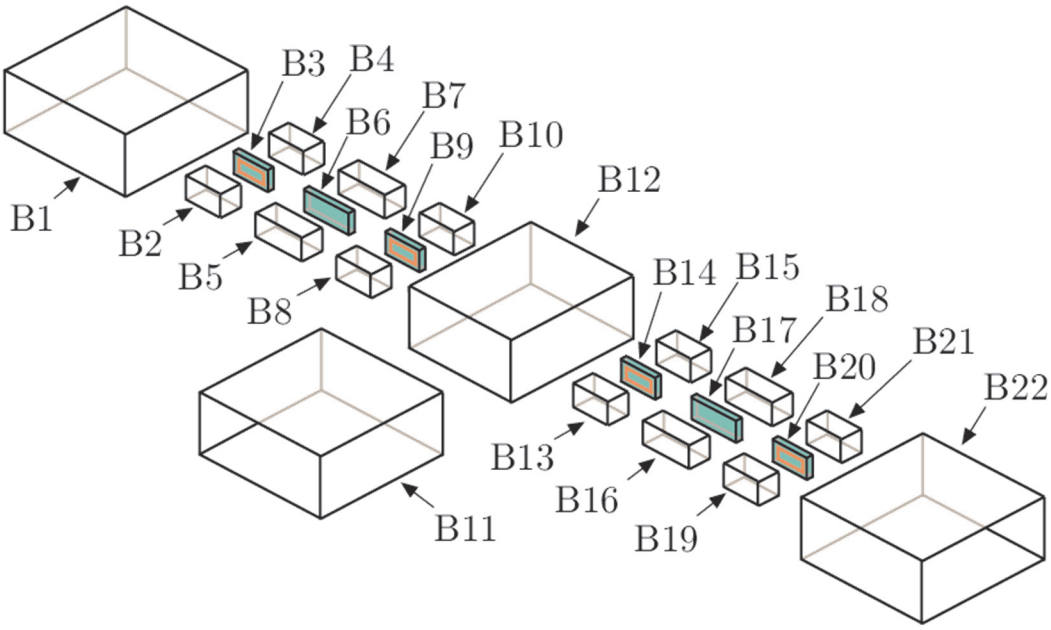

(*b*)

Fig. 4.11. Geometry of the diplexer presented in [9]: (*a*) Sketch of the diplexer geometry, including the ring resonators; (*b*) Segmentation of the diplexer into building blocks.

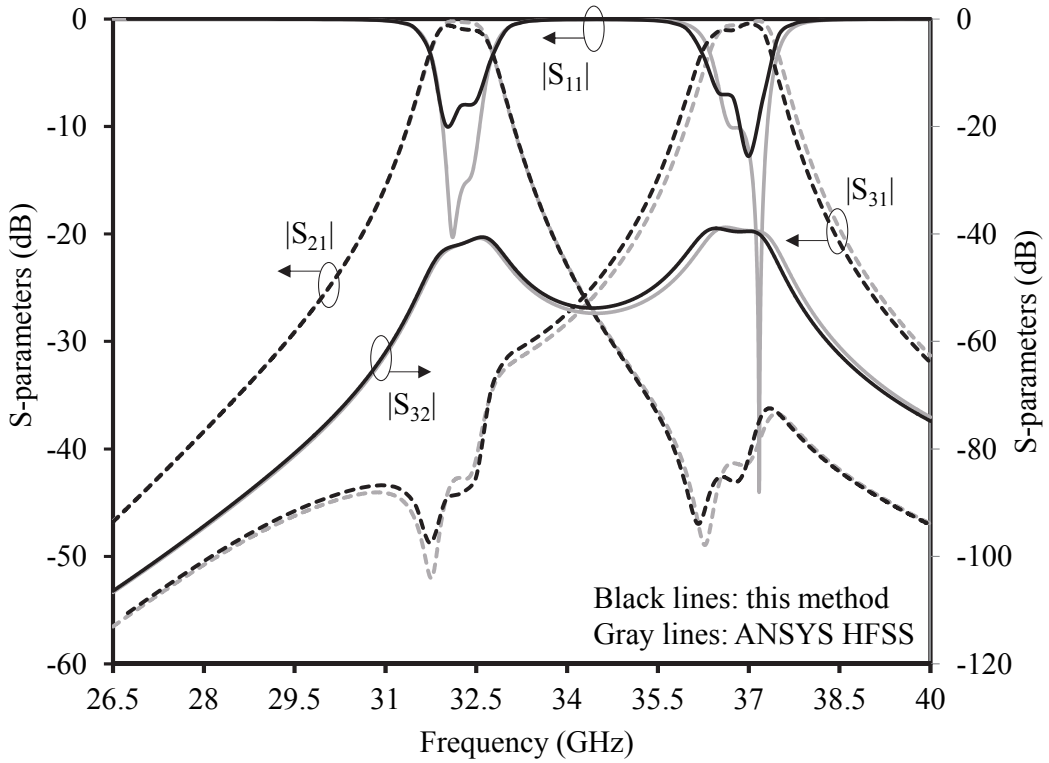

Fig. 4.12. Frequency response of the diplexer of Fig. 4.11: the simulation results of the proposed method are compared with HFSS simulations [6].

ANSYS HFSS	CPU Time (s)
Convergence: 27 points	4967
Interpolating analysis: 18 real frequency points	17919
Total	**22886**

Generalized BI-RME method	CPU Time (s)
BI-RME analysis	34200
MATLAB frequency cascade: 54 frequency points	11286
Total	**45486**

Table XI. Timing comparison for the diplexer based on rectangular ring resonators (RRRs).

ANSYS HFSS	Memory (MB)
Maximum amount	18000

Generalized BI-RME method – coarse mesh	Memory (MB)
Maximum amount	15781

Table XII. Maximum memory requirement comparison for the diplexer based on rectangular ring resonators (RRRs).

4.6 WR-90 waveguide interconnect with two mitered bends

The example proposed in this sub-section represents the first application of the Generalized BI-RME method to the analysis of a circuit with arbitrarily shaped building blocks. In particular, it is presented a simple WR-90 waveguide interconnect with two 90° mitered bends (see Fig. 4.13*a*) [10]. The analysis results are reported in [11]. This structure is filled with a homogeneous medium (air), and, in principle, it could be analyzed in a single shot with the original BI-RME method. However, the segmentation of the component into elementary building blocks that individually better fit within the volume of a box will strongly improve the efficiency of the method. For this reason, the component is segmented into the five blocks shown in Fig. 4.13*b*. Three blocks are simple rectangular boxes, and their GAMs can be calculated by adopting the boxed technique. On the contrary, the two mitered bends must be analyzed adopting the general approach that solve an EFIE problem. The meshes adopted for the analysis of the two arbitrarily shaped blocks are shown in Fig. 4.13*c*. It is noted that only the chamfer region and the interconnecting surfaces are meshed. In particular, on the chamfer surface only the electric basis functions are needed, while only the magnetic basis functions are defined on the interconnecting surfaces. Since only the chamfer surface does not coincide with the external box used to define the Green's functions, the electric wall condition is imposed only on that surface. The analysis required 128 (159) electric basis functions and 234 (258) magnetic basis functions for block AS1 (AS2) (Fig. 4.13*c*). For the EM analysis, a Gaussian integration rule with six points per triangle was used, and $\xi = 3$ and $N_c = 4$ were adopted. Instead, the frequency recombination involved 85 frequency points on the mono-modal frequency band of the WR-90 waveguide (8.2-12.4 GHz): so, a frequency step of 50 MHz. The solution of the EFIE provides the frequency-independent quantities for the calculation of the GAMs; then, by cascading frequency-by-frequency the GAMs, the frequency response reported in Fig. 4.14 is obtained, which is in good agreement with the ANSYS HFSS simulation. A good agreement is observed over the entire frequency band with a matching below the -20 dB.

As shown in Table XIII, the CPU time was about 35 s for the BI-RME analysis, and 0.024 s per frequency point for the cascading procedure. Overall, the proposed method required about 37 seconds of CPU time. In terms of maximum memory allocation, the Generalized BI-RME method has required about 279 MB. As a comparison, HFSS took about 32 seconds for the convergence and about 7 seconds per frequency point with the interpolating method, which required 13 frequency points. The overall CPU time of HFSS was less than two minutes, with an overall memory allocation of about 208 MB. In Table XIII are summarized the timings, while, in Table XIV the maximum amounts of memory required by the ANSYS simulation and by the Generalized BI-RME method for both the structures.

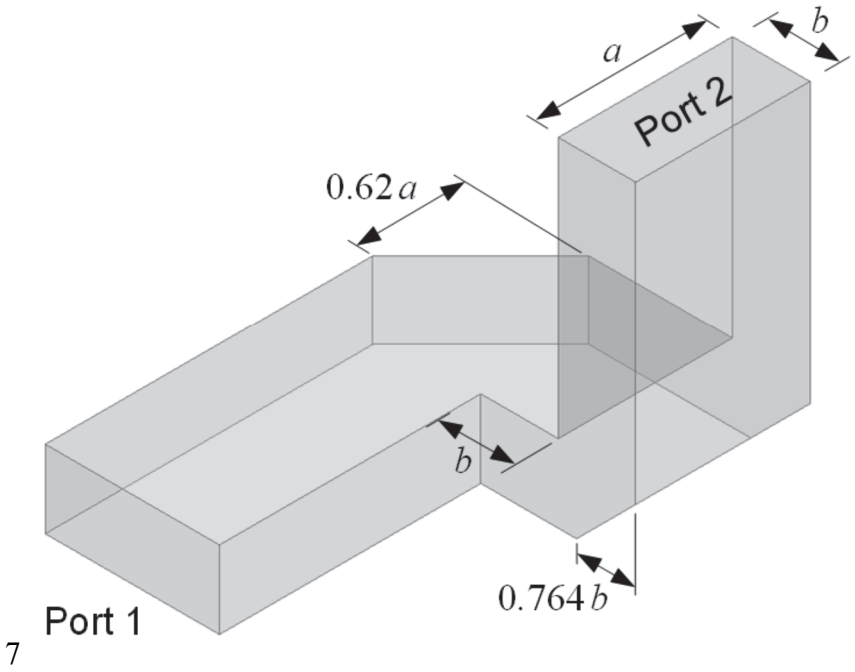

(*a*)

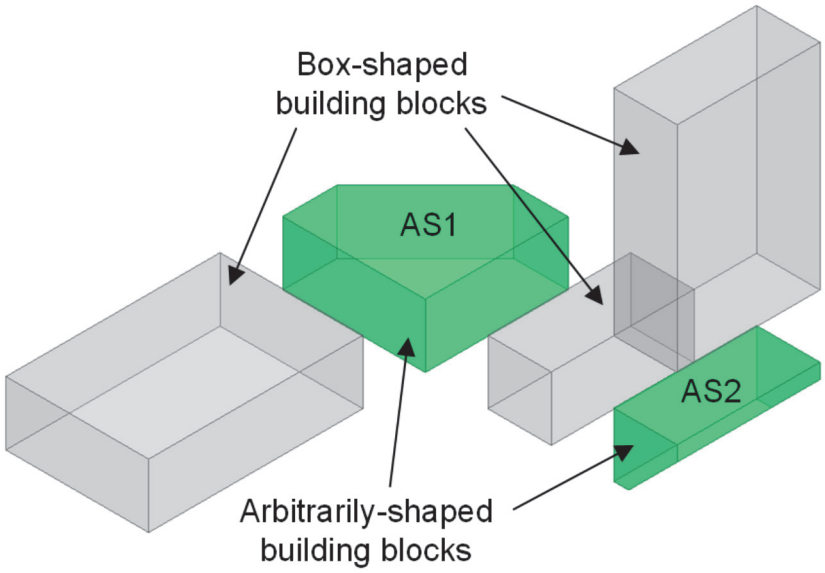

(*b*)

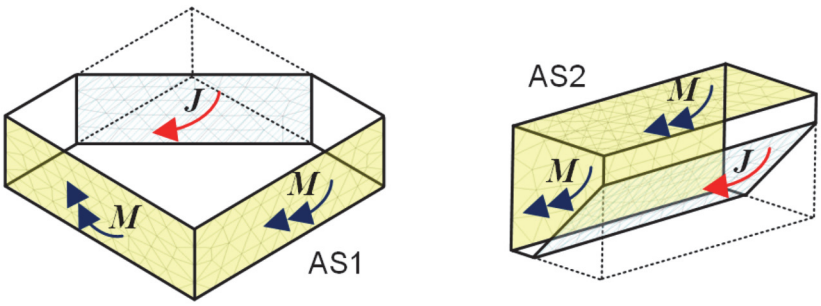

(*c*)

Fig. 4.13. WR-90 waveguide interconnect with two mitered bends (*a* = 22.86 mm, *b* = 10.16 mm) [10]: (*a*) Whole structure; (*b*) Segmented structure with arbitrary shaped building blocks highlighted; (*c*) Mesh adopted for the analysis of the arbitrarily shaped building blocks AS1 and AS2

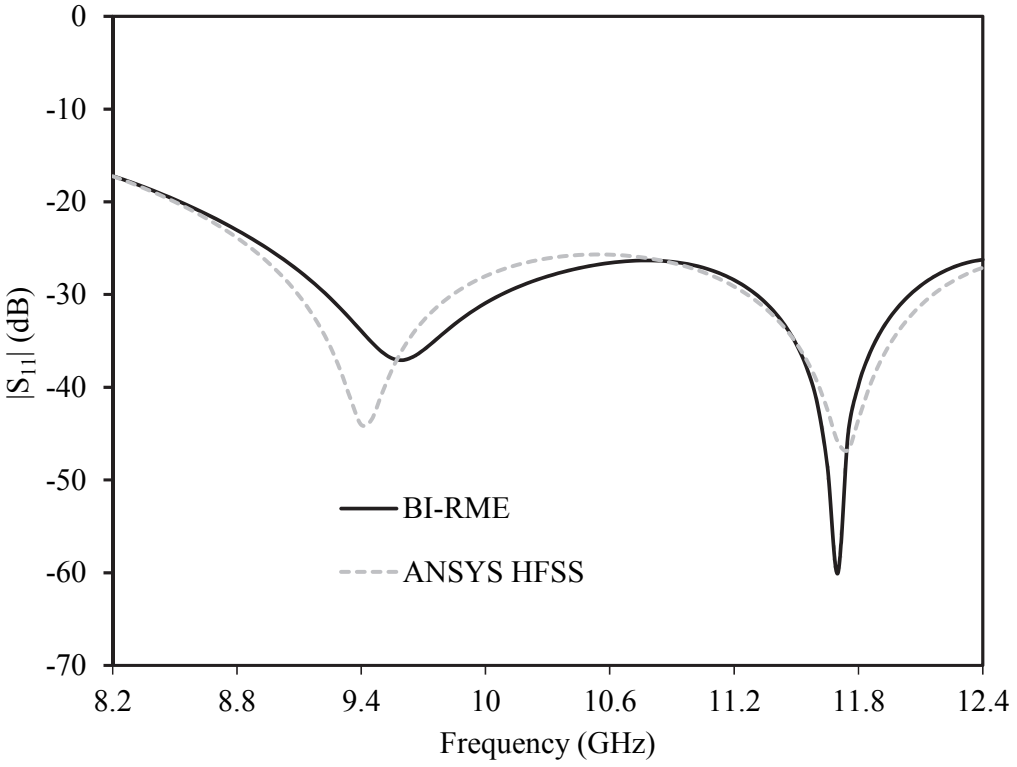

Fig. 4.14. Frequency response of the example of Fig. 4.13: the simulation results of the proposed method are compared with HFSS simulations [11].

ANSYS HFSS	CPU Time (s)
Convergence: 15 points	32
Interpolating analysis: 13 real frequency points	96
Total	**128**

Generalized BI-RME method	CPU Time (s)
BI-RME analysis	35
MATLAB frequency cascade: 85 frequency points	2
Total	**37**

Table XIII. Timing comparison for the WR-90 waveguide interconnect with two mitered bends.

ANSYS HFSS	Memory (MB)
Maximum amount	208

Generalized BI-RME method	Memory (MB)
Maximum amount	279

Table XIV. Maximum memory requirement comparison for the WR-90 waveguide interconnect with two mitered bends.

4.7 WR-90 Riblet coupler with compensating capacitive posts

The second arbitrarily shaped structure is a Riblet junction with compensation metallic post studied in [12] (Fig. 4.15Fig. 4.16*a*). The terminal waveguide are WR90, and all the dimensions of the structure can be found in Fig. 3 and Table I of [12]. The use of the capacitive posts helps to obtain the required 90° of phase difference for this type of coupler. From the computational point of view, the use of the capacitive posts allows transforming the coupler practically from a 2D structure to a fully 3D one. For the BIRME analysis the structure was segmented into twenty-two BBs. Ten building blocks have an arbitrary shape, and the enhanced approach is required to calculate their GAMs. The remaining blocks are just rectangular box and can be analyzed with the boxed technique. In spite of the large number of building blocks, it is noted that the different blocks to be analyzed are a limited number. In fact, from Fig. 4.15*b* it appears that only seven different blocks are repeated identical in the segmented structure. Therefore, they could be analyzed just once, and their GAMs could be reused for the other identical blocks. This significantly speed-up the overall analysis. Depending on the complexity of the block, the number of electric and magnetic basis functions required for the analysis of all the blocks varied from 88 to 375 and from 248 to 1046, respectively. For the EM analysis, a Gaussian integration rule with six points per triangle was used, and $\xi = 4$ and $N_c = 4$ were adopted. Instead, the frequency recombination involved 301 frequency points on the 7.5-10.5 GHz frequency band: so, a frequency step of 10 MHz. The computed scattering parameters are shown in Fig. 4.16. In particular, Fig. 4.16*a* shows the coupling coefficient $|S_{21}|$ and $|S_{31}|$, compared to HFSS simulations. Similarly, Fig. 4.16*b* shows the matching $|S_{11}|=|S_{22}|=|S_{33}|=|S_{44}|$, and isolation $|S_{23}|=|S_{14}|$ of the junction. In all cases the agreement with HFSS simulation is quite good. The analysis results are also reported in [11] and [13].

As shown in Table XV, the CPU time was less than 19 minutes for the BI-RME analysis, and 0.676 s per frequency point for the cascading procedure. Overall, the proposed method required less than 20 minutes of CPU time. In terms of maximum memory allocation, the Generalized BI-RME method has required about 0.249 GB. As a comparison, HFSS took about 14 minutes for the convergence and about 100 seconds per frequency point with the interpolating method, which required 17 frequency points. The overall CPU time of HFSS was about 44 minutes, with an overall memory allocation less than 2.6 GB. In Table XV are summarized the timings, while, in Table XVI the maximum amounts of memory required by the ANSYS simulation and by the Generalized BI-RME method for both the structures.

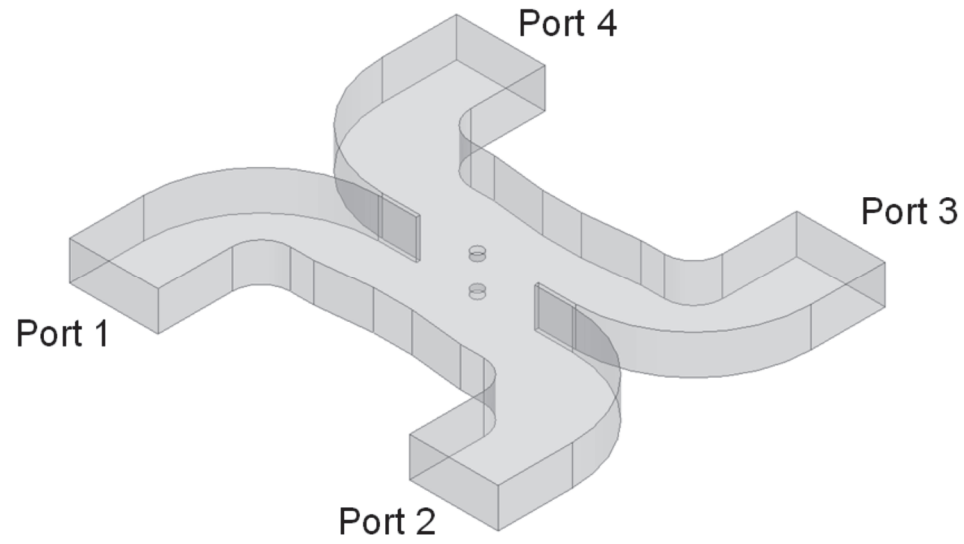

(*a*)

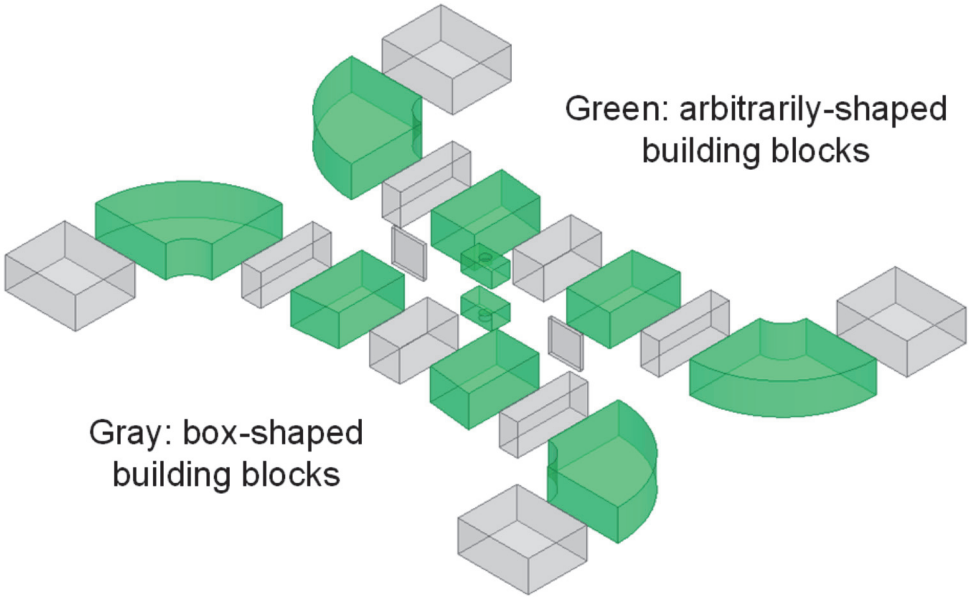

(*b*)

Fig. 4.15. A WR-90 Riblet coupler with compensating capacitive posts [12]: (*a*) Whole structure; (*b*) Segmented structure with arbitrary shaped building blocks highlighted in green.

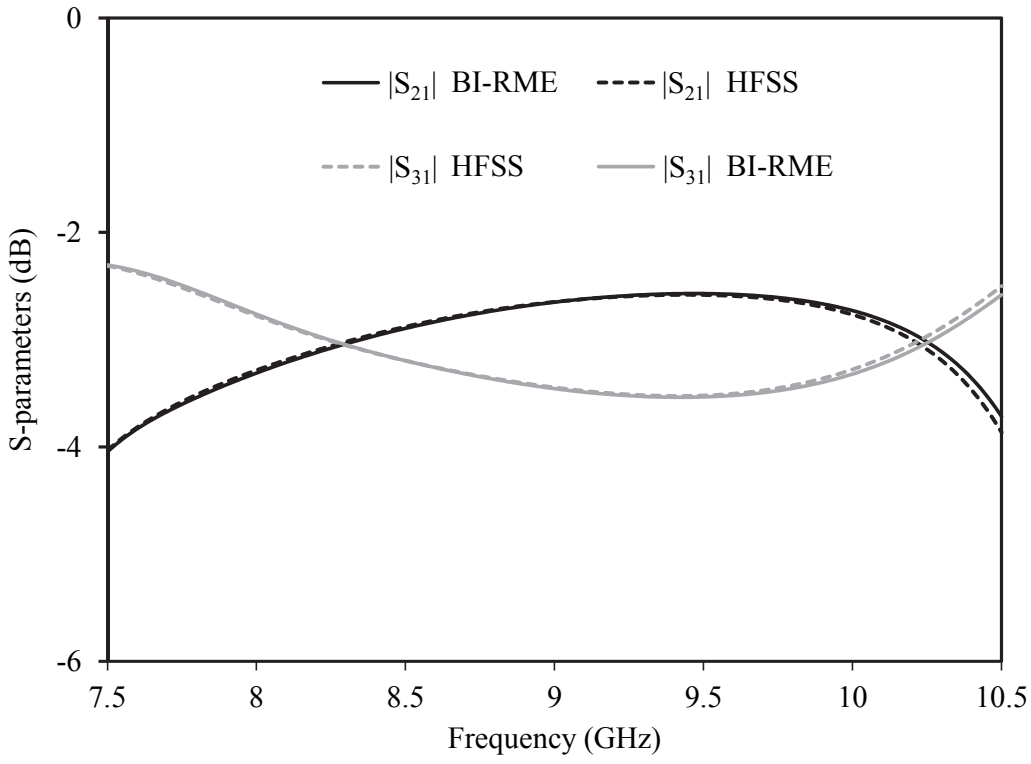

(*a*)

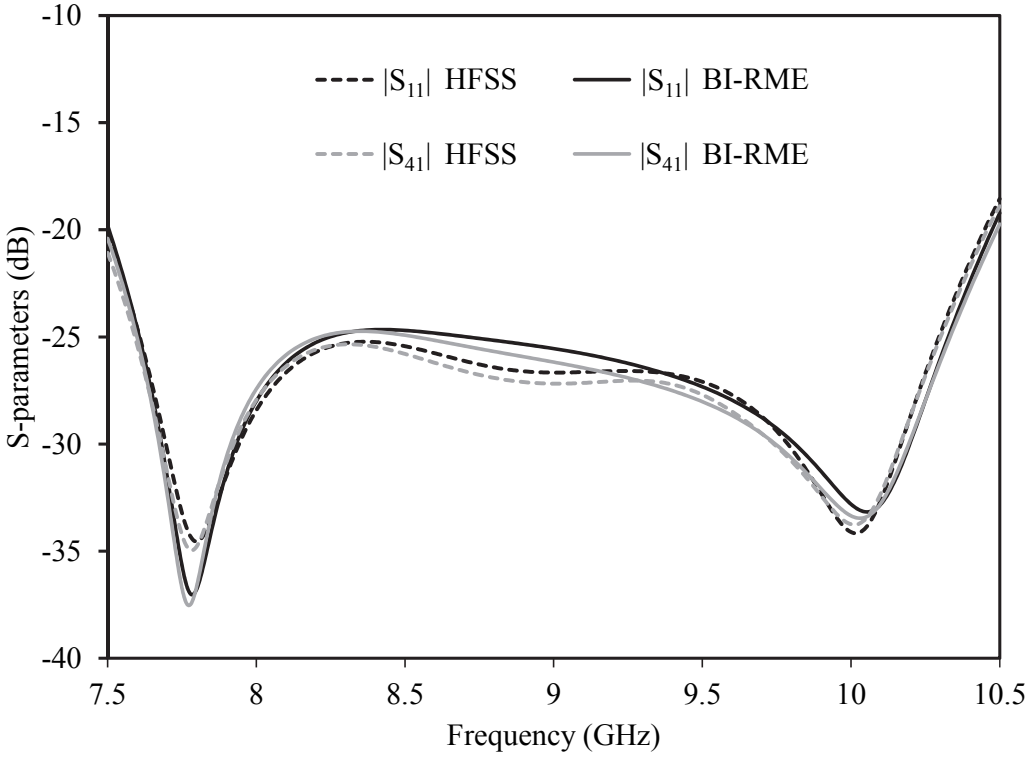

(*b*)

Fig. 4.16. Frequency response of the Riblet coupler of Fig. 4.15, calculated by the BI-RME method is compared with the HFSS simulation [11]: (*a*) Coupling coefficients; (*b*) Matching and isolation.

ANSYS HFSS	CPU Time (s)
Convergence: 20 points	868
Interpolating analysis: 17 real frequency points	1773
Total	**2641**

Generalized BI-RME method	CPU Time (s)
BI-RME analysis	1110
MATLAB frequency cascade: 61 frequency points	41
Total	**1151**

Table XV. Timing comparison for the WR-90 Riblet coupler with compensating capacitive posts.

ANSYS HFSS	Memory (MB)
Maximum amount	2590

Generalized BI-RME method	Memory (MB)
Maximum amount	249

Table XVI. Maximum memory requirement comparison for the WR-90 Riblet coupler with compensating capacitive posts.

4.8 Matched turnstile junction

The matched turnstile junction considered in this sub-section has been proposed in [14] and the analysis results with the Generalized BI-RME method are reported in [15]. This structure is based on the cross section of two rectangular waveguides interconnected with a circular waveguide. The peculiarity of the structure designed in [14] consists in the use of two overlapped cylindrical matching elements (Fig. 4.17*a*). This choice permits a single block machining of the cylindrical waveguide and of the matching elements, thus solving the problem of possible misalignments. As a result, a wideband matching with a return loss better than 30 dB is obtained in the frequency band from 31 GHz to 45 GHz. The analysis was challenged because involved the use of not rectangular shaped terminal ports: in fact, for the circular terminal port, it was necessary to define the RWG basis functions and to project them on the port modal field (the TE_{11} cross-polarized modes) by solving the (2.65). For the BI-RME analysis the proposed turnstile junction has been segmented into six homogeneous building blocks (Fig. 4.17*b*). In particular, blocks B1 and B2 are arbitrarily shaped and the determination of their GAMs requires the solution of the EFIE problem [11], whereas blocks B3-B6 are just boxes, and the GAMs are obtained by directly projecting the Green's functions on the RWG basis functions [6]. The electromagnetic field at the interfaces between building blocks were represented with a total of 2450 RWG basis functions.
For the EM analysis, a Gaussian integration rule with six points per triangle was used, and $\xi = 5$ and $N_c = 4$ were adopted. The simulation results of the BI-RME are compared to the ones calculated by ANSYS HFSS in Fig. 4.18 in the case of the reflection coefficient at the circular port [15]. A good agreement is observed, especially considering the high matching of the junction. It is noted that the HFSS results in [14] are slightly different from the ones reported in Fig. 4.18: this is attributed to a better convergence analysis done in order to produce the ANSYS reference results.
The CPU time required for the preliminary frequency independent BI-RME analysis was less than 3 hours, whereas the GAMs recombination for each frequency point took 0.56 s. In order to have a good representation of the frequency behavior, the frequency range was subdivided into 141 frequency points (100 MHz frequency step). Therefore, the whole analysis required about 3 hours, with a memory allocation of about 0.47 GB. It is worth noting that the GAM reusability is not yet implemented, which would significantly reduce the computing time. As a comparison, HFSS took about one hour and a half for the convergence procedure and, with the interpolating method, more than 20 minutes for each of the 18 frequency points. The overall CPU time was about 8 hours, with an overall memory requirement of about 21 GB. The HFSS timings, as well as the memory requirement, are higher than the ones required to acquire the data presented in [14] but they are necessary to have more precise results. In Table XVII are summarized the timings, while, in Table XVIII the maximum amounts of memory required by the ANSYS simulation and by the Generalized BI-RME method for both the structures.

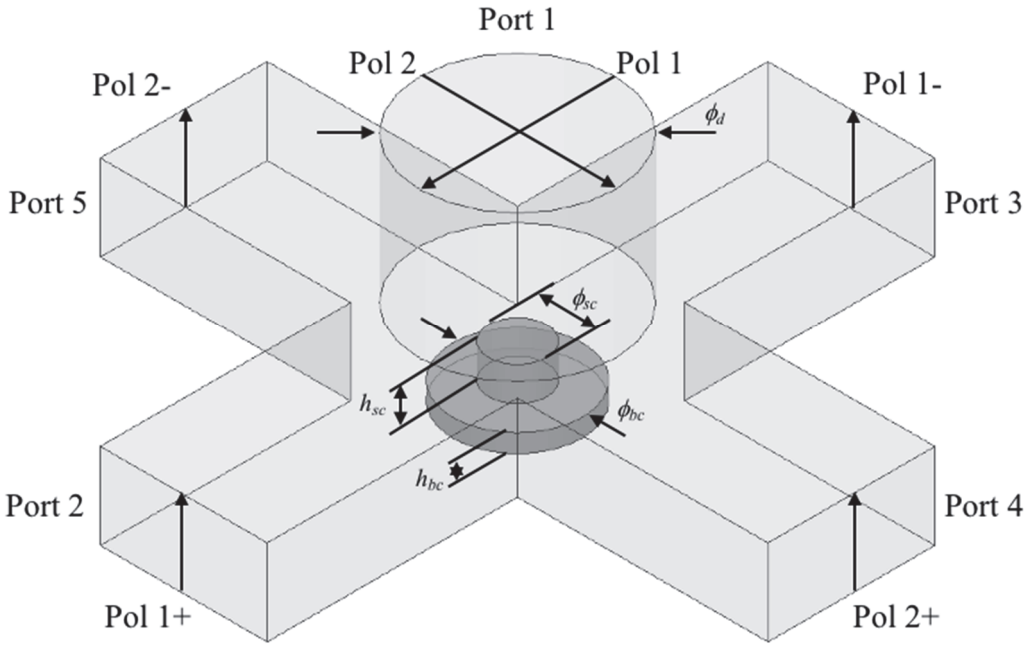

(*a*)

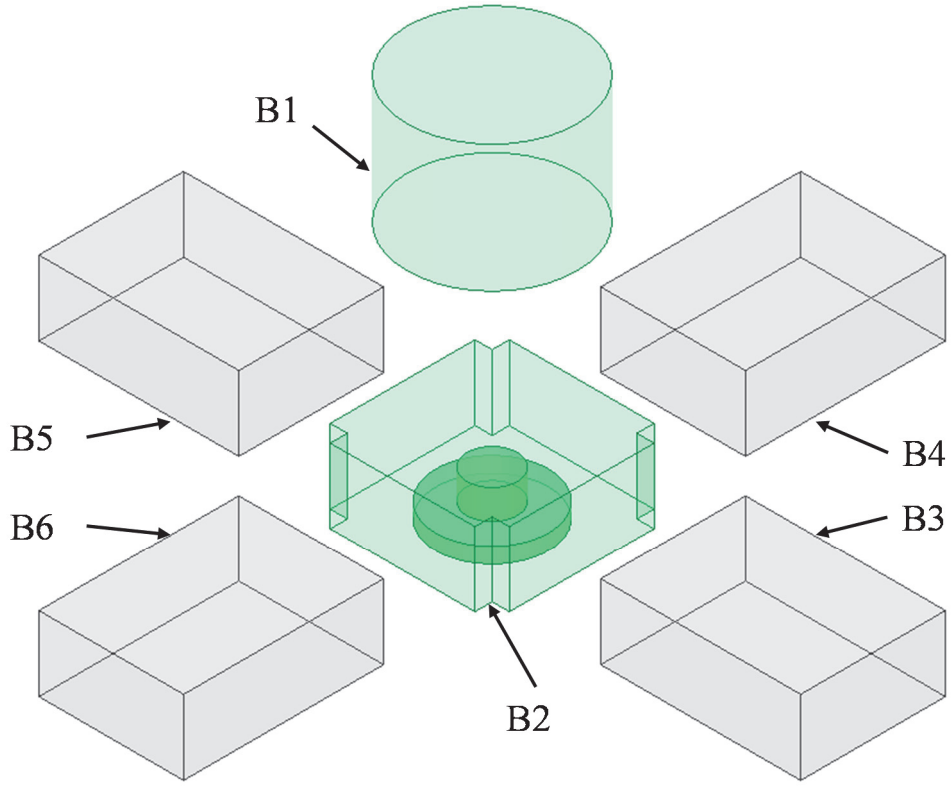

(*b*)

Fig. 4.17. Turnstile junction with superimposed cylinders matching stub: (*a*) Whole structure with the polarizations over each ports; (*b*) Segmented structure with arbitrary shaped building blocks highlighted in green. Dimensions: output rectangular waveguide 6.33 mm × 3.25 mm, circular waveguide diameter ϕ_d = 7.42 mm, ϕ_{sc} = 2.2 mm, ϕ_{bc} = 4.9 mm, h_{sc} = 1.29 mm, h_{bc} = 0.68 mm.

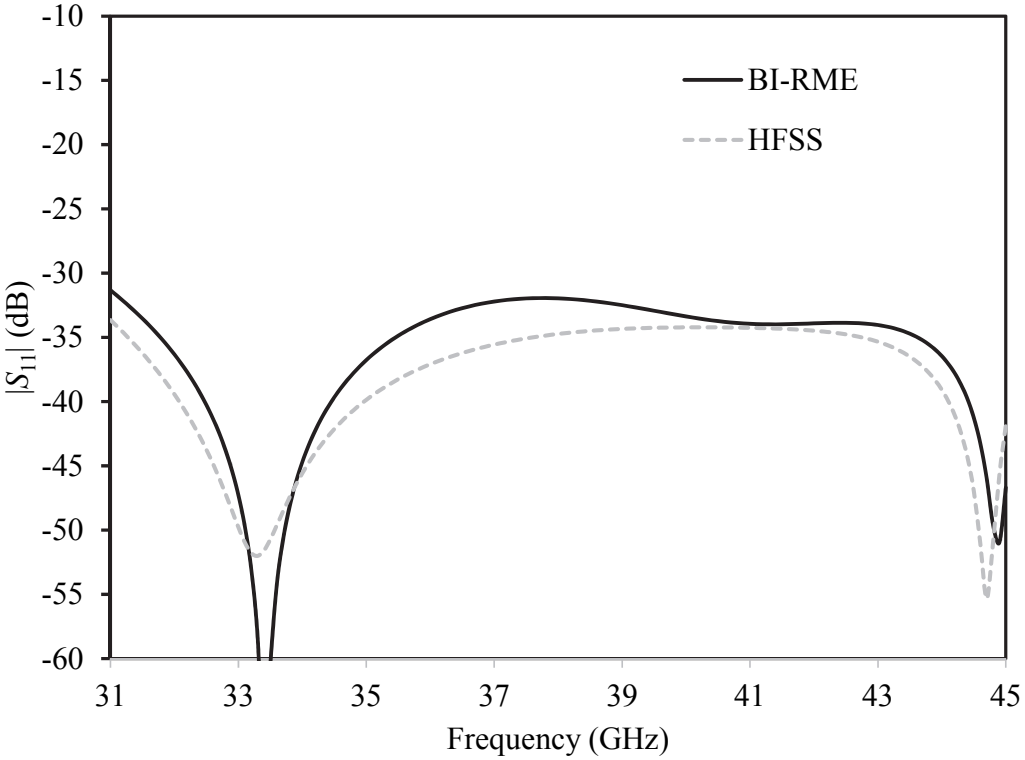

Fig. 4.18. Frequency response of the matched turnstile junction of Fig. 4.17, calculated by the BI-RME method is compared with the HFSS simulation [15]: comparison of the reflection coefficient $|S_{11}|$ at the circular port (identical for both polarizations).

ANSYS HFSS	CPU Time (s)
Convergence: 12 points	3626
Interpolating analysis: 18 real frequency points	21694
Total	**25320**

Generalized BI-RME method	CPU Time (s)
BI-RME analysis	10034
MATLAB frequency cascade: 141 frequency points	80
Total	**10114**

Table XVII. Timing comparison for the matched turnstile junction.

ANSYS HFSS	Memory (MB)
Maximum amount	21100

Generalized BI-RME method	Memory (MB)
Maximum amount	468

Table XVIII. Maximum memory requirement comparison for the matched turnstile junction.

4.9 H-plane WR-75 four-pole dielectric filter

In this sub-section, the results of the analysis of a four-pole dielectric loaded waveguide filter with the Generalized BI-RME method are presented Fig. 4.19. Originally presented in [16], this filter is composed by four full-height full width waveguide (WR-75) cavity loaded with four dielectric resonators with a relative dielectric constant of $\varepsilon_r = 24$. All the filter dimensions are given in the caption of Fig. 4.19*a*. For the BI-RME analysis, the structure is segmented into 15 homogeneously filled building blocks (Fig. 4.19*b*). As already happened for the previous examples, since seven blocks have a "boxed" shape (highlighted in grey), their GAMs are calculated with the algorithm proposed in [6], while for the eight blocks with an "arbitrary" shape (highlighted in green), their GAMs calculation is performed with the more complex approach described in [11] and outlined in Sec. II. As requested by the BI-RME method for the calculation of the Green's functions, each block was closed inside a fictitious rectangular parallelepiped cavity resonator having the minimum possible size, and all the interconnecting surfaces were meshed with a total of 10088 triangles. In particular, for the full-height cylindrical resonators, about 2170 RWG basis functions were required to represent the surface electric current, while about 2110 RWG basis functions for representing the surface magnetic current. Since the upper and lower faces of the cylinder lay on the box surfaces, only the lateral surface of each cylindrical resonator needs to be meshed. On the other hand, for each waveguide cavity resonators, only the interface surfaces with the irises and the cylindrical resonator need the be meshed, with the definition of about 2170 RWG basis function to represent the surface electric current and 3500 RWG basis functions for the magnetic one. Moreover, in order to ensure a good accuracy of the resonant mode expansion, about 1400 modes were retained for the cylindrical resonators, while about 70 modes for the waveguide cavities. Note that the resonators require a considerably high number of modes compared to the cavities ones due to the presence of a high dielectric constant material. As reported in Fig. 4.20, there is a good agreement between the frequency responses calculated with the generalized BI-RME method [17] and the one obtained with a commercial software, ANSYS HFSS, based on the FEM method.

The CPU time required for the BI-RME analysis was about 4 hours, whereas the GAMs recombination for each frequency point took 5.5 s. In order to have a good representation of the frequency behavior, the frequency range was subdivided into 87 frequency points. Therefore, the whole analysis required less than 4.5 hours, with a memory allocation less than 2 GB. Especially in this case, the use of the symmetries and the GAM reusability will significantly reduce the computing time. As a comparison, HFSS took about 13 minutes for the convergence procedure and, with the interpolating method, about 2.5 s for each of the 13 frequency points. The overall CPU time was about an hour, with an overall memory requirement of about 4 GB. In Table XIX are summarized the timings, while, in Table XX the maximum amounts of memory required by the ANSYS simulation and by the Generalized BI-RME method for both the structures.

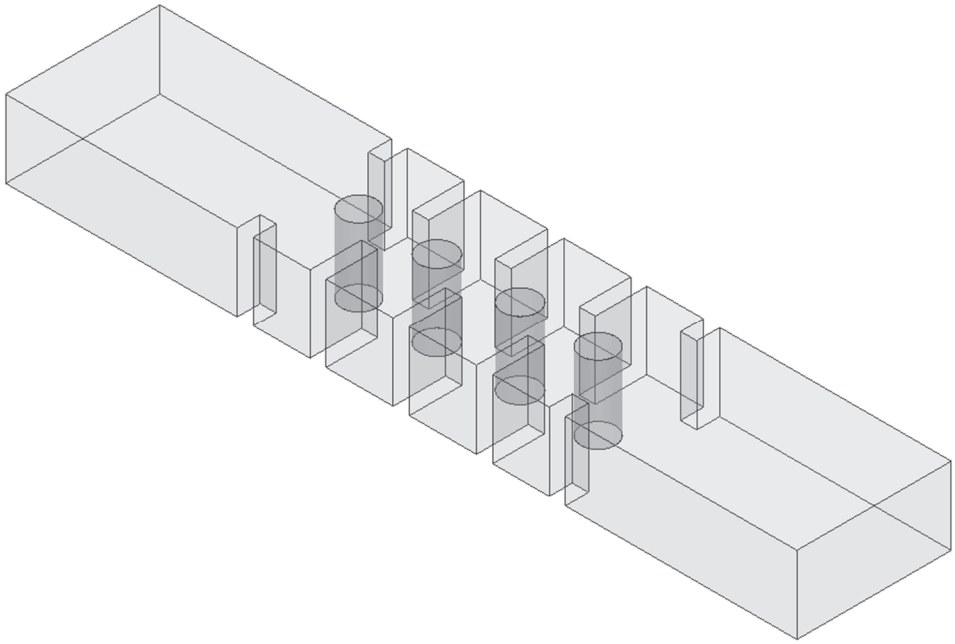

(*a*)

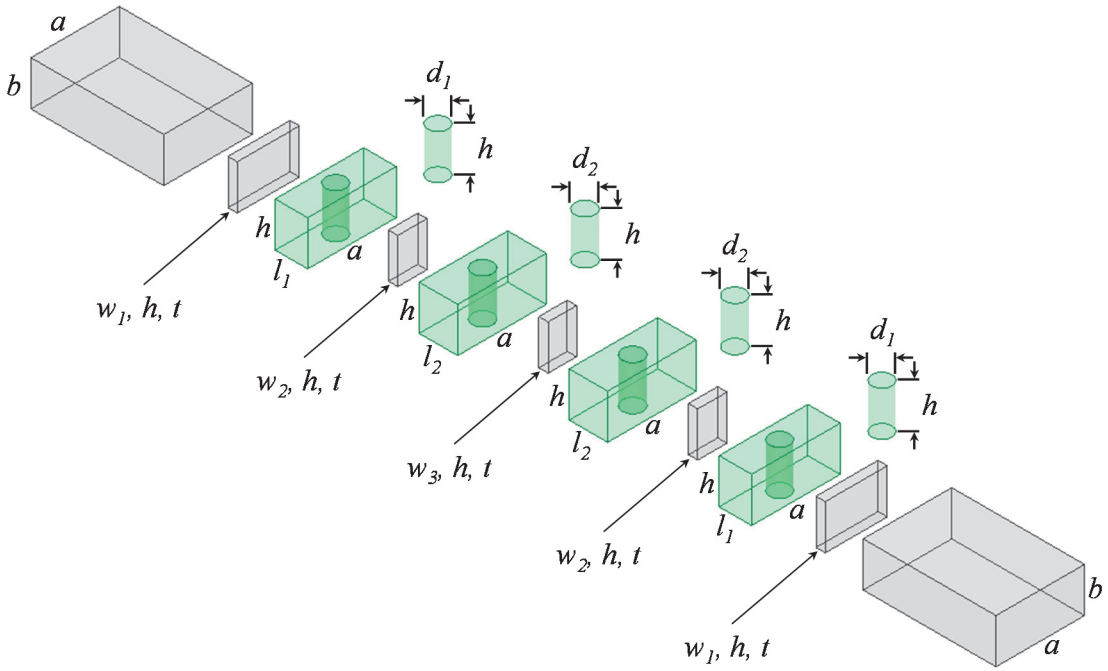

(*b*)

Fig. 4.19. H-plane WR-75 four-pole dielectric filter: (*a*) Geometry of the filter; (*b*) Filter segmented into 15 building blocks. "boxed" building blocks are highlighted in grey while the "arbitrarily" shaped ones in green. Dimensions (in mm): a = 19.05, b = 9.525, l_1 = 6.98, l_2 = 8.28, h = 9.525, w_1 = 13.37, w_2 = 6.286, w_3 = 6.1, t = 2, d_1 = 4.222, d_2 = 4.344, ε_r = 24.

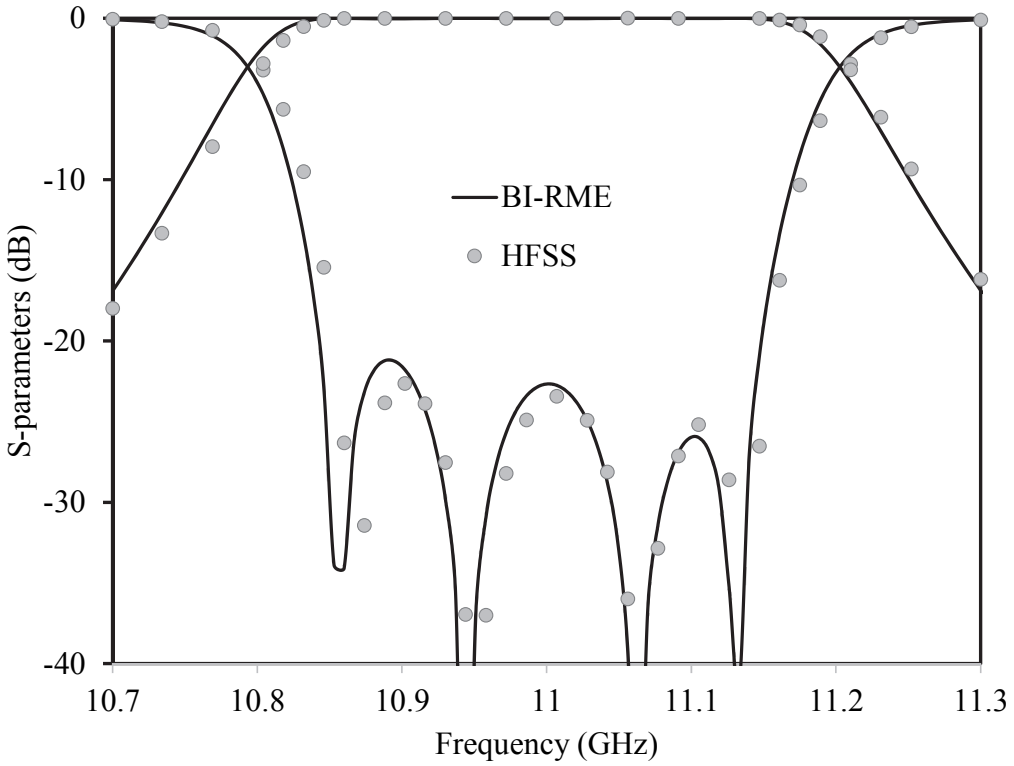

Fig. 4.20. H-plane WR-75 four-pole dielectric filter of Fig. 4.19: comparison between the frequency responses obtained with the generalized BI-RME method and ANSYS HFSS [16].

ANSYS HFSS	CPU Time (s)
Convergence: 15 points	783
Interpolating analysis: 13 real frequency points	1922
Total	**2705**

Generalized BI-RME method	CPU Time (s)
BI-RME analysis	15721
MATLAB frequency cascade: 87 frequency points	475
Total	**16196**

Table XIX. Timing comparison for the H-plane WR-75 four-pole dielectric filter.

ANSYS HFSS	Memory (MB)
Maximum amount	4020

Generalized BI-RME method	Memory (MB)
Maximum amount	1923

Table XX. Maximum memory requirement comparison for the H-plane WR-75 four-pole dielectric filter.

4.10 Four-pole bandpass dielectric "mushrooms" filter

The last proposed example is four-pole dielectric-loaded "mushrooms" bandpass filter (Fig. 4.21). Originally presented in [18], the filter comprises four cylindrical dielectric resonators with relative dielectric constant $\varepsilon_r = 50$, supported by spacers with relative dielectric permittivity approximately equal to one, which are therefore neglected in the analysis. The dimensions of the cavities, irises, and resonators are given in the caption of Fig. 4.21. The filter is segmented into 13 homogeneously-filled building blocks as shown in Fig. 4.21*b*. In particular, five blocks are just boxes (namely the input/output waveguides and the irises), whereas the GAMs of the eight arbitrary shaped blocks (highlighted in green in Fig. 4.21*b*) are obtained with the solution of an EFIE problem. The interconnecting surfaces were meshed with a total of 9308 triangles. In particular, the cavities with the cylindrical holes required 3332 and of 2910 RWG basis functions to represent the surface magnetic and electric currents, respectively. The modal series in the Green's functions were truncated retaining about 50 resonating modes of the box. The analysis of the cylindrical resonators required 2910 RWG basis functions to represent the surface magnetic current and 1400 RWG basis functions for the surface electric current, and about 1300 resonant modes in the Green's function series. Note that the number of modes of the box considered for the cylinder is larger than the one used for the other air-filled arbitrarily shaped blocks, in spite of its smaller volume, because of the presence of the high dielectric constant material.

The frequency response calculated by the generalized BIRME method is shown in Fig. 4.22*a*, together with an ANSYS HFSS analysis and the data taken from [18]. Both the passband response (Fig. 4.22*a*) and the wideband response (Fig. 4.22*b*) show a very good agreement with the other computational techniques. Therefore, even if, as expected, the proposed approach leads to an increase of the dimension of the eigenvalue problem with respect to the specific implementation reported in [18], the generalized BI-RME method preserves the computational accuracy while adding a complete flexibility in the geometry of the component. The analysis results are also reported in [13], [17] and [19].

The CPU time required for the BI-RME analysis was about 9 hours, whereas the GAMs recombination for each frequency point took 6.2 s. In order to have a good representation of the frequency behavior, the frequency range was subdivided into 60 frequency points (5 MHz frequency step). Therefore, the whole analysis required about 9 hours, with a memory allocation of about 2 GB. As for the filter reported in the previous example, the use of the symmetries and the GAM reusability will significantly reduce the computing time. As a comparison, HFSS took about one hour for the convergence procedure and, with the interpolating method, about 18 minutes for each of the 14 frequency points. The overall CPU time was about 5.5 hours, with an overall memory requirement of about 20 GB. The HFSS timings, as well as the memory requirement, are higher than what initially obtained due to the necessity of a finer mesh on the dielectric resonators since, in terms of comparison, it is not correct to use curvilinear elements.

In Table XIX are summarized the timings, while, in Table XX the maximum amounts of memory required by the ANSYS simulation and by the Generalized BI-RME method for both the structures.

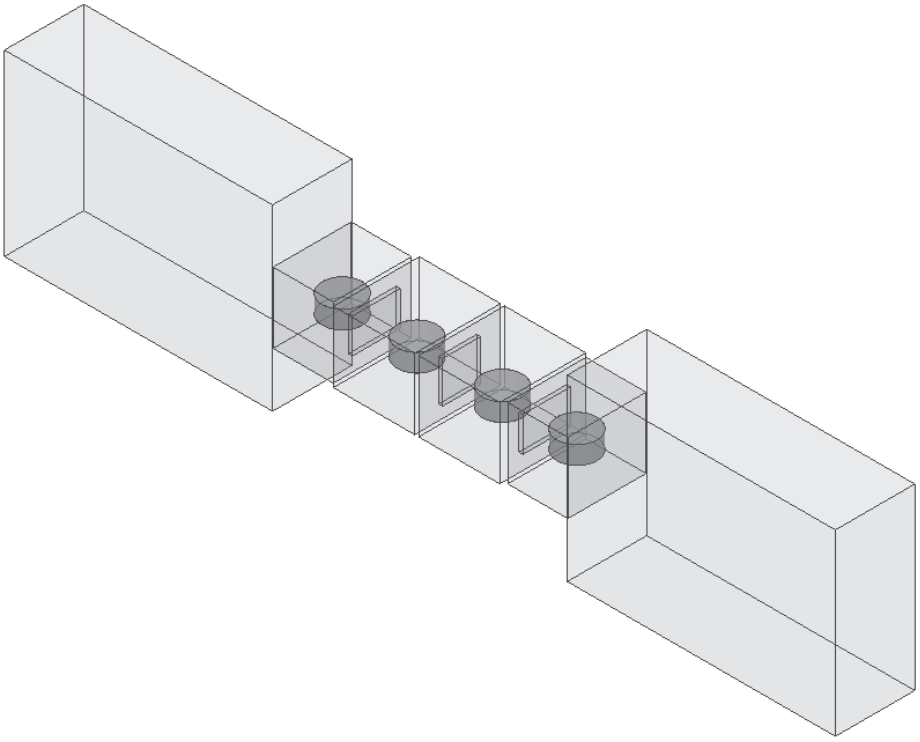

(*a*)

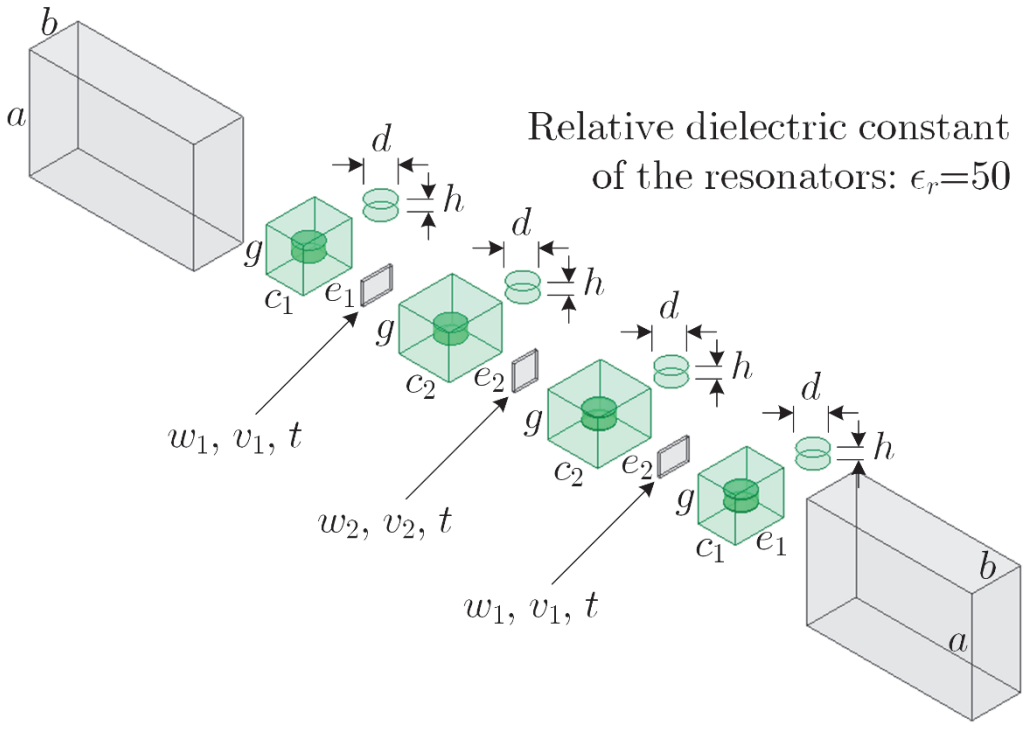

(*b*)

Fig. 4.21. Four-pole bandpass dielectric "mushrooms" filter [18]: (*a*) Geometry of the filter; (*b*) Filter segmented into 13 building blocks. The arbitrarily shaped building blocks are highlighted in green. Dimensions (in mm): a = 22.86, b = 10.16, e_1 = 10.0, c_1 = 7.7, e_2 = 11.0, c_2 = 10.4, g = 9.0, w_1 = 6.08, v_1 = 4.43, w_2 = 4.85, w_2 = 5.27, t = 0.5, d = 5.10, h = 2.3.

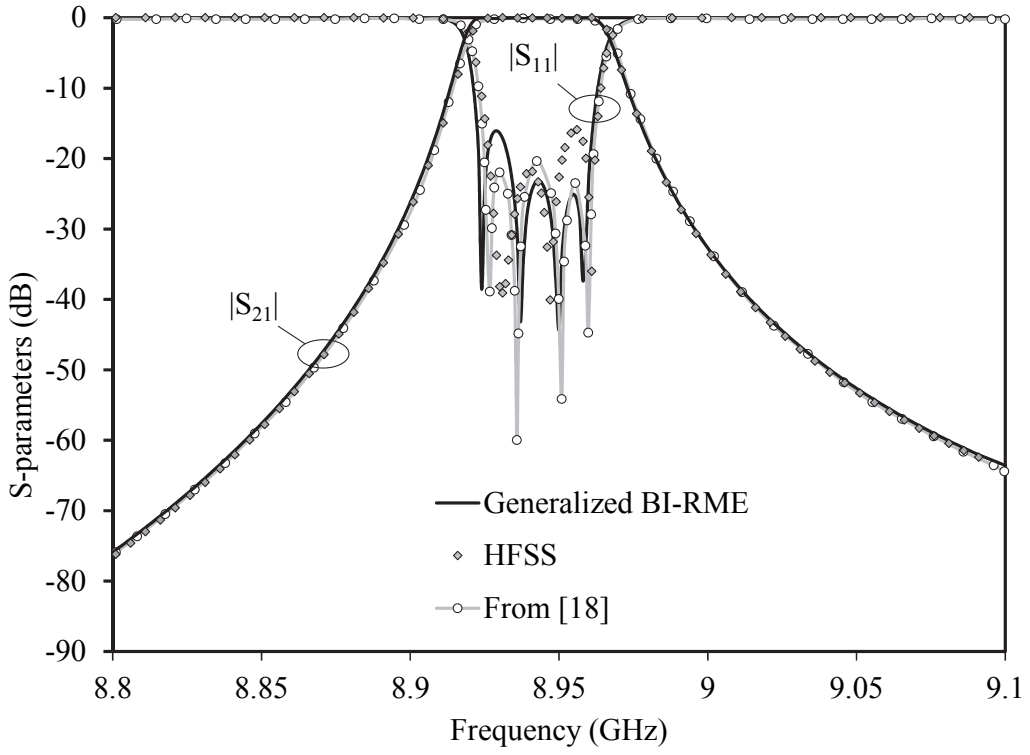

(*a*)

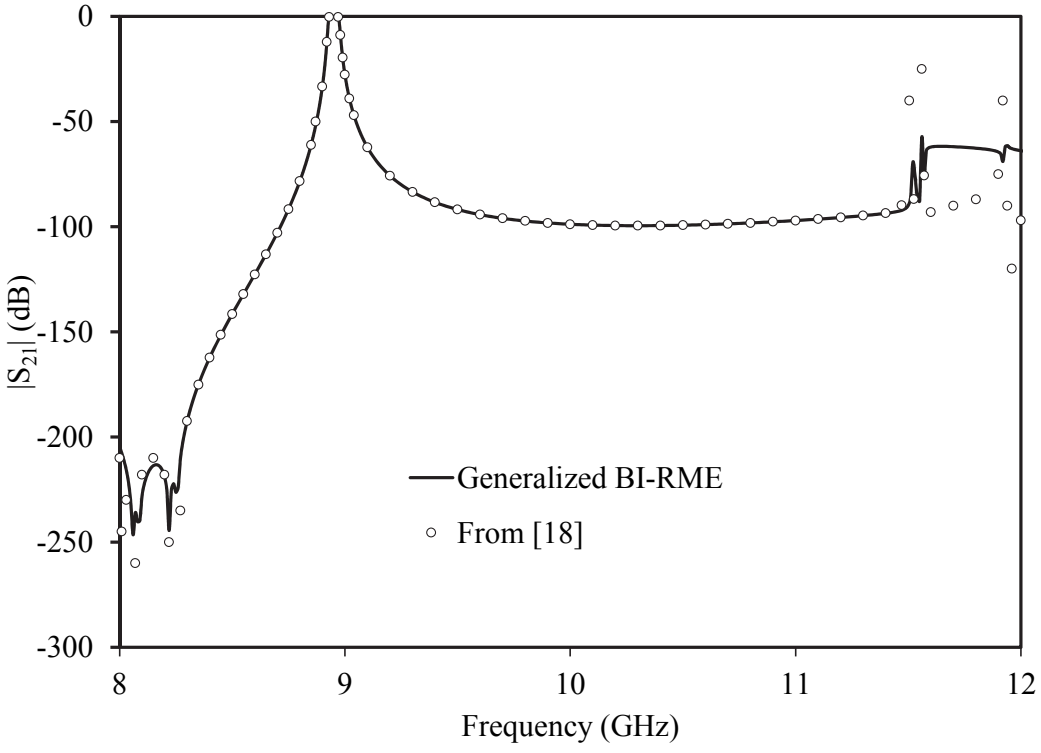

(*b*)

Fig. 4.22. Four-pole bandpass dielectric "mushrooms" filter of Fig. 4.21 ([17] and [19].): (*a*) Passband frequency response calculated by the generalized BI-RME method, compared with HFSS and the results obtained in [18]; (*b*) Wideband frequency response calculated by the generalized BI-RME method, compared with the results obtained in [18].

ANSYS HFSS	CPU Time (s)
Convergence: 5 points	4397
Interpolating analysis: 14 real frequency points	15228
Total	**19625**

Generalized BI-RME method	CPU Time (s)
BI-RME analysis	32724
MATLAB frequency cascade: 60 frequency points	371
Total	**33095**

Table XXI. Timing comparison for the Four-pole bandpass dielectric "mushrooms" filter.

ANSYS HFSS	Memory (MB)
Maximum amount	20400

Generalized BI-RME method	Memory (MB)
Maximum amount	2165

Table XXII. Maximum memory requirement comparison for the Four-pole bandpass dielectric "mushrooms" filter.

Bibliography

[1] C. A. Leal-Sevillano, Y. Tian, M. J. Lancaster, J. A. Ruiz-Cruz, J. R. Montejo-Garai and J. M. Rebollar, "A Micromachined Dual-Band Orthomode Transducer," *IEEE Transactions on Microwave Theory and Techniques*, vol. 62, no. 1, Jan. 2014.

[2] S. Battistutta, M. Bozzi, M. Bressan, M. Pasian and L. Perregrini, "Modeling of Waveguide Components by the BI-RME Method with the Ewald Green's Function and the Segmentation Technique," *2016 IEEE MTT-S International Microwave Symposium (IMS)*, San Francisco, CA, USA, May 22 – 27, 2016.

[3] S. Battistutta, M. Bozzi, M. Bressan, M. Pasian and L. Perregrini, "Application of the BI-RME Method to the Analysis of Piecewise-Homogeneous Waveguide Components," *2016 IEEE MTT-S International Conference on Numerical Electromagnetic and Multiphysics Modeling and Optimization for RF, Microwave, and Terahertz Applications (NEMO),* Beijing, China, July 27-29, 2016.

[4] S. Battistutta, M. Bozzi, M. Bressan, M. Pasian and L. Perregrini, "The BI-RME Method Combined with the Segmentation Technique Applied to the Modeling of 3D Components," *XXI Riunione Nazionale di Elettromagnetismo (XXI RiNEm)*, Parma, Italy, Sept. 12-14, 2016.

[5] S. Bastioli, C. Tomassoni and R. Sorrentino, "A New Class of Waveguide Dual-Mode Filters Using TM and Nonresonating Modes," *IEEE Transactions on Microwave Theory and Techniques*, vol. 58, no. 12, Dec. 2010.

[6] M. Bressan, S. Battistutta, M. Bozzi and L. Perregrini, "Modeling of Inhomogeneous and Lossy Waveguide Components by the Segmentation Technique Combined With the Calculation of Green's Function by Ewald's Method," *IEEE Transactions on Microwave Theory and Techniques*, vol. 66, no. 2, Feb. 2018.

[7] R. Vahldieck and W. J. R. Hoefer, "Computer-aided design of dielectric resonator filters in waveguide sections below cutoff," *IEE Electronics Letters*, vol. 21, no. 19, Sept. 1985.

[8] S. Battistutta, M. Bozzi, M. Bressan, M. Pasian and L. Perregrini, "Modeling of Inhomogeneous and Lossy Components by the BI-RME Method and the Segmentation Technique," *2016 46th European Microwave Conference (EuMC)*, London, UK, Oct. 3–7, 2016.

[9] J. Y. Jin, X. Q. Lin and Q. Xue, "A Miniaturized Evanescent Mode Waveguide Filter Using RRRs," *IEEE Transactions on Microwave Theory and Techniques*, vol. 64, no. 7, July 2016.

[10] J. M. Reiter and F. Arndt, "Rigorous analysis of arbitrarily shaped H- and E-plane discontinuities in rectangular waveguides by a full-wave boundary contour mode-matching method," *IEEE Transactions on Microwave Theory and Techniques*, vol. 43, no. 4, Apr. 1995.

[11] S. Battistutta, M. Bozzi, M. Bressan and L. Perregrini, "Extension of the BI-RME Method to the Analysis of Piecewise-Homogeneous Waveguide Components Including Arbitrarily Shaped Building Blocks," *2017 47th European Microwave Conference (EuMC)*, Nurnberg, DE, Oct. 9–12, 2017.

[12] A. A. Sarhan, M. Tayarani, H. Oraizi, N. Ghadimi and I. Hamidi, "Optimized Broad Band Riblet Short-Slot Waveguide Coupler for X-Band Applications," *International Journal of Scientific & Engineering Research*, vol. 4, no. 8, Aug. 2013.

[13] S. Battistutta, M. Bozzi, M. Bressan and L. Perregrini, "Analysis of Inhomogeneous Waveguide Components by the BI-RME Method," *XXII Riunione Nazionale di Elettromagnetismo (XXII RiNEm)*, Cagliari, Italy, Sept. 03-06, 2018.

[14] D. Dousset, S. Claude and K. Wu, "A Compact High-Performance Orthomode Transducer for the Atacama Large Millimeter Array (ALMA) Band 1 (31–45 GHz)," *IEEE Access*, vol. 1, 2013.

[15] S. Battistutta, M. Bozzi, M. Bressan and L. Perregrini, "Analysis of a Matched Turnstile Junction by the BI-RME Method and the Segmentation Technique," *2018 Baltic URSI Symposium (URSI)*, Poznań, Poland, May 15–17, 2018.

[16] C. Bachiller, H. Esteban, H. Mata, M. A. Valdes, V. E. Boria, A. Belenguer and J. V. Morro, "Hybrid Mode Matching Method for the Efficient Analysis of Metal and Dielectric Rods in H Plane Rectangular Waveguide Devices," *IEEE Transactions on Microwave Theory and Techniques*, vol. 58, no. 12, Dec. 2010.

[17] S. Battistutta, M. Bozzi, M. Bressan and L. Perregrini, "Generalized BI-RME Method applied to the Analysis of Dielectric-Loaded Waveguide Components," *2018 IEEE MTT-S International Conference on Numerical Electromagnetic and Multiphysics Modeling and Optimization for RF, Microwave, and Terahertz Applications (NEMO)*, Reykjavik, Iceland, Aug. 08-10, 2018.

[18] J. Gil, A. A. San Blas, C. Vicente, B. Gimeno, M. Bressan, V. E. Boria, G. Conciauro and M. Maestre, "Full-Wave Analysis and Design of Dielectric-Loaded Waveguide Filters Using a State-Space Integral-Equation Method," *IEEE Transactions on Microwave Theory and Techniques*, vol. 57, no. 1, Jan. 2009.

[19] S. Battistutta, M. Bozzi, M. Bressan and L. Perregrini, "Analysis of Dielectric-Loaded Waveguide Filters by the Generalized BI-RME Method," *2018 48th European Microwave Conference (EuMC)*, Madrid, Spain, Sept. 23–28, 2018.

Chapter 5
Conclusions and future upgrades

Since its creation, the *Boundary Integral-Resonant Mode Expansion* method (BI-RME) has demonstrated to be a very efficient and accurate full-wave method to characterize a microwave component through a mathematical model. However, its specialization to the analysis of a particular class of components was its most important drawback: in order to be applied to a different class of problem, it required an *ad hoc* theory development and code implementation. With the activity descripted in this thesis, this drawback has been overcome by creating a new numerical technique that generalize the BI-RME method through the combination of a particular implementation of it with the segmentation technique. The result, called Generalized BI-RME method, is a numerical technique that permits to analyze completely arbitrary 3D components, filled by piecewise homogeneous and lossy dielectric materials, with the use of simple and well-known RWG basis functions. This is possible by combining an implementation of the BI-RME method with the segmentation technique: in this way, it is possible to use the same theory and code to analyze passive components that spans from the dielectric-loaded filters to the power dividers or to the orthomode transducers.

As explained in Chapter 2, once defined the geometry, the desired circuit is subdivided into homogeneously filled building blocks. Then, it is defined the surface mesh on the building blocks boundary surfaces based on some rules dictated by the successive electromagnetic analysis phase. Each block is analyzed by the BI-RME method subdividing them into two categories based on the block shape. In particular, for the building blocks with a rectangular parallelepiped shape, the analysis is performed with an easier and faster version of the implemented BI-RME method called “boxed” approach; while, for the blocks with a different shape, it is used the general version called “arbitrarily shaped” approach. In particular, in Chapter 3 have been studied the effects of the choice of the segmentation, the mesh and the BI-RME settings on the EM analysis. The results of the electromagnetic analysis of each building block are combined in the post-processing part of the algorithm to form a generalized admittance matrix (GAM) in form of pole expansion, so a wideband and material independent mathematical model of the block behavior. Once obtained the GAMs elements of all the building blocks, they are combined together through a circuital cascade procedure in the frequency domain to obtain the GAM of the entire circuit; then, the admittance matrix behavior is transformed into S-parameters.

In Chapter 4, a series of examples are presented to demonstrate the effectiveness of the proposed algorithm. All the examples are analyzed with the Generalized BI-RME method and the results are

compared with the ones obtained with ANSYS HFSS. In particular, first are reported some examples of structures segmented into boxed blocks; then, the attention is focus on true arbitrarily shaped circuits. In both cases are proposed examples loaded or not with dielectric elements, with or without dielectric losses.

In general, the EM results obtained with the Generalized BI-RME method are in good agreement with the ones of ANSYS HFSS. As already told, even if the results are obtained by choosing the right parameters in order to have a good convergence, a little discrepancy can exist since the proposed method and the FEM implemented into HFSS are always numerical methods. A possible future upgrade could be the implementation of a mesh refinement inside the proposed technique to try to compensate the discrepancies due to the mesh as well as the BI-RME parameters.

Moreover, the maximum memory required by the Generalized BI-RME method is, in general, less than the one of the commercial software. Another necessary consideration is about timing: the proposed method has proved to be a very good numerical technique especially in case of boxed building block. As already told, the Generalized BI-RME method is a homemade project still in the development phase: so, the code structure is designed to have a full control and debug capability and it is not compiled. In this sense, having sometimes timing greater than the one of the commercial software it is not a sign of bad numerical method or implementation but it needs to be interpreted as a point on which it is possible to do better for the next upgrades. In this sense, the use of the block reusability and of the symmetries will help to save a huge amount of computational time. Unfortunately, this requires a full control on the mesh generation that, actually, it is not possible with the adopted mesh generator.

Chapter 6
Highlights of the Ph.D.

The Doctoral activity reported in this thesis is the result of three years (October, 1st 2015 – September, 30th 2018) of research activities on the generalization of the BI-RME method. During this temporal period, the author has published their results on the most important conference proceeding of the microwave panorama. In particular, the *IEEE MTT-S International Microwave Symposium* (IMS - 2016, San Francisco, CA, USA), the *European Microwave Conference* (EuMC - 2016, London, UK; EuMC 2017, Nurnberg, DE; EuMC 2018, Madrid, ES), the *IEEE MTT-S International Conference on Numerical Electromagnetic and Multiphysics Modeling and Optimization for RF, Microwave, and Terahertz Applications* (NEMO - 2016, Beijing, PRC; 2017, Sevilla, ES; 2018, Reykjavik, IS), *Baltic URSI Symposium (URSI* - 2018, Poznań, PL), *IEEE MTT-S International Microwave Workshop Series on Advanced Materials and Processes for RF and THz Applications* (IMWS-AMP – 2017, Pavia, IT). In the publication list are highlighted the conferences on which the author of this thesis has presented its results and on which the presentation has been done by a co-author of the publications. In particular, during the IMS2016 in San Francisco (CA, 2016), the author has won the first prize at the "Graduate Student Challenge" with a work entitled “A New Green, Flexible and Wearable RF Energy-harvesting Approach for IoT”. Moreover, he has collaborated to the creation and management of two international conferences in terms of website and setting up of the paper submission/review process: *2017 IEEE MTT-S International Microwave Workshop Series on Advanced Materials and Processes for RF and THz Applications* (IMWS-AMP 2017) hosted in Pavia (Italy - Sept. 20-22, 2017) as publication and website chair, and the *2018 IEEE International Symposium on Radio-Frequency Integration Technology* (RFIT 2018) hosted in Melbourne (Australia – Aug. 15-17, 2018) as e-Paper Submission & Management Advisor.

On the academic point of view, different seminars and presentations was held during the Ph.D. career and the following doctoral international courses have been followed: “Languages, Problems and Communication Methods of the Scientific Research” and the EuMA International Summer School on Microwave Systems for the IoT. Moreover, the author has given his support to the teaching of the following courses (blackboard exercises, seminars and student coaching): “Circuits and electromagnetic field I”, Bachelor of “Electronics Engineering” and “Linear Electrical Circuits”, Bachelor of “Electronics Engineering”.

Publication list

International Journals

[J-1] M. Bressan, S. Battistutta, M. Bozzi and L. Perregrini, “Modeling of Inhomogeneous and Lossy Waveguide Components by the Segmentation Technique Combined With the Calculation of Green's Function by Ewald's Method,” *IEEE Transactions on Microwave Theory and Techniques*, vol. 66, no. 2, pp. 633-642, Feb. 2018

International Conferences

[C-1] S. Battistutta, M. Bozzi, M. Bressan and L. Perregrini, “Analysis of Dielectric-Loaded Waveguide Filters by the Generalized BI-RME Method,” *2018 48th European Microwave Conference (EuMC)*, Madrid, Spain, Sept. 23–28, 2018. (*presentation held by the fourth author*)

[C-2] S. Battistutta, M. Bozzi, M. Bressan and L. Perregrini, "Generalized BI-RME Method applied to the Analysis of Dielectric-Loaded Waveguide Components," *2018 IEEE MTT-S International Conference on Numerical Electromagnetic and Multiphysics Modeling and Optimization for RF, Microwave, and Terahertz Applications (NEMO)*, Reykjavik, Iceland, Aug. 08-10, 2018. (*presentation held by the fourth author*)

[C-3] S. Battistutta, M. Bozzi, M. Bressan and L. Perregrini, “Analysis of a Matched Turnstile Junction by the BI-RME Method and the Segmentation Technique,” *2018 Baltic URSI Symposium (URSI)*, Poznań, Poland, May 15–17, 2018. (*presentation held by the first author*)

[C-4] S. Battistutta, M. Bozzi, M. Bressan and L. Perregrini, “Extension of the BI-RME Method to the Analysis of Piecewise-Homogeneous Waveguide Components Including Arbitrarily Shaped Building Blocks,” *2017 47th European Microwave Conference (EuMC)*, Nurnberg, DE, Oct. 9–12, 2017. (*presentation held by the first author*)

[C-5] S. Battistutta, M. Bressan, M. Bozzi and L. Perregrini, "Material Characterization Through a Full-Wave Approach Based on the BI-RME Method," *2017 IEEE MTT-S International Microwave Workshop Series on Advanced Materials and Processes for RF and THz Applications (IMWS-AMP)*, Pavia, Italy, Sept. 20-22, 2017. (*presentation held by the first author*)

[C-6] S. Battistutta, M. Bressan, M. Bozzi and L. Perregrini, "A Fast Numerical Technique for the Determination of Electrical Properties of Materials," *2017 IEEE MTT-S International Conference on Numerical Electromagnetic and Multiphysics Modeling and Optimization for RF, Microwave, and Terahertz Applications (NEMO)*, Sevilla, Spain, May 17-19, 2017. (*presentation held by the fourth author*)

[C-7] S. Battistutta, M. Bozzi, M. Bressan, M. Pasian and L. Perregrini, "Modeling of Inhomogeneous and Lossy Components by the BI-RME Method and the Segmentation Technique," *2016 46th European Microwave Conference (EuMC)*, London, UK, Oct. 3–7, 2016. (*presentation held by the first author*)

[C-8] S. Battistutta, M. Bozzi, M. Bressan, M. Pasian and L. Perregrini, "Application of the BI-RME Method to the Analysis of Piecewise-Homogeneous Waveguide Components," *2016 IEEE MTT-S International Conference on Numerical Electromagnetic and Multiphysics Modeling*

and Optimization for RF, Microwave, and Terahertz Applications (NEMO), Beijing, China, July 27-29, 2016. (*presentation held by the fourth author*)

[C-9] S. Battistutta, M. Bozzi, M. Bressan, M. Pasian and L. Perregrini, "Modeling of Waveguide Components by the BI-RME Method with the Ewald Green's Function and the Segmentation Technique," *2016 IEEE MTT-S International Microwave Symposium (IMS)*, San Francisco, CA, USA, May 22 – 27, 2016. (*presentation held by the fourth author*)

National Conferences

[N-1] S. Battistutta, M. Bozzi, M. Bressan and L. Perregrini, "Analysis of Inhomogeneous Waveguide Components by the BI-RME Method," *XXII Riunione Nazionale di Elettromagnetismo (XXII RiNEm)*, Cagliari, Italy, Sept. 03-06, 2018. (*presentation held by the fourth author)*

[N-2] S. Battistutta, M. Bozzi, M. Bressan, M. Pasian and L. Perregrini, "The BI-RME Method Combined with the Segmentation Technique Applied to the Modeling of 3D Components," *XXI Riunione Nazionale di Elettromagnetismo (XXI RiNEm)*, Parma, Italy, Sept. 12-14, 2016. (*presentation held by the first author*)

Appendix

Application to the material characterization

The determination of the complex permittivity of solid, liquid, powdered, and granular materials is becoming more important for several applications. In fact, the exploitation of novel materials (like 3D printable filaments) for the realization of microwave circuits requires a careful determination of their electrical properties [1]-[4]. Moreover, the growing interest for lab-on-chip circuits to be deployed for the realization of Wireless Sensor Networks (WSN) and for Internet of Things (IoT) applications typically requires the determination of the complex permittivity of liquids, powdered and granular materials [5]-[8]. 3Dprinting technology can be adopted for microwave microfluidic sensors, thus achieving a complete Lab-on-Chip approach. Fig. A.1 shows an example of a microfluidic sensor with a complex geometry structure [9].

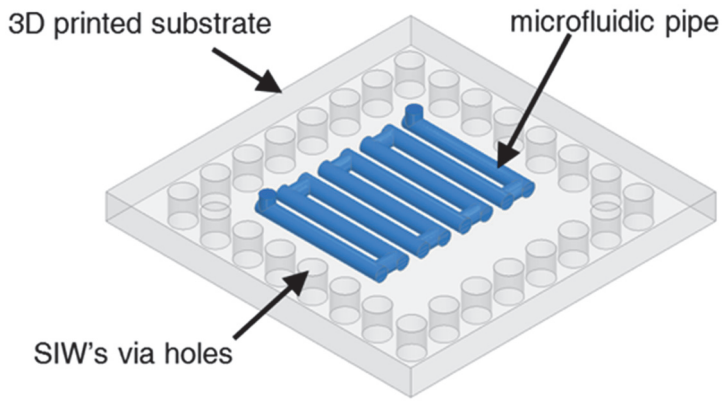

Fig. A.1. Example of a microfluidic sensor based on a SIW cavity [9].

For this kind of complex structures, it is very difficult to find analytical expressions for retrieving the unknown dielectric characteristic of the fluid. Numerical tools are therefore mandatory for the determination of the dielectric parameters. In this sense, the Generalized BI-RME method could found application also on the determination of the dielectric properties of materials thanks to the fact that the complex permittivity appears explicitly in the expression of the generalized admittance matrix (GAM) (2.61). For this purpose, in [10] and [11] it is proposed a possible algorithm applied to a very simple circuit. In particular, the circuit used for the unknown sample testing is a one port waveguide cavity resonator with a thin pipe placed vertically for the characterization of fluids or powders (Fig. A.2). The structure is segmented into homogeneously-filled building blocks and the admittance matrix of each block is represented through a pole-expansion. When using an iterative procedure, the identification of the unknown electrical characteristics of the material does not require repeated full-wave analyses but only circuital matrix recombination. Even if the proposed structure is really simple, only the cavity with

the inductive iris and the pipe need to be realized for the interconnection with a standard waveguide. Moreover, it could be realized with 3D printed material then metallized, to realize it with a low cost. Furthermore, it could be also used to analyze solid materials like the 3D printed filaments by removing the pipe. As shown in Fig. A.2*a*, the proposed structure consists of a resonant cavity of length $c = 13.3$ mm formed by an iris-septum (thickness $g = 1$ mm) in a short-circuited WR-90 rectangular waveguide ($a = 22.86$ mm, $b = 10.16$ mm). The Material Under Test (MUT) is placed in a pipe crossing the cavity ($p = 0.88$ mm). The dimensions of the resonant cavity and of the pipe cross-section, as well as the position of the pipe have been optimized to accommodate the resonant frequencies of materials spanning from air ($\varepsilon' = 1$, $f_r \cong 12.4$ GHz) to water ($\varepsilon' = 80$, $f_r \cong 8.2$ GHz) in the standard X-band frequency range (8.2 GHz – 12.4 GHz). In the BI-RME analysis, the structure has been segmented into two homogeneously-filled blocks (Fig. A.2*b*) and the mesh for the RWG basis functions has been selected in order to have triangles with a mean edge length of about $\lambda_{min}/6$, where λ_{min} is the wavelength at the maximum frequency for the material with the highest value of ε'.

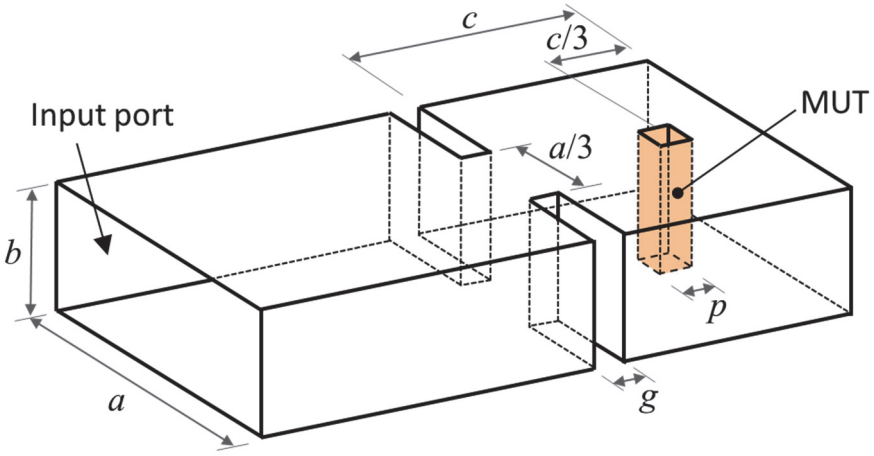

(*a*)

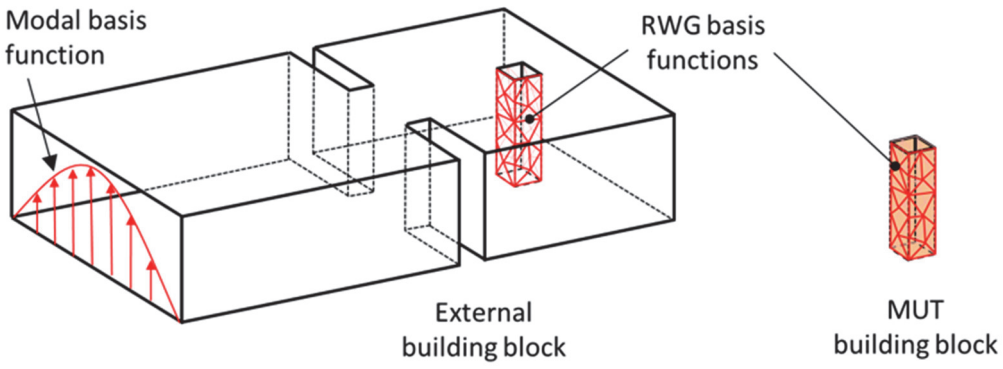

(*b*)

Fig. A.2. The waveguide circuit considered to verify the accuracy of the proposed technique: (*a*) The whole structure including a resonant cavity with a square pipe; (*b*) The structure segmented into two building blocks (the external part and the MUT), whose GAMs are calculated by the B-RME method.

The results of the simulation performed considering three different materials with high and medium-to-low ε' and high and low losses (i.e., MUT#1 $\varepsilon' = 61$, $\varepsilon'' = 6.1$, MUT#2 $\varepsilon' = 30$, $\varepsilon'' = 0.15$, MUT#3 $\varepsilon' = 10$, $\varepsilon'' = 0.1$) are plotted in Fig. A.3 and compared with ANSYS HFSS simulations. The computing time for the calculation of the quantities k_p, A_{ij}, B_{ij}, and C_{ip} appearing in (2.61) was in the order of few minutes. These quantities are independent of the frequency and of the material characteristics and are calculated just once. The frequency-by-frequency computation of the GAMs and their combination required only 0.15 seconds per frequency point.

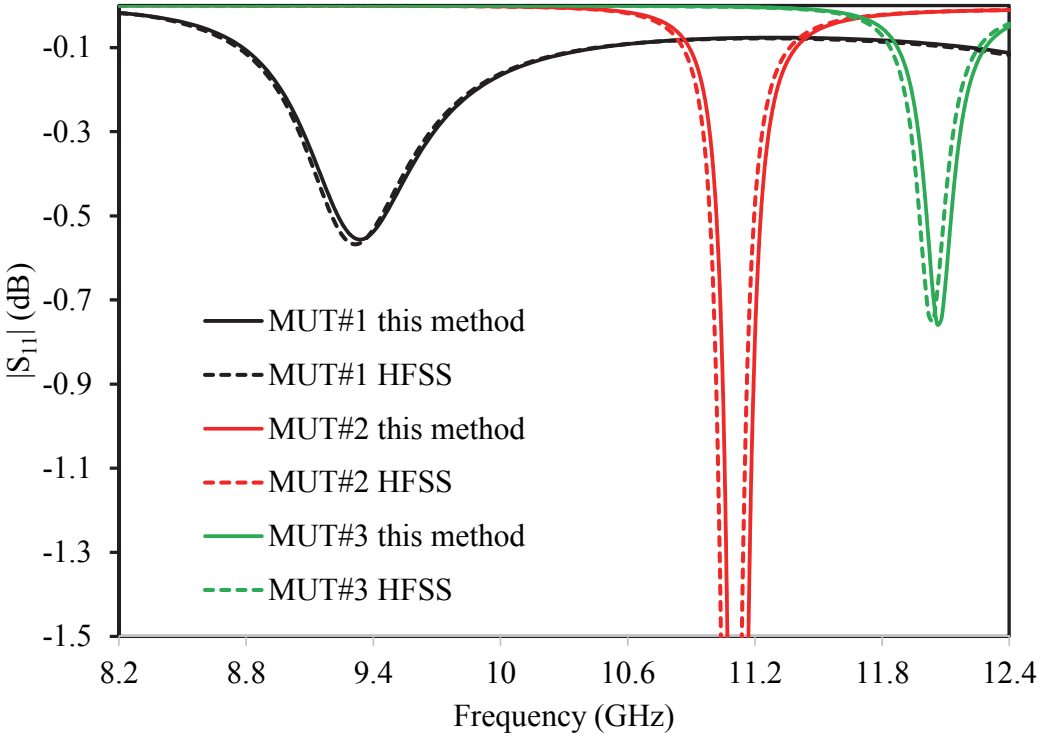

Fig. A.3. Resonance peaks of the reflection when changing the dielectric permittivity of the liquid that flows into the pipe of the structure. The results of the proposed technique are compared with HFSS simulations

The deployment of Wireless Sensor Networks (WSN) requires the realization of lab-on-chip circuits for the measurement of the complex permittivity of different materials. Depending on the application, the material to be sensed, and on the fabrication technology, these sensors may have arbitrary shapes (see, for instance, [9]). Since the proposed method does not require repeated full-wave simulation of the structure when the dielectric constant is changed, it is perfectly suited to setup an automatic system for the dielectric material characterization. Fig. A.4 shows the flowchart of the algorithm. The dashed red rectangle identifies the iterative part, where no full-wave analyses are required and only the circuital combination of GAMs is performed. Indeed, equation (2.61) could be further exploited to calculate also the derivative of the frequency response vs the dielectric constant (and, therefore, of the gradient of the objective function F) in a semi-analytical way. Finally, since the geometry of the sensor is defined *a priori* and does not change, the preliminary calculation involving full-wave analyses (dashed blue rectangle in Fig. A.4) can be performed off-line and their results can be stored and used by the in the processor, which performs the material characterization, without any need to have the full-wave code available on the sensor node.

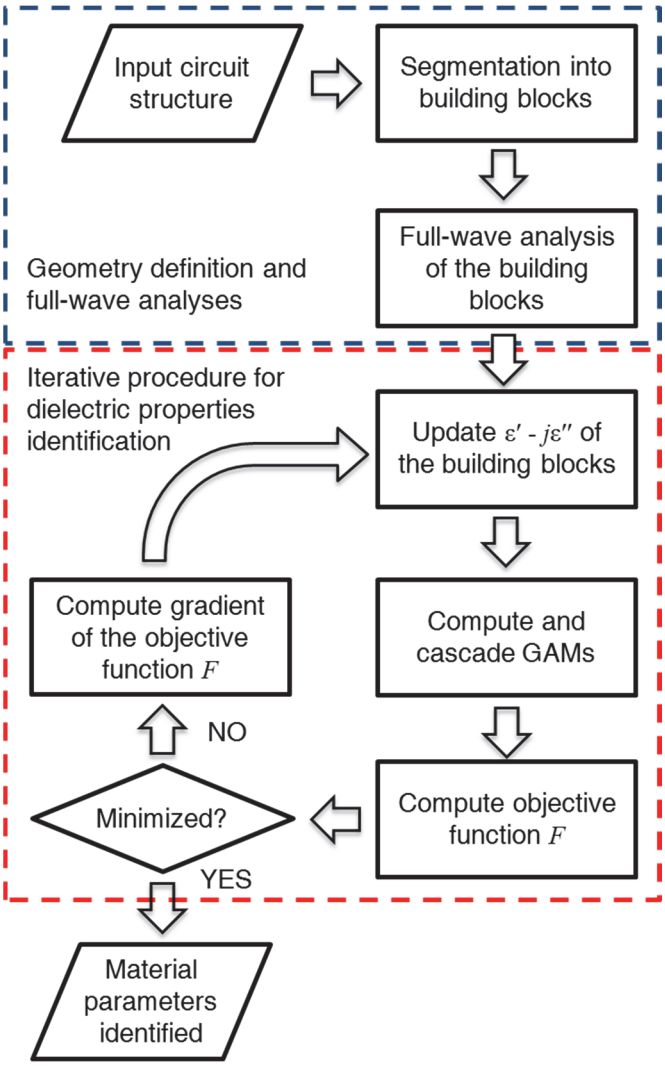

Fig. A.4. Scheme of the procedure for the automatic identification of the electrical properties of an unknown material.

Bibliography

[1] S. Moscato *et al*., "An Innovative Manufacturing Approach for Paper-based Substrate Integrated Waveguide Components and Antennas," *IET Microwave, Antennas & Propag*ation, vol. 10, no. 3, Feb. 2016.

[2] A. Kilian, J. Weinzierl, and L. P. Schmidt, "Permittivity Measurement Techniques at 24 GHz for Automotive Polymer Composites Including Thin Films and Paint Foils," *German Microwave Conference*, Hamburg, Germany, 2008.

[3] R. Moro *et al*., "Textile Microwave Components in Substrate Integrated Waveguide Technology," *IEEE Transactions on Microwave Theory and Techniques*, vol. 63, no. 2, Feb. 2015.

[4] E. Massoni *et al*., "Characterization of 3D-printed dielectric substrates with different infill for microwave applications," *2016 IEEE MTT-S International Microwave Workshop Series on Advanced Materials and Processes for RF and THz Applications*, Chengdu, 2016.

[5] M. Mraović *et al*., "Humidity Sensors Printed on Recycled Paper and Cardboard," *Sensors*, vol. 14, no. 8, Jul. 2014.

[6] A. J. Gimenez *et al*., "Paper-Based ZnO Oxygen Sensor," *IEEE Sensors Journal*, vol. 15, no. 2, Feb. 2015.

[7] J. Sarfraz *et al*., "Printed hydrogen sulphide gas sensor on paper substrate based on polyaniline composite," *Thin Solid Films*, vol. 534, May 2013.

[8] T. Jalkanen *et al*., "Fabrication of Porous Silicon Based Humidity Sensing Elements on Paper," *Journal of Sensors*, vol. 2015, 2015.

[9] S. Moscato *et al*., "Exploiting 3D Printed Substrate for Microfluidic SIW Sensor," *45th European Microwave Conference* (EuMC2015), Paris, France, Sept. 7–10, 2015.

[10] S. Battistutta, M. Bressan, M. Bozzi and L. Perregrini, "Material Characterization Through a Full-Wave Approach Based on the BI-RME Method," *2017 IEEE MTT-S International Microwave Workshop Series on Advanced Materials and Processes for RF and THz Applications (IMWS-AMP)*, Pavia, Italy, Sept. 20-22, 2017.

[11] S. Battistutta, M. Bressan, M. Bozzi and L. Perregrini, "A Fast Numerical Technique for the Determination of Electrical Properties of Materials," *2017 IEEE MTT-S International Conference on Numerical Electromagnetic and Multiphysics Modeling and Optimization for RF, Microwave, and Terahertz Applications (NEMO)*, Sevilla, Spain, May 17-19, 2017.

Acknowledgments

As always, first of all, I would like to thank my future wife, Selene, for her support during all my academic experience, from the Bachelor Degree to the Doctoral one.

Thanks to my family and my girlfriend's one because they have always supported me over several aspects of my life and of my studies.

A big thank to Professors Perregrini and Bressan for their patience and guidance over these years and because they have believed in me.

Thanks to all members of the Microwave Laboratory of the University of Pavia, my "home" during this years: this experience was wonderful.

I know that the following acknowledgment may appear not conventional, but it sincere: I would like to thank the Ph.D... Thanks to these three years, I grew up on the professional point of view as well as on the personal one. It prepared me to the rhythms of working life, to really think as an engineer. Moreover, it allowed me to go to live with my future wife. I had the possibility to participate to the most important conferences on the microwave scenario and to visit beautiful cities like San Francisco, London, Nuremberg… Last, but not least, in these three year I known and worked with beautiful persons that I will always carry in my heart.